Interactions Between Crystal Surfaces in Solution and Agglomeration — a Theoretical Approach

Michael Brunsteiner

A thesis submitted to the University of London in partial fulfilment
of the requirements for the degree of Doctor of Philosophy

University College London
May 2003

Acknowledgements

I would like to thank my supervisor, Prof. Sarah L Price, for her support and for giving me both the freedom I wanted and the guidance I needed.

I would like to thank Mihaly Mezei, Fernando Bresme, John Harding and Gerhard Hummer for helpful discussions about the science.

I would like to thank my family, especially my parents, for their continued support, for letting me do stupid things once in a while and for helping me doing the right thing, eventually.

Teresa, I thank you for all the strength you gave me, for your patience, for tolerating my unhealthy working hours and for the fun you are.

Abstract

Agglomeration can have a crucial impact on the yield of crystallisation processes and the product quality. In this thesis molecular scale modelling is used to gain insights into the mechanism of crystal agglomeration and factors that determine its progress.

The first study analyses the use of the attachment energy model to predict which surfaces of a crystal would be observed and hence the crystal morphology. It is shown that comparatively simple model potentials suffice to provide reasonably accurate morphology predictions within the limitations of the neglect of solvent.

A classical empirical force field for potash alum ($KAl(SO_4)_2{\cdot}12\,H_2O$) is developed. After having established its capability to reproduce experimentally determined properties of the crystal bulk and the solution, different potash alum crystal faces in contact with aqueous solution are modelled via Molecular Dynamics simulations. A range of different methods of modelling polar crystal surfaces, including a novel one, are investigated. The results are used to rationalise experimental results quantifying the agglomerative strength of PA crystallites as a function of super-saturation and the structure of the crystal faces.

Common models for the theoretical prediction of crystal agglomeration include an efficiency parameter which is essentially a material property and a functional of the average force between two particles in solution. A set of Molecular Dynamics simulations of potassium chloride nano-crystallites in aqueous KCl solution is performed in order to establish whether it is possible to obtain reproduceable forces using an explicit water model and an extended system geometry to maintain constant chemical potential of the solution in between two crystal surfaces and a bulk phase. Although the results highlight some interesting aspects, and can give qualitative explanations of agglomeration tendencies, quantitative predictions of agglomeration will require further research.

Contents

1 Introduction **13**

2 Modelling Crystallisation and Agglomeration **18**

2.1 Population Balance Equations 19

2.2 Agglomeration Kernel and Efficiency 22

2.3 Forces between Dispersed Particles 26

2.3.1 DLVO-Theory 27

2.3.2 The State of the Art 28

2.4 Conclusions 34

3 Molecular Simulation **35**

3.1 Introduction 35

3.2 Ab-Initio Methods 37

3.3 Classical Model Potentials 39

3.3.1 Perturbation Theory 40

3.3.2 Model Potentials in Practice 45

3.4 Molecular Mechanics 55

3.5 Molecular Dynamics 57

3.5.1 Integration of the Equations of Motion 58

3.5.2 Boundary Conditions and Cutoffs 59

3.5.3 Ensembles 60

3.5.4 Long Range Interactions 62

3.6 Additional Issues in Molecular Dynamics Simulations 65
3.6.1 Long Range Interactions in Interfacial Systems 66
3.6.2 Charged Systems 68
3.6.3 The Grand Canonical Ensemble 70

4 Crystal Morphologies **74**
4.1 Introduction 74
4.2 Computational Details 76
4.2.1 The Compounds 76
4.2.2 The Model Potentials 77
4.2.3 Attachment Energy Calculations 80
4.2.4 Energy Minimisation 81
4.3 Results & Discussion 82
4.3.1 Theoretical Morphologies 83
4.4 Conclusions 91

5 Force Field Parameterisation for Potash Alum **93**
5.1 Introduction 93
5.2 The Material 95
5.3 The Model Potential 96
5.4 The Strategy 98
5.5 Parameters adopted from the literature 99
5.6 Results 101
5.6.1 The Anhydrates 101
5.6.2 Potash Alum Parameters 103
5.6.3 Structure 105
5.6.4 Local Disorder 107
5.6.5 Aqueous Solutions 108
5.7 Summary 110

6 Electrostatic Long Range Interactions in 2D-periodic Systems 112

6.1 Computational Details . . . 113

6.2 Results and Discussion . . . 114

6.3 Summary . . . 121

7 The Surface Structure of Potash Alum 122

7.1 Introduction . . . 122

7.2 Polar Surfaces . . . 124

7.3 Theoretical Determination of Surface Structures . . . 128

7.3.1 Calculation of Surface Energies . . . 129

7.3.2 Molecular Dynamics . . . 130

7.4 Potash Alum . . . 132

7.4.1 The (220) and (200) Faces . . . 133

7.4.2 The (111) Face . . . 133

7.5 Computational Methods . . . 136

7.5.1 The Model Potential . . . 136

7.5.2 MD-simulations . . . 137

7.6 Results . . . 141

7.6.1 Surface Structures . . . 141

7.7 Discussion . . . 151

7.8 Summary . . . 156

8 Forces Between Nano-Crystallites in Aqueous Solution 157

8.1 Calculating the Potential of Mean Force . . . 158

8.2 Calculation of Inter Particle Forces, the System Geometry . . . 160

8.2.1 Slit-pore at Constant Chemical Potential . . . 163

8.2.2 Direct Simulation of a Particle Reservoir: The Immersed Sandwich 165

8.3 The Material and Model Potentials . . . 168

8.3.1 The Solution . . . 169

8.3.2 The Crystal 170
8.4 Simulation Conditions & Computational Details 172
8.5 Results I, Model Potentials and Rigid Crystals 174
8.6 Results II, Structure and Forces in the Frozen Sandwich 179
8.6.1 Neat Water 180
8.6.2 KCl Solution 189
8.6.3 System Size 193
8.6.4 Explicit Non-Equilibrium 197
8.7 Results III, Structure and Forces obtained with a Mobile Sandwich 200
8.7.1 Motion of the Nano-Crystallites 203
8.7.2 Structure 205
8.7.3 Equilibration 211
8.7.4 Forces 216
8.7.5 Non-Equilibrium 219
8.8 Discussion 230

9 Summary, Conclusions, Outlook **234**

List of Tables

4.1 Crystallographic and thermodynamic data 78
4.2 Summary of the different model potentials 78
4.3 Errors in reproducing the crystal structures and energies 82
4.4 Analysis of faces in terms of interplanar spacings 84
4.5 Attachment energies of pentaerythritol 85

5.1 Results of parameter fitting 100
5.2 Results of lattice energy minimisations 101
5.3 The final parameter set for potash alum 104
5.4 Results of lattice energy minimisations of potash alum 105
5.5 Radii of solvation shells and diffusion coefficients 110

6.1 Geometries and system sizes as used in the calculations 115
6.2 Required CPU time 119

7.1 Details of the potash alum surface simulations 140
7.2 Configurational energies of potash alum (111) slabs 150

8.1 KCl Force field parameters 171
8.2 Lattice parameters and elastic constants (in GPa) of KCl 174
8.3 Setups for Simulations 180
8.4 Details for the equilibrium simulations with mobile crystallites 202
8.5 Number of molecules in the pore and the standard deviations 214

8.6 The 1-D mean square displacement for water and ions in the pore 215
8.7 Average total force between the nano-crystallites 217

List of Figures

2.1 The stages of crystal agglomeration 23
2.2 Modelling crystallisation: the problem hierarchy 34

4.1 The five molecular compounds 77
4.2 Morphologies: ϵ-caprolactam and β-succinic acid 86
4.3 Morphologies: urea and pentaerythritol 89

5.1 Ball and stick model of the content of the potash alum unit cell 95
5.2 The two possible orientations of the sulfate anions in potash alum 97
5.3 The structures of ion-water complexes 106
5.4 Radial distribution functions 108
5.5 Potash alum sample at a pressure of 1 GPa 109
5.6 Radial distribution functions of $Al_2(SO_4)_3$ and K_2SO_4 111

6.1 Radial distribution functions obtained with different treatments of long range interactions 116
6.2 Radial distribution functions obtained with different lengths of the simulation cell 118
6.3 Mass-, charge-density and electrostatic field I 118
6.4 Mass-, charge-density and electrostatic field II 120
6.5 Mass-, charge-density and electrostatic field III 120

7.1 Morphology of potash alum crystals 123

7.2 Screw dislocation on the (111) face of potash alum 124
7.3 Schematical illustration of the different types of surface terminations . . . 125
7.4 Mechanisms for the stabilisation of polar surfaces 126
7.5 Atomic structure of the potash alum surfaces 132
7.6 Possible reconstructions of the polar potash alum (111) face 135
7.7 Cross section of the MD simulation cell 139
7.8 Structure of the (100) and (110) surfaces 143
7.9 Structure of the reconstructed (111) surface 145
7.10 Structure of the charged (111) surfaces 147
7.11 Structure of the polar (111) surfaces and solutions 149

8.1 System geometry for the simulation of a slit pore and bulk 166
8.2 Snapshots of KCl + water systems after 240 ps MD 176
8.3 Average mass and charge densities for the rigid crystal with FF1 177
8.4 Snapshots of the KCl-water interface after 240 ps MD 177
8.5 Time development of the water densities in the pore 182
8.6 Structure of the water in the pore with geometry A 183
8.7 Trajectories of some water oxygens in the 6.0 Å pore 185
8.8 Summation of the Forces 186
8.9 Forces between the crystallites for different lateral distances from the pore center 187
8.10 Averages and RMSD values of the forces for different lateral distances . . . 188
8.11 The average total and structural forces for different surface separations . . 188
8.12 Number of K^+ and Cl^- ions in the pore 189
8.13 Number of water molecules in the pore 190
8.14 Forces as function of lateral ion positions 191
8.15 Snapshots of the pore with $d_p = 6.0$ Å 192
8.16 The average total and structural forces for different surface separations . . 192

8.17 Comparison of the inter surface forces in neat water and in saturated KCl solution . . . 193
8.18 Running averages of forces . . . 195
8.19 Comparison of the calculated structural forces between nano-crystallites with 10 and 12 layers . . . 196
8.20 Structural Forces per area and their RMSDs as a function of the lateral distance to the pore center . . . 197
8.21 Forces between two nano-crystallites approaching each other at a speed of 2 m/s . . . 199
8.22 Forces between two nano-crystallites approaching, mobile vs frozen . . . 201
8.23 200 ps trajectory of the relative positions of the crystallites . . . 204
8.24 200 ps Trajectories of K^+ and Cl^- ions in the pore . . . 205
8.25 The trajectories of two water molecules in a pore with $d_p = 15.6$ Å . . . 206
8.26 Density profiles parallel to the interfaces . . . 207
8.27 Density profiles normal to the surfaces . . . 208
8.28 Pair distribution functions of ions in the pore . . . 210
8.29 Number of water molecules in the pore . . . 213
8.30 Non-equilibrium: force acting between moving crystallites . . . 221
8.31 Non-equilibrium: number of water molecules in the pore . . . 222
8.32 Non-equilibrium: relative K^+ and Cl^- densities . . . 225
8.33 Non-equilibrium: charge density above surface . . . 227
8.34 Non-equilibrium: The average charge density as a function of the distance to the surface . . . 228

Chapter 1

Introduction

Crystallisation of materials from solution is a technique used in a large number of applications, ranging from precipitation and purification of fine chemicals and pharmaceuticals to large scale industrial crystallisation of bulk chemicals.[Mersmann and Braun(2001)] The optimisation of this technique in terms of product quality, purity and yield, power-input and speed is therefore of considerable interest.

One phenomenon that can have a major influence on the outcome [Mersmann and Braun(2001)] of a crystallisation process is crystal agglomeration, i.e., the aggregation of smaller crystals followed by further crystal growth to form a composite larger crystal. The present thesis is part of a PhD program supported by an EPSRC* grant for a project entitled *micro-mechanics of agglomerative crystallisation processes*. It is aimed to contribute to an understanding of the fundamental mechanisms of crystal agglomeration on a molecular level.

To predict crystal aggregation and ultimately agglomeration we need a method for a sufficiently accurate estimation of the forces between crystalline particles in solution.

*The Engineering and Physical Sciences Research Council (EPSRC) is the UK Governments leading funding agency for research and training in engineering and the physical sciences.

So far theoretical approaches to predict the magnitude of forces between macro and meso scopic particles in solution have been confined to semi-empirical models with a limited predictive power. The most widely used of these models, the so called DLVO-theory,[Overbeek(1999)] is a mean field approximation that does not take into account specific intermolecular interactions and the detailed structure of surfaces and liquids. Nonetheless it remained the most accurate theory until not so long ago.

In the early eighties new experimental methods [Israelachvili(1991)] were developed allowing for the measurement of inter-particle forces in unprecedented detail and accuracy. New results obtained with these methods shed some doubt on the applicability of DLVO-theory and extended versions thereof in a number of cases. [Israelachvili and Mcguiggan(1988)] The inter particle force as a function of the particle particle distance was found to have a structure more complex than predicted by mean field theories. Triggered by these experimental results a substantial amount of theoretical work, aimed at revealing the origin and the nature of the involved inter particle forces, was done and published in the last decade. For a recent review see Ref. [Hansen and Lowen(2000)]. It was shown that these hitherto unpredicted forces are due to specific interactions between surfaces and particular solvent molecules, additives or impurities, the microscopic structure of the interstitial solution and spatial correlations between solvated ions. Predicting the influence of these factors quantitatively and from first principles *in silico* could contribute to an efficient control and optimisation of crystallisation processes and thereby reduce the amount of the required and usually costly experiments.

However, most of the theoretical work done so far is concerned with highly idealised model systems and not with realistic models of real materials. This is so because firstly such idealised systems can serve as good models to explain the essential physics that governs inter particle forces. The second, more profane, reason is the fact that most of the theoretical methods used are simply unable to give a realistic and reliable description of anything but the most simple materials because of fundamental shortcomings of the used methods. Science has comparatively reliable and accurate theories for the description

of events on both ends of the length and time-scales in our universe. We can predict the motion of planets and calculate the structure of a hydrogen molecule. Events that fall in between these extremes are generally harder to describe theoretically. A particular challenge are events taking place in disordered systems on the so-called meso-scale, with length and time scales of 10^{-9} - 10^{-3} meters and 10^{-6} - 10^{0} seconds respectively. This corresponds to the characteristic time and length scales found in the description of crystallisation and particle agglomeration.

The theoretical approach I concentrate on here, classical molecular simulation, i.e., Molecular Mechanics/Dynamics or Monte Carlo simulations, can normally only tackle smaller length and, in particular, time scales than those mentioned above. It is, however, a more accurate approach than mean field approximations. The main objective of the present work is to assess the usefulness and the limitations of molecular simulation for understanding and describing the aggregation of crystalline particles in solution. I concentrate thereby on some methodological issues which, while being undoubtedly of importance, have rarely been discussed in the literature so far. Before giving a short outlook on the following chapters two more notes appear to be indicated: Agglomeration and aggregation are, in principal, two different issues. However, as explained in some detail in Chapter 2, we can view aggregation as a necessary first step in the course of an agglomeration event and in the following only this first step will be considered. Therefore the two terms may be used interchangeably on some occasions in this work. Two other concepts that are also different in principle are the aggregation of particles in general and crystals in particular. Here I concentrate on the forces between crystals on close approach and on the structure of the interfaces and the interstitial solution on a microscopic scale. The surfaces of even perfectly spherical particles with a diameter exceeding a few nanometers, can be seen as flat to a good approximation if viewed at a molecular scale and at close distance. Therefore the terms particle and crystal aggregation are also used interchangeably on some occasions and some theoretical results from the literature actually obtained for spherical particles are used to help with the interpretation of features of crystal aggregation.

In Chapter 2 traditional and established theoretical and semi-empirical models for the description of crystallisation and aggregation are reviewed and confronted with more accurate approaches that have been proposed in recent years. A general overview over background of and common methodologies used in classical molecular simulation, and more details about some specific topics required in the following chapters is given in Chapter 3. One ingredient of classical molecular simulation that is of utmost importance for obtaining reliable results is the form and the parameterisation of the energy expression used to calculate intermolecular potentials and forces. As a consequence of the symmetry and the internal structure of the unit cell crystalline particles of a given material always can, and in most cases will, have more than one type of surfaces with a given, and often nearly constant, relative size of these surfaces. This results in a typical shape or morphology (habit). A specific type of molecular simulation is the well established attachment energy method for the prediction of those faces that are observed on grown crystals. In Chapter 4 this method is applied to the crystalline solid state of different organic materials and combined with a variety of different types of intermolecular model potentials. The results are compared to experimental data thereby scrutinising at the same time both our ability to predict crystal morphologies and the usefulness of various types of classical model potentials for the description of intermolecular interactions in the anisotropic interfacial environment.

Due to the large amount of experimental data available, a common theme drawing through the remainder of this thesis is the consideration of inorganic materials. In Chapter 5 a classical model potential for potash alum, a rather complex inorganic material, is devised and tested. Here a model potential of a comparatively simple form is used in order to retain sufficient computational efficiency, so that it can be used in large scale Molecular Dynamics simulations. Another important aspect of classical molecular simulation is the consistent calculation of electrostatic long range interactions. In Chapter 6 various methods to achieve this goal for quasi-two-dimensional systems, such as crystal solution interfaces, are compared in terms of accuracy and computational efficiency. The models devised and the methods described in Chapters 3, 5 and 6 are used in Chapter 7

where an attempt is made to predict the structure of the various surfaces found on potash alum crystals in contact with aqueous solution. This is a particular challenge since the largest of the potash alum faces is a polar surface, this fact rendering traditional methods for the prediction of its structure useless. The proposed structures are discussed in the light of the implications for crystal agglomeration. In Chapter 8 an attempt is made to directly calculate the forces between potassium chloride particles in aqueous solution. In contrast to previous attempts to calculate such forces here the solution including the water molecules is simulated explicitly on an atomic scale. The merits and limitations of proceeding thus are discussed. Finally in Chapter 9 a summary is given of all the work and the results presented in this thesis and promising directions for future work are suggested.

Chapter 2

Modelling Crystallisation and Agglomeration

Crystallisation is a complex process governed by a large number of different parameters, and including events on a broad range of different length and time scales. The latter point renders the theoretical modelling of crystallisation a particular challenge. For modelling the entire process over the whole time-scale one has to coarse grain the system considerably because modelling its microscopic details is computationally not feasible. Thereby we run the risk of over-looking the influence of micro-scale events such as, for example, the influence of specific impurities on crystal morphologies. On the other hand side, if we try to model these micro-scale events explicitly we can only consider a tiny section of the whole system and thereby overlook time- and spatial correlations between this tiny sample and the rest of the system. Notwithstanding these limitations useful theoretical models for crystallisation have been devised and applied. Most of the models used there are based on coarse grained macro-scale descriptions of the system. In Section 2.1 a short overview over these models will be given.

The current work is primarily concerned with one particular aspect of crystallisation, namely with agglomeration. Prediction of the extent of agglomeration via the above mentioned coarse grained models is not possible. Normally agglomeration is either neglected,

which is justifiable in some cases, or it is included by fitting (semi-)empirical models to experimental data.[Mersmann and Braun(2001)] In Section 2.2 ways to include information about particle interactions on a microscopic scale into models for agglomeration are discussed, and in Section 2.3 we review both established and recently developed ways to estimate these interactions via molecular simulation. Finally in Section 2.4 we will draw some conclusions from the literature review to provide a justification for the present work.

2.1 Population Balance Equations

The following account on the theoretical description of crystallisation is essentially a short summary of a chapter in the collection *Crystallization Technology* [Mersmann and Braun(2001)] edited by A. Mersmann which provides comprehensive treatise on theoretical as well as practical aspects of crystallisation.

In the realm of chemical engineering the theoretical description of crystallisation is achieved via a population balance equation (PBE), an integro-differential equation that gives the variation in time of $n(L)$, the number density of crystals as a function of a their respective size L

$$\frac{\partial n}{\partial t} + \frac{\partial (Gn)}{\partial L} + D(L) - B(L) + \sum_k \frac{\dot{V}_i n_i}{V} = 0 \tag{2.1}$$

where L can be the diameter of an approximately spherical particle or the side length of a cuboid crystal. The first term in Eqn. 2.1, the change in the number density with time, equals zero in a continuously driven steady state crystalliser. The second term $\partial Gn/\partial L$ describes the change of n in the size interval dL due to crystal growth rate, $G = dL/dt$, of particles growing into and out of dL. $D(L)$ and $B(L)$ are the death and birth-rate, respectively, arising from the agglomeration, breakage and attrition of crystals. The last term is the sum of all flows entering an leaving the crystalliser. Eqn. 2.1 is only one possible form of a population balance equation. Others, including more terms accounting, for example, for nucleation have been proposed.[Mersmann and Braun(2001)]

In laboratory scale experiments and for theoretical modelling frequently a continuous

reactor is used since a steady state equilibrium is mathematically easier to describe. It is possible to set up such a system so that barely any agglomeration or breakage occur. If, in addition, the solution in such a small scale crystalliser is well mixed so that no dissolution of crystals occurs and the growth rate is the same for all crystals Eqn. 2.1 can be simplified considerably to give

$$\frac{\partial(Gn)}{\partial L} + \sum_k \frac{\dot{V}_i n_i}{V} = 0 \tag{2.2}$$

If the solution fed into the crystalliser is free of crystals and only one volume flow $\dot{V}$ is removed we can simplify further

$$\frac{\partial(Gn)}{\partial L} + \frac{n}{\tau} = 0 \tag{2.3}$$

$\tau = V/\dot{V}_i$ is the mean residence time of the suspension in the crystalliser; here we assume that the solution and the crystals have the same residence time. We can simplify even further by taking the average growth rate G to be independent of the particle size, an assumption which is justified under certain conditions. Now we can write

$$G\ \frac{\partial(n)}{\partial L} + \frac{n}{\tau} = 0 \tag{2.4}$$

which is a simple ordinary differential equation with the solution

$$n = n_0 \exp\left(-\frac{L}{G\tau}\right). \tag{2.5}$$

If we draw a semi-logarithmic plot of the number density against the particle size a straight line results with the negative slope $-1/G\tau$. For a number of materials and conditions crystallisation can be described by Eqn. 2.5. In the majority of cases, however, the assumptions leading to (2.5) are not applicable and size dependent growth rates, agglomeration and attrition play a non-negligible role, leading to deviations from linearity in the experimentally determined $\log(n) - 1/G\tau$ plot. In these cases we have to reconsider Eqn. 2.1. Solution of this general equation is an arduous task, the main difficulty arising because both the birth and death-rates are functionals of the number density distribution

$$B = \mathcal{F}\{n(L)\} \sim \int f(n(L))dL, \qquad D = \mathcal{F}\{n(L)\} \sim \int f(n(L))dL \tag{2.6}$$

and so the very quantity we actually want to calculate is needed as input for the equation. Thus Eqn. 2.1 can only be solved numerically, in most cases with an iterative algorithm. Although this can be done in a reasonable amount of time with state of the art computers [Hounslow et al.(1988)Hounslow, Ryall, and Marshall] it is questionable in how far Eqn. 2.1 can be used for quantitative predictions because kinetic coefficients for nucleation, growth, attrition and agglomeration need to be specified as input. A considerable number of more or less heavily parameterised, semi-empirical relations have been devised to calculate these coefficients from material properties and process parameters [Mersmann et al.(2002)Mersmann, Braun, and Loffelmann]. In most practical work some of these parameters are determined by fitting them to reproduce experimental results,[Mersmann and Braun(2001)] leading to relations and parameters that are only applicable to specific materials and/or conditions.

Smoluchowski investigated agglomeration [von Smoluchowski(1917)] and published 1917 the simple relationship

$$\frac{\mathrm{d}n}{\mathrm{d}t} = -\beta \cdot n^2 \tag{2.7}$$

assuming agglomeration to be a second order process, with the speed of agglomeration being proportional to the square of the number concentration of the particles times a coefficient β, the agglomeration rate or kernel. In most of the theoretical work on agglomeration published since then Smoluchowski's relation is assumed to hold and attention is turned to β. If we allow for size dependent agglomeration and discretise L Eqn. 2.7 turns into a set of differential equations with $\beta = \beta(L)$. Although solving this set of equations is computationally demanding it poses no principal restrictions on the application of Eqn. 2.7. According to Braun et al. [Mersmann and Braun(2001)] more than hundred different kernels, both size dependent and size-independent versions, have been published so far. In the present work we will concentrate on the microscopic factors which determine this coefficient β.

2.2 Agglomeration Kernel and Efficiency

The agglomeration kernel depends on a number of different factors. Estimating the absolute and also the relative contributions of these factors — crystal size, energy dissipation in the reactor, surface properties of the crystal, etc. — has been a notoriously difficult task. Following Mersmann (page 261 in [Mersmann and Braun(2001)]) we divide β into three components

$$\beta = W_{\text{eff}} \beta_{\text{coll}} \beta_L^* \tag{2.8}$$

where β_{coll} is a function of the collision frequency determined by hydrodynamic conditions, β_L^* is a function of the crystal size L. β_{coll} will primarily depend on the type of solvent and on the energy dissipation, i.e., the geometry of the reactor and the agitation rate. In practice β_L^* is frequently taken to be unity. This assumption, being theoretically not justified, still holds surprisingly often, presumably due to an extensive cancellation of errors. For the determination of β_{coll} and β_L^* several more or less rigorous recipes have been proposed.[Mersmann and Braun(2001)] W_{eff} is an efficiency factor, the ratio of attempted to successful (in terms of aggregation) collisions. This factor is found in most common models for the agglomeration kernel, and represents the effect of inter-particle forces on agglomeration. Two equally charged particles, for example, can be expected to repel each other on approach, and thereby avoid aggregation, even if their trajectories would lead to a direct collision in the absence the Coulombic repulsion. These forces result in a low or zero value of W_{eff}.

We can view agglomeration, the factors that influence it, and so ways to describe it, from a slightly different perspective if we divide the process into several stages as sketched in Figure 2.1: The first stage (A) is the approach of two particles caused either by Brownian motion (perikinetic agglomeration) or by a velocity gradient in an agitated or stirred solution (orthokinetic agglomeration). If we neglect long range interactions between the particles, the description of this stage reduces to the problem of calculating collision frequencies between particles of a given size L at a given temperate T in a medium in a given viscosity η.[Mersmann and Braun(2001)] Stage B is to a large extent determined by inter-

Figure 2.1: **The stages of crystal agglomeration**; A: approach of two crystallites on a macroscopic length scale (collision rate dependent); B: for distances between several nanometers and contact the microscopic structure of the solvent and the concentration of the solute and/or impurities determine the effective interactions between the crystallites; C: after contact the accruement of a crystalline bridge between the particles depends primarily on the crystal growth rate and thereby on the super-saturation.

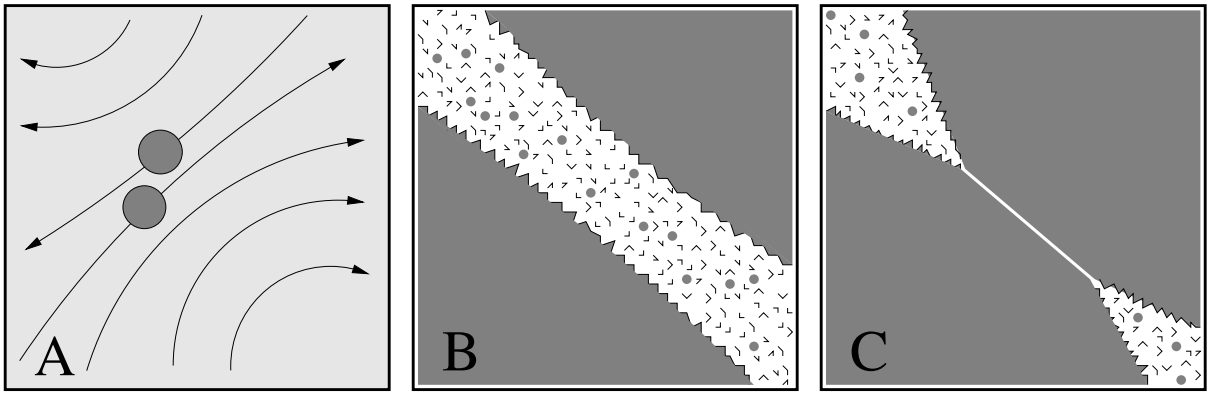

particle forces. Once two particles are closer than a few nanometers two effects come into play: Firstly, the direct electrostatic U_{el} and van der Waals interactions U_{VdW} between the particles become noticeable (i.e. $U = U_{\mathrm{el}} + U_{\mathrm{VdW}} > k_{\mathrm{B}}T$). Secondly the structure of the fluid between the particles is influenced and altered by the immediate vicinity of two surfaces. Specific interactions between the structured surface of the particles and solvent as well as solute molecules can cause a variety of different effects causing both attraction or repulsion, as will be shown in Chapter 8. The value of W_{eff} is to a large extent determined by what happens in stage B. Stage C encompasses phenomena whose occurrence is confined to crystal agglomeration (in contrast to aggregation of non-crystalline particles such as colloids or biological vesicles). Here a solid bridge has formed between the two particles and the agglomeration process is completed by further growth of this bridge.

Here we make the following assumptions: i) The effect of the conditions governing stage A (L, T, η, etc) on agglomeration is given by the parameters β_{coll} and β_L^*. These parameters can be calculated with reasonable accuracy using established relations.[Mersmann and Braun(2001)] ii) The importance of stage C will depend on the

super-saturation, the agglomerative bond growth rate and on the yield-strength of this bond. Normally it is not known whether the structure of the solid bridge formed between the two particles is crystalline or amorphous. Therefore the yield-strength cannot be estimated. However, for low up to medium energy input into the reactor (i.e. low stirring rates) we expect agglomeration to be practically irreversible after stage B, and in these cases we do not have to consider stage C. iii) In many cases stage B will have a pronounced effect on the agglomeration rate. If we can determine the forces in stage B with reasonable accuracy as a function of, e.g., the concentration and identity of additives we have a powerful tool for finding new means to control agglomeration "in silico", without having to to rely on lengthy and expensive experiments.

Both stage A and C will not be considered in this work where we want to concentrate on the efficiency parameter W_{eff} and its determination from first principles. The state of the art of determining W_{eff} is either fitting it to experimental data [Gardner et al.(1998)Gardner, Theis, and Young] or calculating it as a function of the interactions and forces between two particles. [Elimelech et al.(1985)Elimelech, Gregory, Jia, and Williams] For the latter strategy we need: 1) the average forces $F(r)$ between or the interaction energy $U(r)$ of two particles in the solution as a function of their distance r, 2) a relation to calculate W_{eff} from $F(r)$ or $U(r)$. Here we want stress that if the agglomerating particles are in any medium other than vacuum, the energy $U(r)$ must actually be a free energy or more precisely the potential of mean force between the two particles.

The first prototype of such a function, relating $F(r)$ to W_{eff}, was proposed by Fuchs in 1934 in the context of the coagulation of charged aerosols.[Fuchs(1934)] The author starts from a generalised version of Smoluchowskis equation (Eqn. 2.7) and considers the influence of the repulsive force between equally charged particles on their collision frequency. With χ being the probability of a collision between two charged particles, and

this probability for un-charged particles being one, Fuchs arrives at

$$\frac{1}{\chi} = W_{\text{eff}} = 2a \int_{2a}^{\infty} \frac{1}{r^2} \exp\left(\frac{\phi(r)}{k_{\text{B}}T}\right) \mathrm{d}r \tag{2.9}$$

In (2.9) a is the radius of the particles, T the temperature and $\phi(r)$ is the potential of the electrostatic force $\int_r^{\infty} F(r)\mathrm{d}r$. Later, in 1970, Spielman proposed a modification of Eqn. 2.9 by including the dependence of the relative diffusivity D_{12} of two particles 1 and 2 on their separation. With $D_{12}^{\infty} = \lim_{r\to\infty} D_{12} = \lim_{r\to\infty}(D_1 + D_2)$ he arrives at

$$\frac{1}{\chi} = W_{\text{eff}} = 2a \int_{2a}^{\infty} \frac{D_{12}^{\infty}}{D_{12}} \frac{1}{r^2} \exp\left(\frac{\phi(r)}{k_{\text{B}}T}\right) \mathrm{d}r \tag{2.10}$$

Both equations 2.9 and 2.10 have been applied to various systems such as polystyrene Latex suspensions [Han and Lee(2002)], protein adsorption onto silica surfaces [Docoslis et al.(2001)Docoslis, Wu, Giese, and Van oss] and zeolite growth [Nikolakis et al.(2000)Nikolakis, Kokkoli, Tirrell, Tsapatsis, and Vlachos]. Common to all this work is that the inter particle forces (see point 2 above) were calculated by some, possibly extended, version of the so-called DLVO-theory which is in fact a very crude way of assessing these forces. Both the DLVO-theory and other more accurate methods for calculating $F(r)$ are discussed in the next section.

A quite different ansatz for solving the same problem was made by Kallay et al.[Kallay and Zalac(2002)]. They assume that, at least for particles in the nanometer size range, the *transition state theory* can be applied to estimate the aggregation rate β. We write for the aggregation between two particles A and B

$$A + B \rightleftharpoons AB^{\ddagger} \rightarrow AB \tag{2.11}$$

$AB^{\ddagger}$ is the *activated complex*, i.e., the structure of the agglomerate on top of the activation energy barrier $\Delta^{\ddagger}G^{\circ}$, which in this case is the height of the free energy barrier between the separated and the attached (or agglomerated) particles. Using the formulation of Eyring as given, e.g., in Ref. [McQuarrie and Simon(1997)] we obtain an expression for the reaction rate or, in this case, the rate of agglomeration

$$\beta = \frac{k_{\text{B}}T}{hc^{\circ}} \exp\left(-\Delta^{\ddagger}G^{\circ}/RT\right) \tag{2.12}$$

If we calculate the force $F(r)$ between two particles $\Delta G(r)$ is, again, nothing else but the potential of mean force, i.e., $\int_r^\infty F(r)\mathrm{d}r$. This formalism is appealing because, in contrast to Eqns. 2.9 and 2.10, we directly arrive at an aggregation rate. However, to which extent this equation can be applied to crystal agglomeration in general is unclear. Kallay et al.,[Kallay and Zalac(2002)] in proposing this model used rather rough estimates for $\Delta G(r)$ in two highly idealised model systems. From their results it is not possible to draw a clear conclusion concerning the usefulness of the model. In any case, in both Equations 2.9 and 2.10, we need the average force or the potential of mean force between the particles as a function of their distance. This quantity will be the major issue of the present work.

2.3 Forces between Dispersed Particles

In the last 20 years a large amount of work, experimental as well as theoretical, has been devoted to the estimation of forces between meso-scopic particles in solution. To our knowledge none of the publications in this field deals explicitly with crystal agglomeration. There is, however, a large body of literature on the interactions between idealised surfaces, between colloidal particles in solution and on the general features of what is called electrostatic double layer (ESD) interactions. The bulk of this work is concerned with the interactions between charged particles or macro-ions in aqueous solution. We expect these results to be of particular relevance for the problem at hand because here we are concerned with the interactions between ionic nano-crystallites in ionic aqueous solutions. Most, if not all, crystals in an aqueous solution will be charged to some extent. Even surfaces as simple as, for example, the (100) faces of alkali halides have been shown to carry a net charge in solution.[**?**] For ionic crystals the anions and cations in the solution will in most cases have a different affinity to a given surface [Oyen and Hentschke(2002)] For polar surfaces, i.e., surfaces with a non-vanishing dipole moment perpendicular to that surface, we can expect this phenomenon to be even more pronounced. Many molecular crystals have surface groups that can undergo ionisation or dissociation. Both effects,

the preferred attachment of specific ions from solution and surface group ionisation will depend strongly on parameters such as the pH, the concentration of various ionic species, additives and impurities in the solution, etc. Rationalising the influence of each of these parameters can provide a means for effectively controlling agglomeration and ultimately the yield and quality of the crystalline product.

2.3.1 DLVO-Theory

The DLVO-theory,[Derjaguin and Landau(1941), Verwey and Overbeek(1948)] named so after the initials of its authors (Derjaguin, Landau, Verwey, Overbeek) is a theory of the stability of colloidal dispersions. Only recently the journal *Advances in Colloid and Interface Science* published a comprehensive discussion of the DLVO theory.[Overbeek(1999)] In spite of its simplicity this model for the forces between dispersed nano and microparticles can be used to describe at least qualitatively a wide range of systems. The effective force is calculated as a sum of two contributions: attractive van der Waals and repulsive electrostatic interactions.

For intermolecular forces, the van der Waals contribution will be discussed in some detail in Section 3.3. In the DLVO-theory the interactions between all the atoms in two macroscopic bodies are integrated over the volumes of the two bodies. For example, for two spheres with radii r_1 and r_2 at a separation D the van der Waals potential is given by

$$E_{VdW} = -\frac{A}{6D}\left(\frac{r_1 r_2}{r_1 + r_2}\right) \tag{2.13}$$

Expressions similar to (2.13) result for different pairs of ideal shapes (cylinders, semi-infinite surfaces, etc.; see Ref. [Mersmann and Braun(2001)], p. 252). The parameter A is the so-called Hamaker-constant.[Hamaker(1937)] If only dispersion is allowed for, A can be approximated by the London theory.[London(1930)] A more accurate calculation was proposed by Lifshitz [Lifshitz(1956)]. The Hamaker constant can also be determined empirically by directly measuring the force between two particles and in addition there are a few alternative theoretical approaches.[Ackler et al.(1996)Ackler, French, and Chiang] In

a recent article Thennadil et al.[Thennadil and Garcia-rubio(2001)] find a comparatively simple theoretical approach to give good agreement with another high level theoretical approach for polystyrene spheres in water. In a rather sobering article Ackler et al.[Ackler et al.(1996)Ackler, French, and Chiang] compare values of the Hamaker constant for a range of materials. They find that, depending on the material, these values can differ wildly (10-700%) between theoretical and experimental, as well as in between different theoretical, methods. However, the VdW forces are basically determined by material properties and therefore not easy to manipulate (which is what we want to do here). In addition for charged particles at small separations, the more important contribution is the electrostatic interaction.

The term electrostatic interactions in the context of the DLVO-theory refers solely to the forces caused by the overlap of two charge distributions of equal sign above charged surfaces or spheres in solution. These distributions and their interaction is calculated within the framework of the Poisson-Boltzmann equation for point charges in a dielectric continuum

$$\nabla^2\phi(r) = -\frac{1}{\epsilon_0\epsilon}\rho(r) \tag{2.14}$$

where $\phi(r)$ is the electrostatic potential and $\rho(r)$ is the average charge density at a distance r from a central ion. There is a number of ways for solving this equation for various boundary conditions.[Biesheuvel(2001)] A consequence of employing this mean field approximation for calculating the forces due to the electrostatic interactions is that these forces between two equally charged particles can only be repulsive over the whole range of possible separations. This appears to be plausible but is wrong in some cases. This and other short-comings of the DLVO-theory will be discussed in the next section.

2.3.2 The State of the Art

In addition to the electrostatic and the VdW contributions of the classic DLVO-theory some authors have included other forces due to hydration of the surfaces [Yotsumoto and Yoon(1993)] or to Lewis acid-base interactions between the

surfaces.[Van oss et al.(1999)Van oss, Docoslis, Wu, and Giese] It is unclear, however, to which extent shortcomings of the theory can be corrected for by simply adding additional terms. Many of the papers published in the last two decades that mention the DLVO-theory do so in a negative way, i.e., they present results that can not be explained with DLVO. Two specific kinds of experiment have contributed to discrediting the DLVO theory: Firstly it became possible in the early eighties to measure forces between curved surfaces with an un-precedented accuracy and resolution.[Israelachvili and Mcguiggan(1988)] The results obtained with the so-called *surface force apparatus* disagree with the DLVO predictions in many cases.[Israelachvili(1991)] Secondly the advent of more powerful computer hardware and algorithms made it possible to scrutinise the DLVO force predictions on a microscopic scale. The experimental results were confirmed and the molecular resolution of computer simulation studies made it possible to propose explanations for the disagreement with DLVO. These findings, however, were not un-disputed. A number of different mechanisms were proposed to explain the non-DLVO forces as they are now called. In a recent article on this matter Ninham complains about a "plethora of force".[Ninham(1999)] For a recent and comprehensive review of publications in this field see Ref. [Hansen and Lowen(2000)]. Here we will only look at the findings published in a few selected and recently published papers that are interesting in the context of the present work. In particular we will try to establish which simplifications included in the DLVO-theory and other methods must be dismissed for getting a sufficiently realistic model and reliable results for the forces between particles in solution.

One phenomenon not predicted by DLVO-theory that seems to be well established by now is the fact that like-charged particles in ionic solution can have attractive interactions in the presence of counter ions with a valency $\nu \geq 2$. This effect is caused by both entropic and energetic factors originating from ion-ion correlations in the vicinity of the charged surfaces. An example for this effect can be found in a paper by Wu et al.[Wu et al.(1999)Wu, Bratko, Blanch, and Prausnitz] who perform Monte Carlo simulations of macro-ions in a primitive model electrolyte (hard sphere micro-ions in solvent modelled as continuum with dielectric permittivity of water). They compare their results

with results obtained with DLVO and the Sogami-Ise theory (SI), another mean field theory, developed to overcome some of the limitations of DLVO. The authors find that with divalent counter-ions charged particles attract each other at a separation of roughly 1.2 micro-ion diameters while both SI and DLVO predict repulsion for all particle separations. In another paper [Wu et al.(2000)Wu, Bratko, Blanch, and Prausnitz] the same authors compare interaction forces between like-charged and oppositely charged macro-ions in a primitive model electrolyte. They find the repulsive and attractive forces obtained for like and oppositely charged macro-ions to be not symmetric which is also in qualitative disagreement with DLVO predictions.

Rouzina and Bloomfield [Rouzina and Bloomfield(1996)] define a dimensionless constant Γ

$$\Gamma = \frac{z^2 l_B}{a} \tag{2.15}$$

where a is the average separation of counter-ions in the solution layer next to the charged surface, z is the counter-ion valence and l_B is the Bjerrum length defined as $l_B = e^2/(4\pi\epsilon\epsilon_0 k_{\mathrm{B}} T)$, which is the separation between two unit charges (e) in a solvent of dielectric constant ϵ, where the electrostatic energy equals the thermal energy $k_{\mathrm{B}} T$. The authors find that this parameter can be used to predict whether the interactions between like charged particles in a solution is purely repulsive or whether they attract each other at a distance of about one ionic diameter. Later Wu and Prausnitz found [Wu and Prausnitz(2002)] that, once properly renormalised, the results of a number of other studies confirm the findings of Rouzina and Bloomfield. This result is appealing because it shows a relatively simple way to estimate the boundaries of the regime in parameter space where aggregation of like charged particles can be expected. The values of parameters needed to calculate Γ can be determined in a comparatively simple simulation of a single particle-solution interface. However, this result cannot be used for quantitative predictions.

Greberg and Kjellander [Greberg and Kjellander(1998)] investigated a similar system using a solution of the reference hyper-netted chain equa-

tion [Lado et al.(1983)Lado, Foiles, and Ashcroft] (RHNC) as simulation method. This method can in principle yield results equivalent to Monte Carlo simulations of simple anisotropic systems such as a primitive model electrolyte in a slit-pore with planar charged walls. In contrast to the model of Wu et al., as discussed above, they used counter and co-ions with different sizes. They find that under these conditions and with a particular size ratio between co- and counter-ions the charge distribution above a charged surface can undergo fluctuations (charge-inversion) with the consequence that equally charged macro-particles can also attract each other in the presence of mono-valent counter-ions.

Nearly all of the paper published so far in this field use the primitive model electrolyte to simulate the solution. Hence specific correlations between the solvent molecules (water in most cases) and the ions and surfaces are not accounted for because the solvent is modelled as a continuum solely characterised by its dielectric constant ϵ. Burak and Andelman [Burak and Andelman(2001)] proposed an extension of the Poisson Boltzmann equation (PBE, Eqn. 2.14) that includes the effect of ion-solvent correlations. They compare results for a primitive model electrolyte between two equally charged surfaces obtained with their method with results obtained with the the unmodified PBE. The authors conclude that solvent mediated forces, related to ion-solvent correlations are another mechanism that can induce inter-surface attraction. For some cases (mono-valent ions, small separation, large surface charge) these forces are the leading mechanism for surface attraction.

A more rigorous attempt to include ion-solvent correlations was proposed by Marčelja.[Marcelja(1997)] He extended the primitive model by using an effective potential for the ion-ion interactions. This effective potential is a sum of the bare Coulomb interactions, scaled by the dielectric constant as in the primitive model, and a short range oscillating contribution. The latter is obtained by separate MC or MD simulations of the bulk solution in which the potential of mean force between two ions is calculated. The short range contribution is this potential of mean force minus the Coulomb force. Marčelja finds that the implicit inclusion of the ion-solvent interactions via effective po-

tentials reveals new insights. The charge density profile above the surface is altered compared to the PBE description of the system and for 1:1 electrolytes the repulsion at short separations is noticeably increased. In a subsequent publication by Otto and Patey [Otto and Patey(2000)] Marčelja's findings were qualitatively confirmed but here the authors find that the measured inter-surface forces are very sensitive to the precise form of the effective potentials used and marked differences in the forces can be observed with effective potentials that differ by not more than their respective error-bars. Moreover both Marčelja and Otto and Patey state that reliable results can only be obtained by including effective surface-ion potentials in addition to the ion-ion potentials.

A more direct attempt to include the effect of ion-solvent correlations was made by Lee et al.[Lee et al.(2002)Lee, Chan, and Tang]. They perform Monte Carlo simulations of a solution between planar charged surfaces where the solution consists of ions, hard spheres interacting via a Coulomb term and uncharged hard spheres representing the solvent. They find increased repulsion between the surfaces independent of the valency of the ions. Apart from showing that inclusion of explicit ion-solvent interactions has some influence on the measured inter surface forces, this result is not very helpful because an uncharged hard sphere is a very poor model for water, the solvent present in most interesting "real world" systems.

Inclusion of both solvent-ion and ion-ion correlations in the solution between two isolated structure-less spherical macro-particles, both charged and un-charged was considered by Kinoshita et al.[Kinoshita et al.(1996)Kinoshita, Iba, and Harada] using the reference hyper-netted chain-theory.[Lado et al.(1983)Lado, Foiles, and Ashcroft] Both the ions and the solvent were modelled as hard spheres. However, the solvent particles were given a dipole as well as a quadrupole-moment thereby comprising a more realistic model for water. The authors [Kinoshita et al.(1996)Kinoshita, Iba, and Harada] find that the interactions between charged particles in solution are substantially influenced by the size of the counter-ions, with a trend opposite to that found with primitive model electrolytes. they also find that the presence of apolar particles in trace amounts leads to a considerable enhancement of the attractive interaction between neutral macro-particles. The

model Kinoshita et al. use appears to be quite realistic. However, in addition to other shortcomings of the Reference Hyper-netted Chain approach, macro-particles or surfaces with an explicit molecular structure cannot be easily included into this model.

To our knowledge there has been published only one attempt to simulate an ionic solution in a slit pore including an explicit water model (TIP4P-FQ [Rick(2001)]) so far. In particular for small surface surface separations Yang et al.[Yang et al.(2002)Yang, Yiacoumi, and Tsouris] find pronounced differences between their results and results obtained with a primitive model electrolyte. The ion distribution functions across the pore are different and the anions (Cl) show a markedly different surface adsorption behaviour than the cations (Na). Although it appears to be the most advanced study so far the method proposed by Yang et al.[Yang et al.(2002)Yang, Yiacoumi, and Tsouris] has still some shortcomings: The authors imposed the condition of over-all charge neutrality of the system which is not necessarily a valid assumption especially for small pore widths. More importantly a the ion densities in the pore as a function of the pore width are estimated by grand canonical ensemble simulations using, again, a primitive model electrolyte, before performing the simulations with the explicit solvent. The water density for a given pore width is approximated with an ad-hoc approach of dubious validity. The reason for this is simply that grand canonical ensemble (GCE) simulation (see Section 3) has to be used for estimating these densities and for now there seems to be no GCE algorithm that is powerful enough to cope with an aqueous ionic solution with an explicit water model at ambient conditions. This is also the very reason why up to now practically all the research done for electrolyte solutions in confined geometries has used the primitive model, or some modifications thereof, instead of more realistic descriptions of the solution. Since the presence of explicit water can apparently alter the ion density profiles and structure of the solution in a pore [Yang et al.(2002)Yang, Yiacoumi, and Tsouris] there is good reason to expect this also to apply for the over all densities of water as well as of the ions.

Figure 2.2: **Modelling crystallisation: the problem hierarchy**

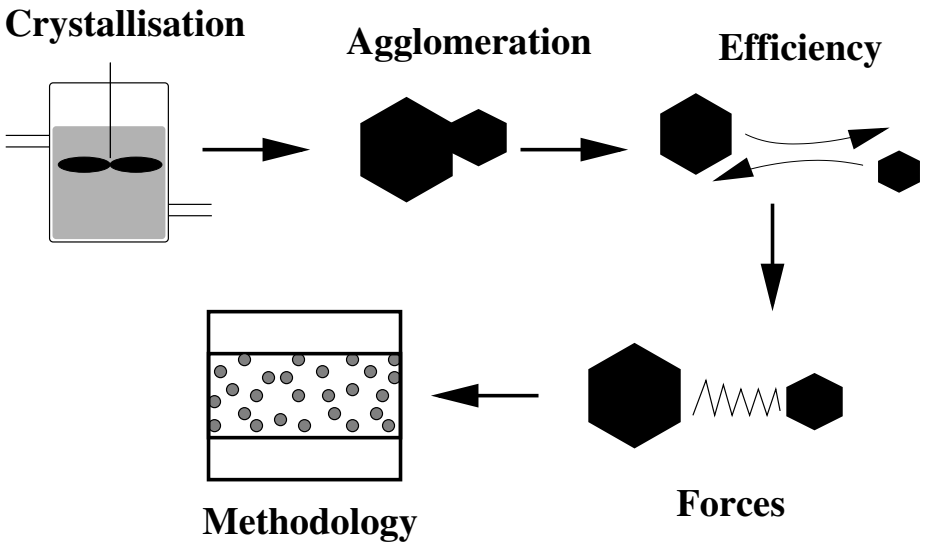

2.4 Conclusions

Starting from crystallisation we have gone all the way down to molecular simulation. We have seen that if we want to find a realistic model for crystallisation a hierarchy of problems ensues as shown in Figure 2.2. Apparently one root of the crystallisation problem tree is the inability of molecular simulation to make reliable predictions for the forces between meso-scale particles in solution. Thus, if we want to have a model for the interactions and forces between particles in solution that is able to make reliable quantitative predictions, we have to include realistic and explicit descriptions of ion-ion and ion-solvent interactions, as well as a model for the detailed structure of the surfaces. If we attempt to do this we face, as indicated above, formidable methodological problems. Thus most of the work described in this thesis has essentially been done to shed some light onto these problems and to test whether we can obtain any quantitative and reliable results for the forces between meso-scale particles in solution.

Chapter 3

Molecular Simulation

3.1 Introduction

Computer simulation of matter at the atomic scale has a history nearly as long as the computer itself. The first general purpose electronic computer, the *Electronic Numerical Integrator and Computer* or ENIAC, was developed during the second world war at the University of Pennsylvania. An improved version, the *mathematical and numerical integrator and computer* or MANIAC, was developed, by a team under Nicholas Metropolis, who was also to run the first scientific problem — complex calculations involving the hydrogen bomb design — on the ENIAC in 1945. The method he devised and used then, the *Metropolis Monte Carlo* algorithm [Metropolis et al.(1953)Metropolis, Rosenbluth, Rosenbluth, Teller, and Teller] (MC), is one of the three principal algorithms applied in most of the work in classical molecular simulation. The other two being *Molecular Mechanics* and its time dependent version *Molecular Dynamics*. Molecular Dynamics (MD), was first introduced in the late 1950's by Alder and Wainwright [Alder and Wainwright(1959)] who simulated the dynamic trajectories of a sample of hard spheres. Other milestones include the first dynamic simulation of a realistic liquid by Rahman in 1964 [Rahman(1964)] and the first simulation of water by Stillinger and Rahman in 1971 [Rahman and Stillinger(1971)]. By

now molecular simulation has become a standard method applied to a wide range of problems in physical, theoretical and bio-chemistry.

Molecular Mechanics/Dynamics and Monte Carlo simulations represent only one area of computer simulation of matter and are normally confined to samples containing between 10^2 and 10^9 atoms. For the simulation of macroscopic samples of liquids, at the price of less detail, we can use various methods from the realm of *computational fluid dynamics* (CFD) [Wesseling(2000)]. There are also methods that were developed to bridge the gap between micro- and macroscopic simulation (meso-scale simulations), such as *smooth particle applied mechanics* (SPAM) [Hoover and Hoover(2001)] or *dissipative particle dynamics* (DPD).[Hoogerbrugge and Koelman(1992)] On the other end of the (length and time) scale, i.e., for very small systems containing less than 10^3 atoms we can include quantum mechanical effects in our simulations to get an approximate solution of the Schrödinger equation and investigate the electronic structure of the material (*ab initio calculations*). Recipes used here [Jensen(1999)] include the self consistent iterative solution of the Hartree Fock equations (HF-SCF) and, although this is not a *true* ab-initio method, density functional theory (DFT). One entirely different approach for the calculation of the microscopic structure and statistical mechanics of simple fluids is based on numerical solutions of the Ornstein Zernike equation (Percus-Yevick, hyper-netted chain equations)[Hansen and McDonald(1996)] and extensions thereof for not so simple fluids [Lado et al.(1983)Lado, Foiles, and Ashcroft].

The methods used in this work are Molecular Dynamics and its "static" version Molecular Mechanics. We also perform a limited number of ab-initio calculations. The latter, however, are only used as auxiliary tool in the development of classical model potentials as discussed below. Therefore and because we used a well known standard program package [Frisch et al.(1998)Frisch, Trucks, Schlegel, Scuseria, Robb, Cheeseman, Zakrzewski, Montgomery, Jr.,
as a "black box" for this task we will discuss these methods only very briefly in Section 3.2. In Section 3.3 we try to give a short rationale of the physical basis of the terms used in the energy expression in classical molecular simulation followed by a discussion of the practical implementation of these terms in commonly used simulation software.

Given a means for calculating the potential energy of a molecular configuration and the resulting forces on the atoms/molecules one can proceed in two ways: i) search the configuration space of the considered sample to find the structures with the lowest energies (Molecular Mechanics, Section 3.4), ii) calculate the structure and/or the dynamics of the system at a finite temperature (Monte Carlo, Molecular Dynamics, Section 3.6.3 and 3.5). Due to the vast amount of knowledge accumulated in the last 50 years in this field this account cannot be more than a very short overview. For a more comprehensive description of these methodologies we refer to the textbooks by Allen and Tildesley [Allen and Tildesley(1987)] and by Frenkel and Smit.[Frenkel and Smit(2001)]

3.2 Ab-Initio Methods

One approach to the determination of intermolecular potentials and forces between two molecules is the calculation of the electronic density of the molecular complex ab initio. Thereby the time independent Schroedinger equation is solved numerically – and approximately – for the system of interest. Various methods are available for this purpose. Unless an explicit reference is given most of the information given in this section was taken from the book *Computational chemistry* by Frank Jensen.[Jensen(1999)]

Within a molecule the masses of the nuclei are much greater than the electronic masses, hence the electrons can respond almost instantaneously to any change in the nuclear positions. Thus we can think of the electrons as moving in an external field of fixed nuclei. Within this, so-called, Born-Oppenheimer approximation the nuclear kinetic energy term can be neglected and the nuclear-nuclear repulsion term can be considered a constant. These two terms can therefore be removed from the Hamiltonian in the time independent Schrödinger equation. What remains is termed the electronic Schrödinger equation

$$\hat{H}\Psi(\vec{r};\vec{R}) = E\Psi(\vec{r};\vec{R}) \tag{3.1}$$

with $\vec{r}$ and $\vec{R}$ being the electronic and nuclear coordinates respectively. The notation implies that the electronic wave-function depends on the nuclear positions only paramet-

rically – a different wave-function is defined for each nuclear configuration. Usually the wave function of the system is represented by a finite sum of some analytic basis functions. Normally Gaussians are used for this purpose nowadays for reasons of computational efficiency. The actual set of such functions used for the calculations is called the basis set. The total electronic wave-function must be anti-symmetric with respect to the exchange of two electron coordinates. This can be achieved by building it from *Slater Determinants* — the sum of all possible permutations of the basis functions used. Minimisation of the energy of the system leads to a set of so-called Hartree-Fock equations which can be solved iteratively resulting in the self consistent field (SCF) orbitals (HF-SCF-method). Repeating the calculation with different nuclear arrangements allows the potential energy surface to be mapped out and the equilibrium geometries to be found.

With this most basic way to calculate ab initio energies one electron can not "see" all the other electrons but rather a smeared out average charge-distribution, i.e., The model does not take electron-electron correlation into account. There is a number of approximate methods available to correct for this deficiency. For a review on such advanced methods including density functional theory (DFT) see for example Refs. [Jensen(1999), Levine(1991)].

If one performs ab-initio calculations for the purpose of calculating intermolecular interactions and/or parameterising/validating classical forcefields not only the energy of the whole system E_{ab} has got to be determined but also the energies of the two isolated molecules a and b because the quantity of interest in this case is the intermolecular interaction energy or the energy difference

$$\Delta E = E_{ab} - E_a - E_b \tag{3.2}$$

The method is called the *super-molecular approach* and its main drawback can be seen immediately when considering the magnitude of the terms in (3.2). ΔE is normally smaller than 20 kJ/mol whereas the terms E_{ab} and $E_a + E_b$ – even for the smallest molecules – usually exceed 10^6 kJ/mol. The problem even worsens due to the so called *basis set superposition* error (BSSE). This additional error is caused by the fact that for calculations

involving the dimer the electrons of both molecules have available not only the orbitals on their own nuclei, but also the orbitals on the nuclei of the other molecule. This is not the case for the calculations for the two monomers. Consequently the dimer basis set is larger than that of each monomer resulting in an artificial lowering of the dimer energy relative to the energies of the two monomers. There are methods to correct – to a certain extent – for the BSSE, the most frequently used being probably a procedure called *counterpoise correction* [van Duijneveldt et al.(1994)van Duijneveldt, van Duijneveldt-van Derijdt, and van Lenthe]. An example for the consequences of such a correction is given by Tzeli et al. for the acetylene-water system [Tzeli et al.(2000)Tzeli, Mavridis, and Xantheas]. They found that inclusion of BSSE corrections alters the equilibrium geometry of the global minimum and the features of the potential energy surface around it on a qualitative scale.

Until not long ago it was not possible to calculate E_{ab} with an error smaller than the interaction energy ΔE itself with reasonable computational effort. Since then methods and computer speed improved considerably. To summarise, however, one can say that in order to accurately calculate non-covalent molecular interaction energies by ab initio methods quite extensive basis sets and elaborate correction schemes have to be employed. Methods that take a good part of the electron correlation into account are still extremely inefficient in terms of the involved computational effort ($\propto N^5$ or worse). Density functional theory is considerably more efficient in accounting for electron correlation but performs poorly when estimating the contribution of dispersion (see 3.3.1) to the energies and forces.[van Mourik and Gdanitz(2002)] Therefore it is desirable to have alternative ways for the calculation of intermolecular potentials and forces especially for medium-sized or large systems.

3.3 Classical Model Potentials

The basic assumption that enables us to simulate materials at the atomic scale with systems containing up to 10^6 molecules over time intervals of up to one micro second is the *classical approximation*. This has turned out to be a reasonable approximation for all but

the smallest atoms/molecules such as neon or hydrogen, provided we can exclude and are not interested in any changes of the bonding topology or the oxidation states of the involved molecules. The molecules are treated as classical objects, i.e., they are localised and have well defined position and momentum at any given point in time. Atoms or molecules are modeled as hard spheres (*billiard balls*) or soft spheres that interact via potentials derived (semi)empirically [Williams(2001)] or from perturbation theory.[Stone(1985)] These model potentials are normally comparatively simple parameterised functions of the particle coordinates. A set of such functions and parameters, a so-called *force field*, provides the full energy expression for a given system. In the following we first present the physical background of the various terms in classical model potentials as derived with intermolecular perturbation theory. In a second part we discuss the practical implementation of model potentials and various simplifications and approximations made there.

3.3.1 Perturbation Theory

Instead of calculating the total energy of a dimer and subtracting the monomer energies, as done in the super-molecular approach, one can go for a direct calculation of the interactions, i.e., the energy difference by a perturbation approach. The individual contributions to the interaction potential can be calculated with a much smaller computational effort and can – as an additional benefit – provide insight into the origin of the contributions to the potential. Perturbation Theory is the most rigorous approach for the derivation of classical model potentials

The total intermolecular energy U_{tot} can be partitioned into different contributions each of which in turn can be attributed to distinctive physical principles. The most common way of doing this decomposition is given by

$$U_{tot} = U_{er} + U_{el} + U_{ind} + U_{disp} \tag{3.3}$$

The main contribution at short distances is due to the exchange-repulsion energy U_{er} caused by electron exchange and charge overlap effects. The electrostatic energy U_{el} represents the Coulomb interaction between the unperturbed charge distributions of the

molecules. The induction (or polarisation) term U_{ind} arises due to the modification of the charge density of one molecule caused by the permanent multipole moments of the other. Finally there is the dispersion energy term U_{disp}, which is the only kind of attractive interaction between uncharged and non-polar molecules. It can be attributed to the interaction of the instantaneous fluctuations in the charge densities. The theoretical basis of this decomposition is briefly sketched in the following paragraphs.

The simplest way to derive an expression for each of the terms in (3.3) is to employ the Rayleigh-Schrödinger perturbation method.[Buckingham(1967)] A short description of this method follows. For a more elaborate derivation the reader is referred to [Jeziorski et al.(1994)Jeziorski, Moszynski, and Szalewicz] and references therein.

The eigenvalue problem for the electronic Hamiltonian $\hat{H}$ of the dimer AB can be written as

$$\left(\hat{H}_0 + \zeta\hat{V}\right)\Psi_{AB} = E_{AB}\Psi_{AB} \tag{3.4}$$

where the unperturbed operator $\hat{H}_0 = \hat{H}_A + \hat{H}_B$ is the sum of the electronic monomer Hamiltonians $\hat{H}_A$ and $\hat{H}_B$. The perturbation operator $\hat{V}$, defined as the difference between $\hat{H}_0$ and the total Hamiltonian $\hat{H}$, collects the interactions between the electrons of each monomer with the other monomer respectively. The parameter ζ with $0 \leq \zeta \leq 1$ defines the order of the perturbation expansion. For $\zeta = 0$ the system is represented as the sum of the two unperturbed molecules, i. e., $E_{AB}(\zeta = 0) = E_A + E_B \equiv E_0$ and $\Psi_{AB}(\zeta = 0) = \Psi_A + \Psi_B \equiv \Psi_0$. This situation can be regarded as the zeroth order approximation which is valid only for infinite separation of the involved particles. For $\zeta = 1$ the perturbation is fully turned on and $E_{AB}(\zeta = 1)$ and $\Psi_{AB}(\zeta = 1)$ become the exact energy and wave function respectively of the interacting dimer.

The interaction energy $E_{int} = E_{AB} - E_0$ and the wave-function Ψ_{AB} can be expanded as power series in ζ

$$E_{int}(\zeta) = \sum_{n=0}^{\infty} \zeta^n E^{(n)} \tag{3.5}$$

$$\Psi_{AB}(\zeta) = \sum_{n=0}^{\infty} \zeta^n \Psi^{(n)} \tag{3.6}$$

Whether (3.5) and (3.6) converge for $\zeta \to 1$ depends on the system considered. When introducing the normalisation condition

$$\langle \Psi_0 | \Psi_{AB}(\zeta) \rangle = 1 \tag{3.7}$$

the expression for the interaction energy takes the form

$$E_{int}(\zeta) = \langle \Psi_0 | \zeta \hat{V} | \Psi_{AB}(\zeta) \rangle \tag{3.8}$$

Hence $E^{(n)}$ – the *polarisation energy* of nth order – is given by

$$E^{(n)} = \langle \Psi_0 | \hat{V} | \Psi^{(n-1)} \rangle \tag{3.9}$$

The terms $E^{(n)}$ in (3.5) up to $n = 3$ can be given a physical interpretation and they can be rigorously related to monomer properties, which considerably facilitates their estimation and practical evaluation. However, when two molecules approach each other and overlap between the two charge-distributions occurs the formalism breaks down and one has to go back to a semi-empirical description of the interactions. The decomposition in (3.3) includes essentially all terms $E^{(n)}$ up to second order in E_{int} that give important contributions for most molecular compounds. In the following paragraphs expressions for each of these terms and ways for their practical calculation will be given.

Electrostatic For the interactions of molecular species carrying permanent multipole moments the electrostatic energy is the first order term and usually the most important contribution to E_{int}. It is strictly pairwise additive and given by

$$U_{el} = \langle \Psi_A \Psi_B | \hat{V} | \Psi_A \Psi_B \rangle \tag{3.10}$$

It can be expressed in terms of the total charge distribution ρ_A and ρ_B of the monomers.

$$U_{el} = \int \cdots \int \frac{\rho_A(\mathbf{r}_1)\rho_B(\mathbf{r}_2)}{r_{12}} \mathrm{d}\mathbf{r}_1^3 \mathrm{d}\mathbf{r}_2^3 \tag{3.11}$$

For practical calculations this expression is not very helpful. It can be replaced by a function of R, the vector between the centres of the two molecules and Ω, a set of angles

describing the relative orientation of the vector R and the molecule fixed axes.

$$U_{el} = \sum_{l_1 l_2} \sum_{k_1 k_2} \binom{l_1 + l_2}{l_1} Q^A_{l_1,k_1} Q^B_{l_2,k_2} \bar{S}^{k_1,k_2}_{l_1,l_2,l_1+l_2}(\Omega) R^{-l_1-l_2-1} \tag{3.12}$$

where the Q_{lk} are the permanent multipole moments of the isolated molecules and the so called *normalised $\bar{S}$ functions*, $\bar{S}^{k_1,k_2}_{l_1,l_2,l_1+l_2}$, are expansion functions for the orientational dependence of $U(R,\Omega)$.[Stone(1996)]

As opposed to most empirical potentials that model the electrostatic interactions merely by partial charges, i. e. mono-poles situated at atomic centres, this kind of model potential can represent anisotropic features of the charge distribution around a molecule quite well. In principle molecules of arbitrary shape can be modelled. However, for molecules with a shape far from spherical the convergence of (3.12) is quite poor. For such cases *distributed multipole analysis*[Stone(1985)] (DMA) can yield a better representation than central multipoles, as used in (3.12). Here multipoles can be assigned to arbitrarily chosen sites within a molecule, usually a site on every atom. Thus geometric features like d-orbitals or π-electron clouds within aromatic compounds can be modeled in an intuitive way.

The calculation of the distributed multipoles for a given molecule is accomplished analysing the monomer charge densities which is a relatively cheap ab-initio calculation. Use of DMA in the context of dynamic simulations is still in an early stage, and the computational effort involved is between one and two orders of magnitude greater than for traditional point-charge models. Considering, however, that the speed of computer hardware typically increases by one order of magnitude in approximately six years the application of DMA in the context of MD or MC can be assumed to become feasable in the near future, even for relatively large systems containing in excess of thousand atoms. This is definitely enough to model dynamically the solid state of most small up to medium sized organic molecules, in order to predict crystal structures and possible polymorphs from first principles, including temperature effects. This is a field of research where accurate model potentials such as those discussed here have already been applied very succesfully.[Beyer et al.(2001)Beyer, Lewis, and Price]

Induction This is a second order term arising from the perturbations of the charge density of molecule A due to static electric field generated by the unperturbed monomer B and vice versa. It is given by

$$U_{ind}^{A} = -\sum_{n_A \neq 0} \frac{| < \Psi_A^0 \Psi_B^0 | \hat{V} | \Psi_A^n \Psi_B^0 > |^2}{E_N^A - E_0^A} \tag{3.13}$$

with an equivalent term for U_{ind}^{B}.

By applying a multipole expansion, the interaction energy of A can be expressed in terms of the permanent multipole moments of B and the polarisabilities of A, plus the orientation dependent functions. Thus it is possible — similar as for the electrostatic energy — to derive analytic functions starting from (3.13) to describe the induction interaction quantitatively[Celebi et al.(2000)Celebi, Angyan, Dehez, Millot, and Chipot] in terms of properties of the two isolated molecules. However, ab-initio calculations of polarisabilities are very demanding, let alone the necessity to allow for the movement of charges within the molecule. There are methods that try to mimic a kind of induction effect by allowing for polarisabilities of the molecules, the simplest of which being the so called shell model[Dick and Overhauser(1958)]. It is, however, unclear to which extent artifacts can be introduced into the model by proceeding thus.

For the interaction energy of ions the dispersion term changes as R^{-4} and hence gives a non-negligible contribution. For (di)polar molecules the leading induction term goes as R^{-6} and will usually be very small. When dealing with non-ionic materials it is thus common practice to neglect anisotropy and to absorb it empirically into the dispersion term by fitting to a spherical potential $\propto R^{-6}$.

Dispersion The dispersion interaction is the only attractive component between uncharged spherically symmetric molecules (i. e. neutral atoms).

$$U_{disp} = -\sum_{n^A \neq 0, n^B \neq 0} \frac{| < \Psi_A^0 \Psi_B^0 | \hat{V} | \Psi_A^n \Psi_B^n > |}{E_n^A - E_0^A + E_n^B - E_0^B} \tag{3.14}$$

By the very definition the dispersion interaction represents a pure intermolecular correlation effect. It may be viewed as the stabilising energetic effect of the correlations of

instantaneous multipole moments of the monomers. Application of a central multipole expansion results in

$$U_{disp} = - \sum_{n=6,8,10,...} \frac{C_N}{R^n} \tag{3.15}$$

Basically there is a way to calculate the coefficients C_N from monomer properties[Jeziorski et al.(1994)Jeziorski, Moszynski, and Szalewicz], however, usually one employs more approximate methods for their estimation or fits them to experimental data.

Short-Range When two molecules approach each other their respective charge distributions will overlap. On the one hand side attraction will result since the electrons can exchange between the molecules and thus move over an extended space — a sort of quantum mechanical entropic effect. On the other hand side this attraction is dominated by an exponentially increasing repulsion due to the Pauli exclusion principle. Both effects are usually taken together and modelled by an exponential term in the intermolecular potential. When the charge distribution around molecules is anisotropic this applies naturally to the repulsion as well. The description of repulsion interactions by anisotropic potentials which are assumed to be proportional to an exponential function of the charge overlap, has been accomplished[Hermida-ramon et al.(1998)Hermida-ramon, Engkvist, and Karlstrom, Nobeli et al.(1998)Nobeli, Price, and Wheatley]. Such models, however, have only been applied to a few simple molecular species so far and more work needs to be done to establish their applicability.

3.3.2 Model Potentials in Practice

One can calculate intermolecular potentials and forces with perturbation theoretical methods up to an accuracy better than one percent [Jeziorski et al.(1994)Jeziorski, Moszynski, and Szalewicz] and ways have been found to include the induction and repulsion in a non-empirical fash-

ion [Hayes and Stone(1984), Stone(1993)]. However, in practice and in most cases one settles for a compromise when dealing with medium sized or large molecules since the computational effort involved in a complete perturbation theoretical treatment becomes formidable for such systems.

There are a few features common to most classical model potentials: They are atom-atom potentials. Thereby the individual molecules are represented by an assembly of so called interaction-sites. Frequently — but not necessarily — the positions of these sites coincide with the positions of the atoms in the molecule. There are force fields that define additional interaction sites at, e. g., the position of a chemical bond or a lone electron pair. Each interaction site has certain properties quantified by a set of parameters. These parameters determine the interaction energy and force (and possibly torques) between two such sites as a function of their separation and, for anisotropic potentials, also their orientation. The interaction between two molecules is assumed to be the sum of the interactions of all possible pairs of sites. The actual total configurational energy U_{tot} of an ensemble of interacting molecules is given by

$$U_{tot} = \sum_{i<j} u_{ij} + \sum_{i<j<k} u_{ijk} + \sum_{i<j<k<l} u_{ijkl} + \cdots \tag{3.16}$$

Here u_{ij} are pair, u_{ijk} three-body-potentials, etc. Such *more-body* potentials take account for the fact that the interaction energy of two molecules is modified in the presence of a third, fourth, etc molecule. The main contribution to the non-additive part of the energy is due to the three-body interaction. Terms of higher order are usually negligibly small and, additionally, tend to cancel out each other. Calculations of three-body interactions are typically limited to those based on the triple-dipole dispersion term of Axilrod and Teller.[Axilrod and Teller(1943)] Such calculations commonly contribute 5-10% to the pairwise additive energy of the liquid phase. For water trimers Groenenboom et al.[Groenenboom et al.(2000)Groenenboom, Mas, Bukowski, Szalewicz, Wormer, and Van der avoird] find three-body interactions to contribute about 15% of the trimer binding energy at the hydrogen bonded equilibrium geometry and 30% or more to the hydrogen bond rearrangement barriers. In this case the dominant three-body interactions are the second-

and third-order polarisation effects. Since the calculation of three-body interactions is a computationally expensive task — the effort for the calculation of the three-body contribution in (3.16) goes with N the number of particles as N^3 — it is commonly assumed that the outcome of molecular interactions can be adequately attributed to the effect of *effective* two-body interactions alone. In practice one uses force field parameters for the pair interactions that have been fitted to reproduce experimental bulk properties of a material. As a consequence such empirical pair potentials partially absorb the three (and higher) body terms implicitly.

Another common feature of classical force fields, partially inspired by perturbation theory, partially by practical considerations, is the partitioning of the energy expression into in a sum of Van der Waals, electrostatic and intramolecular interactions

$$U = U_{VdW}(\{\mathbf{r}^N\}) + U_{el}(\{\mathbf{r}^N\}) + U_{intra}(\{\mathbf{r}^N\}) \tag{3.17}$$

as functions of the coordinates $\{\mathbf{r}^N\}$ of all atoms or interaction sites.

Van der Waals Interactions Van der Waals der Waals forces include the repulsion due to overlap and three different types of attractive contributions: [Atkins(1988)] the Keesom, Debeye, and London forces. The Keesom forces are the attractive forces between permanent dipole molecules, averaged over all possible mutual orientations of the molecules. The Debeye forces are the attractive forces between a permanent dipole molecule and an induced dipole molecule. An induced dipole molecule is a non-polar molecule which was made (induced) to become a dipole molecule by the electrostatic field emitted by another dipole molecule. London forces are attractive forces between two non-polar molecules caused by spontaneous fluctuations of the charge distribution around a molecule resulting in fluctuating net dipole moments. All these energy contributions vary as the sixth inverse power of the distance between two molecules. The Keesom forces are implicitly taken into account if we provide the simulated molecules with explicit point dipole moments or approximate such a dipole moment by partial charges on the different interaction sites in a molecule. The Debeye forces are true many-body interactions. Their calculation is

cumbersome but in many cases they can be neglected or included in the form of an effective dispersion term. If this is not the case one has to use methods to account explicitly for polarisability of molecules as described further below. In most cases the dispersion represents the main contribution to the attractive VdW interactions.

The simplest model for the van der Waals interactions between atoms is the hard sphere model [Alder and Wainwright(1959)] where atoms are characterised solely by the diameter d of this sphere, with the interaction potential

$$U(r_{ij}) = \begin{cases} \infty & r_{ij} \leq d \\ 0 & r_{ij} > d \end{cases} \tag{3.18}$$

where r_{ij} is the distance between two spheres i and j. d can, for example, be derived from the second Virial gas coefficient. Despite its simplicity this model can provide some insights into the structure and dynamics of simple liquids.[Hansen and McDonald(1996)]. Interestingly enough the hard-sphere potential results in an effective attraction in dense fluids for atoms that are close enough. This phenomenon is solely due to steric effects: two neighbouring atoms experience collisions from other atoms in the medium primarily in the direction towards each other because no other atoms are left in the space between them and hence collisions that would push them in the opposite direction cannot take place.

The first step towards a more realistic description of the interactions between atoms is to replace the hard by a soft sphere. The most accurate choice for this interaction would be an anisotropic exponential function. In most cases however and mostly for numerical convenience the repulsion is described by an isotropic inverse power law, U $\propto r_{ij}^{-n}$ with $9 < n < 16$. This soft repulsion can be complemented by a term accounting for the attraction due to dispersion forces varying as r_{ij}^{-6} giving, for example, the frequently used Lennard Jones potential

$$U_{\mathrm{LJ}}(r_{ij}) \;=\; 4\,\epsilon\,\left\{\left(\frac{\sigma_{ij}}{r_{ij}}\right)^{12} - \left(\frac{\sigma_{ij}}{r_{ij}}\right)^{6}\right\} \;=\; A\,r_{ij}^{-12} - B\,r_{ij}^{-6} \tag{3.19}$$

A generalisation of the Lennard Jones potential for anisotropic interactions between non-

spherical molecules is the Gay-Berne potential.[Gay and Berne(1981)] If an exponential term for the repulsion is used instead of the polynomial term the so-called Buckingham potential is obtained.

$$U_{\mathrm{Buck}}(r_{ij}) = A_{ij}\exp(-r_{ij}/\rho_{ij}) - C_{ij}r_{ij}^{-6} \tag{3.20}$$

The parameters in Eqs. 3.19 and 3.20 are usually determined by fitting them to reproduce experimental data such as crystal structures, lattice energies or elastic constants.[Williams(1966)] In order to avoid extensive calculations and experiments and to retain a certain degree of generality non-bonded parameters, e. g., σ and ϵ are usually taken to be site-properties, i. e., for the interaction of two different sites (atom-types) mixing rules like those given in (3.21) are used to generate the according parameters in a rather ad hoc fashion.

$$\sigma_{ij} = \frac{1}{2}\big(\sigma_i + \sigma_j\big), \qquad \epsilon_{ij} = \sqrt{\epsilon_i\ \epsilon_j} \tag{3.21}$$

Although these equations are very simple they can successfully model a number of physical properties of gases, liquids [Verlet(1967)] and solids [Williams(1966), Williams(2001)], and one of the two expressions 3.19 or 3.20 is used to describe the van der Waals interactions in most of the commonly used force fields.[Brooks et al.(1983)Brooks, Bruccoleri, Olafson, States, Swaminathan, and Karplus, Scott et al.(1999)Scott, Hunenberger, Tironi, Mark, Billeter, Fennen, Torda, Huber, Kruger, and Van gun Halgren(1999)]

Electrostatic Interactions The electrostatic contribution to the intermolecular interactions is the most important in a wide range of interesting systems. Molecules with sufficiently stiff bonds, bond and torsional angles can be seen as rigid bodies to a good approximation. In such a case the electrostatic interactions can by described rigorously by a sum of pairwise interactions between electrostatic multipoles on each interaction site.[Stone(1985)] A distributed multipole analysis is performed calculating partial charges and higher multipoles for a number of interaction sites in the molecule. In this analysis the electrostatic potential arising from the charge overlap of two basis functions is written

in terms of a multipole expansion around a point between the two nuclei. These moments are calculated directly from the density matrix and the basis functions. The highest non-vanishing term is the sum of the angular momenta for the two basis functions. Thus the electrostatic potential outside the charge-distribution can be described exactly — within the limitations given by the ab-initio method used and the quality of the basis set — by a few terms of this series, provided that distributed multipoles are assigned for each pair of basis functions. This, however, would mean that $\approx M^2$ different sites (M being the size of the basis set) would be required. In practice only the nuclei and possibly the midpoints of the bonds are selected as multipole points and all the pair expansion points are moved to the nearest multipole point. This series converges rapidly, provided the distance moved is not too great. For a consistent treatment the multipole series should be truncated at a given power $n = l_1 + l_2 + 1$ of the inter-site distance r, l_1 and l_2 being the angular momenta for the two basis functions, and not at a given multipole. Therefore a DMA up to hexadeca-pole is required to include quadrupole-quadrupole interaction energies and all other terms for $n \leq 5$ which can be expected to reproduce the electrostatic interactions for molecules with mainly s and p orbitals, i. e., the majority of organic compounds, reasonably well. This method of calculating electrostatic forces has been successfully applied [Price(2000)] in modeling (primarily organic) molecular materials.

Due to the relatively high computational cost involved in the calculation of interactions between dipoles and higher multipoles, other, simpler models for the electrostatic interactions are applied in most classical model potentials. These simpler models generally terminate the series expansion of the electrostatic interactions after the first term, i.e., they allow only for monopole-monopole interactions between each pair of interaction sites.

$$U_{\mathrm{Coul}}(r_{ij}) = \frac{q_i q_j}{4\pi\epsilon_0 r_{ij}} \tag{3.22}$$

Theoretically one could position an arbitrary amount of such monopoles, represented by *partial charges* q_i, at different sites within a molecule, and, by choosing appropriate values for the q_i, obtain a representation of the charge density around the molecule, and

thereby the intermolecular interactions, to any desired accuracy. The common approach, however, is to allow only for as many partial charges, i.e, electrostatic interaction sites, q_i in a molecule as there are atoms. For all but the simplest molecules the resulting number of monopoles is too small to give an accurate description of the electrostatic interactions even at long range. Nevertheless the limited degree of anisotropy introduced by this model provides reasonable accuracy for many materials and due to the computational cost of more accurate methods it is still the only possible choice in some cases.

The generation of partial charges for the electrostatic interaction sites calculated with this model is no straightforward task. The partial charge model is artificial and consequently there is no single "correct" method for the charge derivation. A rather simple and computationally cheap method is the assignment of charges to atoms according to their relative electro-negativity in an iterative process.[Gasteiger and Marsili(1980)] An approvement of such relatively crude approximations can be achieved by inclusion of additional constraints such as the reproduction of dipole-moments.[No et al.(1990)No, Grant, and Scheraga] In the most direct approach partial charges are derived from optimising the fit between the classical Coulomb model for the electrostatic potential and the quantum mechanical molecular electrostatic potential evaluated at many points around the molecule (so called ESPD-charges).[Maple et al.(1994)Maple, Hwang, Stockfisch, Dinur, Waldman, Ewig, and Hagler] While being quite demanding in terms of the computational effort these methods can yield quite wrong results for the electrostatic potential in certain regions of space just outside the molecular surface.[Jensen(1999)] Mulliken Population analysis[Mulliken(1955)] and similar methods[owdin(1970)] provide a way for partitioning the wave function of a molecule in terms of the basis functions and thereby distributing the electrons into atomic contributions. However apart from other deficiencies[Jensen(1999)] this method produces charges that reflect mostly properties of the basis sets used rather than the actual distribution itself. Yet another method is partitioning the wave-function itself rather than the basis-functions by analysing it in topological terms by the method of *Atoms in Molecules*.[Bader(1990)] Atomic partial charges calculated with this algorithm

have — as opposed to the other concepts of partial charges — the unique and desirable property of being well defined quantities that can be derived in a physically unambiguous way. In the Atoms in Molecules method the total electron probability density $\rho(\vec{r})$ around the molecule is divided in subspaces by generating a vector field $\nabla\rho(\vec{r})$. The nuclei are the attractors of the gradient vector field of the electron density. The space of the molecule is partitioned into basins, a basin being the sub-volume Ω_A of space traversed by the trajectories terminating at a given nucleus A. Since a single attractor is associated with each basin, an atom is defined as the union of an attractor and its basin. To obtain partial charges finally the electron density in each basin is summed up.

$$q_A = \int_{\Omega_A} \rho(\vec{r}) d\vec{r} \tag{3.23}$$

It is questionable, however, whether this method will yield a particularly good representation of the electrostatic potential, and multipoles derived with the AIM formalism tend to have very poor convergence properties.[Stone and Alderton(1985)] Virtually no information is available about its usefulness in molecular simulation applications.

To summarise one can say that there is no unique way of determining partial charges and the above mentioned methods can give quite different results for the same molecule in many occasions. Nevertheless the partial charge model can be seen as a useful first approximation if care is taken in the derivation of the charges [Bayly et al.(1993)Bayly, Cieplak, Cornell, and Kollman], especially for organic molecules and bio-molecular systems.[Cornell et al.(1993)Cornell, Cieplak, Bayly, and Kollman]

Intramolecular Terms In classical Molecular Mechanics simulations the molecules are frequently assumed to be rigid. For small molecules like, e. g., water or methane this is often a good approximation. For larger molecules, however, the intramolecular degrees of freedom can not be neglected. In a simple approximation the energy contributions due to the variations of bond-lengths b and bond-angles α can be quantified by harmonic and

Morse potentials of the form

$$U_{\text{bond}}(b) = D\{[1-\exp(-\beta(b-b_{eq}))]^2 - 1\} \quad (3.24)$$

$$U_{\text{ang}}(\alpha) = \frac{1}{2}k_a(\alpha-\alpha_{eq})^2 \quad (3.25)$$

where the superscript eq designates the equilibrium value of the bond between atoms labelled i and j and the angle formed by the atoms labelled i, j and k respectively. k^b_{ij} and k^a_{ijk} are the corresponding force constants quantifying the *stiffness* of a bond or angle. Potentials for torsional degrees of freedom can be described by

$$U_{tors}(\theta_{ijkl}) = k_d\,(1+\cos(n\theta_{ijkl})) \quad (3.26)$$

where θ_{ijkl} is a dihedral angle defined by four atoms $ijkl$ and n being its periodicity. More sophisticated forcefields like MM3[Allinger et al.(1989)Allinger, Yuh, and Lii] include anharmonic terms into (3.25) and (3.26).

Polarisability Due the substantial computational cost involved the induction energy involving polarisability of atoms and molecules is frequently not accounted for in classical molecular simulation. Instead one tries to include the average effect of polarisability by choosing appropriate fixed partial charges as, for example, in the popular SPC/E water model.[Berendsen et al.(1987)Berendsen, Grigera, and Straatsma] Triggered by the ever increasing performance of state of the art computers, more effort is being put into methods that account for polarisability in organic and bio-molecular molecules in recent years.[Kaminski et al.(2002)Kaminski, Stern, Berne, Friesner, Cao, Murphy, Zhou, and Halgren, Halgren and Damm(2001)] However, the traditional realm of polarisable classical force fields has been the simulation of inorganic and ionic systems. For such systems, the use of force field methods is not straightforward and their successes depend strongly on the type of compound under investigation. While the character of organic or biochemical molecules allows a natural separation into bonding and non-bonding interactions, this separation is frequently not possible for inorganic systems such as metal alloys. Static partial charges can be difficult to define for inorganic systems. Especially for

ionic materials polarisation can frequently not be neglected due to the high charge densities found on ions resulting in a strong electrostatic field that can easily polarise neighbouring molecules. Here the most popular model has been the so-called shell model [Dick and Overhauser(1958)]. Each atom is represented by a core and a massless shell connected by a harmonic spring. Partial charges are assigned to both the core and the shell, with the sum of both charges being the nominal charge of the ion. The relative positions of the shells for a given molecular configuration is determined self consistently in an iterative fitting process. The relatively widespread use of this model is probably in part due to its intuitive nature, the core resembling the atomic nucleus and the shell the electron cloud surrounding the nucleus. At this point, however, the analogy ends already because in most cases both the ratio between the charges on the core and the shell as well as the force constant of the spring are determined empirically by fitting to structural properties of the material.[Catlow and Cormack(1987)] Successful applications of the shell model include the physi-sorption of molecules on surfaces [Kim et al.(1994)Kim, Moller, Tildesley, and Quirke], the diffusion of molecules in the cage structure of zeolites [Catlow and Thomas(1992)] and the prediction of the crystal structure and polymorphs of inorganic materials.[Catlow et al.(1993)Catlow, Thomas, Freeman, Wright, and Bell]

In some cases it is possible for classical force fields to retain a reasonably predictive power even when polarisability of ions is not taken in account explicitly, as shown for materials such as various simple fluorides [Bingham et al.(1989)Bingham, Cormack, and Catlow] or clay minerals.[Hartzell et al.(1998)Hartzell, Cygan, and Nagy]

To summarise this section we state that the development of classical model potentials has become a well established field of science by now. There are examples for empirical force fields performing impressingly well even for problems known to be quite problematic.[Wawak et al.(1998)Wawak, Pillardy, Liwo, Gibson, and Scheraga] Such a good performance, however, is not given throughout and generally it is dangerous to rely on the results without giving careful consideration to whether the accuracy of the

force field used is good enough for the properties being simulated.

3.4 Molecular Mechanics

If we are interested in the relative internal energies of different configurations of a given system or in the structure of *the* most stable configuration at low temperatures and in some physical properties of the system in this structure, and if we cannot afford to treat the whole system on an ab-initio basis, the method of choice is Molecular Mechanics. Typical applications of this method are crystal structure prediction [Motherwell et al.(2002)Motherwell, Ammon, Dunitz, Dzyabchenko, Erk, Gavezzotti, Hofmann, Leus and protein folding.[Klepeis et al.(2003)Klepeis, Pieja, and Floudas] Given the molecular content and connectivity in the system of interest, we can propose an initial configuration. This initial configuration can be a mere (educated) guess or a configuration obtained from experiments such as X-ray diffraction or NOE-NMR. Frequently the assumption is made that the most stable structure (e.g., the configuration of a protein *in vivo* or the structure of a grown crystal) corresponds to the structure with the lowest internal energy. After applying a suitable model potential, as discussed in Section 3.3, to the system the energy and its first derivatives with respect the all particle coordinates are calculated and then the structure is systematically modified in discrete s.pdf downhill along the energy gradient to obtain the lowest energy configuration or the energy minimum. This procedure, called *steepest decent* energy minimisation, is the simplest algorithm for finding a minimum on an energy hyper surface. Other methods such as *conjugate gradient* or *Newton Raphson* minimisation include more then one of a number of successive gradient vectors in calculating the new particle positions, vary the step length or include higher derivatives of the energy. For a comprehensive account on these and various other methods of minimisation see Reference [Press et al.(1994)Press, Teukolsky, Vetterling, and Flannery]. Advanced methods can improve the speed at which the minimum is found considerably but the identity of the found minimum will essentially be the same.

This sounds straight forward enough but for all but the most simple systems the search

for the global energy minimum in the configuration space is a non trivial task. The reason for this is that a system with N atoms has $3N - C$ configurational degrees of freedom (C being the number of constraints imposed on the system such as fixed bond-lengths, normally $C \ll 3N$). That is, a particular configuration of the system is represented by a point on the energy hyper surface in an $(3N - C)$-dimensional configuration space. This hyper surface may and in most cases will have count-less *local minima*. In which of these minima the energy minimisation routine ends up depends, of course, very sensitively on the initial configuration and not on the relative depth of this minimum.

One method devised to overcome this so-called *multiple minima problem* is *simulated annealing*.[Kirkpatrick et al.(1983)Kirkpatrick, Gelatt, and Vecchi] Here the system is simulated with Molecular Dynamics or Monte Carlo algorithms (to be discussed in Sections 3.5 and 3.6.3) at a finite temperature. Then the temperature is lowered gradually down to zero Kelvin. Thus the configuration space is explored more thoroughly but there is still no guarantee that the global minimum is found. A number of more or less sophisticated algorithms for searching the global energy minimum of a given system, such as hyper-surface deformation and genetic algorithms have been proposed in recent years (see Reference [Wales and Scheraga(1999)] and references therein) but for none of these it can be shown that it will necessarily find the global minimum of a moderately complex system within a reasonable amount of time. Hence global optimisation must be seen as an unresolved problem and is indeed a field of active research.

Another limitation of Molecular Mechanics is its complete neglect of entropic effects. The average structure of a given system at a finite temperature corresponds to the *free* energy minimum rather then the minimum of the internal energy. To which degree the energy minimum and the free energy minimum structures differ will depend very sensitively on the particular system under consideration and can hardly be predicted by simple means. In a first order approximation one can include entropic effects via the so-called harmonic approximation. In a normal mode analysis, the characteristic vibrations of an energy-minimised system (at zero K) and the corresponding frequencies are determined assuming the potential is harmonic in all degrees of free-

dom. The vibrational contributions to the free energy are calculated as a function of these frequencies [Taylor et al.(1997)Taylor, Barrera, Allan, and Barron]. The validity of this model decreases with increasing temperature but for simple materials results can agree with Molecular Dynamics and experimental results up to temperatures $T > 1000$ K.[Allan et al.(2001)Allan, Barrera, Barron, and Taylor]

While Molecular Mechanics can find and investigate the structures and properties of (free) energy minima it generally cannot provide any information about how the system gets there in the first place. The structure of a crystal grown from solution might well be influenced by the properties of the solvent or impurities while the crystal nucleus is formed. Possibly the internal structure of this initial seed is separated from the global minimum for a given material by energy barriers too high to be overcome under "normal" conditions. In particular in the field of bio-molecular chemistry it has been a long standing debate whether the native *in vivo* structure of a protein must necessarily correspond to the lowest (free) energy configuration or to what extent the complex kinetics of protein folding may cause the protein to end up in a local rather than a global minimum.[Miller and Wales(1999), Dinner and Karplus(1998), Doye and Wales(1996), Dill(1993), Dill et al.(1993)Dill, Fiebig, and Chan]

Notwithstanding all the limitations mentioned above, the method of Molecular Mechanics has provided a number of valuable insights into the structure and properties of various materials and thereby assisted and complemented experiment and theoretical models.[Wawak et al.(1998)Wawak, Pillardy, Liwo, Gibson, and Scheraga, Beyer and Price(2000), Motherwell et al.(2002)Motherwell, Ammon, Dunitz, Dzyabchenko, Erk, Gavezzot

3.5 Molecular Dynamics

Molecular Dynamics is used to investigate the time dependent evolution of a molecular system. While this procedure is normally more expensive in terms of the required computational resources than Molecular Mechanics, it can be used to obtain a wealth of additional information. One can study the structure of a system at finite temperatures,

investigate the nature of transition states in the configurational hyper space, directly calculate quantities that depend on fluctuations such as thermal expansivity and numerous other properties.[Allen and Tildesley(1987), Frenkel and Smit(2001)]

3.5.1 Integration of the Equations of Motion

The (analytical) derivatives of the energy expression, with respect to the coordinates of all the atoms in the system, give the forces acting on the atoms for a given configuration of the system. Thus, given the coordinates, velocities and forces of all particles we can integrate the classical Newtonian equations of motion numerically over a small time increment Δt, typically around 10^{-12} seconds, to obtain a new set of atomic coordinates. This cycle, force calculation $\rightleftarrows$ numerical integration, is repeated to obtain the trajectory of the system in phase space over the desired amount of time. There exits a number of ways for the numerical and approximate integration of Newtons second law $F_i = m_i a_i$ [Press et al.(1994)Press, Teukolsky, Vetterling, and Flannery, Vesely(2001)] (F_i is the net force acting on particle i at a given point in time, resulting in its acceleration $a_i = d^2 r_i/dt^2$). In most of the available software, however, a version of the simple *Verlet algorithm* [Verlet(1967)] is used. The position r of each particle at time $t+\Delta t$ is calculated from its positions at time t and $t - \Delta t$ and the acceleration $a = F/m$ at time t as

$$r(t + \Delta t) = 2r(t) = r(t - \Delta t) + a(t)\Delta t^2 + O(\Delta t^4) \tag{3.27}$$

Despite its simplicity this algorithm is exact up to third order in Δt. In addition, it is one of a group of so-called symplectic algorithms. Such algorithms [Posch et al.(1990)Posch, Hoover, and Holian, Holian et al.(1990)Holian, Degroot, Hoover, and Hoover] are time reversible and very stable in terms of long term energy conservation. Similar algorithms that are frequently used in MD programs and that explicitly include the velocity in the equations of motion, giving thereby a more accurate estimate of the velocities at time t, are the *velocity Verlet* [Allen and Tildesley(1987)] and the *leap frog* [R. P. Feynman and Sands(1963)] algorithm. The latter is the standard integrator

in DL_POLY [Smith and T.R. Forester(2001)], the MD program we use for most of the calculations reported in this thesis.

3.5.2 Boundary Conditions and Cutoffs

One problem associated with Molecular Dynamics and molecular simulation in general is the small system size or particle number, N, that can be simulated within a reasonable amount of computer time. Currently we can only simulate systems with up to $N \sim 10^6$ particles. For typical densities of liquids or solids this corresponds to system sizes of L = 10-100 nm, with L being the side length of a cubic box. With such an unfavourable ratio between volume and surface of the system boundary effects, i.e., interactions between particles and the container wall are going to have a major influence on the calculated properties of the system. Often one is not interested in these boundary effects but rather in bulk properties of the system. The solution for this problem is the application of so-called periodic boundary conditions (PBC). Here the box containing the system and all its content are repeated periodically in all three dimensions. Particles approaching a boundary are not pushed back but are allowed to cross this wall unimpeded to enter the system with the same momentum through the opposite wall of the system. PBCs are normally combined with the so-called *nearest image convention* or a spherical cutoff. In the former case each particle only interacts with the closest of all its periodic images, in the latter, each particle only interacts with the closest of all its periodic images of each other particle only if the radial distance to this image is smaller than a given maximum distance, the so called cutoff-radius. Particles separated by a distance longer than this cutoff do not "see" each other. The application of such a spherical cutoff, typically taken to be between eight and sixteen Ångstrom, is justified for materials that only interact via VdW potentials because in that case interactions between particles further apart than about ten Å can be safely neglected. If there are electrostatic interactions between particles, so-called long range interactions interactions, proportional to the inter-particle distance r as r^{-n}, with $n \leq 3$, we can still use periodic boundary conditions but the interactions

between a primary particle and *all* periodic images of the atoms in the system have to be considered. (see Section 3.5.4).

3.5.3 Ensembles

The trajectory of the system in phase space generated by straight forward application of the cycle *force calculation* $\rightleftarrows$ *numerical integration* for a fixed number N of atoms in a constant volume V corresponds to the so-called micro-canonical or NVE-ensemble. The system is isolated in that it can exchange neither matter nor energy with its surroundings and the trajectory lies on an energy hyper sphere in the $6N$-dimensional phase space. Most experimental setups operate under conditions of constant temperature, T, and volume, V, or temperature and pressure, P, rather than volume and internal energy, E. If we want to compare simulation to experimental results it is therefore often desirable to simulate a system at constant temperature (and pressure) with the energy (and the volume) fluctuating around some average values. The statistical mechanical ensembles corresponding to these conditions are the canonical (NVT) and the isobaric-isothermal (NPT) ensemble, respectively. Alternatively we might want to simulate an *open system*, i.e., a system that can exchange matter with a reservoir, where the condition of constant N is replaced by constant chemical potential, μ, leading from the canonical to the grand canonical (μVT) ensemble. A number of other ensembles have been devised and used in simulation work, but they are used rarely. We note that in the thermodynamic limit, i.e., for $N \rightarrow \infty$ the average properties converge for all the ensembles described. A rigorous statistical mechanical derivation of the various ensembles is beyond the scope of this work. For a more in-depth account see, e.g., Reference [McQuarrie(2000)].

In DL_POLY, the software we use here, there are various algorithms implemented for generating canonical and NPT ensembles, the physically most rigorous of which are the methods devised by Nose and Hoover.[Holian et al.(1990)Holian, Degroot, Hoover, and Hoover] For most of the simulations reported in the following we use the so-called Nose-Hoover thermostat, for

obtaining a trajectory in the the canonical ensemble. From the velocities of the particles and their masses, the kinetic energy is calculated at each timestep and the integration algorithm is modified so that the acceleration of each particle is scaled by a factor α. The resulting equations of motion are

$$\frac{dr(t)}{dt} = v(t) \tag{3.28}$$

$$\frac{dv(t)}{dt} = F(t)/m - \alpha(t)v(t) \tag{3.29}$$

The factor α is given by the first order differential equation

$$\frac{d\alpha(t)}{dt} = \frac{1}{\tau}\left(\frac{E_{kin}}{E_{\rm kin}^{\rm targ}} - 1\right) \tag{3.30}$$

Here $E_{\rm kin}$ is the instantaneous kinetic energy at time t and $E_{\rm kin}^{\rm targ}$ is the desired or target kinetic energy corresponding to the desired temperature. In combination with the *leap frog* algorithm the position r and velocity v of a particle at time t in a simulation with timestep Δt are calculated according to

$$v(t+\frac{1}{2}\Delta t) = v(t-\frac{1}{2}\Delta t) + \Delta t\left[F(t)/m - \alpha(t)v(t)\right] \tag{3.31}$$

$$v(t) = \frac{1}{2}\left[v(t-\frac{1}{2}\Delta t) + v(t+\frac{1}{2}\Delta t)\right] \tag{3.32}$$

$$r(t+\frac{1}{2}\Delta t) = r(t) + \Delta t v(t+\frac{1}{2}\Delta t) \tag{3.33}$$

$$\alpha(t+\Delta t) = \alpha(t-\frac{1}{2}\Delta t) + \frac{\Delta t}{\tau^2}\left(\frac{E_{kin}}{E_{\rm kin}^{\rm targ}} - 1\right) \tag{3.34}$$

$$\alpha(t) = \frac{1}{2}\left[\alpha(t-\frac{1}{2}\Delta t) + \alpha(t+\frac{1}{2}\Delta t)\right] \tag{3.35}$$

Note that in the *leap frog* algorithm the velocities and positions are updated out of sync by $\frac{1}{2}\Delta t$ and the velocities at time t required for updating the coordinates at time $t+\Delta t$ are approximated by Equation 3.32.

It has been shown [Hoover(1985)] that this algorithm reproduces the canonical ensemble. It produces an set of points in the 6N dimensional phase space where the probability $p(E)$ of finding a point corresponding to a state with internal energy E at an inverse

temperature β is given by

$$p(E) = \frac{\exp(-\beta E)}{\int \exp(-\beta E)\, d\mathbf{p} d\mathbf{q}} \tag{3.36}$$

The expression in the denominator, an integral over the coordinates $\mathbf{q}$ and moments $\mathbf{p}$ of all particles, is the classical statistical mechanical partition function for the canonical ensemble.

3.5.4 Long Range Interactions

In principle the interaction between two particles separated by a distance r goes to zero only for $r \to \infty$. As discussed in Section 3.3.1 all intermolecular interactions can be written as a power series in r, $\sum_n c_n r^{-n}$. Interactions for which the leading term in the series is an inverse power of n with $n > 3$ (such as the van der Waals interactions where the leading term corresponds to the term with $n = 6$), are generally assumed to decay fast enough, so that all interactions beyond a large enough cutoff radius r_c can be ignored without affecting the calculated properties qualitatively. If the van der Waals interactions are approximated by a Lennard Jones potential (see Equ. 3.19) the cutoff radius is frequently taken to be $r_c = 2.5\,\sigma$. Applying such a cutoff is no longer a reasonable choice for terms with $n \leq 3$, i.e., for electrostatic interactions between charges (n=1), charges and dipoles (n=2) and dipole-dipole interactions (n=3). This is most clearly to be seen by analytically calculating an estimate for the error ΔE_c introduced by neglecting the interactions beyond r_c between a particle and all the other particles surrounding it. If the primary particle interacts with the other particles via a pair-potential $u(r) = r^{-n}$ and we approximate the pair distribution beyond the cutoff being unity we can estimate ΔE_c by

$$\Delta E_c \propto \int_{r_c}^{\infty} u(r) 4\pi r^2 dr. \tag{3.37}$$

The proportionality constant depends on the average particle density, ρ, in the system, but from Equation 3.37 it is clear that for $n \geq 3$ the integral diverges and hence for all densities $\rho > 0$ an unacceptable error is introduced by neglecting the interactions beyond a finite cutoff r_c. For a long time this fact has been known

and accounted for in the field of theoretical inorganic crystallography. The method most commonly used to cope with this problem is Ewald Summation.[Ewald(1921)] It took until the early nineties for it to become generally accepted that for fluids consisting of charged or polar molecules, the application of a cutoff radius to the Coulomb interactions can lead to severe artifacts in structural and especially in dynamic results. [Schreiber and Steinhauser(1992), Boresch and Steinhauser(1997)] Since then most of the commonly used academic and commercial software for Molecular Dynamics simulations includes Ewald summation routines and/or a number of alternative algorithms for consistent calculation of the long range interactions that have been devised in the last two decades. For a overview over these methods see, e.g., References [Toukmaji and Board Jr.(1996), Sagui and Darden(1999)]. In the following we describe Ewald Summation as well as the Reaction Field Formalism, an alternative method to account for electrostatic long range interactions.

Ewald Summation

Ewald summation and its variations [Toukmaji and Board Jr.(1996)], are methods, for treating all interactions between charges. The concept of periodic boundary conditions is taken literally by assuming the system to be composed of an infinite number of periodic boxes. The N particles with charges q_i in the central box, the only part of the system that is explicitly simulated, interact not only with each other but additionally with all the periodic replicas in the surrounding infinite number of boxes. For a cubic central box the electrostatic energy U_{el} is given by

$$U_{el} = \sum_{\mathbf{n}} \left(\sum_{i<j}^{N} q_i q_j |\vec{r}_{ij} + \mathbf{n}|^{-1} \right) \tag{3.38}$$

The sum over $\mathbf{n}$ is the sum over all simple cubic lattice points, $\mathbf{n} = n_x L + n_y L + n_z L$, n_x, n_y, n_z being integer and L the side length of the cubic box. In order to manage this summation, the Coulomb potential u_{Coul} for each pair of particles is written as a sum of

two terms

$$u_{Coul} = \frac{q_i q_j}{r_{ij}} = \frac{q_i q_j}{r_{ij}} \operatorname{erfc}(\kappa r_{ij}) + \frac{q_i q_j}{r_{ij}} \operatorname{erf}(\kappa r_{ij}) \tag{3.39}$$

where erf and erfc are the error function and the complementary error function respectively. The complementary error function renders the first term of the sum short ranged, leaving the long range contribution of the coulomb potential essentially to the second term. The relative weight of the two terms is controlled by the parameter κ. The second term can be calculated by exploiting the periodic nature of the whole system. After applying a three dimensional Fourier transformation to this term the summation can be done conveniently in reciprocal space.

$$\begin{aligned} U_{ew} = \quad & \sum_{i<j} \left(\sum_{|\mathbf{n}|=0}^{\infty} \frac{q_i q_j}{|\vec{r}_{ij}+\mathbf{n}|} \operatorname{erfc}(\kappa|\vec{r}_{ij}+\mathbf{n}|) \quad + \right. \\ & \left. \frac{1}{\pi L^3} \sum_{\mathbf{k}\neq\mathbf{0}} q_i q_j \frac{4\pi^2}{k^2} \exp(\frac{-k^2}{4\kappa^2}) \cos(\mathbf{k}\mathbf{r}_{ij}) \right) \quad - \frac{\kappa}{\sqrt{(\pi)}} \sum_{i=1}^{N} q_i^2 \end{aligned} \tag{3.40}$$

The last term of equation 3.40 is the so called self-term which has to be subtracted in order to correct for the interaction of particles with themselves. If κ is chosen properly, the summation of the first term for all pairs can be confined to the central box. In other words, the summation of the first term in equation 3.40 stops at $|\mathbf{n}| = 0$. The second term is a sum over reciprocal vectors $\mathbf{k} = 2\pi\mathbf{n}/L$, how many of these have to be included depends on the value of κ. Optimally parameterised [Fincham(1994), Adams and Durey(1986)] the EW method has an execution time which scales as $N^{3/2}$ where N is the number of particles.

Reaction Field

In the reaction field method [Barker and Watts(1973), Neumann(1985)] it is assumed that any given molecule is surrounded by a spherical cavity of finite radius within which the electrostatic interactions are calculated explicitly. Outside the cavity the system is treated as a dielectric continuum. The occurrence of any net dipole within the cavity induces a polarisation in the dielectric, which in turn interacts with the molecule. The model allows

the replacement of the infinite Coulomb sum by a finite sum plus the reaction field. The effective pair potential is given by

$$u(r_{ij}) = q_i q_j \left(\frac{1}{r_{ij}} + \frac{(\epsilon_{RF} - 1)}{(2\epsilon_{RF} + 1)} \frac{r_{ij}^2}{r_c^3} \right) \tag{3.41}$$

with r_c the radius of the cavity and ϵ_{RF} the dielectric constant outside the cavity. This expression unfortunately leads to large fluctuations in the system Coulombic energy, due to the large step in the function at the cavity boundary, and, therefore, usually the reaction field potential is smoothened by a tapering function.

Hummer et al. introduced an extended version [Hummer et al.(1994)Hummer, Soumpasis, and Neumann] of this concept, a *generalised reaction field* (GRF) with a Coulomb potential of the form

$$u_{GRF}(r_{ij}) = \frac{q_i q_j}{r_{ij}} \left(1 - \frac{r_{ij}}{r_c} \right)^4 \left(1 + \frac{r_{ij}}{5r_c} + \frac{2r_{ij}^2}{5r_c^2} \right) \tag{3.42}$$

$u_{GRF}(r)$ and all its derivatives are monotonic and of alternating sign, just like $\frac{1}{r}$, and $u_{GRF}(r)$ and its derivatives up to third order vanish at the cutoff r_c. This screened Coulomb interaction model yields results for test systems that agree very well with Ewald Summation data while retaining its computational efficiency of cutoff based methods.[Hummer et al.(1994)Hummer, Soumpasis, and Neumann]

3.6 Additional Issues in Molecular Dynamics Simulations

For obtaining some of the results reported in this thesis we use methods and algorithms that, unlike the methods presented in the preceding sections, are not included in most standard molecular simulation software. These methods and some background are briefly discussed in the following.

3.6.1 Long Range Interactions in Interfacial Systems

For inter-facial systems with a pseudo 2-D periodicity a consistent calculation of the long range interactions is a comparatively intricate task. As discussed in Section 3.5.4 there have essentially been three principal approaches for treating long range interactions in systems periodic in three dimensions, all used in combination with periodic boundary conditions: 1) do not consider long range interactions at all by using a spherical cutoff for the, possibly switched or shifted, Coulomb potential, 2) use a cutoff and account for interactions beyond the cutoff radius via a reaction field, 3) use *true* periodic boundary conditions by employing Ewald Summation or any equivalent method like Particle Mesh Ewald, Particle-Particle particle-Mesh or Fast Multipole Analysis.[Sagui and Darden(1999)] For inter-facial systems both the first [Perera and Berkowitz(1993), Bocker et al.(1995)Bocker, Nazmutdinov, Spohr, and Heinzinger, Marmier et al.(1999)Marmier, Hoang, Girardet, and Lynden-bell, Wensink et al.(2000)Wensink, Hoffmann, Apol, and Berendsen] and a, possibly modified, version of the third [Shelley and Patey(1996), Feller et al.(1996)Feller, Pastor, Rojnuckarin, Bogusz, and Brooks, Spohr(1997), Oyen and Hentschke(2002)] of these approaches have been used frequently while we found only one reference for an application of the second approach.[Hummer and Soumpasis(1994)] Comparisons of the first approach with more advanced methods consistently conclude that approach 1 can easily lead to serious artifacts and should be avoided whenever possible.[Shelley and Patey(1996), Feller et al.(1996)Feller, Pastor, Rojnuckarin, Bogusz, and Brooks, Spohr(1997)]

Conventional Ewald Summation cannot be applied straight-forwardly to inter-facial systems with periodicity in only two dimensions because an artificial periodicity in the direction perpendicular to the interface would be introduced, resulting in additional forces not to be found in real 2-D systems. The earliest attempt to calculate the long range interactions consistently in such a system is a 2-D version of Ewald Summation.[Heyes et al.(1977)Heyes, Barber, and Clarke] It is the most rigorous way to

tackle this problem and at the same time the most expensive one, the required CPU time scaling with N^2, where N is the number of particles in the system. One conceptually very simple alternative is to use conventional 3-D Ewald Summation in combination with a geometry of the simulation box that ensures there to be a vacuum slab of sufficient thickness between the layers representing the system of interest. This approach has the advantage that one can use most common MD simulation packages, including DL_POLY, without modification. The disadvantage is the fact that here the simulation box in the direction has to be quite large to include the vacuum slab. Since the number of reciprocal space vectors used in the Ewald Summation is proportional to the volume of the simulation box for a given accuracy, the computational effort involved is substantial. Only recently it has been shown [Yeh and Berkowitz(1999)] that the thickness of the required vacuum slab, and therefore the length of the simulation cell in the direction perpendicular to the interface(s), can be reduced considerably by adding a term U_{dip}, proportional to the square of the net dipole moment component in that direction, to the total electrostatic energy function U_{el} of the system:

$$U_{el} = U_{ew} + \frac{1}{3V}\mathbf{M}_z^2 = U_{ew} + U_{dip,z} \tag{3.43}$$

U_{ew} is the electrostatic energy calculated by Ewald Summation for conducting boundary conditions, as defined in Equation 3.40, V is the volume of the simulation box and $\mathbf{M}_z$ is the component of the net dipole moment in the z-direction (here taken to perpendicular to the interface). The derivation of this expression was originally done in a seminal paper by de Leeuw et al. in the context of Ewald Summation [Leeuw et al.(1980)Leeuw, Perram, and Smith]. We stress, however, that it is generally applicable for correcting the electrostatic energy of systems finite in three or less dimensions independent of the method used to calculate the remainder of the energy expression.[Hummer(2002)] In fact there has been a some debate on whether this correction term should be used in the comparison of crystal bulk lattice energies or not.[Van eijck and Kroon(2000), Wedemeyer et al.(2000)Wedemeyer, Arnautova, Pillardy, Wawak, Czaplewski, and Scheraga,

Pillardy et al.(2000)Pillardy, Wawak, Arnautova, Czaplewski, and Scheraga, Kantorovich(1999), Kantorovich and Tupitsyn(1999)] For crystals that are definitely finite in at least one dimension the application of this term seems to be less controversial.[Yeh and Berkowitz(1999), Kantorovich(1999), Kantorovich and Tupitsyn(1999)]

During the last decade a number of alternative methods that claim to combine accuracy and computational efficiency have been proposed and compared.[Widmann and Adolf(1997), Jorge and Seaton(2002)] However, none of these methods seems to be decidedly more efficient than 3-D Ewald with the correction term, as discussed above [Yeh and Berkowitz(1999)]. In addition the implementation of this latter method is considerably easier than most of the other methods. Therefore I implemented the dipole correction term, Eqn. 3.43, into DL_POLY. In addition I also implemented the generalised reaction field (GRF) method [Hummer et al.(1994)Hummer, Soumpasis, and Neumann], see Equation 3.42 in Section 3.5.4. In Chapter 6 the results obtained in a number of test calculations are going to be presented.

3.6.2 Charged Systems

If the enclosing boundaries are chosen to be wide enough then all systems can be made overall neutral. However, there are many systems that carry a permanent net charge on a micro or meso scale, e.g., some colloids or micelles in biological systems [Kuhn and Rehage(1997)] or lattice defects in crystals.[De souza and Maier(2003)] Simulation of such systems can be difficult if the region of interest, for example, the surface of an ionic crystal in solution, is charged and the entire neutral system, the crystal and the surrounding ionic solution containing more charged crystals and the corresponding number of counter ions in this case, is too big too be modelled with microscopic resolution. One way to go in such a case is coarse graining the system thereby making simulation of the entire neutral system feasible at the price of loos-

ing information about the detailed molecular structure in the interesting part of the system. The solution outside a charged colloid can be represented as continuum and the charge density be calculated by numerical solution of the Poisson Boltzmann equation. This approach is often taken when calculating and comparing the energies of different configurations of a protein [Miteva et al.(1997)Miteva, Demirev, and Karshikoff, Vila et al.(1998)Vila, Ripoll, Vorobjev, and Scheraga, Wagner and Simonson(1999)].

If we want to model a charged section of an over-all neutral system at molecular resolution this system is normally going to be so small that we have to apply periodic boundary conditions to avoid undesired wall effects and a pronounced system size dependence of the results. A periodically repeated system with a net charge in the repeat unit, however, formally has an infinite energy. If we use a spherical cutoff scheme, and only consider interactions with the nearest of the periodic neighbours, the energy is going to be finite even for a system with a net charge. However, we are then confronted with the well known negative effects of cutting the Coulomb interactions at a finite distance.[Shelley and Patey(1996), Feller et al.(1996)Feller, Pastor, Rojnuckarin, Bogusz, and Brooks, Spohr(1997)]

One possible solution is to simulate only the interesting part of the system and add the appropriate number of counter ions to ensure that the system has no net charge, as often done for charged biological molecules such as DNA.[Lyubartsev and Laaksonen(1998)] This, however, is an ad hoc solution since we cannot know in advance how large the simulated system has to be to ensure the correct concentration and density gradient and ultimately the location of the counter ions.

It seems to be common misunderstanding that Ewald Summation can only be applied to over-all neutral systems. In fact it can be applied to charged systems provided some precautions are taken.[Refson()] The k=0 term of the reciprocal space sum in Eqn. 3.40 takes the form

$$U_{ew}^{k=0} = \frac{1}{k^2} \exp\left(-\frac{k^2}{4\kappa^2}\right) \left|\sum_{i=1}^{N} q_i\right|^2 \tag{3.44}$$

which is zero in the case of electro-neutrality but infinite otherwise. Its omission from the sum in Eqn. 3.40 is physically equivalent to adding a uniform jelly of charge which exactly

neutralises the net-charge. In most standard implementations of Ewald Summation this term is not included by default because the simulated systems are expected to be neutral anyway. However there is yet another term, non-zero only for charged systems, which is generally also omitted by default. This is the term accounting for the interactions of the background charge density (the jelly) with the explicit atomic charges in the simulation cell in real space.

$$U_{ew}^{chg} = \frac{\pi}{2V\kappa^2} \left| \sum_{i=1}^{N} q_i \right|^2 \tag{3.45}$$

If this term is included any apparent net-charge in a simulated system is consistently neutralised by a uniform background charge, rendering the total energy of the periodically repeated system finite. Since we performed a number of MD simulations of charged systems I implemented (3.45) into DL_POLY.

The background charge is of course not present in a real system, and can therefore be seen as an artifact that invalidates any results obtained for this system. However, we can just as well take the view that this uniform background charge is a first order approximation to the generally non-uniform charge distribution that surrounds a charged sub-system *in vivo*. Thus it is unclear whether the artifacts introduced by the implicit background charge or those introduced by explicitly neutralising the system with counter ions are larger. The answer to this question probably depends considerably on the particular system studied. For completeness we add that if the free energy of solvation of charged molecules is calculated, or molecular dynamic simulations at constant pressure are performed for charged systems, the system size dependence of the results can be reduced considerably by additional terms in the energy expression.[Hummer et al.(1996)Hummer, Pratt, and Garcia, Bogusz et al.(1998)Bogusz, Cheatham, and Brooks]

3.6.3 The Grand Canonical Ensemble

The Grand canonical Ensemble (GCE) represents an open system where, in addition to the volume and the temperature, the chemical potential, μ, is

held constant rather than the number of particles. This type of ensemble is particularly useful for simulating confined systems in contact with a (virtual) reservoir. Examples for this kind of system include liquids or gases in porous materials [Channon et al.(1998)Channon, Catlow, Gorman, and Jackson, Grey et al.(2002)Grey, Nicholson, Gale, and Peterson] and water in the active site of enzymes.[Kamberaj and Helms(2001)] Such systems are in equilibrium with a bulk phase at constant values of density and temperature. The values of the density in the confined region is generally not equal to the corresponding value in the bulk. Since we do not know the density this region cannot be simulated in any of the common ensembles (NVE, NVT, NPT). Simulating the bulk phase and the equilibration explicitly is in most cases not computationally feasible because of the large system sizes and time-scales involved. Simulation in the grand canonical ensemble ensures that the density and the density gradient in the confined system are in equilibrium with a bulk phase, at the same chemical potential. Molecular simulation of the grand canonical ensemble is most frequently performed in the context of Monte Carlo simulation. Here we only give a brief outline of the method. For more detailed accounts we refer to the literature; a good and concise introduction to Metropolis Monte Carlo can be found, for example, in Ref. [Hansen and McDonald(1996)] while the extension to grand canonical ensemble is discussed in some detail in Ref. [and Nicholson and Parsonage(1982)]

The canonical ensemble average $\langle A \rangle$ of any quantity $A(\mathbf{r}^N)$ that is a function of the particle coordinates in a system at constant N, V and T, is given by [McQuarrie(2000)]

$$\langle A \rangle = \frac{\int A(\mathbf{r}^N) \exp\left(-\beta E(\mathbf{r}^N)\right) d\mathbf{r}^N}{\int \exp\left(-\beta E(\mathbf{r}^N)\right) d\mathbf{r}^N} \tag{3.46}$$

We can replace the integrals in Eqn. 3.46 by sums and generate a large number M of random configurations $\mathbf{r}^N$ for the given values of N, V and T to get an estimate of A.

$$\langle A \rangle \simeq \frac{\sum_{m=1}^{M} A(\mathbf{r}^N(m)) \exp\left(-\beta E(\mathbf{r}^N(m))\right)}{\sum_{m=1}^{M} \exp\left(-\beta E(\mathbf{r}^N(m))\right)} \tag{3.47}$$

This, however, would be very inefficient since at densities corresponding to a dense gas or a liquid most of the randomly chosen configurations would include overlapping particles.

This results in a high energy and a vanishing contribution to the sums in (3.47). The Metropolis Monte Carlo algorithm uses *importance sampling* to concentrate on configurations that give substantial contributions. Regions in phase space that give the largest contributions to the sums in (3.47) are also sampled most frequently. Results of this *biased* sampling must be corrected by weighing each configuration accordingly. If we sample on a Boltzmann distribution these weights are nothing else but the Boltzmann factor and (3.47) reduces to

$$\langle A \rangle \simeq \frac{1}{M} \sum_{1}^{M} A(m) \tag{3.48}$$

The algorithm that produces a set of configurations with a Boltzmann distribution, the Metropolis Monte Carlo algorithm, starts from any initial configuration and performs random moves (or rotations) of randomly chosen particles. After each move the resulting change in the internal energy of the system ΔE is calculated. At the same time a random number ζ is generated, evenly distributed over the interval $[0, 1)$. The new configuration is only accepted if

$$\exp\left(-\beta \Delta E\right) > \zeta \tag{3.49}$$

Otherwise it is rejected and the old configuration is counted once more. It is common practice to limit the maximum length of a random move so that approximately half of all moves are accepted, thereby maximising the numerical efficiency of the algorithm. By modifying the term in the exponential in (3.49) appropriately, one can generalise the method to produce other ensembles, such as the NPT ensemble.[Allen and Tildesley(1987), Hansen and McDonald(1996)]

If we want to simulate the grand canonical or μVT-ensemble, we allow not only for particle movements but also for fluctuations of the particle number N. This is accomplished by repeated insertion and deletion of particles into/from the simulation volume according to the probabilities

$$P_{ins} = \frac{1}{N+1} \exp\left(B - \beta \Delta E\right) \tag{3.50}$$

$$P_{del} = N \exp\left(-B - \beta \Delta E\right) \tag{3.51}$$

This is one commonly adopted notation devised originally by Adams.[Adams(1975)] Here $B = \beta\mu' + log(\bar{N})$, $\beta = 1/k_B T$, μ' is the *excess* chemical potential and $\bar{N}$ is the mean number of particles. The system is constrained by the applied parameters B, V and T. It can be shown that Eqns. 3.50 and 3.51, in combination with a conventional NVT Monte Carlo algorithm, generate a grand canonical ensemble and consequently a system with constant average chemical potential.[Adams(1975)] Although it has not yet been proven rigorously that this is also true in combination with an MD simulation, this heuristic assumption has been made.[Lupkowski and Vanswol(1991)]

No matter whether we use MD or MC, there is one problem that complicates grand canonical simulation algorithms: with decreasing temperature, increasing density and stronger inter-molecular interactions, the probability for inserting a particle at a randomly chosen position in the system becomes vanishingly small, resulting in very poor statistics, insufficient exploration of the phase space, and therefore inaccurate and eventually useless results. Although considerable progress has been made, and a number of improved algorithms have been proposed over the last two decades [Mezei(1987), Shing and Azadipour(1992), Vega et al.(1994)Vega, Shing, and Rull, Shelley and Patey(1994), Yau et al.(1994)Yau, Liem, and Chan, Macedonia and Maginn(1999)], this problem cannot be considered as resolved. Since this problem directly affects the present work it will be discussed in somewhat more detail in Section 8.2.1.

Chapter 4

Crystal Morphologies

4.1 Introduction

In the context of crystallography the term morphology (or habit) refers to the macroscopic appearance of a crystal which is characterised by a set of surfaces and their relative areas. The prediction and the control of crystal morphologies is a field of active research [Grimbergen et al.(1998)Grimbergen, Reedijk, Meekes, and Bennema, Liu et al.(1995)Liu, Boek, Briels, and Bennema, Boek et al.(1994)Boek, Briels, and Feil] because of its importance in industrial processing. The shapes of crystals are fundamental to many methods for purification and separation.

There are several theoretical methods available for the calculation of the morphological importance (MI), i.e., the relative size of crystal faces. The oldest is the empirical BFDH-rule [Bravais(1886), Friedel(1907), Donnay and Harker(1937)], due to Bravais, Friedel, Donnay and Harker, which assumes that the MI of a given face with Miller indices hkl is proportional to the interplanar distance d_{hkl} between two layers of this face. In a seminal paper published 1954 by Hartman and Perdok[Hartman and Perdok(1954)] the authors introduced two new concepts: the attachment energy (E_{att}) and periodic bond chains (PBC). PBCs are periodically repeated chains of strong intermolecular interactions, for example, when the molecules are hydrogen bonded, parallel to a given face. Those faces

containing at least two different PBCs (F-faces) are assumed to grow layer by layer. They can be expected to be the slowest growing faces and are therefore likely to be observed in the crystal habit. The attachment energy, E_{att} is defined as the energy released when one additional growth slice of thickness d_{hkl} is attached to the crystal face identified by the Miller indices hkl. The MI of the F-faces is estimated by assuming that the growth velocity R_{hkl} of each F-face is proportional its attachment energy. Later Hartman and Bennema showed that this assumption is a valid approximation for F-faces below the roughening temperature [Hartman and Bennema(1980)].

The attachment energy method is widely used for morphology predictions for organic molecules as a routine modelling method. More elaborate models which include the effect of solvent etc. [Vandervoort(1991), Liu et al.(1995)Liu, Boek, Briels, and Bennema, Winn and Doherty(1998)] are being developed. Examples of at least qualitatively correct predictions with the attachment energy model include crystals of aspirin [Meenan(1997)], 4-aminobenzophenone [Qingwu et al.(1997)Qingwu, Sheen, Shepherd, Sherwood, Simpson, and Hammond], sodium chlorate [Clydesdale et al.(1998)Clydesdale, Roberts, Telfer, Saunders, Pugh, Jackson, and Meena β-succinic acid [Clydesdale et al.(1991)Clydesdale, Docherty, and Roberts] and *alpha*-lactose mono-hydrate [Clydesdale et al.(1997)Clydesdale, Roberts, Telfer, and Grant]. Usually attachment energies are calculated for a number of faces with d_{hkl} above a certain threshold and the growing faces are identified by drawing a Wulff plot with $R_{hkl} \propto |E_{att}|$, that is, the faces with the highest (least negative) attachment energies are expected to be flat faces. Faces where there are strong attractive interactions between the layers, giving more negative attachment energies, grow more rapidly and hence grow out and are not observed. (The faces corresponding to larger R_{hkl} values lie outside the enclosed volume of the predicted morphology on the Wulff plot.) Thus the attachment energies often reflect whether strong interactions (PBCs) lie within the face or link its growth layers. Hence the calculation of PBCs is frequently omitted. This assumption is justified for crystals with sufficiently isotropic interactions between the growth units [Berkovitch-Yellin(1985)].

One prerequisite for the calculation of attachment energies is an intermolecular model potential or force-field. Force-fields of varying degrees of sophistication are available in abundance for several classes of chemical compounds. [Hobza et al.(1997)Hobza, Kabelac, Sponer, Mejzlik, and Vondrasek, Gundertofte et al.(1996)Gundertofte, Liljefors, and Norrby, Halgren(1999)] Quite a few of these model potentials and parameter sets have been used for attachment energy calculations. The purpose of the present study is to investigate systematically how sensitive the results of attachment energy morphology predictions are to the use of specific model potentials. In most published crystal morphology predictions, only one force-field is used, or at best some minor variations are considered [Docherty and Roberts(1988)]. In this paper we compare predicted morphologies of five different organic compounds obtained with a range of different intermolecular model potentials which are widely used for modelling organic crystal structures. Variations in both the repulsion-dispersion parameters and in the accuracy of the electrostatic model are considered. The ability of each model potential to reproduce the crystal structure and lattice energy was also considered, as the usual criterion for suitability for modelling the condensed phases of the molecule.

4.2 Computational Details

4.2.1 The Compounds

The five different compounds chosen for the morphological analysis are β-succinic acid (β-SA), hexamethylene-tetramine (HMT), pentaerythritol (PE), urea and ϵ-caprolactam (ϵ-CL) (Figure 4.1). They are chosen to cover a range of different functional groups, types of intermolecular interactions and space-groups. The crystallographic properties of each compound are given in Table 4.1. All the crystal structures, except for ϵ-caprolactam, were determined by neutron diffraction and consequently can be used without correcting the hydrogen positions. For ϵ-caprolactam the covalent carbon-hydrogen

Figure 4.1: **The five molecular compounds whose crystal morphologies are investigated**

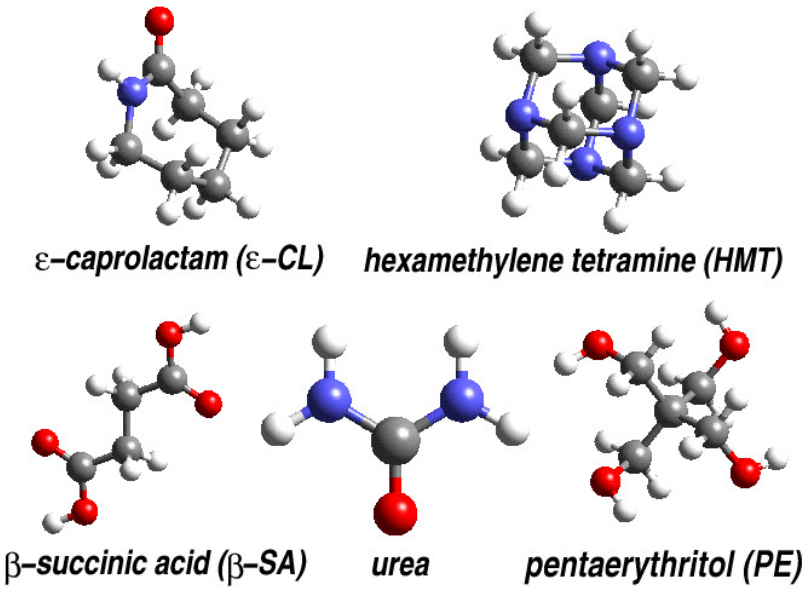

and nitrogen-hydrogen bond-lengths are normalised to 1.092 and 1.009 Å respectively [Allen et al.(1987)Allen, Kennard, Watson, Brammer, Orpen, and Taylor] to correct for the errors in X-ray location of hydrogen atoms.

4.2.2 The Model Potentials

In Table 4.2 the atom-atom intermolecular potentials used here are summarised, They are described in more detail below. The molecules are treated as rigid bodies in all calculations. For the attachment energy calculations this does not make any difference since attachment energies do not include intramolecular contributions by definition. For the lattice energy minimisations one can expect the rigid body model to be a good approximation for most of the compounds considered here. The **GF force-field** was developed by Gavezzotti and Filippini [Filippini and Gavezzotti(1993), Gavezzotti and Filippini(1994)] to model organic crystal structures with the computationally simple functional form of an exp-6 potential, with the interaction between atom i in one molecule, and atom j in

Table 4.1: **Crystallographic and thermodynamic data and the corresponding references for the investigated compounds.**

Compound	T/K[a]	Z	SG	a/
ϵ-CL [Winkler and Dunitz(1975)]	295	8	C2/c	19.
HMT [Kampermann et al.(1995)Kampermann, Sabine, Craven, and Mcmullan]	15	2	I$\bar{4}$3m	6.
PE [Semmingsen(1988)]	295	2	I$\bar{4}$	6.
β-SA [Leviel et al.(1981)Leviel, Auvert, and Savariault]	77	2	P21/c	5.
urea [Swaminathan et al.(1984)Swaminathan, Craven, Spackman, and Stewart]	12	2	P$\bar{4}$21m	5.

[a]Temperature of structure determination

Table 4.2: **Summary of the different model potentials.**

Label	Electrostatic	Repulsion-Dispersion
GF	—	exp-6 [Filippini and Gavezzotti(1993), Gavezzotti and Filippini(19
CVFF	empirical atomic charges	LJ [Hagler et al.(1979)Hagler, Dauber, and Lifson]
CGLJ	ab initio atomic charges	LJ [Hagler et al.(1979)Hagler, Dauber, and Lifson]
CGEX	ab initio atomic charges	exp-6 [Williams and Cox(1984), Coombes et al.(1996)Coombes, P
DMEX	ab initio atomic multipoles	exp-6 [Williams and Cox(1984), Coombes et al.(1996)Coombes, P

another, separated by a distance r_{ij}, having the form:

$$V_{ij} = A_{ij} \exp\left(-Br_{ij}\right) - C_{ij} r_{ij}^{-6} \tag{4.1}$$

Thus the electrostatic interactions are absorbed into the repulsion-dispersion parameters. To allow this a separate set of exp-6 parameters has to be determined for each possible pair of atom types.

The **Consistent Valence Force-field, CVFF**, is part of the OFF module of the commercial molecular modelling package *Cerius*^{2}[Mol(1999)] and is widely used in indus-

trial morphology prediction. The non-bonded energy part of the CVFF potential is the form most commonly used in Molecular Mechanics force-fields. It comprises a Lennard-Jones (LJ) type expression for the repulsion-dispersion part of the potential whereas the electrostatic interactions are approximated by the assigning partial charges q_i to each atomic site:

$$V_{ij} = A_{ij} r_{ij}^{-12} - B_{ij} r_{ij}^{-6} + \frac{q_i q_j}{r_{ij}} \tag{4.2}$$

For the compounds investigated here, the CVFF parameters are essentially those of the force-field for amino-acids derived by Hagler and Lifson [Hagler et al.(1974)Hagler, Euler, and Lifson, Hagler et al.(1979)Hagler, Dauber, and Lifson] by fitting to crystal structures and sublimation energies of amides and carboxylic acids. The partial charges for the CVFF force-field are calculated using so called *bond increments* as implemented in *Cerius*^{2}.[Mol(1999)]

A more accurate method of describing the electrostatic interactions is to use atomic charges derived from the ab initio charge distribution of the molecule. Electrostatic potential derived (ESPD) charges are determined by minimising the least-squares difference between the quantum mechanical electrostatic potential, calculated ab initio, and the potential generated from the atomic partial charges, on some points on a grid located around the van der Waals surface of the molecule. For this task the CHELPG algorithm [Chirlian and Francl(1987), Breneman and Wiberg(1990)] as implemented in Gaussian98 [M. J. Frisch et al.(1998)] is used here. The required electronic structure calculations are performed with Gaussian98 at the second order Moller-Plesset (MP2) level with the 6-31G++ basis set. The resulting ESPD atomic charges are combined with the same Lennard-Jones repulsion dispersion potential as used in the CVFF model, to give **CGLJ model**.

In order to assess the importance of the way the repulsion-dispersion interactions are represented, the ESPD charges are also combined with an exp-6 potential, which has been developed for crystal structure modelling by empirical fit-

ting in conjunction with realistic electrostatic models. For the **CGEX model**, the empirical parameters used for the exp-6 potential are those fitted to azahydrocarbon crystal structures by Williams [Williams and Cox(1984)]. The parameters required to describe hydrogen bonding protons are taken from the extension to this set, H(-N) [Coombes et al.(1996)Coombes, Price, Willock, and Leslie] and H(-O) [Beyer and Price(2000)], which were fitted to compounds with N-H $\cdots$ O=C/N hydrogen bonds and carboxylic acid crystal structures respectively.

DMEX, the most sophisticated model potential used in modelling the crystal structures of polar organic molecules, uses a realistic electrostatic model which represents the charge distribution around each atom as a multipole series. The anisotropic multipole moments represent the electrostatic effects from non-spherical features such as lone pair and π electron density, which can be important in representing the directionality of hydrogen bonding and π-π interactions. The distributed multipole analysis (DMA) used in this study [Stone(1985)] was derived from the same wave-function as the ESPD atomic charge model, by analysing the density matrix using the program GDMA [Stone(1998)]. The electrostatic contribution to the lattice and attachment energies includes all terms in the multipole expansion up to r_{ij}^{-5} thus involving atomic multipoles up to hexadecapole. The DMEX model potential combines the DMA electrostatic model with the same exp-6 model used in CGEX.[Williams and Cox(1984)]

4.2.3 Attachment Energy Calculations

The attachment energy is a well defined quantity. There are, however, different algorithms for its calculation. The programs *Cerius*^{2}[Mol(1999)] and HABIT [Clydesdale et al.(1991)Clydesdale, Docherty, and Roberts] divide the perfect crystal lattice into molecules within and outside of a slice of thickness d_{hkl} parallel to the face (hkl). The summation of the interaction energy between the molecules within the slice provides the slice energy, and the difference between the slice and the lattice energy is twice the attachment energy. The programs ORIENT

[Stone et al.(2000)Stone, Dullweber, Engkvist, Fraschini, Hodges, Meredith, Popelier, and Wales, Engkvist et al.(2000)Engkvist, Price, and Stone] and MARVIN [Rohl and Gay(1996)] build an infinite crystal in two dimensions only, representing each surface. In MARVIN, an additional layer built on top of that surface, which can optionally be relaxed before the attachment energy is calculated directly. In ORIENT, a single nano-crystallite consisting of only one surface unit cell of thickness d_{hkl}, with the same geometry and orientation as in the bulk of the crystal, is placed on the surface in the crystallographic position to give the attachment energy [Stone et al.(2000)Stone, Dullweber, Engkvist, Fraschini, Hodges, Meredith, Popelier, and Wales, Engkvist et al.(2000)Engkvist, Price, and Stone].

If the surface unit cell contains more than one non-equivalent building unit, there may be different attachment energies for a given face depending on where the crystal is cut. In such cases, usually the less negative attachment energy is used in constructing the morphology, since one can assume that the slower growing part of the face will give the dominant contribution to the overall growth velocity.

Attachment energy calculations are performed using ORIENT for the CGEX and DMEX model potentials. The morphology module of *Cerius*^{2} is used for the corresponding calculations with the CGLJ, GF and CVFF model potentials. Care is taken to use the appropriate methodologies in the programs [Mol(1999), Engkvist et al.(2000)Engkvist, Price, and Stone] to account for electrostatic long-range interactions. Finally the calculation and visualisation of the Wulff-plot morphologies corresponding to the attachment energies is done with the morphology module of *Cerius*^{2} [Mol(1999)] as is the calculation of periodic bond chains (PBCs).

4.2.4 Energy Minimisation

The lattice energy minimisations for all the isotropic atom-atom potentials are carried out using the so called *Smart Minimiser* included in *Cerius*^{2}, in which different minimisation algorithms are used, subject to the stage of the minimisation and the steepness of the

Table 4.3: **Errors in reproducing the crystal structures and energies by lattice energy minimisation with different model potentials.** The errors, ΔE, are given in kJ mol^{-1} as the absolute difference between the calculated lattice energy and the experimental enthalpy of sublimation, $\Delta E_{\mathrm{latt}} - \Delta H_{\mathrm{sub}}$. σ is the rms deviation of the lattice parameters a, b and c in percent.

	ϵ-CL		HMT		PE		β-SA		urea	
	ΔE	σ	ΔE	σ	ΔE	σ	ΔE	σ	ΔE	σ
CVFF	0.55	3.53	34.43	0.72	-41.91	3.24	-10.08	1.14	30.92	2.24
GF	-6.53	3.96	22.94	1.59	1.13	4.54	-11.32	1.56	-9.80	7.85
CGLJ	-10.21	2.39	34.43	0.72	35.36	2.96	-43.17	1.40	-0.04	2.93
CGEX	4.68	3.06	4.94	1.15	-6.65	1.33	6.41	1.72	9.03	4.13
DMEX	-18.90	9.88	9.18	1.15	-20.58	2.14	-13.61	1.18	18.37	8.13

energy-gradient. The repulsion-dispersion contribution is summed directly to 30 Å and Ewald summation is used for the electrostatic contribution to the lattice energy. The program DMAREL [Willock et al.(1995)Willock, Price, Leslie, and Catlow] which uses a modified Newton-Raphson algorithm is used for the lattice energy minimisations with the anisotropic atom-atom potential DMEX. The long range electrostatic interactions, up to dipole-dipole, are calculated with the Ewald summation method, and the interactions between higher multipoles and the repulsion-dispersion contributions are directly summed to 15 Å. All lattice energy minimisations start at the experimental structure.

4.3 Results & Discussion

The results of the lattice energy minimisations are summarised in Table 4.3. Many of the reproductions of the crystal structure and lattice energy are well within the accuracy that can be expected in comparing lattice energy minima with finite temperature crystal structures and heats of sublimation. Differences of a few percent in the cell

lengths can be attributed to the neglect of temperature effects on the crystal lattice and molecular structure [Beyer and Price(2000)]. Differences between the experimental lattice energy and the heat of sublimation of less than about $\pm$ 10 kJ mol^{-1} are not significant[Gavezzotti and Filippini(1997)], as these are likely to represent thermodynamic approximations and experimental error. Although not constrained, the space-group symmetry is conserved except for urea with the GF and DMEX force-fields. The small energy lowering for an orthorhombic distortion on lattice energy minimisation may reflect the neglect of zero-point and thermal motions averaging over the two equivalent structures, as well as errors in the model potential [Day et al.(2001)Day, Price, and Leslie]. The worst reproduction is a considerable shearing of the unit cell of the ϵ-caprolactam structure with the DMEX force-field, which corresponds to a volume change of 4.7 %. This shearing is very sensitive to the length of the rigid C-H bonds and the reproduction would be much better with the shorter C-H bonds used in parameterising the potential. All of the force-fields model at least one of the crystal structures within the accuracy of static lattice energy minimisation, and none are satisfactory for all the molecules considered here. However, crystal structure reproduction is a severe test of a force-field, and although there are some serious errors in the lattice energies, morphology calculations only rely on relative attachment energies. Hence, the results in Table 4.3 confirm that all the force-fields might reasonably be considered for use in a morphology modelling study, although all are clearly limited in accuracy by the neglect of polarisation and the other assumptions made in their derivation.

4.3.1 Theoretical Morphologies

A BFDH analysis is carried out for each of the compounds and only those faces with the larger interplanar distances d_{hkl} were used. The threshold value for d_{hkl}, below which the faces are no longer considered, is chosen to be at a natural break in the d_{hkl} values and so that the retained faces include all the experimentally observed faces, as shown in Table 4.4.

Table 4.4: **Analysis of faces in terms of interplanar spacings (d_{hkl} in Å).** The Miller indices of experimentally observed faces are given in bold font. For each compound only faces above the horizontal bar are considered in the calculations of attachment energies. The type of face, T, indicates whether a given face is flat (F) or not (x).

ϵ-CL			PE			β-SA			urea			HMT		
hkl	d_{hkl}	T	*hkl*	d_{hkl}	T	*hkl*	d_{hkl}	T	*hkl*	d_{hkl}	T	*hkl*	d_{hkl}	T
200	8.91	F	**101**	4.99	F	**100**	5.46	F	**001**	4.68	F	**110**	4.90	F
110	7.13	F	**002**	4.37	F	**110**	4.63	x	**110**	3.94	F	200	3.46	x
11$\bar{1}$	6.02	F	110	4.30	F	**020**	4.38	F	101	3.58	x	21$\bar{1}$	2.83	x
111	5.18	x	112	3.07	x	**011**	4.34	F	**111**	3.01	x	310	2.19	x
31$\bar{1}$	4.82	x	200	3.04	x	11$\bar{1}$	3.48	x	200	2.78	x	22$\bar{2}$	2.00	x
20$\bar{2}$	4.75	x	103	2.63	x	120	3.42	x	210	2.49	x	420	1.55	x
310	4.72	x	211	2.60	x	**111**	3.32	F	201	2.39	x	44$\bar{2}$	1.15	x
002	4.42	F	22$\bar{2}$	1.93	x	021	3.29	x	21$\bar{1}$	2.20	x	62$\bar{2}$	1.04	x
11$\bar{2}$	4.05	x	20$\bar{4}$	1.77	x	12$\bar{1}$	2.87	x	102	2.16				
40$\bar{2}$	3.99	x	40$\bar{2}$	1.44	x	121	2.77	x	112	2.01				

Also indicated is which faces have two periodic bond chains and so can be considered to be F-faces by Hartman-Perdok analysis. All molecules whose interaction with a neighbour is more stable than -10 kJ mol^{-1}, calculated with the GF force-field are considered as bonds for the subsequent Hartman-Perdok analysis. This is an ad hoc energy cutoff, and since the designation of F-faces depends quite sensitively on the value of this threshold, I emphasise that this analysis is merely indicative.

Generally the attachment energies of a given face obtained with the various model potentials differ considerably, as do the lattice energies; as an example, the attachment energies calculated for pentaerythritol are given in Table 4.5. Since the MI of a face is determined by its relative rather than by the absolute attachment energy, these differences are not necessarily reflected in the resulting morphologies.

Table 4.5: **Attachment energies of pentaerythritol faces** in units of kJ/mol unitcells; obtained with different model potentials.

hkl	CVFF	GF	CGLJ	DMEX	CGEX
101	-61.46	-83.14	-96.50	-82.74	-82.12
002	-42.72	-53.76	-44.12	-38.10	-40.42
110	-89.08	-125.23	-152.67	-129.57	-127.72
112	-98.91	-137.15	-162.98	-137.68	-136.50
200	-79.91	-106.36	-115.90	-105.07	-98.43

Hexamethylene Tetramine

The predicted morphologies of hexamethylene tetramine match the experimental habit, in which only {110} faces are observed [Davey and Rütti(1976)] for all the model potentials. The BFDH algorithm gives the same correct result. This can be ascribed to the unusual high symmetry of the unit cell ($I\bar{4}3m$) as well as of the molecule itself. There are only two different sets of equivalent faces with $|h| + |k| + |l| < 4$, namely {110} and {200}. Since higher indexed faces are usually rough due to geometric reasons alone, only these two faces are candidates for the crystal habit. The molecules have a shape very close to spherical and there are no polar groups on their surfaces. Thus the intermolecular interactions within the crystal are not directional and any kinetic effects on the growth velocity can be assumed to be isotropic for all faces. The same reasoning applies to the influence of any solvent. Thus by far the greatest effect on the morphology can be ascribed to energetic differences between the faces. The attachment energy for the {200} faces is at least fifty percent greater in magnitude than for the {110} faces for all the model potentials. Approximately the same ratio is found for the interplanar spacings d_{hkl} of the two sets of faces. Thus the resulting habit shows {110} faces only no matter which force-field is used. The difference of the ratio between the two attachment energies of the {110} and {200} faces does not exceed five percent for any pair a model potentials, although

Figure 4.2: **Experimental (vapour grown) and calculated morphologies** of ϵ-caprolactam (left) and β-succinic acid (right).

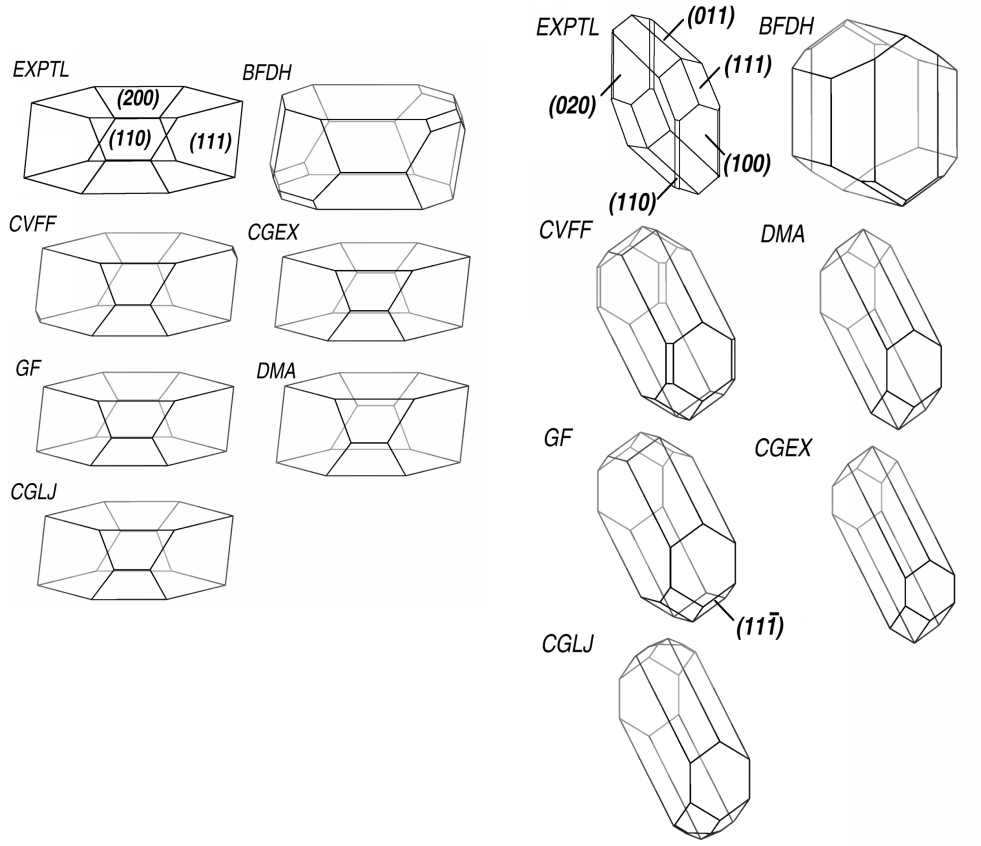

there are considerable differences in the absolute values. Thus, the influence of geometric factors is so overwhelming for hexamethylene tetramine that almost any force-field would predict the correct morphology.

ϵ-Caprolactam

The experimental habit of vapour grown ϵ-caprolactam [Walker et al.(1998)Walker, Roberts, and Maginn] is contrasted with the results of the theoretical predictions in Figure 4.2. The growth morphologies predicted by the attachment energies all reproduce the shape of the vapour grown crystal [Walker et al.(1998)Walker, Roberts, and Maginn], independent of

the model potential used. The BFDH model predicts additional faces which are not observed. There are only small quantitative differences between the five attachment energy morphologies. The aspect ratio between the {200} and the {111} faces varies somewhat but these differences are probably too small to provide any evidence for assessing the quality of the model potentials.

Essentially the same morphology of ϵ-caprolactam was predicted by Walker et al. [Walker et al.(1998)Walker, Roberts, and Maginn] from attachment energies calculated using the DREIDING force-field [Mayo et al.(1990)Mayo, Olafson, and Goddard] combined with partial charges obtained with the charge equilibration method [Rappe and Goddard(1991)]. Geertman and Heijden [Geertman and Vanderheijden(1992)] predicted the growth of small additional faces. They calculated attachment energies treating the ϵ-caprolactam growth unit to be the dimer as well as the monomer units used here. The habits resulting from their monomer calculations show $\{\bar{2}02\}$ and $\{\bar{3}\bar{1}1\}$ faces whereas results of the dimer-calculations predict the growth of $\{20\bar{1}\}$ faces, but generally predicted the experimental morphology better. These calculations used a force-field which combined an exp-6 potential with parameters of undefined origin with Mulliken charges obtained from a semi-empirical (PM3) charge density. The differences between their and our results may be due to the differences in the model potentials used.

β-Succinic Acid

None of the theoretical predictions for β-succinic acid matches the experimental morphology [Berkovitch-Yellin(1985)] exactly, as shown in Figure 4.2. There is not a single calculated morphology that shows all the experimental faces and only these. However, DMEX and CGEX, the force-fields that can be expected to provide the best description of the intermolecular interactions, give rather similar morphologies, that differ somewhat from the experimental structure as well as from the structures predicted with the BFDH algorithm and the GF, CGLJ and CVFF force-fields. The differences between the the experimental

morphology and the theoretical results obtained with the DMEX, CGLJ and CGEX force-fields may be due to shortcomings in the attachment energy model instead of weaknesses of the model potentials. This assumption is confirmed by published results of the β-succinic acid morphology [Berkovitch-Yellin(1985)] obtained with yet another model potential (LJ-parameters of Hagler and Lifson [Hagler et al.(1979)Hagler, Dauber, and Lifson] combined with multipoles up to quadrupole derived from deformation density maps obtained from X-ray diffraction data). These predicted β-succinic acid habits show the same deficiencies as the better force-fields used here, namely that the $\{100\}$ faces are too big while the $\{011\}$ faces are too small. All the model potentials used here, while generally giving somewhat different results, incorrectly predict the growth of the $\{11\bar{1}\}$ family of faces. The two strong hydrogen bonds found in β-succinic acid crystals, and therefore most periodic bond chains, are perpendicular to this face. This is confirmed by a PBC analysis (Table 4.4): $\{11\bar{1}\}$ is not an F-face and thus, according to Hartman-Perdok theory the attachment energy, is not appropriate as a measure for its growth rate.

Two other published theoretical morphologies of β-succinic acid [Rohl and Gay(1996), Docherty and Roberts(1988)] obtained with the CVFF and the Hagler and Lifson force-fields make essentially the same morphological predictions. These force-fields all have essentially the same parameters for β-succinic acid and hence the similarities in the calculated habits. The only appreciable difference between these results and our predictions is that the published predictions did not properly consider the $\{11\bar{1}\}$ faces.

Urea

The experimental habit of vapour grown urea and theoretical predictions are shown in Figure 4.3. The BFDH prediction is very poor, but all attachment energy calculations correctly predict that the morphology is dominated by the $\{001\}$ and $\{110\}$ faces. The experimental aspect ratio of "ca 1.5" determined by Docherty et al.[Docherty et al.(1993)Docherty, Roberts, Saunders, Black, and Davey], is rather smaller than that suggested by the growth rates for the $< 001 >$ and $< 110 >$

Figure 4.3: **Experimental (vapour grown) and calculated morphologies** of urea (left); experimental (from aqueous solution) and calculated morphologies of pentaerythritol (right).

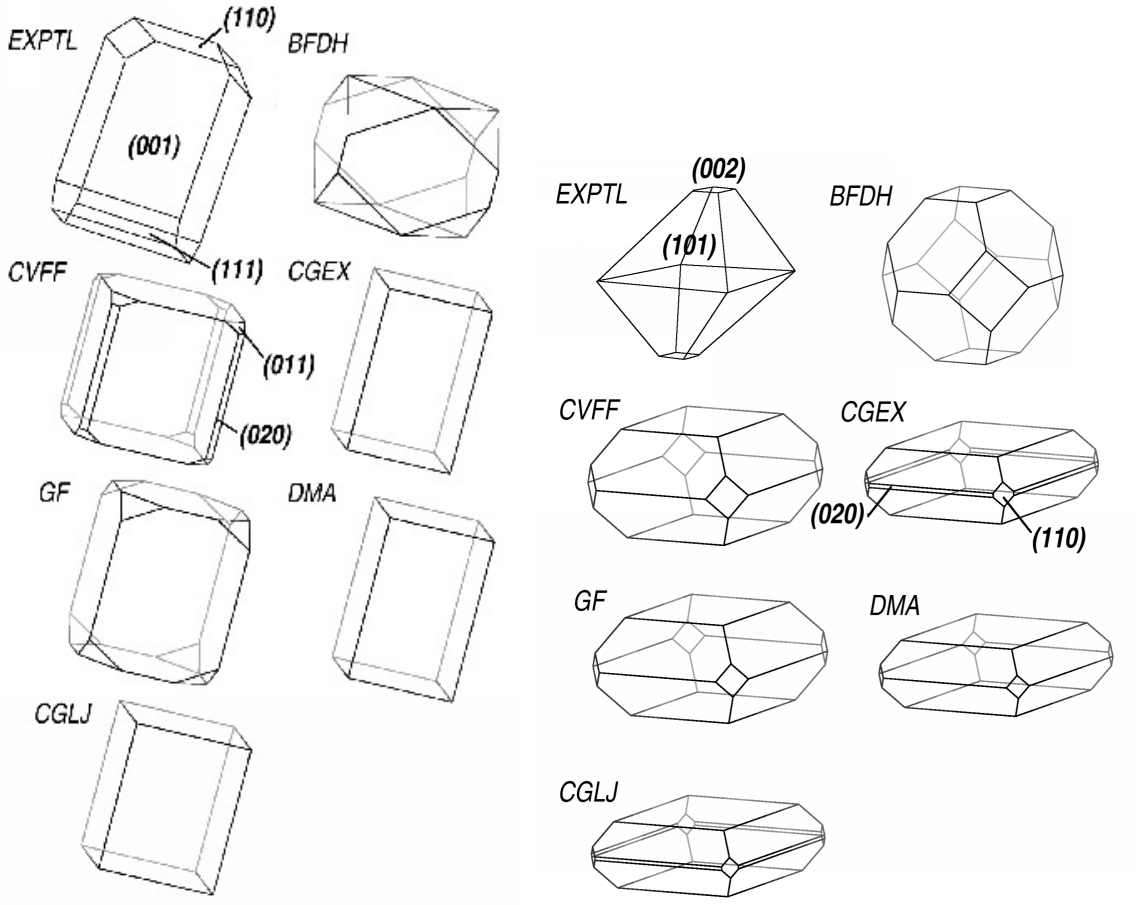

directions reported by Feigelson et al.[Feigelson et al.(1985)Feigelson, Route, and Kao]. However, the aspect ratio is probably very sensitive to the conditions used, as when urea crystals are grown from pure aqueous solutions the aspect ratio can exceed 50:1. [Davey et al.(1986)Davey, Fila, and J.] Thus, although there is some variation in the ratio between the attachment energies $E_{att}(001)/E_{att}(110)$, all the attachment energy predictions are probably within experimental variations, and all the force-fields are satisfactory in this respect.

The experimental morphology also shows small {111} faces [Docherty et al.(1993)Docherty, Roberts, Saunders, Black, and Davey]. These are polar cap facets, that show that growth velocities in the $< 111 >$ and in the $< \bar{1}\bar{1}\bar{1} >$ directions are not equal, to the extent that only one of these faces is observed. Various reasons have been put forward to explain the polar cap facets [Docherty et al.(1993)Docherty, Roberts, Saunders, Black, and Davey, George et al.(1995)George, Harris, Rohl, and Gay, Engkvist et al.(2000)Engkvist, Price, and Stone], as the attachment energy model cannot predict such polar effects on crystal habits by definition.

The attachment energy model predicts some additional faces for the CVFF and GF force-fields. The morphological importance of the {101} set of faces for the GF and CVFF force-fields, and the {200} set of faces with the CVFF force-field is comparatively small. The attachment energy for these faces is just below the appearance threshold for most of the other force-fields. All the habits predicted with force-fields which have an ab initio based electrostatic model (the CGLJ, CGEX and the DMEX potentials) are qualitatively equivalent, differing only in the aspect ratio. The case of urea demonstrates once more that deficiencies in the morphological predictions are more due to shortcomings in the attachment energy model than in the potential models.

Pentaerythritol

The calculated habits for pentaerythritol are shown in Figure 4.3, along with the morphology for crystals grown in aqueous solution [Su et al.(1992)Su, Li, Pan, Wu, and Yang] which is the only experimental morphology available. The strong influence of polar solvents on the morphology of crystals therefore limits the comparisons that can be made. The growth of the two most prominent sets of faces ({001} and {101}) is correctly predicted with all models including the BFDH algorithm. Attachment energy calculations with all force-fields result in poor predictions for the aspect ratio, the relative morphological importance of the {001} and the {101} faces. All force-fields incorrectly predict the

growth of {110} faces, and the CGLJ and CGEX force-fields also predict small {200} faces, which are also not observed in the experimental habit for the solution grown crystals.

The large difference between the attachment energy predictions of the aspect ratio and the experimental morphology when grown from aqueous solution certainly reflects the influence of the solvent. The {001} and {101} faces of pentaerythritol have totally different surface structures, with the (101) face providing a high density of polar sites in contact with the solution, while the (001) face is covered with relatively non-polar aliphatic residues.

Thus, the major shortcoming in the predictions is from the lack of inclusion of solvent effects in the the attachment energy model, and, relative to this, the variations due to changes in the force-field are negligible.

4.4 Conclusions

A range of various model potentials was used to calculate attachment energies of five different organic crystals. In most cases the usage of different force-fields results only in minor differences for the habits predicted with the attachment energy model, with qualitative and often reasonable quantitative agreement between the more rigorously derived force-fields, despite considerable variations in the absolute values of the attachment energies.

While theoretical and experimental vapour-grown morphologies agree for hexamethylene tetramine and ϵ-caprolactam, in other cases there are significant discrepancies between the experimental and the set of theoretical habits. In the case of succinic acid, the attachment energy predicts the appearance of a small face that is not observed, because it is not a flat F-face, and so the attachment energy growth rate is an inappropriate underestimate. Urea shows polar facets, and the known morphology of pentaerythritol is likely to be considerably affected by solvent, two effects that cannot be included in attachment energy predictions.

Recently, a number of new, more accurate and more elaborate methods for the

theoretical prediction of crystal morphologies have been developed [Vandervoort(1991), Liu et al.(1995)Liu, Boek, Briels, and Bennema, Winn and Doherty(1998)], which try to include the habit modifying effect of solvents and impurities. Such simulations will be much more sensitive to the model potential used, particularly to the balance between the solute-solute and solute-solvent interactions. The type of variations in morphology with force-field seen in this study will be more significant when more realistic methods of predicting morphologies are established.

Hence one can conclude that theoretical morphologies as calculated with the attachment energy model are relatively insensitive to the model potential used. Any theoretically reasonable potential, that gives a satisfactory reproduction of the crystal structure and lattice energy, is likely to predict the crystal morphology as well as can be expected within the limitations of the attachment energy model. Nevertheless, the attachment energy model has been shown to be a considerable improvement on the BFDH method. In all cases, the attachment energy model gives a useful estimation of the morphology, suitable for chemical engineering, or for eliminating poorly growing hypothetical crystal structures in crystal structure prediction. [Beyer et al.(2001)Beyer, Day, and Price]

Chapter 5

Force Field Parameterisation for Potash Alum

5.1 Introduction

In this chapter a classical interaction model potential for potash alum, $KAl(SO_4)_2 \cdot 12\,H_2O$ is derived and tested. In Chapter 7 of this thesis this force field will be used to investigate the structure of potash alum surfaces in contact with aqueous solution. Thus we must aim to construct a forcefield that provides a good representation of the intermolecular interactions in the crystal, in the aqueous solution and their balance at the critical interface. With the advent of more powerful computers and more efficient algorithms, most theoretical studies on inorganic and/or ionic systems nowadays use density functional theory [Gonze et al.(2002)Gonze, Beuken, Caracas, Detraux, Fuchs, Rignanese, Sindic, Verstraete, Zerah, Jol or periodic Hartree-Fock [Dovesi et al.(2000)Dovesi, Orlando, Roetti, Pisani, and Saunders], methods that take quantum mechanical effects explicitly in account. Here we want to obtain information about the dynamics of the system performing Molecular Dynamics simulations of comparatively large systems (several thousands of atoms). The system-size and time-scales involved in these calculations forbid the usage of *ab initio* methods and we must therefore use a classical model potential. Most of the work on classical

(semi-)empirical force fields published so far concentrates on modelling of organic molecules and bio-molecular systems. Although a substantial amount of work has been done modeling inorganic and ionic materials the methods and results have been treated rather stepmotherly in comparison. Force field parameters for some of the components of potash alum and their interactions are available in the literature, but a comprehensive model for this material has not been devised yet. One difficulty when modelling inorganic materials with classical model potentials is that the degree of transferability of the force field parameters is normally very limited. Thus a model potential has to be re-parameterised for each new material, for example, the parameters of a Cl-Cl Lennard Jones potential would be different for KCl and NaCl. The character of organic molecules allows a natural separation into bonding and non-bonding interactions. This separation is frequently not possible for inorganic materials. Due to the higher charge densities found particularly in ionic systems molecular interactions are often dominated by polarisation and charge transfer effects, features whose representation with classical model potentials is not a straight forward task. Models to simulate polarisation (see Section 3.3.2), such as the shell model, do exist, but so far these models have been mainly parameterised and applied for static lattice energy minimisations. It has not been shown clearly whether they comprise a reliable concept for Molecular Dynamics simulations of ionic materials. It could be suspected that the consideration of polarisability is of particular importance when establishing the structure of a solution above a surfaces, i.e., in a highly anisotropic system, but some of the results published so far are controversial. Yeh et al. found [Yeh and Berkowitz(2000)] the differences in the results obtained with a polarisable and a non-polarisable water model when simulating the structure of water upon a surface to be negligible. Oyen et al. simulated an aqueous sodium chloride solution at the NaCl (001) interface [Oyen and Hentschke(2002)] and found different adsorption behaviour of ions on the surface with polarisable and non-polarisable water models respectively. Hence, the explicit inclusion of polarisability into the model may be important, in particular when simulating surfaces. However, since the according algorithms increase the computational effort considerably we try to manage with a rigid

Figure 5.1: **Ball and stick model of the content of the potash alum unit cell**; atom types are identified by colours: green: K, magenta: Al, red: O, white: H, yellow: S

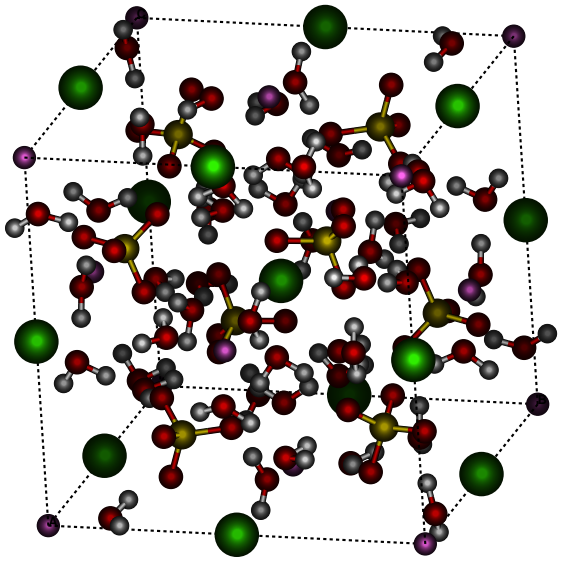

ion potential. By requiring the force field to fulfill a number of rather stringent criteria, as detailed below, we expect it to provide a reasonable approximation for describing the structural features of potash alum solution interfaces.

5.2 The Material

The cubic unit cell of potash alum (space-group $Pa\bar{3}$) contains four formula units $KAl(SO_4)_2 \cdot 12$ (see Figure 5.1). The lattice parameter is 12.157 Å. The structure of the potash alum unit cell has so far only been determined with X-ray diffraction [Larson and Cromer(1967)]. Therefore the positions of the hydrogen atoms in the unit cell are not known. To get a reasonable estimate of the structure including the hydrogen atoms for comparison with our calculated results we use the hydrogen positions in an $NH_4Al(SO_4)_2 \cdot 12$ unit cell as determined by neutron diffraction. [Larson and Cromer(1967)] Since potash alum and $NH_4Al(SO_4)_2 \cdot 12$ not only have

the same space group but also nearly identical lattice parameters the hydrogen positions obtained by superimposing the two lattices give a reasonable first estimate. The structure obtained thus is further refined by keeping the positions of all atoms in the potash alum unit cell apart from the hydrogens fixed while minimising the energy of the unit cell. The oxygen-hydrogen distance and the bond-angles in the water molecules are thereby constrained to the values used in the water model that we use in our simulations. Any difference between the hydrogen positions resulting from this procedure and the experimental structure is probably much smaller than the uncertainty of positions obtained by neutron diffraction.

A distinctive feature of potash alum is a particular type of local crystal disorder observed at finite temperatures.[Sakuntala et al.(2000)Sakuntala, Akhilesh, Chandra Shekar, and Sahu] As shown in Figure 5.2 each sulfate anion can be found in one of two different orientations, A and B. The resulting *dynamical disorder* varies with temperature and pressure. According to X-Ray data between 70 and 90 percent of the sulfate groups are to be found in orientation A under ambient conditions [Sakuntala et al.(2000)Sakuntala, Akhilesh, Chandra Shekar, and Sahu].

The potash alum unit cell contains a large number of crystal waters. The force field parameters will have to be tuned accurately to prevent the crystal from turning into a liquid at elevated temperatures. Reproducing the solid state of the material and the correct proportion of disordered sulfated ions at room temperature is an arduous task as shown below. However, once these features are properly reproduced in a simulation one can be confident that the force field is also able to model other properties of the material with a reasonable degree of accuracy.

5.3 The Model Potential

The functional forms commonly used for classical empirical model potentials have already been outlined in Section 3.3.2. Here we give only a short summary of the of the energy

Figure 5.2: **The two possible orientations of the sulfate anions in potash alum**. Each sulfate bounces back and forth between the two orientations with a high frequency. At room temperature on average between 10 and 30 % of the sulfate ions are found in the energetically less favourable orientation A.

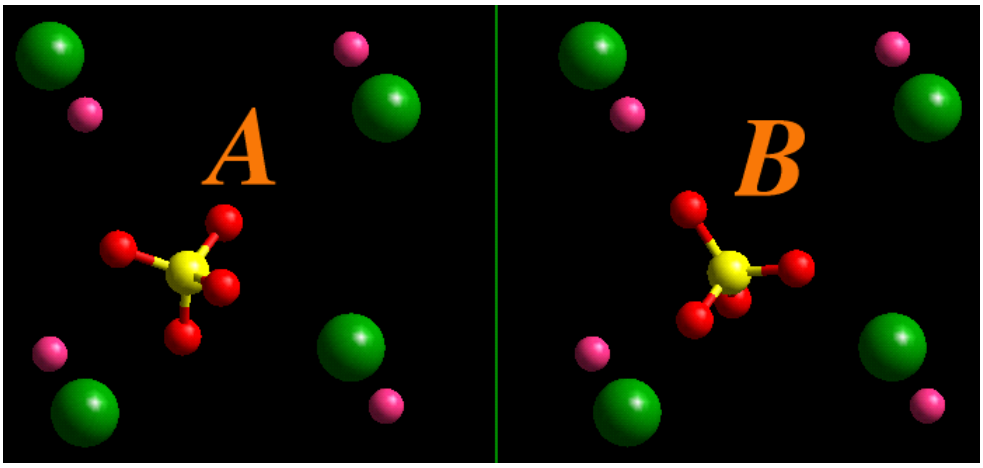

expression we use for potash alum. Following most of the work published on the modelling of inorganic materials we use a Lennard Jones and/or Buckingham potentials (Eqns. 3.20 and 3.19) to describe the van der Waals interactions between the atomic sites and a simple Coulomb term (eqn. 3.22) to account for the electrostatic interactions. For the ions we use nominal charges while for the oxygen atoms in the water and the sulfate groups partial charges are adjusted to account for the polarisation in an average manner. While the water molecules are kept rigid the intramolecular degrees of freedom of the sulfate groups are described by Morse (bond stretching, Eqn. 3.24) and harmonic potentials (bond angle bending, Eqn. 3.25).

For the sake of consistency we model the water-water and the water-ion interactions within the crystal and in the solution with the same model potentials. The polarisation and thereby higher electrostatic moments of the water molecules might differ somewhat in the crystal and the solution. However, if we look at the structure of the water in the crystal we see that it forms two hex-aquo complexes with the K^+ and Al^{3+} cations. The structures of these complexes can be expected to be quite similar to the corresponding

ions with their first solvation shell in an aqueous solution. In fact we can view the potash alum crystal as "frozen" and super saturated aqueous solution of $KAl(SO_4)_2$. Therefore we expect that a non-polarisable water model with parameters fitted to reproduce the crystal structure can also be used for the simulation of the solution and vice versa.

5.4 The Strategy

The parameters A_{ij}, C_{ij}, etc in equations 3.20 - 3.24 have to be determined so that experimental properties of the simulated compound are reproduced to a certain accuracy. The following criteria are used for fitting the parameters:

- Reproduction of the crystal structure of PA upon lattice energy minimisation.
- Reproduction of the elastic constants of PA upon lattice energy minimisation.
- Reproduction of the crystal structure of PA at ambient conditions (300 K, 1 atm).
- Reproduction of structure of $[SO_4(H_2O)_6]^{2-}$ and $[Al(H_2O)_6]^{3+}$ clusters as derived from high level ab initio calculations

In addition to these criteria we also require the force field to give reasonable structures of the three anhydrates $K_2(SO_4)$, $Al_2(SO_4)_3$ and $KAl(SO_4)_2$ upon lattice energy minimisation. This last criterion ensures a certain degree of transferability of the potential. This is important because with a model potential as simple as the one used here one could possibly find parameters that, on the one hand side, seem to reproduce certain properties of the material reasonably well while being, on the other hand side, physically not reasonable and providing useless results for properties that have not (yet) been tested. This danger is reduced if we can show that the obtained parameters can also reproduce the structures of other materials.

The following strategy was adopted to generate the required force field parameters:

1. Use parameters published previously for similar substances where ever this appears to be reasonable.

2. Fit the cation-sulfate and sulfate-sulfate interactions as well as the sulfate atomic charges to reproduce the crystal structures of $Al_2(SO_4)_3$, $KAl(SO_4)_2$ and K_2SO_4.

3. fit the water sulfate and water cation interactions to reproduce the crystal structure of potash alum at 0 and 300 K,

4. evaluate the parameter set by simulating aqueous solutions of K_2SO_4 and $Al_2(SO_4)_3$.

5.5 Parameters adopted from the literature

The SPC/E water model: This widely used rigid model provides good results for many properties of liquid water [Berendsen et al.(1987)Berendsen, Grigera, and Straatsma]. It has a considerably higher dipole moment than the isolated water molecule, a feature that can, at least partially, make up for the missing polarisability.

Intramolecular parameters for SO_4^{2-}: Morse and harmonic potential parameters for S-O bond stretching and O-S-O angle bending were fitted by Allen et al.[Allan et al.(1993)Allan, Rohl, Gay, Catlow, Davey, and Mackrodt] to reproduce crystal structures of a range of different sulfates of mono and divalent cations.

K^+-H_2O VdW parameters: Borodin et al.[Borodin et al.(2001)Borodin, Bell, Li, Bedrov, and Smith] fitted Buckingham potential parameters to reproduce structures of a range of different K^+-SPC/E water clusters minimised at the MP2 level with large basis sets.

Apart from the water-water interactions these parameters were merely used as initial values in the fitting procedure and some of them are different in the final version of the force field.

Table 5.1: **Results of parameter fitting** for K_2SO_4, $Al_2(SO_4)_3$ and $KAl(SO_4)_2$ and the transferable parameters (in units of eV and Å)

atom types	pot.-type	parameter values		
		K_2SO_4, (PKS)		
K-O_S	Buckingham	A = 1400.4462	ρ = 0.2971	C = 0.0
O_S-O_S	Lennard Jones	ϵ = 6.74e-03	σ = 3.30	
O_S-S-O_S	harmonic	k_a = 15.0	α_0 = 109.47°	
S-O_S	Morse	D = 5.0	β = 1.2	b_0 = 1.505
O_S	Coulomb	q = -0.8233		
		$Al_2(SO_4)_3$, (PAS)		
Al-O_S	Buckingham	A = 1000.08	ρ = 0.238359	C = 0.0
O_S-O_S	Buckingham	A = 123535.8	ρ = 0.20	C = 25.98
O_S-S-O_S	harmonic	k_a = 15.0	α_0 = 109.47°	
S-O_S	Morse	D = 50.0	β = 9.2	b_0 = 1.505
O_S	Coulomb	q = -1.30		
		$KAl(SO_4)_2$, (PKAS)		
Al-O_S	Buckingham	A = 900.0	ρ = 0.27	C = 0.0
K-O_S	Buckingham	A = 1560.47	ρ = 0.287925	C = 0.0
O_S-O_S	Buckingham	A = 103585.02	ρ = 0.18	C = 25.98
O_S-S-O_S	harmonic	k_a = 15.0	α_0 = 109.47°	
S-O_S	Morse	D = 5.0	β = 1.2	b_0 = 1.4392
O_S	Coulomb	q = -1.1		
		transferable parameters, (PTR)		
Al-O_S	Buckingham	A = 1000.0	ρ = 0.2670	C = 0.0
K-O_S	Buckingham	A = 2121.0	ρ = 0.2924	C = 2.8422e+03
O_S-O_S	Lennard-Jones	ϵ = 1.4113e-02	σ = 2.798	
O_S-S-O_S	harmonic	k_a = 15.0	α_0 = 109.47°	
S-O_S	Morse	D = 5.0	β = 1.2	b_0 = 1.505
O_S	Coulomb	q = -1.05		

Table 5.2: **Results of lattice energy minimisations**; For each material the experimental lattice parameters (in Å) and the volume of the unit cell are given. Deviations from the experimental values are given in percent for each of the parameter sets given in Table 5.1.

	K_2SO_4			$Al_2(SO_4)_3$			$KAl(SO_4)_2$		
	exptl	PKS	PTR	exptl	PAS	PTR	exptl	PKAS	PTR
a	5.723	+0.54	+2.14	8.025	+0.64	+1.34	4.71	-0.06	+4.26
b	9.999	-0.22	-0.69	8.025	+0.64	+1.34	4.71	-0.06	+4.26
c	7.422	-0.20	-1.95	21.357	+0.05	-2.64	8.01	-0.63	+0.03
V	424.7	+0.12	-0.54	1191.1	+1.34	-0.01	153.9	-0.76	+8.74

5.6 Results

5.6.1 The Anhydrates

Before trying to get a transferable model potential for K_2SO_4, $Al_2(SO_4)_3$ and $KAl(SO_4)_2$ we optimise the forcefield parameters for each of the compounds separately. The resulting parameters are given in Table 5.1 and the results of lattice energy minimisations with these parameters are given in Table 5.2. The differences between experimental and calculated lattice parameters and unit cell volumes are very reasonable, i.e. small, for all three of the compounds. The average and the largest deviation from the experimental value are 0.44 and 1.34 % respectively. However, these good results are only obtained with quite different sets of forcefield parameters. The van der Waals parameters of the sulfate-sulfate interactions and the charge on the sulfur oxygen as well as the the stiffness and equilibrium length of the S-O bond vary considerably. These differences are presumably due to the different valence, ranging from I to III, of the involved cat-ions, resulting in considerable differences in the magnitude and orientation of the polarisation of the sulfate ion. It is questionable whether the involved modifications of the sulfate electronic structure could be modelled decisively better with a simple shell model for the oxygens because it is

unclear whether the polarisability of the whole sulfate molecule can be modelled as a superposition of four (or five) isotropic polarisabilities on the included atoms. The charge of -2 e on the sulfate ion cannot be considered as localised on any of the atomic sites. The whereabouts of the corresponding charge density will probably depend very sensitively on the positions of the surrounding ions. Especially for those compounds containing Al(III) not only polarisation but also a certain amount of charge transfer takes place. Hence the formal charges for the ions used here will not provide a realistic description of the system — a drawback which cannot be compensated for by using a shell model but rather by an appropriate modification of the parameters for the van der Waals interactions. An alternative way to cope with the problems sketched above would be the usage of a variable-charge model [Martin and K.(1981), Ghosez et al.(1998)Ghosez, Michenaud, and Gonze, Gale(2000)]. Since, however, we do not have any MD-software that includes such a model and we would have to reparametrise the whole force field from scratch we do not consider this method here.

Given the points made above it is not surprising that the generation of a transferable set of interaction parameters for the compounds considered here turns out to be quite arduous a task. As partial charge for the sulfate oxygen we use -1.05 e, the approximate mean of the values obtained in the course of the parameter fitting for the separate compounds. This value we consider as a reasonable approximation since it is quite close to values for the same atomic site given in previously published forcefields (CVFF[Mol(1999)], OPLS[Cannon et al.(1994)Cannon, Pettitt, and Mccammon]). For the intramolecular potential (bond stretching and angle bending) parameters for the sulfate ion we use those published by Allen et al.[Allan et al.(1993)Allan, Rohl, Gay, Catlow, Davey, and Mackrodt] since no modification of these parameters results in better minimised structures for all three compounds. The attempt to use GULP[Gale(1997)] for fitting the van der Waals parameters for the sulfate-sulfate and the different sulfate-cation interactions in a concerted fashion fails because for virtually all the calculations the resulting parameters scarcely differ from the input values, i.e., usually the attempted optimisations get stuck in local minima very

close to the starting points. Thus we go for a brute force method, minimising the lattice energy for all three compounds using all possible combinations of a range of different values for the van der Waals parameters. The best five or so of the resulting parameter sets are further optimised *manually* resulting in the final transferable parameters as given in Table 5.1. In Table 5.2 the results of the lattice energy minimisations for the three different compounds with the transferable parameters are opposed to the results obtained when using the parameters fitted for each compound separately. Not surprisingly the transferable force field (PTR) performs worse than the individually fitted parameter sets for all three of the materials. While the highest deviation from cell parameters and cell volume for K_2SO_4 and $Al_2(SO_4)_3$ is 2.64 % the cell volume of $KAl(SO_4)_2$ calculated here is 8.74 % larger than its experimental value. Nevertheless the transferable parameters are are expected to be good enough for our purposes since 1) The minimisations were done without space group constraints in all cases and the symmetry was conserved throughout. 2) The results for K_2SO_4 and $Al_2(SO_4)_3$ are reasonable. 3) The cause of the poor result for $KAl(SO_4)_2$ is irrelevant for the system of interest (potash alum crystal and solution) because here the highly charged Al^{3+} cation is always shielded by a water layer. (The experimental rate constant for the exchange of water molecules in the $Al(OH_2)_6^{3+}$ complex is 1.29 s [Rudolph et al.(2000)Rudolph, Mason, and Pye] and, as shown below, the proposed force field provides a good representation of the $Al(OH_2)_6^{3+}$ complex)

5.6.2 Potash Alum Parameters

Only after the derivation of interaction parameters for the ionic components with some degree of transferability as described in the previous section we attempt to parameterise the crucial water-ion interactions to complete the force-field for potash alum. For the water-water non-bonded interactions and the geometry of the water we use the well known and thoroughly tested SPC/E water model[Berendsen et al.(1987)Berendsen, Grigera, and Straatsma]. In a first attempt the ion-water interactions are derived by fitting parameters to reproduce the experimental

Table 5.3: **The final parameter set for potash alum** (units: eV, Åand e).

atom types	pot.-type		param
O_W-O_W	Lennard-Jones	ϵ = 6.727e-03	σ =
O_W-O_S	Lennard-Jones	ϵ = 6.727e-03	σ =
O_S-O_S	Lennard-Jones	ϵ = 1.411e-02	σ =
Al-O_S	Buckingham	A = 1000.0	ρ =
Al-O_W	Buckingham	A = 1000.0	ρ =
K-O_S	Buckingham	A = 2121.0	ρ =
K-O_W	Buckingham	A = 2121.0	ρ =
O_S-S-O_S	harmonic	k_b = 15.0	α_0 =
S-O_S	Morse	D = 5.0	β =

atomic charges	
q(O_W) = -0.8476 [Berendsen et al.(1987)Berendsen, Grigera, and Straatsma]	q(H) = 0.4238
q(O_S) = -1.05[Allan et al.(1993)Allan, Rohl, Gay, Catlow, Davey, and Mackrodt]	q(Al) = 3.0

crystal structure and elastic constants using the GULP[Gale(1997)] software. Additionally we try fitting the parameters to reproduce the structures of $[Al(OH_6)]^{3+}$ and $[SO_4(OH_6)]^{2-}$ clusters which have been published as a result of high level ab initio calculations [Rudolph et al.(2000)Rudolph, Mason, and Pye, Pye and Rudolph(2001)]. The resulting parameter set turns out to give good results upon lattice energy minimisation. However, when modelling the material at 300 K and a pressure of zero Pascal in an NPT Molecular Dynamics simulation the obtained parameters lead to *melting* of the crystal. In an extensive procedure guided to a minor degree by chemical intuition and to a larger one by trial and error the parameters are further optimised and fine-tuned. The final parameter set, henceforth referred to as PAFF, is given in Table 5.3. In the following

Table 5.4: **Results of lattice energy minimisations of potash alum.**

	exp	minim.	Δ[%]		exp	minim.	Δ[%]
Lattice parameters / Å				Elastic constants / 10^{11} Dyn/cm^2			
a/Å	12.157	12.096	-0.50	e_{11}	2.47	4.88	+98
b/Å	12.157	12.096	-0.50	e_{12}	1.03	1.61	+56
c/Å	12.157	12.096	-0.50	e_{44}	0.87	1.01	+16
V/Å^3	1796.7	1769.8	-1.50				
Average distance between selected atom types / Å							
O1-S	1.4830	1.4601	-1.544	O2-Al	1.9077	1.8968	-0.571
O1-O1	2.4213	2.3840	-1.540	O2-O1	2.6830	2.5999	-3.097
O2-K	2.9825	2.9926	+0.339	O2-O2	2.6666	2.6646	-0.075

sections various results obtained with PAFF are presented and compared to experiment.

5.6.3 Structure

In Table 5.4 results are given of lattice energy minimisation of potash alum with PAFF and compared to experimental values. The results are quite satisfactory apart from the elastic constants. The latter, however, are supposed to be larger as a result of theoretical calculations than as obtained in experiment because in real crystals we usually find defects such as vacancies, grain boundaries, etc. while the theoretical model corresponds to a perfect crystal. The size of the variation between the simulated perfect and the "real" elastic properties depends on material, measurement conditions, etc. Here we consider it sufficient to get elastic constants that are positive and preferably larger (0-100%) than the experimental values. The structures of $[Al(H_2O)_6]^{3+}$ and $[SO_4(H_2O)_6]^{2-}$ clusters after energy minimisation using our force field are shown in Figure 5.3. The aluminium-oxygen distance of 1.946 Å in the $[Al(H_2O)_6]^{3+}$ cluster ob-

Figure 5.3: **The structures of ion-water complexes** obtained with our force field (PAFF). The calculated geometries are compared to experimental results (exp) and ab-initio calculations (ai); a) distance between aluminium ion and water oxygens, b) distance between sulfate and water oxygens

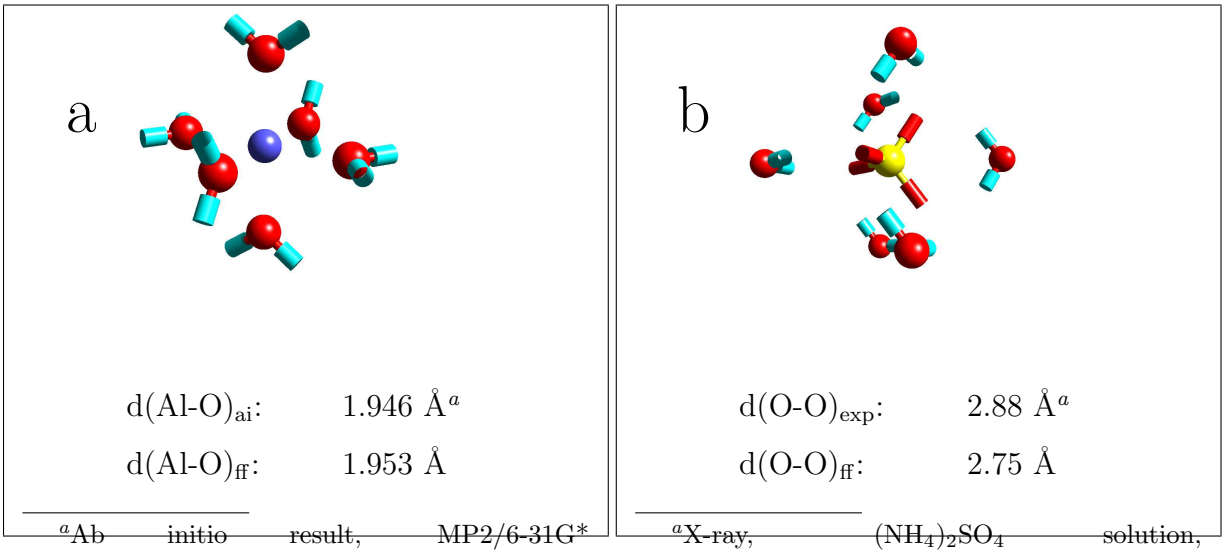

tained with our force field compares well with the result of high level ab initio calculations [Rudolph et al.(2000)Rudolph, Mason, and Pye] (1.953 Å). The distance calculated here between sulfate and water oxygens in the $[SO_4(H_2O)_6]^{2-}$ cluster is 2.75 Å. The only value for this distance we found in the literature is somewhat higher with 2.88 Å. This reference value, however, is an experimental value as obtained for the complex in solution at 298 K. Thus the difference between the two distances can be attributed to the thermal motion. Here we not only scrutinise the model by performing lattice energy minimisations of potash alum but also MD simulations of the crystal at finite temperatures. For this task we use the MD-program DL_POLY [Smith and Forester(1996)]. A super-cell of $2 \times 2 \times 2$ unit cells of the experimental crystal structure is built and used as starting configuration. Electrostatic long range interactions are accounted for with the Ewald Summation method while the VdW interactions are included up to a cutoff distance of 12 Å. The pressure is held constant at zero Pascal using an isotropic Nose-Hoover type baro-state with a relaxation time constant of one pico second.[Hoover(1985)] Temperature is held

constant at 300 Kelvin with a Nose-Hoover thermostat and a relaxation time constant of 0.1 pico seconds.[Hoover(1985)]

The average lattice parameter obtained with MD simulation of the crystal at 300 K and zero pressure is 12.185 Å which is only 0.2 % larger than the experimental value [Larson and Cromer(1967)]. The crystal structure at ambient conditions is well conserved as can be seen by comparing the calculated radial distribution functions as shown in Figure 5.4. The first maxima of the pair correlation functions coincide generally quite well with the *experimental* values, shown as delta functions. The small deviations in pcfs including sulfate oxygens are mainly due to the the orientational disorder of the sulfate groups.

5.6.4 Local Disorder

For quantifying the degree of disorder we define the order parameter

$$\mathrm{O}_{PA} = \frac{\mathrm{N_A}}{\mathrm{N_A} + \mathrm{N_B}} \tag{5.1}$$

where $\mathrm{N_A}$ and $\mathrm{N_B}$ are the average numbers of sulfate ions per unit-cell in the A and B orientation, respectively. With the force field proposed here MD simulation at 300 K and zero pressure gives a degree of disorder of $\mathrm{O}_{PA} \approx 0.95$. This is slightly larger than the experimental value but considering the high uncertainty of the experimental value still acceptable. Here we also present one result obtained for PA at a pressure of 1 GPa. In Figure 5.5 we show the value of O_{PA} obtained in the course of an MD simulation at 1 GPa and 300 K. After about 40 ps there is complete disorder, i.e., on average half of the sulfate ions are to be found in either orientation. On the rigth hand side of Figure 5.5 we see a snapshot of the simulated crystal at t=55 ps. While there is no order in the sulfate orientations the metal atoms are still ordered and close to their ideal lattice positions. In an interesting paper by Sakuntala et al.[Sakuntala et al.(2000)Sakuntala, Akhilesh, Chandra Shekar, and Sahu] the authors find that depending on the initial degree of orientational disorder the potash alum crystal undergoes different solid-solid phase transitions at elevated pressures. Crystals with low

Figure 5.4: **Radial distribution functions** obtained for various pairs of atom types in an MD simulation of potash alum at 300 K. The average structure at this temperature as obtained with X-ray diffraction in experiment is indicated by delta functions

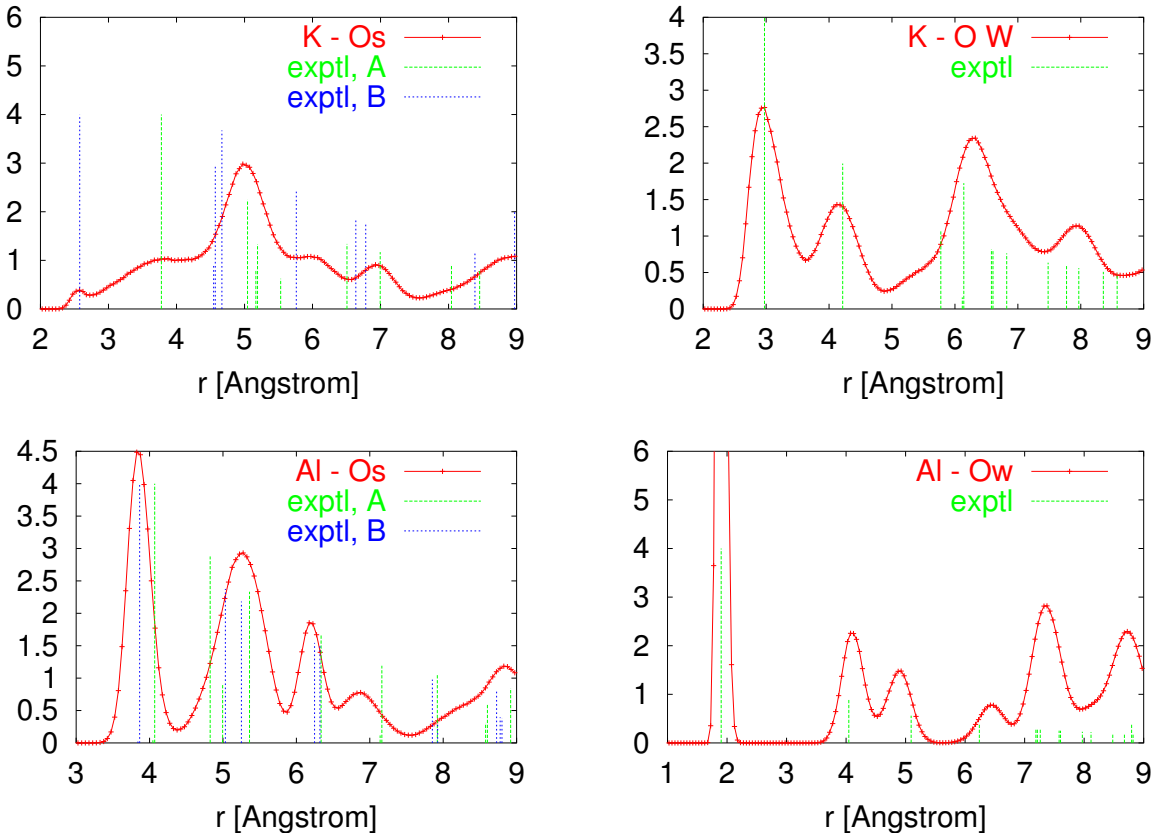

degree of initial disorder ($O_{PA} \approx 0.9$) undergo structural transformation to a disorder-free phase at 1.5 GPa irreversibly while samples with high degree of initial disorder ($O_{PA} \approx 0.75$) remain in the cubic phase and subsequently become amorphous upon further pressurising. As a future project it would be interesting to explore whether our force field can reproduce the phase diagram of potash alum at higher pressures.

5.6.5 Aqueous Solutions

In the following we show results of MD simulations of aqueous solutions of K_2SO_4 and $Al_2(SO_4)_3$. The simulated systems contained eight K_2SO_4 in 436 H_2O and eight $Al_2(SO_4)_3$

Figure 5.5: **Potash alum sample at a pressure of 1 GPa and a temperature of 300 K**; left: time development of the order parameter for the sulfate orientation; right: snapshot of the simulation cell after 55 ps.

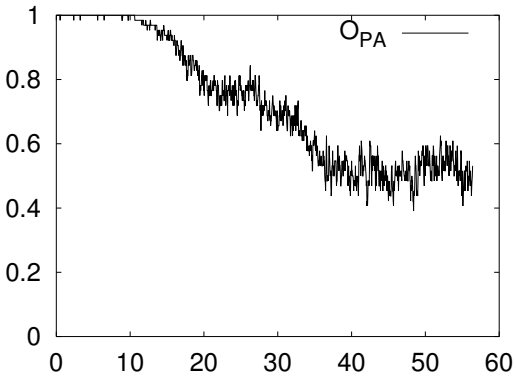

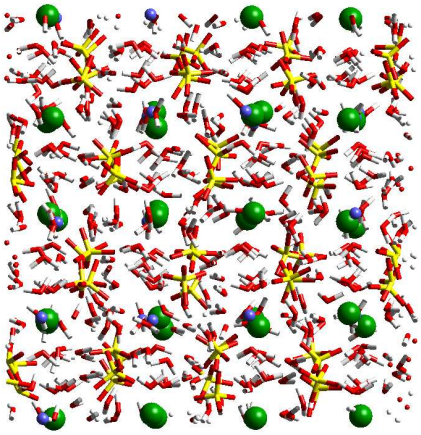

in 800 H_2O respectively. Pressure and temperature were held constant with Nose Hoover baro- and thermostats [Hoover(1985)] at zero Pa and 300 K respectively. The structural data given in Table 5.5 looks satisfactory. The average radius of the first solvation shell for the different ionic species was taken to be the the distance of the first maximum of the corresponding radial distribution function from the origin. The resulting values are in good agreement with experimental values. The average number of water molecules in the first solvation shell are only given for the sake of completeness since here the experimental values tend to be inaccurate and hard to interpret. It was mentioned above that the potash alum crystal can be seen as a highly super-saturated and frozen solution of $KAl(SO_4)_2$. This assumption is confirmed by the data in Table 5.5 and the radial distribution functions between the various components in the $Al_2(SO_4)_3$ and K_2SO_4 solutions shown in Figure 5.6. The first maxima of the distribution functions are for

Table 5.5: **Radii of solvation shells (<>, in Å) and diffusion coefficients** (D, in $10^{-9}m^2/s$) obtained in MD simulations of K_2SO_4 and $Al_2(SO_4)_3$ solutions at 300 K.

	MD	exptl.	ref.		MD	exptl
			K_2SO_4			$Al_2($
$\langle K - O_W \rangle$	2.74	2.79	[Marcus(1988)]	$\langle Al - O_W \rangle$	1.91	1.90
$\langle O_S - O_W \rangle$	2.68	2.79	[Caminiti et al.(1979)Caminiti, G., and G.]	D (Al^{3+})	0.82	
$\langle S - O_W \rangle$ /	3.71	3.7-3.9	[Ohtaki and Radnai(1993)]			
coord. no. (K^+)	6.7	6-7	[Marcus(1988)]			
coord. no. (SO_4^{2-})	12.8	6-14	[Ohtaki and Radnai(1993)]			
D (K^+)	1.4	2.0	[McCall and Douglas(1965)]			

K^+-O(SO_4^{2-}): 2.67 Å(solution), 2.6 Å(crystal); for Al^{3+}-O(SO_4^{2-}): 1.6, 3.9 Å(solution), 3.8,4.05 Å(crystal). In the Al^{3+}-O(SO_4^{2-}) distribution function we find contact ion pairs with an Al^{3+}-O(SO_4^{2-}) distance of only 1.6 Å. This is encouraging because the occurrence of contact pairs between aluminium and an-ions in aqueous solutions is generally not found with other an-ions such as ClO_4^-, Cl^- or NO_3^- but was confirmed experimentally for SO_4^{2-}. [Rudolph et al.(2000)Rudolph, Mason, and Pye]

5.7 Summary

We have developed a classical empirical model potential, PAFF, for potash alum and its aqueous solution. The force field is to some extent transferable and gives reasonable results for the crystal structures of the various anhydrates. The crystal structure of potash alum is well reproduced at both zero and 300 K. We could also reproduce the partial orientational disorder of the sulfate ions and some structural and dynamical properties of the aqueous solutions. Non withstanding the simple form of this force field we have found to provide reasonably good results for a range of properties of the material. Thus

Figure 5.6: **Radial distribution functions** between the components of $Al_2(SO_4)_3$ (top) and K_2SO_4 (bottom) aqueous solutions; O_W: water oxygen, O_S sulfate oxygen.

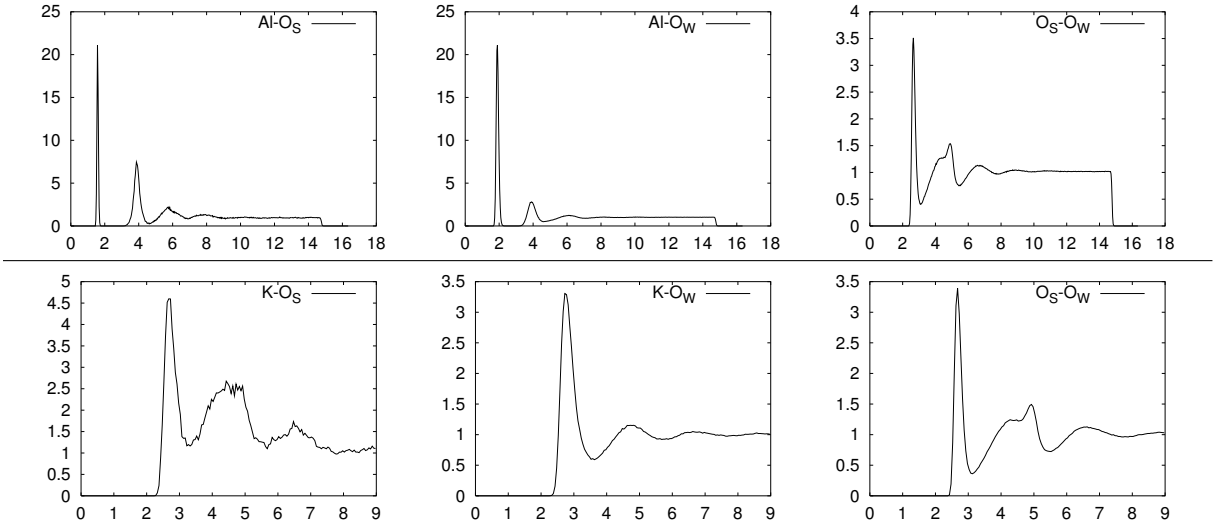

we expect it to be accurate enough to give a realistic model of the solid liquid interface between potash alum and its aqueous solution as modelled in Section 7.

Chapter 6

Electrostatic Long Range Interactions in 2D-periodic Systems

For systems periodic in two dimensions the summation methods discussed in Section 3.6.1 have only been tested for a small range of materials and geometries. There is no comprehensive analysis to be found in the literature, particularly for interfaces including a dielectric crystalline material, as used here, Therefore we perform a number of test calculations for a simple two-dimensional model system. We want to establish the best combination of accuracy and computational efficiency for the atomistic simulation of systems of the type considered in the following chapters. In particular we will compare results obtained with Ewald Summation[Allen and Tildesley(1987)] with those obtained with a generalised reaction field (GRF).[Hummer et al.(1994)Hummer, Soumpasis, and Neumann] Both algorithms were originally developed to account for the long range interactions in isotropic systems with periodicity in three dimensions. For such systems GRF was found [Hummer et al.(1994)Hummer, Soumpasis, and Neumann] to produce results for a range of properties of liquid systems that are virtually indistinguishable from those obtained with Ewald Summation, at a notedly lower computational cost. Ewald Summation and the equivalent Smooth Particle Mesh Ewald have been shown to account correctly for long range interactions in systems with periodicity in only two dimensions when cer-

tain precautions are taken. [Yeh and Berkowitz(1999)] Here we investigate whether this can also be achieved with a generalised reaction field. We compare results obtained from Molecular Dynamics simulations of a system consisting of pure water upon a crystal slab of KCl using a number of different ways to account for the electrostatic long range interactions. These include i) simple truncation and shifting of the electrostatic interactions (SHI), ii) tapering the Coulomb potential via a generalised reaction field (GRF), iii) Ewald Summation (EW), iv) Smooth Particle Mesh Ewald (SPME). Each of the methods is used both with and without a dipole correction term (MZ) as explained in Section 3.5.4. EW and SPME are equivalent and give identical results if properly parameterised. We include both methods here to compare their efficiency in terms of the required CPU time.

6.1 Computational Details

Details of the methods used to sum the electrostatic interactions are given in Section 3.5.4. The system we simulate consists of a KCl-slab of varying thickness with the (110) or (100) face exposed to a layer of liquid water. Periodic boundary conditions are applied in the direction parallel to the surface. The length of the simulation cell in the direction perpendicular to the interface, L_z, is chosen so that an empty region of at least 20 Å separates the periodic replicas of the crystal+water slabs. The entire KCl crystal is taken to be rigid, i.e., all ions are constrained to their experimental bulk lattice positions. For modelling the water we use the extended simple point charge model (SPC/E) [Berendsen et al.(1987)Berendsen, Grigera, and Straatsma] which describes the water-water interactions by a combination of a Lennard Jones potential between the oxygen sites and Coulomb interactions between partial charges on the oxygens and hydrogens. For the interactions between water and the crystal components K^+ and Cl^- we also use a combination of Lennard-Jones and Coulomb potentials with a set of parameters devised by Dang et al. and first published in Ref. [Rasaiah and Lynden-bell(2001)]. The temperature is held constant with a Nose-Hoover thermostat [Hoover(1985)] using a relaxation time of 0.1 ps. The time-step used is two femto seconds and all simulations include 40 ps

equilibration and 200 ps production time.

6.2 Results and Discussion

We simulated the system using the four approaches: shifted Coulomb potential, generalised reaction field, Ewald Summation and Smooth Particle Mesh Ewald, each with and without a dipole correction term (indicated by "MZ" attached to the acronym). We also varied the size of the simulation box, the thickness of the crystal slab, the number of water molecules and the Ewald parameters. The simulation parameters used in the test runs are summarised in Table 6.1.

In particular we are interested in the dependence of the liquid structure on the method chosen to account for the long range interactions and on the other parameters that are varied in our simulations. Therefore we calculate and compare radial distribution functions (RDF) between the water oxygens (O-O) and between water and the crystal atoms (O-Cl, O-K). All results for the (110) face are compared with those obtained with the pmz1 and pmz2 parameter sets since it has been shown that Ewald Summation in combination with the dipole correction term gives results that are equivalent to a full 2-D Ewald Summation.[Yeh and Berkowitz(1999), Crozier et al.(2000)Crozier, Rowley, Spohr, and Henderson]

The only difference between ew1 and ew2 are the parameters of the Ewald Summation algorithm. The real and reciprocal space cutoffs and the convergence factor α chosen there correspond to an approximate relative accuracy [Smith and T.R. Forester(2001)] of the calculated forces of 1.0×10^{-6} (ew1) and 5.0×10^{-6} (ew2) respectively. The ewmz simulation is performed with the same relative accuracy as ew2, but here we include a dipole correction term to minimise the electrostatic interactions between the simulation cell content and its periodic replicas in the direction perpendicular to the surface. The O-O, Cl^--O and K^+-O RDFs obtained with ew1, ew2 and ewmz (not shown here) are virtually indistinguishable. Also the average mass and charge density along the z-axes as well as the electrostatic field do not show any clear trend when increasing the accuracy or

Table 6.1: **Geometries and system sizes as used in the calculations.** The top section represents a comparable set of simulations with different methods to account for long range interactions. The bottommost five parameter sets are used for comparing results obtained with different system sizes, numbers of solvent and crystal atoms

label	method[a]	face[b]	N_w[c]	N$\parallel$[d]	N$\dashv$[e]	L_z [f]	α,$\vec{k}_{max}$[g]
shi	SHI	110	356	8	25.1×22.2	67.5	—
shimz	SHIMZ	110	356	8	25.1×22.2	67.5	—
grf	GRF	110	356	8	25.1×22.2	67.5	—
grfmz	GRFMZ	110	356	8	25.1×22.2	67.5	—
ew1	EW	110	356	8	25.1×22.2	67.5	0.35, 6, 6, 12
ew2	EW	110	356	8	25.1×22.2	67.5	0.31, 8, 7, 21
pmz1	SPMEMZ	110	356	8	25.1×22.2	67.5	0.31, 8, 8, 32
pmz2	SPMEMZ	110	623	9	31.1×31.4	67.5	0.31,16,16,32
pmz3	SPMEMZ	100	315	7	22.2×22.2	67.5	0.31, 8, 8, 32
pmz4	SPMEMZ	100	315	7	22.2×22.2	80.1	0.31, 8, 8, 32
pmz5	SPMEMZ	100	315	7	22.2×22.2	120.0	0.31, 8, 8, 64
pmz6	PMEMZ	100	315	11	22.2×22.2	80.1	0.31, 8, 8, 32

[a]Method used to calculate Coulomb interactions, Addition of MZ means that a dipole correction term is included

[b]Miller indices of the crystal surface

[c]Number of water molecules

[d]Number of crystal layers parallel to the surface

[e]Size of the simulation box perpendicular the surface in Å^2

[f]Length of the simulation cell perpendicular to the surface in Å

[g]Parameters for Ewald Summation, α given in Å^{-1}

Figure 6.1: **Radial distribution functions obtained with different treatments of long range interactions**, the labels correspond to those given in Table 6.1; units of the x-axes are Å; since only relative values are relevant here no units are given for the y-axes.

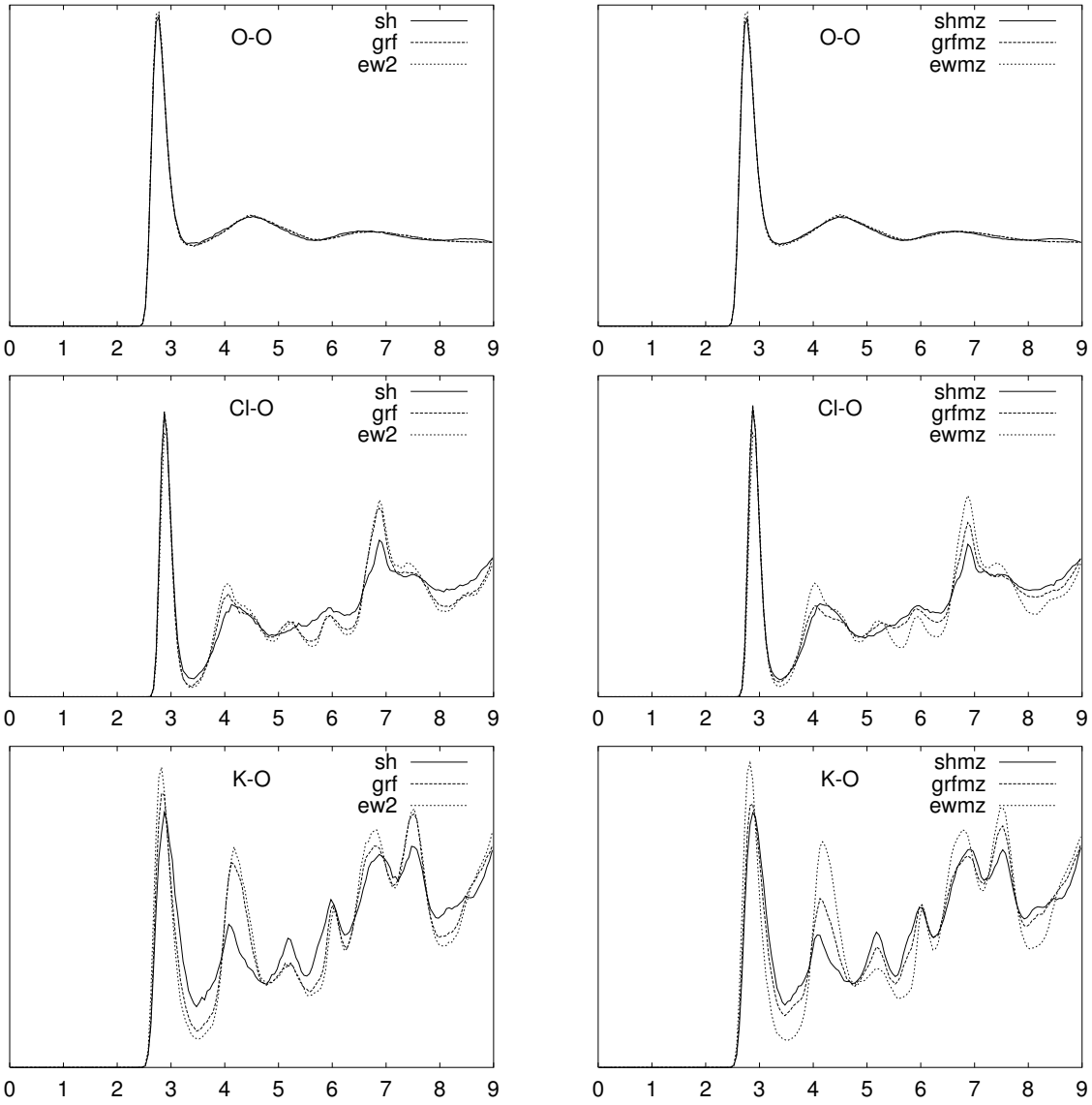

using the dipole correction. This agrees with results of Yeh et al. who found the dipole correction to be crucial only for systems with permanent electric field perpendicular to the surface [Yeh and Berkowitz(1999)]. It also shows that the lower of the two Ewald precisions used here is sufficient to account for the long range interactions in the systems studied here.

If we compare the Cl^--O and K^+-O RDFs for sh, grf and ew2 we can clearly observe differences, as shown in Figure 6.1. The largest deviations from pmz1 we get with shi, the grf result lying in between. The differences are negligible again for the O-O RDFs. For the three methods complemented by the dipole correction (shmz, grfmz, ewmz) we find the same trend. Interestingly enough the grf result is much closer to both ew2 and ewmz, which are virtually identical here, as grfmz.

With the same time-step, temperature, etc. we performed simulations of 315 water molecules upon a 100 KCl surface using SPME combined with MZ only but for different lengths of the simulation box and different numbers of k-vectors for the reciprocal Ewald sum in the z-direction. Results are given in Figures 6.2 and 6.3. The consistency of the results for simulations of the same inter-facial system with an extension in the z-direction ranging from 67 to 120 Å, and a corresponding vacuum between the crystal+water slabs ranging from to 25 to 70 Å, shows that the method used is definitely applicable for the efficient simulation of inter-facial systems. We conclude that for the system geometry used here and with non-polar crystal surfaces, a vacuum slab of 25 Å thickness suffices to effectively mimic a system that is periodic in only two dimensions and confined by an infinite vacuum in the third dimension.

Figure 6.2: **Radial distribution functions obtained with different lengths of the simulation cell**; units of the x-axes are Å; since only relative values are relevant no units are given for the y-axes here.

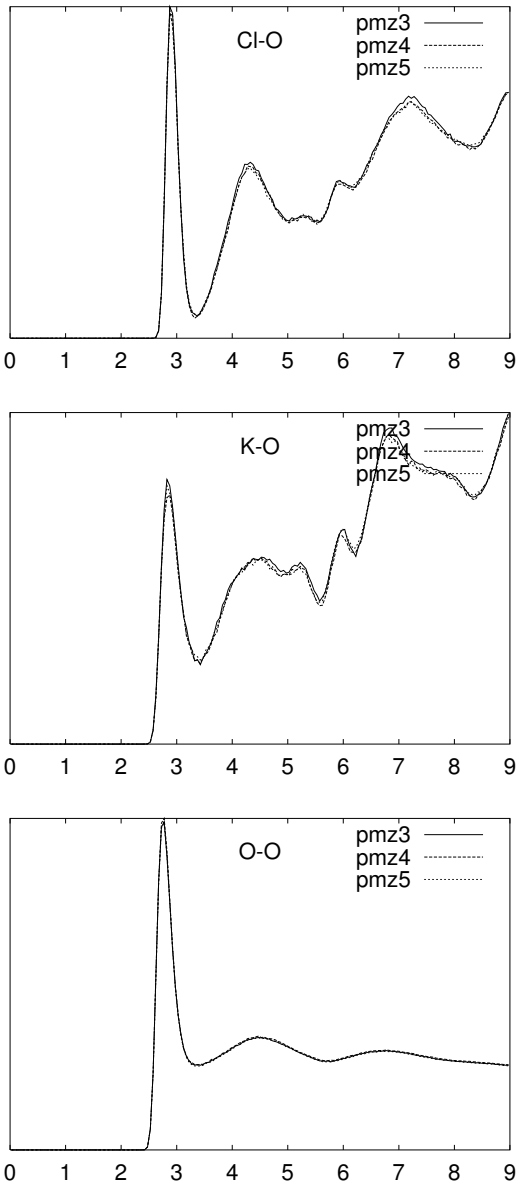

Figure 6.3: **Mass-, charge-density and electrostatic field, φ, in the direction perpendicular to the crystal-water interface for different lengths of the simulation cell**; φ is calculated by numerical integration of the charge-density ρ_q(z). The curves are perfectly co-incident, pmz4 and 5 are off-set for clarity

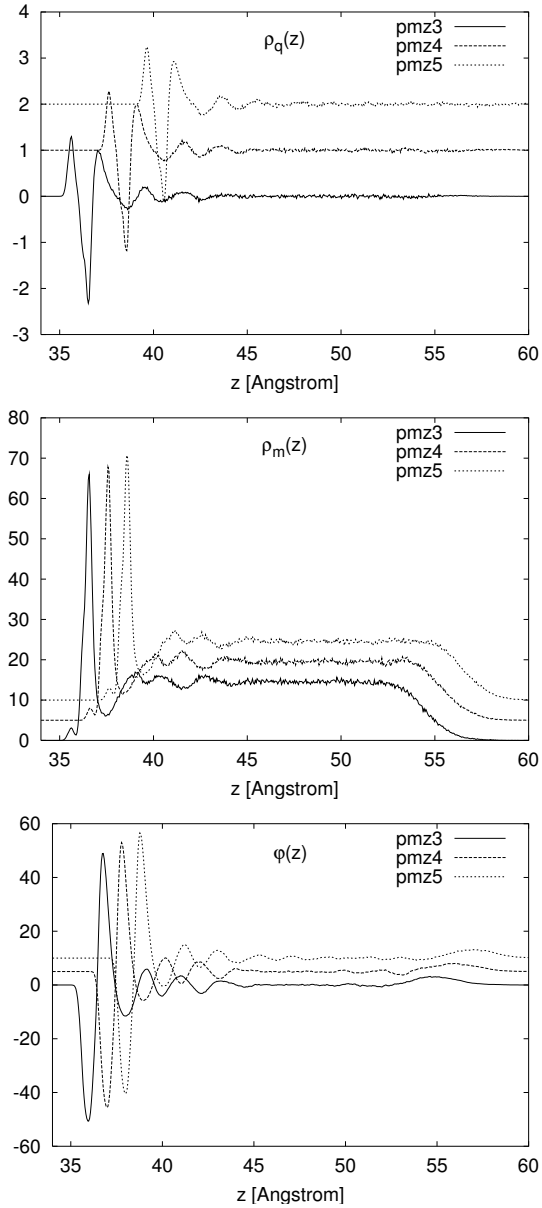

Table 6.2: **Required CPU time for different methods** for calculating long range interactions

method	SHI	GRF	EW	EW	EW	SPME	SPME	SPME
precision $[10^{-6}]^a$			100	5	1	100	5	1
$t_{CPU}^{rel}{}^b$	1.00	1.24	2.34	3.42	3.81	1.82	1.85	1.85

[a]Precision parameter as given in DL_POLYinput for Ewald methods
[b]CPU time required relative to SHI

In Figure 6.4 we compare structural features obtained with the simulations labelled pmz1 and pmz2 in Table 6.1. These results show the effect of increasing the size of the simulation cell in the direction parallel to the surface. In Figure 6.5 we compare results of the simulations labelled pmz4 and pmz6 in Table 6.1. Here we can see the effect of increasing the thickness of the crystal slab in the direction perpendicular to the surface (pmz4: 13.3 Å, pmz6: 22.2 Å). In none of the diagrams shown in Figures 6.4 and 6.5 there are appreciable differences between the two crystal sizes considered. Hence we can draw the straight forward conclusion that the smaller of the two systems is large enough to reproduce features of the infinite surface.

One important aspect of methods for MD simulations is their computational efficiency, i.e., their execution speed. In Table 6.2 we compare the CPU time required on a single processor of an SGI Octane for simulating 200 femto seconds real-time of a crystal water system as described above. The result is not surprising: the smooth particle mesh Ewald algorithm turns out to be a good combination of accuracy and computational efficiency. The generalised reaction field gives similar structural results as obtained with Ewald Summation and is about 30% faster than SPME. Nevertheless we prefer the latter method because its usefulness is well established and the applicability of GRF would have to be shown anew for each different system or geometry.

Figure 6.4: **Mass-, charge-density and electrostatic field in the direction perpendicular to the crystal-water interface**, for $L_x \times L_y = 557.6$ Å^2 (pmz1) and $L_x \times L_y = 975.7$ Å^2 (pmz2); since only relative values are relevant here no units are given for the y-axes.

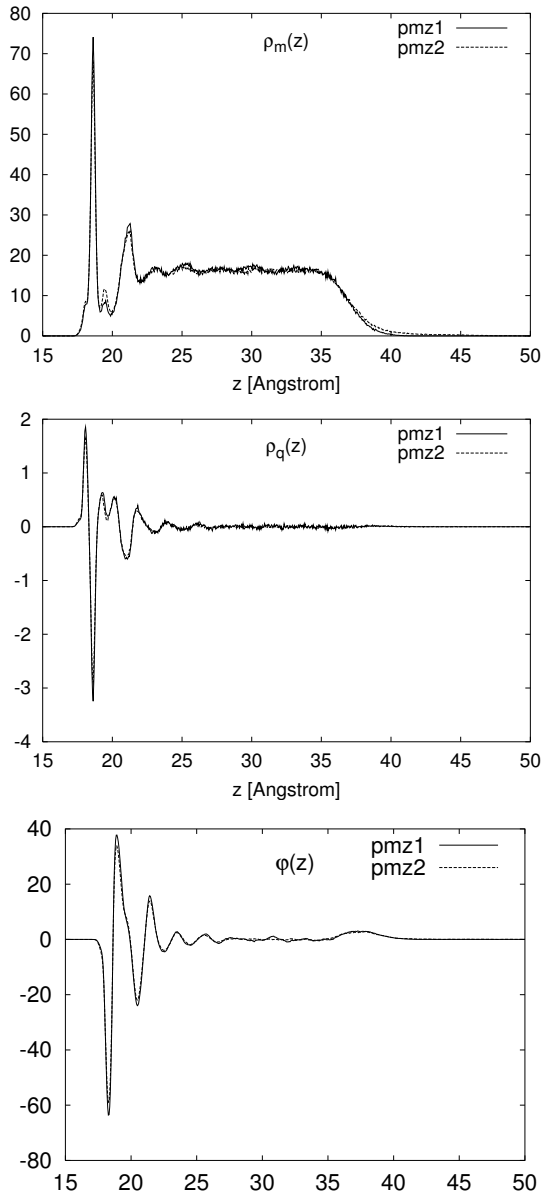

Figure 6.5: **Mass-, charge-density and electrostatic field in the direction perpendicular to the crystal-water interface**, for crystal slabs of 7 (pmz4) and 11 (pmz6) layers; since only relative values are relevant here no units are given for the y-axes.

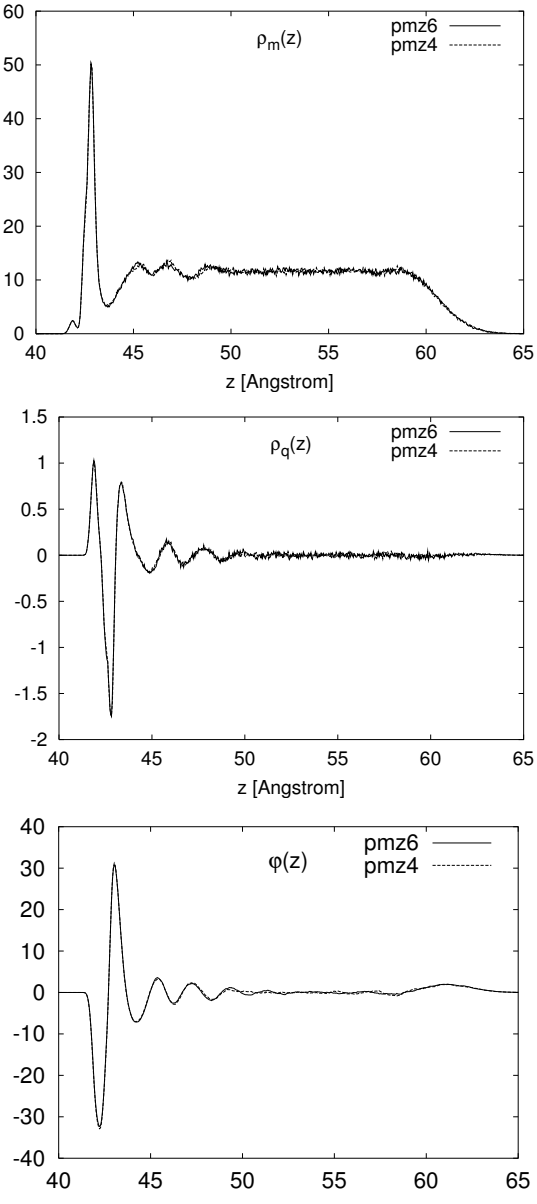

6.3 Summary

We have investigated structural properties of a thin water layer above a KCl crystal slab using a range of system sizes and methods to account for the electrostatic long range interactions in pseudo two dimensional systems. It has been shown before [Yeh and Berkowitz(1999)] that 3D-Ewald Summation with an empty region of sufficient thickness between the slabs can account accurately for the the long range interactions in such a system geometry. The main question here was whether this accuracy can also be achieved with a generalised reaction field, an algorithm that is normally faster than SPME. Indeed the results obtained with a GRF are much closer to the SPME results than those obtained by truncating the Coulomb potential. Nevertheless we find that the best combination between accuracy and efficiency is SPME because GRF turned out to be only about 30% faster. Moreover the physical implication of GRF giving different results for a non-polar system, depending on whether the dipole correction term is applied or not, is unclear. For the particular system studied here a crystal slab of 22.2×22.2×13.3 Å (corresponding to 175 pairs of KCl ions) and a water layer with a thickness of approximately 20 Å (corresponding to 315 H_2O molecules) are sufficient to give results convergent with system size. An empty space of at least 25 Å between two neighbouring periodic replicas of crystal-liquid slabs combined with a relative accuracy of the Ewald Summation of 5.0×10^{-6} can effectively cancel the influence of these periodic replicas on the molecular structure within a liquid layer provided the simulation cell has no permanent dipole moment. In the latter case the undesired interaction with the periodic replicas can be removed very efficiently by applying a dipole correction term as shown by Yeh et al.[Yeh and Berkowitz(1999)]

Chapter 7

The Surface Structure of Potash Alum

7.1 Introduction

Knowledge of the detailed structure of surfaces is of importance in a number of fields including catalysis[Sinfelt(2002)], crystal growth[Vlieg(2002)], separation techniques[Haberlein and Tschiersch(1994)], semi-conductors and industrially applied nano structures.[Talapin et al.(2002)Talapin, Poznyak, Gaponik, Rogach, and Eychmuller] The structure of the involved crystal surfaces is also a prerequisite if we want to accurately determine the forces between two nano crystallites separated by an aqueous solution. Here I will concentrate on potash alum (PA) but I will also try to draw some general conclusions for the theoretical methods of determinating surface structures.

PA crystals in aqueous solution are usually terminated by large (111) and smaller (100) and (110) faces as shown in Figure 7.1. The fact that the PA (111) face is a so-called polar surface results in some difficulties for the determination of its structure, and this problem will be discussed extensively in the following. Both the (111) and the (100) faces of PA have been shown to grow via a screw dislocation mechanism [Vanenckevort et al.(1981)Vanenckevort, Bennema, and Vanderlinden,

Figure 7.1: **Morphology of potash alum crystals**. a) as calculated with the attachment energy method using the model potential derived in Chapter 5; b) as grown from aqueous solution (photograph from Amara et al.[Amara et al.(2001)Amara, Ratsimba, Wilhelm, and Delmas])

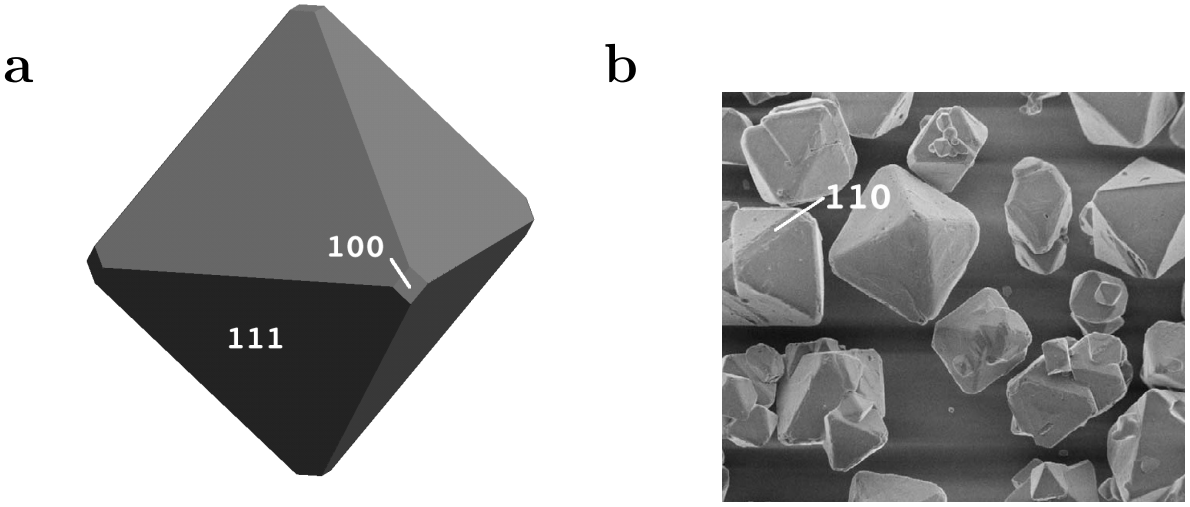

Reyhani et al.(1999)Reyhani, Freij, and Parkinson] (see also Figure 7.2). Therefore we can expect the surface to be flat over large regions. The atomic structure of a crystal unit cell on surfaces is usually different from its counterpart in the bulk crystal. The actual difference between bulk and surface structure can range from a minute relaxation of the atoms in the outermost surface layers due to the anisotropic environment up to a full scale reconstruction.

Neither experimental nor theoretical results for the detailed atomic scale structure of PA surfaces have been published so far. We do, however, know the forces necessary to detach two PA crystallites agglomerated in aqueous solution.[Pratola et al.(2002)Pratola, Simons, and Jones] From these values for different pairs of the growing faces one can draw conclusions about the relative bonding strength between the faces. Since this bonding strength, or *stickiness*, must be largely determined by the atomic scale structure of the surfaces I will try to rationalise the relative strengths of the agglomerative bonds in terms of the surface structure obtained in this study.

Figure 7.2: **Screw dislocation on the (111) face of PA**; the dimensions of this photograph (6×6 μm) suggest that the PA surfaces are flat for approximately 0.2 μm which is the size of about 160 PA unit-cells. (photograph by Reyhani et al. [Reyhani et al.(1999)Reyhani, Freij, and Parkinson])

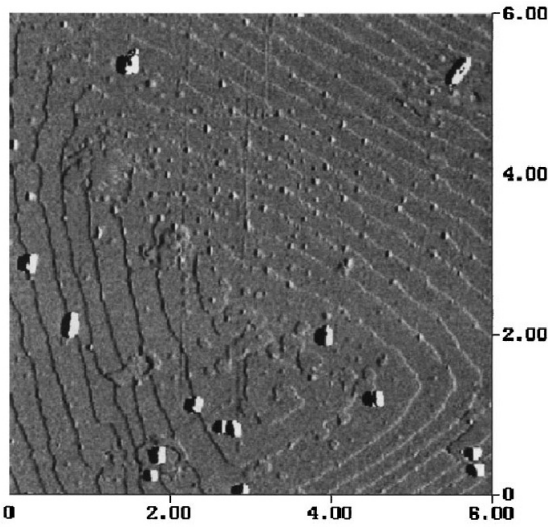

The next section is a brief excursus on the phenomenon of polar crystal surfaces, discussing both theoretical and experimental observations. In Section 7.3 common methods used for the theoretical prediction of surface structures are reviewed, followed by an account of the *ideal* surfaces of PA, as obtained by cleaving the perfect bulk crystal structure in Section 7.4. Section 7.5 summarises some details of the computational methods used here. In Section 7.6 and 7.7 results are presented and discussed, respectively, followed by a summary in Section 7.8.

7.2 Polar Surfaces

Polar surfaces are defined as surfaces with a finite dipole moment perpendicular to the surface plane in the repeat unit. Three fundamental types of surfaces of ionic materials are shown in Figure 7.3. The categorisation (types I-III) was introduced by Tasker [Tasker(1979)]. Both type II and III surfaces have layers with alternating net

Figure 7.3: **Schematical illustration of the different types of surface terminations**. Crystal slabs are shown in side view the dashed line indicating the position of the surface. The repeat unit is indicated by the curly brackets. The dipole moment of the polar surface can be eliminated by reconstructing (rec) or charging (chg) the crystal slab. Versions 1 and 2 of rec and chg will in most cases *not* give the same surface energy.

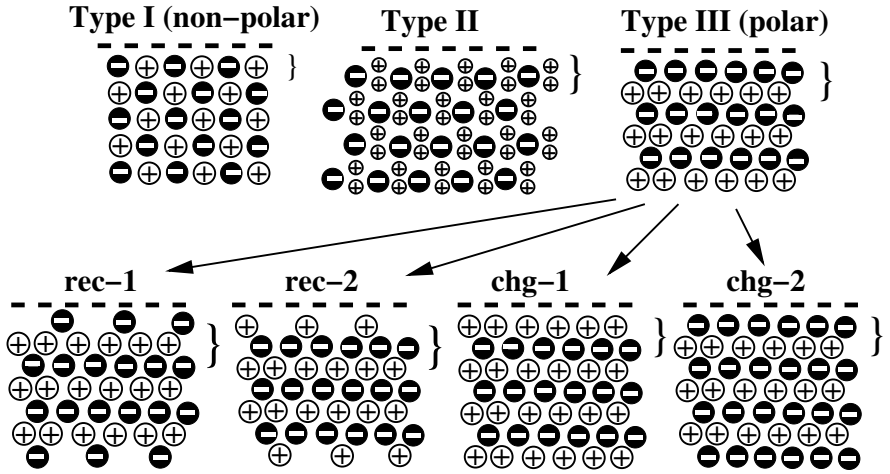

charges perpendicular to the surface but in type II faces the stoichiometric repeat unit can be defined so that a zero net dipole moment results. Tasker argued that a polar or type III surface can not exist on a real crystal because the dipole moment perpendicular to this surface, and therefore also the surface energy, diverges as the crystal grows. He concluded that for all crystals with a theoretical type III surface this surface will reconstruct while growing, ending up as some version of a type II surface (rec-1 and rec-2 in Figure 7.3). However, Taskers statement "They [the polar surfaces] therefore cannot exist as a simple termination of the bulk structure"[Tasker(1979)] is strictly valid only for perfect surfaces in contact with vacuum. For most technologically interesting cases we are facing surfaces in contact with a gas or liquid phase. Here we always have counter ions and/or polar molecules adsorbed onto the surface rendering the system charge neutral again if it was charged in the first place and/or reducing a possible dipole moment. In fact *real* polar surfaces can be stabilised by one out of six mechanisms shown schematically in Figure 7.4, or any combination thereof.

Figure 7.4: **Mechanisms for the stabilisation of polar surfaces**

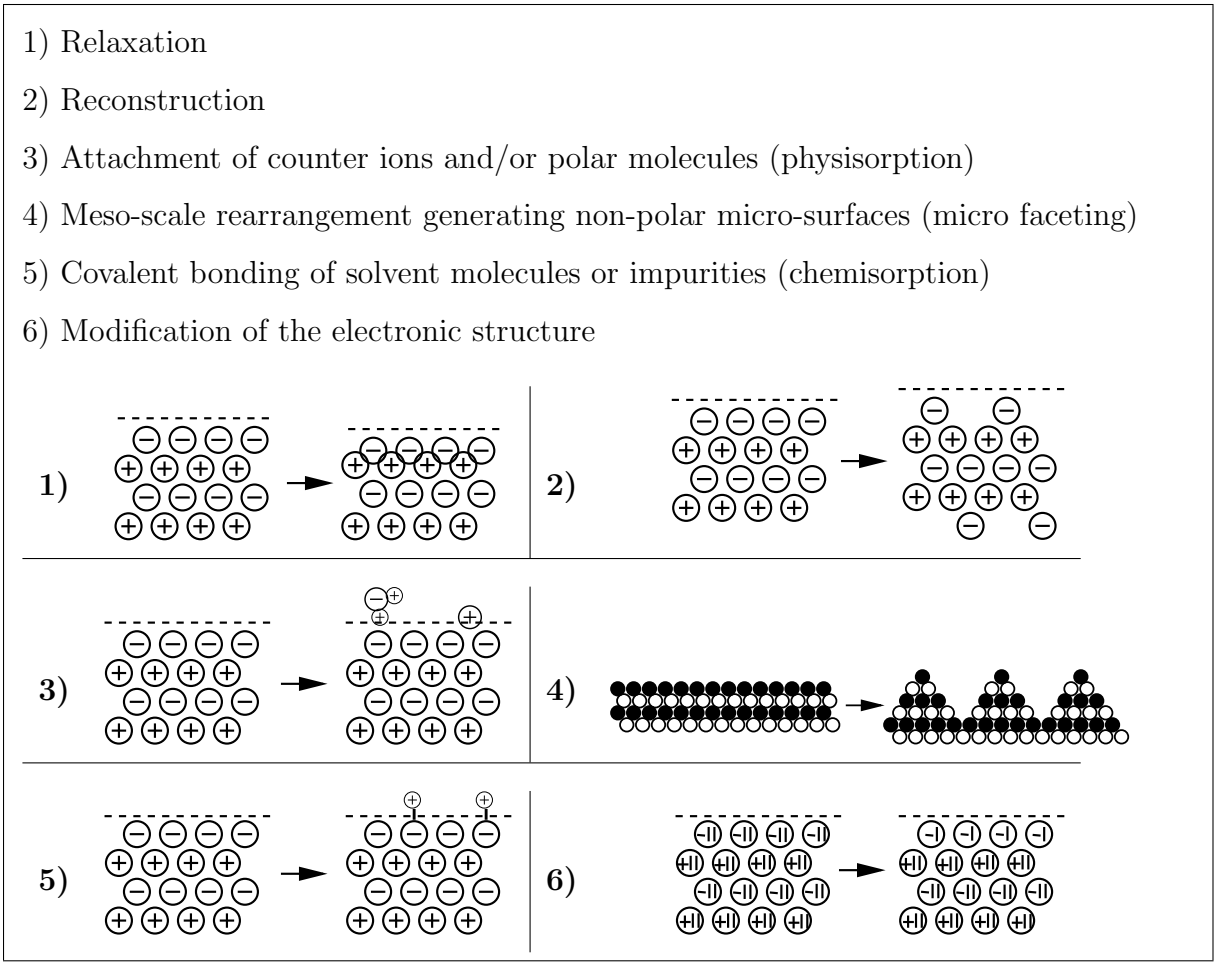

In the literature the terms relaxation and reconstruction are not always well defined and sometimes they are even used inter changeably. Here the term reconstruction will only be used for a modification of the surface structure that includes a stoichiometric change of the surface unit cell content as compared to the bulk unit cell. Relaxation is defined as a simple rearrangement of the atoms or molecules in the surface unit cell.

One must be careful when dealing with molecular crystals containing polar molecules or some semiconductors, prominent examples being urea [Engkvist et al.(2000)Engkvist, Price, and Stone] and zinc blende [Maki et al.(1999)Maki, Ichinose, Sekiguchi, Ohashi, Nishihara, Haneda, and Tanaka]. Here the dipole moment of a polar surface can not be completely eliminated by means of

a simple reconstruction, and there is no way to define the repeat unit so as to obtain a Type I or Type II face. Consequently the structure of the (hkl) surface will differ from its $(\bar{h}\bar{k}\bar{l})$ counterpart. Recently Harding extended the concept of Tasker to such materials which, unlike PA, cannot be reconstructed to have a mirror plane in the crystal parallel to a polar surface.[Harding(1999)]

In the last decade several new and sophisticated methods for the experimental investigation of surface structures such as surface X-ray diffraction, low energy electron diffraction (LEED), scanning tunneling microscopy (STM), atomic force microscopy (AFM) and grazing incident X-ray defraction (GIXD) have been developed or considerably improved. Polar surfaces can have a number of technologically interesting properties and the improved experimental equipment triggered a large number of publications on their microscopic structure. All the above mentioned mechanisms for the stabilisation of polar surfaces or combinations thereof have been confirmed experimentally for different materials: GIXD experiments on CoO (111) surfaces reveal [Mocuta et al.(2000)Mocuta, Barbier, and Renaud] that here the surface is stabilised by creation of a (non-polar) spinel Co_3O_4 structure in the outermost layers. Using GIXD Barbier et al. found that NiO (111) surfaces are terminated by a flat defect free polar surface which is stabilised by adsorption of light elements such as CO or O_2.[Barbier et al.(1998)Barbier, Renaud, and Stierle]. The same authors find two years later, also with GIXD, that NiO (111) is terminated by an octopolar reconstruction. No hydroxylation of the Ni-terminated layer was found with increasing H_2O partial pressure above the surface.[Barbier et al.(2000)Barbier, Mocuta, Kuhlenbeck, Peters, Richter, and Renaud] The same type of reconstruction was shown to occur on WO_3 (001) faces with STM experiments.[Jones et al.(1996)Jones, Rawlings, Foord, Egdell, Pethica, Wanklyn, Parker, and Oliver] AFM observations reveal that Jarosite (001) faces have a polar termination.[Becker and Gasharova(2001)] The authors of this study show theoretically that here the surface dipole moment can be reduced to a large extent by extensive relaxation. ZnO (111) surfaces show un-reconstructed polar terminations and Carlsson

showed theoretically with DFT calculations that a metallisation of these surfaces enables charge transfer between the surfaces to eliminate the dipole.[Carlsson(2001)] This result was confirmed by another theoretical study revealing that water adsorbed on this surface cannot dissociate thereby excluding its stabilisation by the bonding of hydroxy ions and protons.[Wander and Harrison(2001)] The (001) surface of CeO_2 investigated with STM and LEED was found to be terminated by a reconstructed half occupied oxygen layer.[Norenberg and Harding(2001)] The extent of oxygen coverage varies with the kind of preparation, the annealing temperature and the composition of the gas phase. A termination with a lower oxygen coverage is stabilised by a reduction of surface Ce^{4+} to Ce^{3+}.

The emerging picture is that at higher temperatures polar surfaces are stabilised by non-stoichiometric reconstructions or micro-faceting, while at lower temperatures the attachment of counter-ions, physisorption of impurities/solvents or the chemisorption of primarily hydroxyl anions or protons eliminates the dipole moment.

7.3 Theoretical Determination of Surface Structures

The relative stability of different surfaces at a given temperature is determined by their surface free energies or surface tensions [Safran(1994)]. Surface free energies are by no means easy to calculate theoretically. Not only does it require extensive computational resources but the proper algorithm for its calculation, i.e., essentially the choice of the path used in a thermodynamic integration scheme [Allen and Tildesley(1987)] is not well established and still a matter of debate.[Hodel et al.(1993)Hodel, Simonson, Fox, and Brunger, Smith and Lynden-bell(1999), Grochola et al.(2002)Grochola, Russo, Snook, and Yarovsky] Consequently attempts to calculate this quantity have been limited to a small number of comparatively simple materials such as Lennard-Jones crystals [Broughton and Gilmer(1986), Smith and Lynden-bell(1999)], pure metals [Grochola et al.(2002)Grochola, Russo, Snook, and Yarovsky] or simple alloys. [Lill and Broughton(2000)]

An alternative is to use surface energies instead of free energies, and assume that the ratios between the free energies of different surface terminations are close to the ratios between the surface energies of those structures. This is strictly true only at zero Kelvin, and for finite temperatures this essentially assumes that the entropic contributions to the surface free energies are constant or at least vary much less than the energetic contributions between different surface terminations. Although this assumption is not generally true, it is probably safe in most cases to expect at least the order of the energies to be the same as the order of the free energies. Consequently one assumes that the termination with the lowest surface energy is the most stable structure. This assumption has been frequently adopted and numerous examples of using relative surface energies, calculated with either empirical classical model potentials or diverse ab initio or DFT methods, can be found in the literature. Examples of inorganic materials include perovskite titanate [Heifets et al.(2000)Heifets, Kotomin, and Maier], forsterite [Watson et al.(1997)Watson, Oliver, and Parker], aragonit [Aquilano et al.(1997)Aquilano, Rubbo, Catti, and Pavese] and various metal oxides [Conesa(1995), Gillan et al.(1996)Gillan, Kantorovich, and Lindan, Nygren et al.(1996)Nygren, Pettersson, Freitag, Staemmler, Gay, and Rohl].

Another way to estimate the stability of a given surface termination is to perform a Molecular Dynamics simulation of the surface, possibly in contact with a liquid phase or impurities. Thereby we can assess kinetic factors and structural features due to the finite temperature that cannot be observed with Molecular Mechanics and energy minimisation. While we cannot easily calculate surface (free) energies we can learn something about the relative stability of different surfaces or surface terminations by comparing the dynamics and the relaxation of the considered terminations.

7.3.1 Calculation of Surface Energies

Because of the polar and/or non-stoichiometric nature of the surfaces considered here the calculation of their surface energies is not possible. Therefore only a short account will

be given here on the theoretical calculation of surface energies.

For simple and non-polar surfaces the energy E_{surf} of a crystal vacuum interface at zero Kelvin can be readily calculated via Molecular Mechanics calculations. The total energies $E_{stack}(N)$ of stacks consisting of N surface unit cell layers are calculated for different values of N. With A being the surface area per unit cell and E_{latt} the lattice energy of one crystal unit cell in the bulk, the surface energy per unit area is obtained as

$$E_{\text{surf}} = \lim_{N\to\infty} \left(\frac{1}{N} E_{\text{stack}}(N) - E_{\text{latt}} \right) \frac{1}{2A} \tag{7.1}$$

Although this method is frequently used, by considering up to about ten layers, surface energies obtained as differences between slab energies and independently determined bulk energy (E_{latt}) will diverge with slab thickness. [Fiorentini and Methfessel(1996), Boettger et al.(1998)Boettger, Smith, Birkenheuer, Rosch, Trickey, Sabin, and Apell] As an alternative way to calculate E_{surf} we can write[Fiorentini and Methfessel(1996)]

$$E_{\text{stack}}(N) \approx 2E_{surf} + NE_{\text{latt}} \tag{7.2}$$

That is for large N the stack energy becomes a linear function of N. If we use this relationship to define the lattice energy E_{latt} both E_{slab} and E_{latt} are calculated in a consistent way. Thus one obtains convergent surface energies with increasing N provided the lowest order electrostatic moment of the unit cell at the surface is the quadrupole or of higher order In this case usually the energies of up to only a couple of layers (N<10) have to be calculated. However, for the (111) faces of potash alum the dipole moment prevents either method of calculating the surface energies to be applied.

7.3.2 Molecular Dynamics

Most of the theoretical investigations of surface structures have so far concentrated on the pure crystal surface or a surface with a limited number of adsorbed molecules or defects. For surfaces in contact with vacuum or a dilute gas phase this is a valid model. If, however, we are interested in the structure of a surface in contact with a

liquid at room or higher temperatures such calculations can only be of limited usefulness. Using DFT simulations Wright et al.[Wright et al.(2001)Wright, Cygan, and Slater] showed that adsorbed water molecules can stabilise surfaces resulting in less pronounced relaxation for a range of different carbonates. Performing MD simulations Baudin et al.[Baudin et al.(2000)Baudin, Wojcik, and Hermansson] showed for ceria that the relative stability of surfaces next to vacuum can change with temperature. The structure of a PA crystal surface in contact with an aqueous solution at 300 K will possibly differ qualitatively from the vacuum interface at zero Kelvin. Here I will not compare surface energies as obtained by energy minimisation of crystal slabs with different surface terminations but rather try to establish the most stable of these terminations by performing MD simulations of the surfaces in contact with aqueous PA solution. By investigating the system using MD simulations, temperature and solvent effects can be accounted for in the most natural way. The straight forward calculation, and thereby comparison, of surface energies is not possible with MD at finite temperatures. Assessing surface free energies, while possible in principle, is computationally not feasable with the means at our disposal. However, I only need to determine *the* most stable version of a given face (hkl). An unstable surface will evolve towards a nearby stable version in the course of an MD simulation and subsequently the conformational energy will converge to and fluctuate around some mean value. Thus we can establish the structure of a stable surface without knowing the actual value of the surface (free) energy. Given the complex structure of the PA (111) surface we are likely to find several different "stable" surfaces, corresponding to local free energy minima, when starting the MD from different initial structures or surface cuts. As criterion for choosing the most stable structure out of these local minima one can use the average configurational energy and/or the RMSD of the molecules/ions at or close to the surface. If the dimensions of the simulation cell and the total number of molecules are the same for each system I can directly compare the average energies. This criterion together with the stability, i.e. the RMSD, of the atoms/molecules in the outermost surface sub-layer can be used to determine the most stable surface structure.

Figure 7.5: **Atomic structure of the potash alum surfaces**, each slab contains four PA unit cells, side view, surfaces on top.

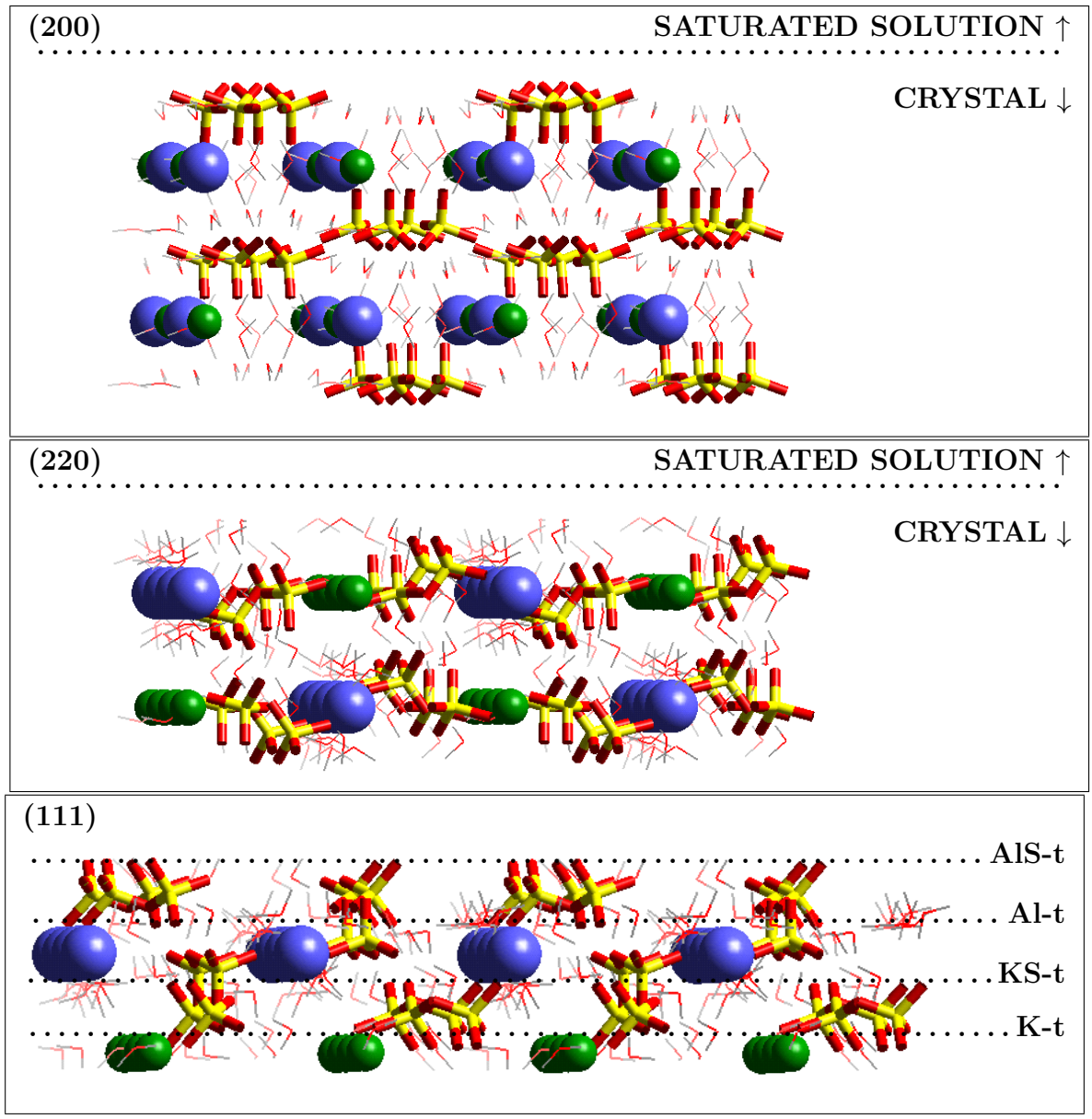

7.4 Potash Alum

The unit cell of PA is relatively large and its structure intricate. There are several different ways to cut the crystal parallel to a given face hkl. Figure 7.5 shows the microscopic

structure of PA crystal slabs cut along the surface planes of the three growing faces.

7.4.1 The (220) and (200) Faces

The (110) and the (100) faces of potash alum both have two identical repeat units in the surface unit cell. Therefore, according to crystallographic terminology, we label these surfaces (220) and (200) in the following. For the (220) face the high symmetry of the unit cell leaves us with only one possible cut to obtain a flat surface as shown in Figure 7.5. Although the (200) face would allow for at least three different cuts, only the one termination shown in Figure 7.5 results in a surface with a vanishing dipole moment perpendicular to that surface. We can safely assume that if there is only one way of cutting a non-polar surface then a possibly relaxed version of this surface is going to be the very termination to be found on the real potash alum (200) surface.

7.4.2 The (111) Face

A transverse section of the (111) surface as shown in Figure 7.5 reveals its polar nature. Each of the four possible simple cuts produces a polar Type III surface, a consequence of the alternating staggering of positively (K^+ or Al^{3+}) and negatively charged (SO_4^{2-}) sub-layers. The most important question raised in this chapter is: Which of the four possible surface terminations (AlS-t, Al-t, KS-t or K-t in Figure 7.5) is found on PA (111) surfaces in contact with solution and which of the six mechanisms presented in Figure 7.4 act(s) to reduce the dipole moment and/or to stabilise the resulting polar surface ? For narrowing down the possible answers to the second part of the question we make some assumptions: Modification of the electronic structure on the surfaces, as often proposed for polar oxide surfaces/semiconductors, will play a negligible role for strongly ionic crystals such as PA. Considering experimental microscopic data [Vanenckevort et al.(1981)Vanenckevort, Bennema, and Vanderlinden, Reyhani et al.(1999)Reyhani, Freij, and Parkinson], micro-faceting can also be excluded. The fifth mechanism given in Figure 7.4 could play a role for PA surfaces through the

partially covalent bonding of hydroxy anions to surface aluminium ions. This process, however, must be expected to depend very sensitively on the pH of the solution. There is no straightforward way to include pH-effects into classical MD simulations and this would also require additional force field parameterisations. Therefore we can only speculate about its possible influence. In the following we will concentrate on the first three mechanisms listed in Figure 7.4, i.e., we investigate the relative contributions of relaxation, reconstruction and the attachment of counter-ions or polar solvent molecules to the stabilisation of the PA (111) surface.

Due to the highly symmetric crystal structure of PA it is possible to construct charged as well as reconstructed slabs with identical surface terminations on both sides of the slab as sketched in Figure 7.3. The most stable of these terminations must be the experimentally observed one because there is no conceivable reason for the (111) and the $(\bar{1}\bar{1}\bar{1})$ having a different termination. By reconstructing the terminating positive or negative sub-layers subject to the conditions of over-all charge neutrality and zero dipole moment we can produce four different (111) slabs in a way that the two surfaces become symmetric and energetically equivalent again. Thereby the the Type III surfaces sketched in Figure 7.5 are transformed to Type II surfaces. Because the K^+ and the Al^{3+} layers have a different total charge the slab would remain polar if one just relocated half of the sulfate ions above a K^+ or Al^{3+} layer to the opposite surface. In these cases the cation layer directly beneath the terminating sulfate layer has to be duplicated additionally in order to get a symmetric and non-polar slab. Schematical diagrams of the four different reconstructions are shown in Figure 7.6. In most of the attempts to predict the structure of polar surfaces theoretically with classical model potentials this strategy is adopted [Nygren et al.(1996)Nygren, Pettersson, Freitag, Staemmler, Gay, and Rohl, Pojani et al.(1997)Pojani, Finocchi, Goniakowski, and Noguera,
Norenberg and Harding(2001), Barbier et al.(1998)Barbier, Renaud, and Stierle] unless the symmetry of the crystal forbids such a simple reconstruction. Alternatively one can leave both the (111) and the $(\bar{1}\bar{1}\bar{1})$ face being terminated by the same either positively or negatively charged sub-layer resulting in a crystal with a vanishing total

Figure 7.6: **Possible reconstructions (Type III ⇒ Type II) of the polar potash alum (111) face**. The Position of the two surfaces of each slab are indicated by the dashed bold lines. The many bulk unit cells which would separate the two faces have been omitted for clarity. Note that – other than suggested in this simplified diagram – the number of sulfate ions in the two terminating sulfate layers of the AlS-t and KS-t terminations are different (three vs one per surface unit cell) due to the different charges of the adjacent Al^{3+} and K^{+} layers respectively.

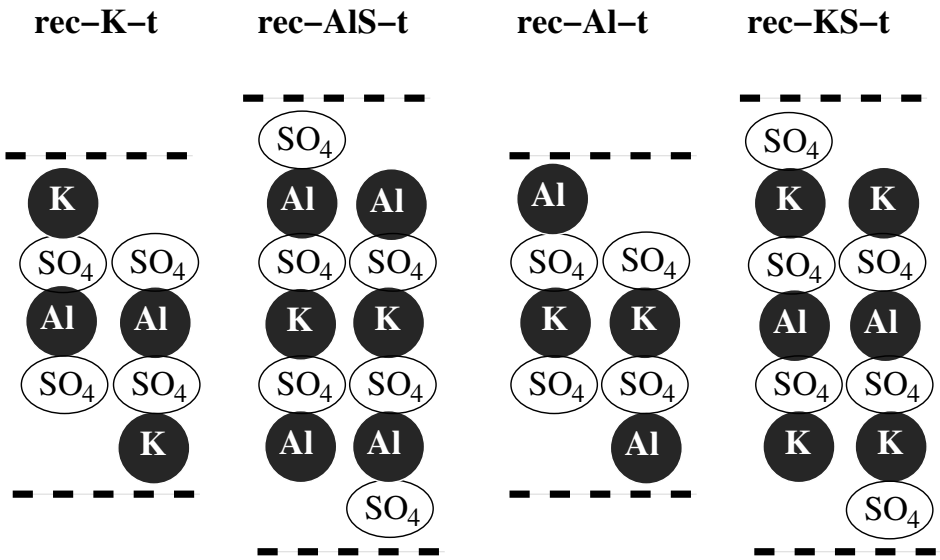

dipole moment and a finite net charge (chg-1 and chg-2 in Figure 7.3). This apparent net charge is the very reason why this kind of structure is usually not considered since most attempts to reconstruct a polar surface were done under the constraint of over-all charge neutrality. As discussed in Section 7.2 other mechanisms than reconstruction, most notably the attachment of counter ions and polar solvent molecules, can stabilise polar surfaces in contact with a liquid phase. Thus there seems to be no good reason for discarding the charged surface slabs, and so four reconstructed as well as the four charged surface terminations will be considered.

The complex structure of potash alum would allow for a considerably larger number of different cuts, but all, apart from the eight surface structures considered here, would either result in a very rough surface prone to dissolution or they would differ only by the number of water molecules on the surface. The latter does not count as different cut

because in the simulation the surface is in contact with an abundance of water molecules from the solution.

7.5 Computational Methods

To estimate the relative stability of the different proposed terminations MD simulations with all eight surface terminations defined above are performed. Additional simulations were done with the two non-polar (200) and (220) faces to obtain information about the structure of the solution above these faces. In the following some technical details of the computations are given.

7.5.1 The Model Potential

For all the calculations reported here I used the empirical potential developed in Chapter 5. There it was shown that this force field can reproduce the structure of PA at room temperature. Further evidence for the usefulness of this potential is shown in Figure 7.1, where the theoretical morphology as calculated with the attachment energy method is compared to photographs of potash alum crystals grown from aqueous solution. Although the theoretical morphology does not predict the small (220) faces observed in experiment the potential can still be considered adequate when considering that the attachment energy model does not take in account the influence of the solution (see Section 4). For ions and water molecules in solution the same model potentials were used as in the crystal slab.

The reliability of empirical classical model potentials, such as the one used here has always been a matter of debate. In using model potentials parameterised to reproduce bulk properties to model surfaces, the potentials are assumed to be independent of co-ordination environment, which is a poor approximation for polarisation contributions. With the advent of faster computers and powerful and efficient versions of *ab initio* methods such as periodic HF and DFT algorithms the

usefulness of empirical force fields are increasingly put under scrutiny. The (110) face was predicted to be the most stable surface of SnO_2 with both DFT and with empirical methods but the relative stability found with DFT for (100) and (101) disagrees with earlier shell-model predictions.[Oviedo and Gillan(2000)] The theoretical predictions for low index rutile surfaces obtained with a transferable variable-charge Ti-O inter-atomic potential and with ab-initio methods also show some differences.[Swamy et al.(2002)Swamy, Muscat, Gale, and Harrison] In contrast, the relative surface energies and surface relaxation in the α-Al_2O_3 (0001) surface, calculated with periodic HF, DFT and classical empirical models agree qualitatively and the quantitative differences are within the experimental error ranges for all three methods. The (100) and (110) surface relaxations in $SrTiO_3$ and $BaTiO_3$ perovskite thin films as calculated by means of a semi-empirical shell model, agree well with experiment and with DFT calculations [Heifets et al.(2000)Heifets, Kotomin, and Maier]. Watson et al. found empirical model potentials to be well suited to the predictions of surface structures of forsterite [Watson et al.(1997)Watson, Oliver, and Parker]. These examples represent only a small fraction of the calculations of surface properties published so far. Generally classical model potentials seem to be only of limited accuracy but they still can provide valuable qualitative insights. For MD simulations of large systems, such as those presented here, there is no alternative yet.

7.5.2 MD-simulations

MD simulations are performed of a saturated PA solution adjacent to PA crystal slabs with different surface terminations exposed to the solution. The crystal slabs consist of layers of 2×2 surface unit cells, the number of layers varying between 3.0 and 3.75 for different terminations as detailed below.

Although the real surface in contact with aqueous solution will certainly differ from the bulk structure, the latter can be used as a good starting configuration for MD simulations since the real structure of the most stable surface is expected to differ not too much

from the bulk structure. This is because the modified surface must return to the bulk structure eventually in the course of crystal growth, and if the surface was very different from the bulk a considerable amount of reconstruction would have to take place to allow crystal growth to proceed. This reconstruction would result in a large free energy penalty hampering crystal growth for a given face, and therefore it is unlikely to occur if this face is observed in experiment.

The slab terminations considered are the two non-polar surfaces (labelled 100-t and 110-t) and eight different (111) surfaces. The simulation cell geometry used in all cases is shown in Figure 7.7. The crystal slab is placed on one end of the box with the interesting surface perpendicular to the z-direction and facing the solution layer. At least the uppermost three sub-layers of sulfate ions and cations in the crystal slab, including the corresponding amount of crystal water molecules, were allowed to move freely according to the intermolecular forces due to all the other molecules in the system while the remaining part of the crystal was held rigid (or frozen in the DL_POLYterminology) in the course of the simulation (as indicated by flexible and rigid in Figure 7.7).

The length of the box in the z-dimension is in all cases 70 Å. In all simulations the solution consists of six sulfate three aluminium and three potassium ions in 576 water molecules, corresponding to a PA solution at the saturation concentration at 300 K of 121.2 g anhydrous PA per 1 kg solution. With the resulting thickness of the solution layer, z_s, between 15 and 20 Å, this leaves a vacuum slab of $z_v \approx 25$ Å.

More details on the geometries and other features of the different simulations are given in Table 7.1. Each of the four charged or non-reconstructed (111) slabs was set up in two different ways: 1) the *charged version* (see chg-1 or chg-2 in Figure 7.3), 2) the *polar version*, corresponding essentially to three layers of the slab shown in Figure 7.5 (see pol-1 or pol-2 in Figure 7.3) The structure of the surface exposed to the solution is identical for both the charged and the polar version. They differ only by an additional rigid sub-layer at the bottom leaving the charged version with its net charge but with a zero dipole moment. According to the label assigned to each surface in Figure 7.5 and to whether the charged or polar version was used the simulation runs are labelled chg-

Figure 7.7: **Cross section of the MD simulation cell**. Each system consists of a PA crystal slab with one of the considered surfaces or surface terminations in the xy-plane, adjacent to a layer of saturated PA solution. Only the atoms in the sub-layers of the crystal slab close to the solution are allowed to move (flexible); the remaining atoms of the crystal are frozen (rigid). Periodic boundary conditions are imposed in all dimensions; the gas phase region is introduced to approximate an effectively two-dimensional system.

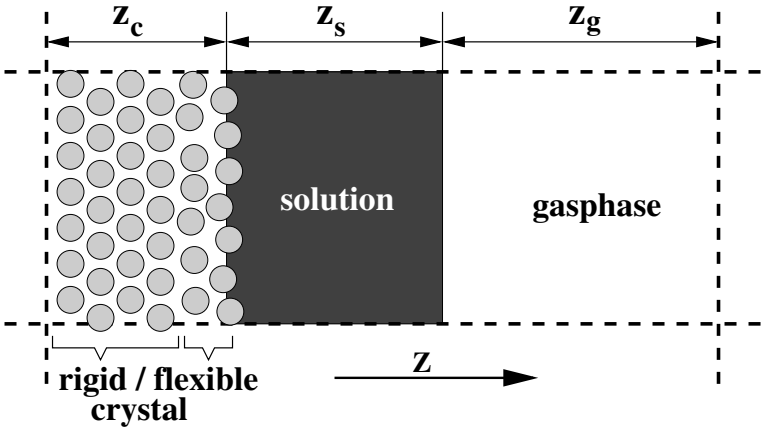

AlS-t, pol-AlS-t, chg-Al-t, etc. The reason for setting up simulations with the polar in addition to the charged slabs is that both setups are unrealistic in different ways: The polar slab has a permanent dipole moment which would not be there in a real crystal while the charge-density of the entire charged slab, in contrast to the surface, is surely higher than it would be in reality. Comparing the results obtained with both setups allows us to estimate the nature and magnitude of any artifacts that are possibly introduced by either method. Four simulations were done with reconstructed aluminium and potassium terminated surfaces as sketched and labelled in Figure 7.6.

Theoretically one could eliminate the net-charge in the systems with the charged slabs by choosing the appropriate ratio of anions and cations in the solution. However, proceeding thus would be very expensive in terms of computational resources because we needed to simulate relatively large solution slabs on both sides of the crystal slab and since we do not know the width of the charged double layer a priori the choice of the thickness of these solution slabs and the relative ionic concentration would be

Table 7.1: **Details of the PA surface simulations**

label	surf[a]	occ[b]	N_l[c]	x×y/Å^2[d]	label	surf	occ	N_l	x×y/Å^2
chg-AlS-t	SO_4^{2-}	1.0	3.75	34.38×29.78	chg-Al-t	Al^{3+}	1.0	3.25	34.38×29.78
pol-AlS-t	SO_4^{2-}	1.0	3.0	34.38×29.78	pol-Al-t	Al^{3+}	1.0	3.0	34.38×29.78
rec-AlS-t	SO_4^{2-}	0.75	3.625	34.38×29.78	rec-Al-t	Al^{3+}	0.5	3.0	34.38×29.78
chg-KS-t	SO_4^{2-}	1.0	3.75	34.38×29.78	chg-K-t	K^+	1.0	3.25	34.38×29.78
pol-KS-t	SO_4^{2-}	1.0	3.0	34.38×29.78	pol-K-t	K^+	1.0	3.0	34.38×29.78
rec-KS-t	SO_4^{2-}	0.25	3.375	34.38×29.78	rec-K-t	K^+	0.5	3.0	34.38×29.78
200-t	SO_4^{2-}	1.0	3.0	24.31×24.31	220-t	all	1.0	3.0	34.38×24.31

[a]Type of ions in the outermost surface layer

[b]Occupancy of the outermost surface layer, 1 for a full layer as in the bulk, 0.5 for a half layer, etc.

[c]Number of layers of surface unit cells in the slab, each layer consists of four sub-layers, each sub-layer contains 16 ions of only one type, all ions are equally weighted.

[d]Size of the rectangular cross-section of the box perpendicular to the z-dimension

unclear. To leave the different systems as comparable as possible, and in order to avoid biasing the system in an arbitrary manner, I chose to use identical ionic concentrations in all simulations. If one uses the 3-D Ewald Summation technique to account for the electrostatic long range interaction in a simulation, any net charge is formally compensated for by the introduction of a homogeneously distributed background charge of the same magnitude and the opposite sign (see Section 3.6.2). Such a homogeneous background charge density can be seen as a simple approximation of the effect of the diffuse and non-homogeneous counter ion cloud to be found above real charged surfaces in aqueous solutions.[Adamson and Gast(1997)]

All systems were equilibrated for at least 50 ps with the entire crystal slab held rigid. After this equilibration period, the atoms in the uppermost sub-layers of the crystal slab were allowed to move freely. The overall simulation time for each of the the different systems is at least 200 ps. The most stable terminations were simulated for consid-

erably longer time spans which are specified in the results section. The MD simulations are performed with a modified version of DL_POLY.[Smith and Forester(1996)] The time-step used with the leap-frog algorithm is 0.002 pico seconds. Correction terms for the energy and forces of polar [Yeh and Berkowitz(1999)] and the energy of charged systems [Bogusz et al.(1998)Bogusz, Cheatham, and Brooks] are applied as described in Chapter 3. The temperature is kept constant at 300 K with an isotropic Nose-Hoover thermostat[Hoover(1985)] using a relaxation time constant of 0.1 pico seconds. A SHAKE-like algorithm [Smith and Fincham(1993)] is used to keep the water molecules rigid.

7.6 Results

7.6.1 Surface Structures

The main result of the MD simulations of the solution above the different PA surfaces is the structure of the flexible part of the surface and the adjacent solution. Hence snapshots of configurations in the simulation cell as obtained after equilibration of the different systems are plotted and compared. Although snapshots of MD simulations can be helpful for understanding certain points, a more concise picture of the interesting parts of the configuration can be gained from time averaged one dimensional density distribution functions. For assessing the stability of the surfaces, the motions of the atoms near the surface in the direction perpendicular to the surface plane (here the z-dimension) are particularly relevant. If the surface is stable we get a well defined peak for each each ion or molecule in each sub-layer. The width of these peaks can be taken as an estimate of the root mean square displacement (RMSD) in the z-direction. The one-dimensional RMSD of atoms in a simple crystal at 300 K can be expected to lie between 0.2 and 0.25 Å [Dove(1993)]. Since here we are dealing with a surface we must expect this number to be a lower boundary to the RMSD of the atoms and molecules when the displacement is defined relative to the average position of the atom in the relaxed surface rather than as the distance to the ideal lattice position.

The (100) and (110) Faces

The structure of the two systems with the non-polar PA surfaces are shown in Figure 7.8. On both surfaces the flexible layers are relatively stable. The dissolution of one single ion, corresponding to a small peak at approximately z = 0 Å in the density distributions given on the right hand side, can be seen above the (100) surface. The rest of this surface, however, remains stable over the whole simulation time of 600 ps. The peaks between z = −5 and −20 Å in the density distribution plots correspond to the flexible Al^{3+}, K^+ and sulfate layers. Not surprisingly they become broader with increasing z but even the width of the broadest peak, corresponding to the uppermost sulfate layer at z ≈ −6 Å, would not exceed ∼ 2 Å, which is appropriate for surface atoms in a stable interface at a temperature of 300 K. In the density distribution plots the structure of the PA solution above the surface is given as well. The solution layer is ∼ 25 Å thick, barely any ordering of ions occurs apart from the fact that the K^+ ions get closer to the surface than Al^{3+}. The reason for this is probably that Al^{3+} ions are always surrounded by a very tight and persistent hydration shell of six water molecules. The exchange rate of the waters in the K^+ hydration shell is faster by about eight orders of magnitude.[Rudolph et al.(2000)Rudolph, Mason, and Pye, **?**] The water molecules closest to the surface are also very tightly bound and hardly any exchange of these waters happens in the course of the simulation. Therefore and in contrast to potassium ions there will always be at least two relatively rigid layers of water between any aluminium ion and the surface. The potassium ions never attach directly to this surface, i.e., there is always at least one water molecule between the solution potassium ions and each surface sulfate oxygen atom.

In the snapshot of the (110) surface in Figure 7.8 two of the K^+ ions are about 2 Å from their ideal lattice positions but there was no sign of a real dissolution of the surface. Within a simulation time of 600 ps the two K^+ ions diffused even further away from the surface as to be seen by the small peaks between z = -2 and -3 Å in the density distribution plots on the right hand side but eventually they returned to a position nearer to their ideal

Figure 7.8: **Structure of the (100) and (110) surfaces and the solution**, snapshots and z-density distribution functions. The thick dashed line marks the surface and the thin dashed line marks the boundary between rigid and flexible ions. The abscissa in the distribution function plots corresponds to the z-dimension in Figure 7.7 with units of Å. For easier comparison the peaks in the density distribution function plots have been normalised so that their maxima are approximately at equal heights and a horizontal brace connects a layer in the snapshot with the corresponding peak in the distribution function plot. The crystal water is neither included into the snapshots nor into the distribution function plots for clarity. The water considered here includes only water present in the solution in the initial configuration which is valid since very few of the crystal waters diffused into the solution.

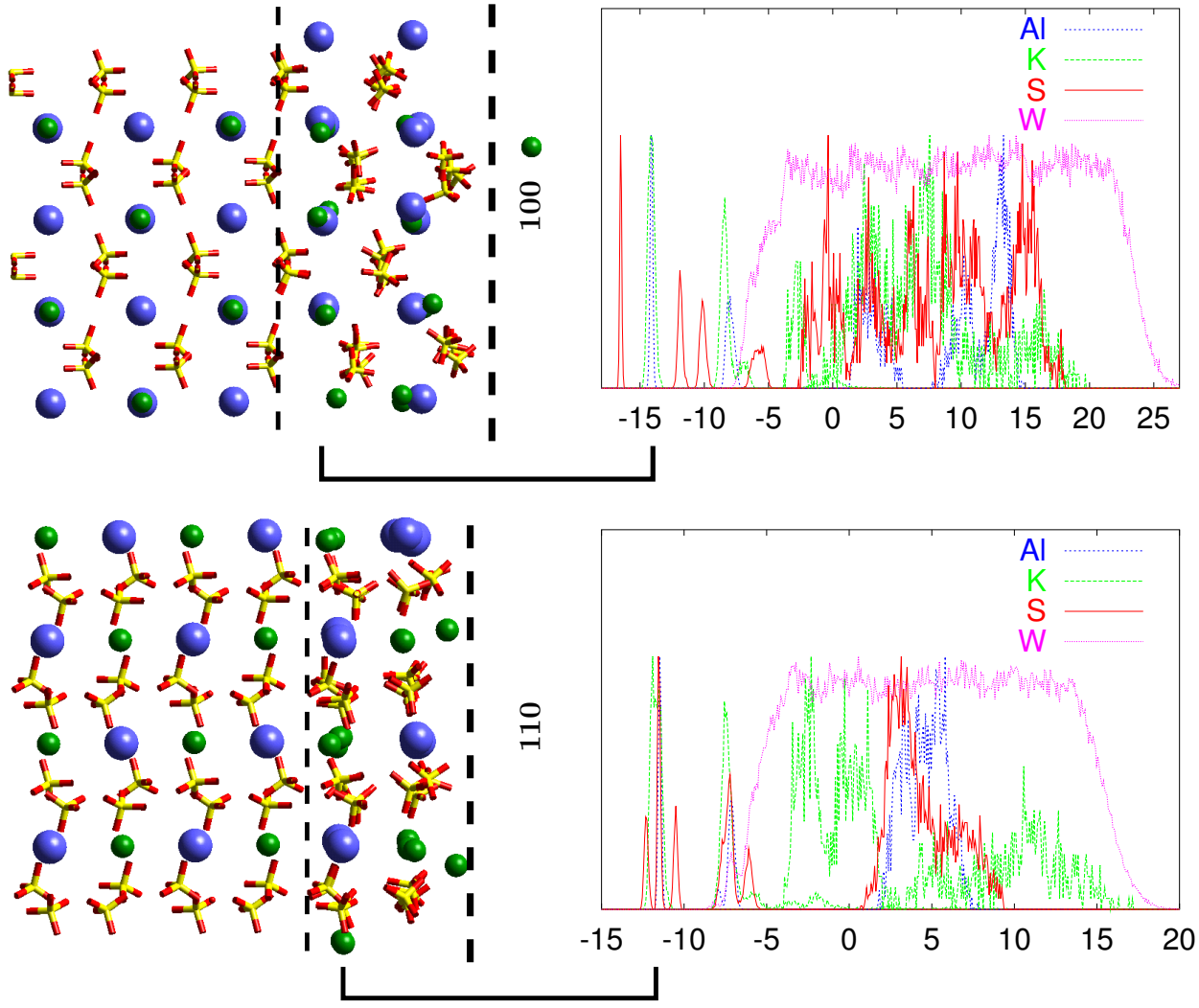

lattice positions. Just as in the (100) surface the remaining ions in the surface remain stable. The solution above the (110) surface shows a more ordered structure than it does above the (100) surface. Again the potassium ions get closer to the surface than Al^{3+} and sulfate ions. Here this trend is more pronounced than it is for the (100) surface.

The (111) Face

Both the K-t and KS-t (111) surfaces turn out to be unstable. More than half the ions in the outermost surface layer of all the reconstructed, the charged and the polar K-t and KS-t terminations show a clear tendency to dissolve into the solution after less than 100 pico seconds of simulation. Therefore only the results for the AlS-t and Al-t terminations are presented here in some detail.

Structure of the Reconstructed Systems For the reconstructed AlS-t surface, initially defined in Figure 7.6 the diagrams in Figure 7.9 show clearly its stability. Here the atoms in the four uppermost surface sub-layers, three sulfate and one aluminium, were allowed to move. The width of the distribution functions for these atoms are smaller than 1.5 Å and remained so over a period of 800 ps. Although the rec-AlS-t slab is overall neutral it represents a Type II face having charged sub-layers. It is probably the resulting local electrostatic field that causes the structuring of the solution which is more pronounced here than it is above the non-polar (100) and (110) faces. Again a potassium peak at about z = 0 Å comes next to the surface followed by aluminium and sulfate peaks at roughly identical positions further away from the surface. Going further out the solution becomes increasingly disordered. The most notable observation here is that the potassium ions come in direct contact with the surface sulfate ions with no interstitial water molecules.

The rec-Al-t system, shown in Figure 7.9 shows a somewhat broader outermost aluminium peak but it still can be regarded as stable surface termination. Due to the highly charged aluminium ions directly on the surface the local electrostatic field is stronger than it is in the rec-AlS-t system and therefore the structure of the solution ions is even

Figure 7.9: **Structure of the reconstructed (111) surface and the solution**; The arrows in the snapshot of the rec-Al-t system show the K^+ ions that have attached to the surface from the solution. Adjacent Al^{3+} ions are drawn smaller for clarity. See caption of Figure 7.8 for more explanations.

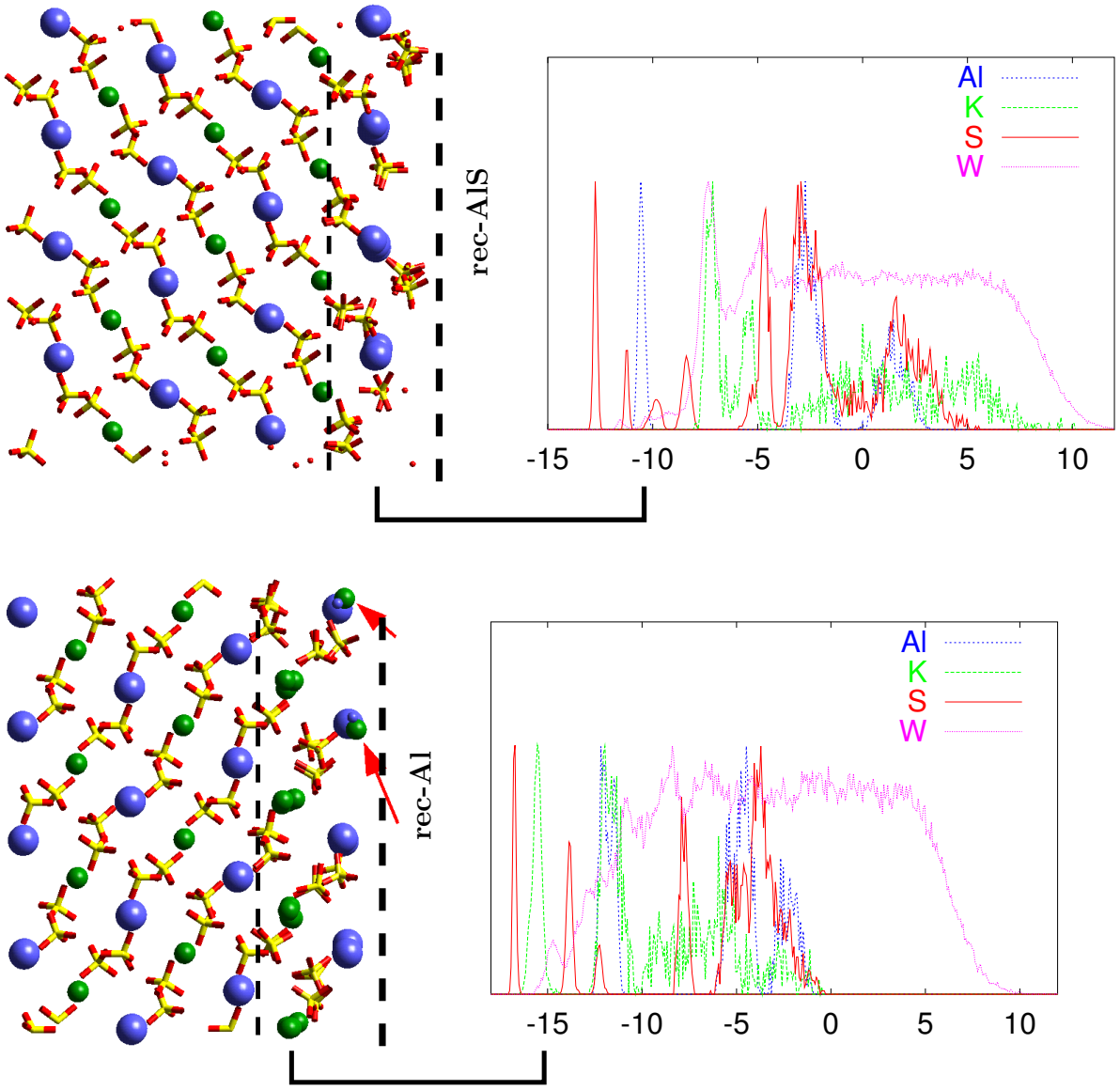

more distinctive here. Surprisingly and in spite of the positive charge of the outermost crystal layer the potassium ions get still closer to the surface than the sulfates. Here half of the ions in the uppermost aluminium layer have been removed in the course of the reconstruction of the slab. At closer inspection it turns out that potassium diffuses into the empty aluminium pockets left by this reconstruction (see Figure 7.9). Being at z≈0 Å at the start of the simulation the first K^+ ion covers the distance to the surface site in ∼200 ps and stays in this position for 600 ps before diffusing back into the solution. The second attaches after 600 ps and stays there for 400 ps until the end of the simulation. This behaviour could be induced by the assumed artificial reconstruction of the surface. *In vivo* such a persistent attachment of K^+ ions in Al-sites is a very unlikely scenario because this would come down to one component of PA (the potassium ions) acting as an inhibitor for the growth of PA since the potassium ions got stuck in a "wrong" position on the surface.

Structure of the Charged Systems The structures of the two net-charged crystal slabs and the adjacent solutions (chg-AlS and chg-Al) are shown in Figure 7.10. The flexible surface layers, one aluminium and 3 sulfate, in the chg-AlS system are stable. As compared to the other (111) terminations investigated here the z-RMSD of the surface atoms is the lowest for this system. The solution above the surface including the water is well ordered.

An interesting result was obtained with the chg-Al system. The surface layer in the snapshot in Figure 7.10 looks quite stable. The solution slab, however, looks different from the other systems studied so far. The ions in the solution show a very clear ordering along in the z-dimension perpendicular to the surface. Closest to the surface are two water layers followed by a succession of four distinctive sulfate and aluminium peaks (surface–Al^{3+}–H_2O–H_2O–SO_4^{2-}–Al^{3+}–SO_4^{2-}–Al^{3+}). Even further away from the surface are all the potassium ions which partially evaporate together with a couple of hydration waters into the gas phase. The magnitude of the net-charge of the PA slab in the chg-Al system (32 e per simulation box) is twice as large than it is in the chg-AlS system. The resulting

Figure 7.10: **Structure of the charged (111) surfaces and solutions**; See caption of Figure 7.8 for more explanations.

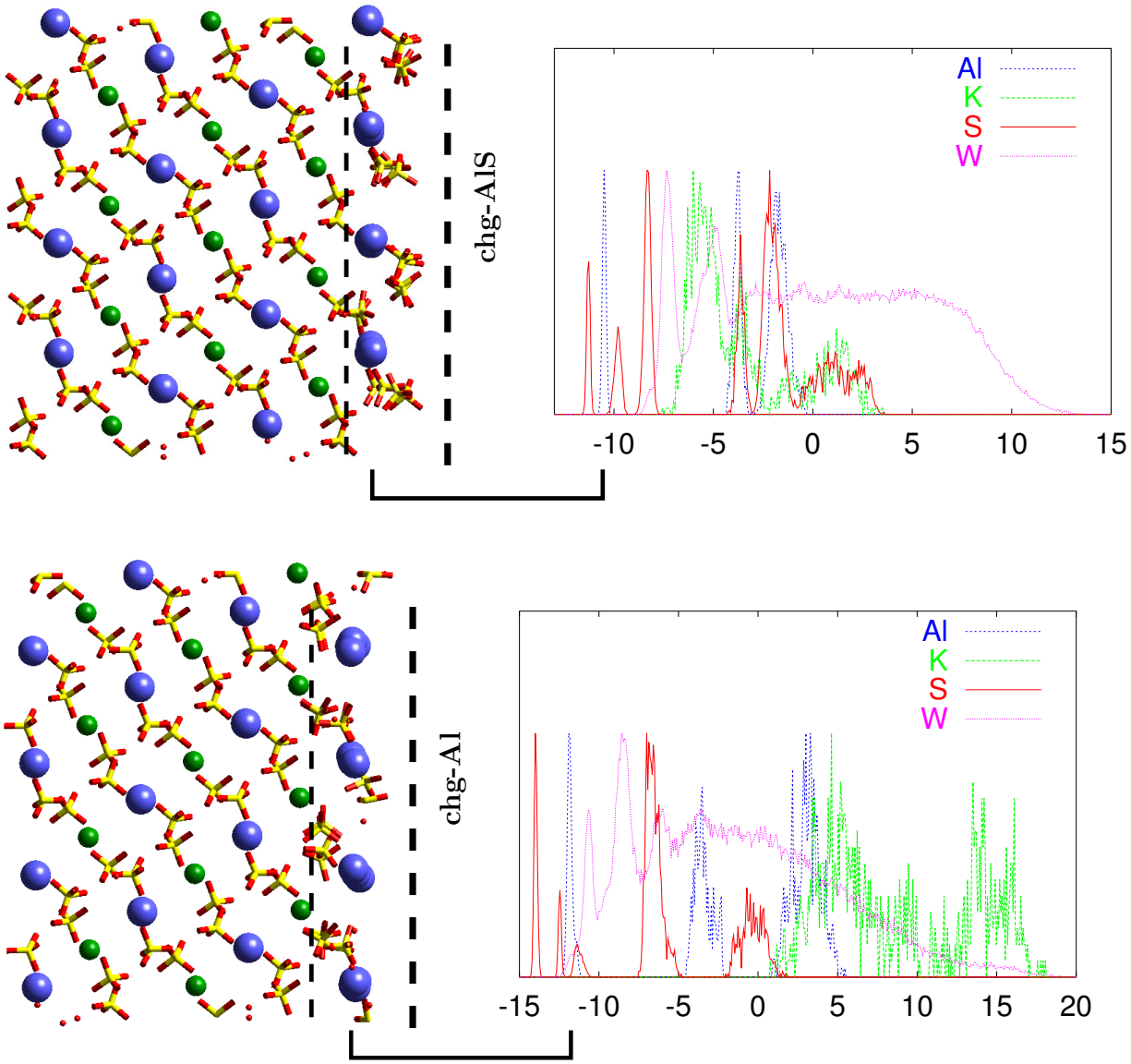

high charge density probably causes the ionic layering in the solution and the resulting oscillating charge density. The very ragged gas liquid interface is clearly an artifact due to the small system size. It is somewhat surprising that in spite of the high charge density in the slab the structure of the flexible surface layers is barely distorted and the atoms in the surface remain very close to their ideal lattice positions.

To make sure that no artifacts were introduced by holding majority of the crystal ions rigid in the simulations the chg-AlS-t system was simulated for 400 pico seconds with one additional layer of each K^+ and Al^{3+} and the according number of sulfate and water molecules flexible. Here the width of z-distribution functions of the outermost surface ions (not shown here) increases slightly but the surface remains stable and no dissolution of ions into the solution is observed

Structure of the Polar Systems The results obtained with the polar slabs are shown in Figure 7.11. In the pol-Al system the terminating two sulfate and one aluminium layer including the water molecules complexing these ions were un-constrained. In the pol-AlS system the flexible part consists of three sulfate, one aluminium and the according water molecules respectively. The snapshots reveal that both surfaces remain flat and stable over the simulation period of 200 pico seconds for pol-Al and two nano seconds for pol-AlS. However, the structure of both surfaces differ considerably from the bulk crystal structure. In the pol-AlS surface the distance between the surface aluminium layer and the first rigid aluminium layer in the bulk increases notedly as compared to the ideal crystal structure. In the pol-AlS density distribution plot the position of the aluminium peak with respect to the three sulfate peaks is shifted towards the surface. In the pol-Al surface the same out-bound relocation happens to the sulfate peaks with respect to the aluminium layers. In both cases this pronounced relaxation leads to a decrease in the net z-dipole moment. Especially in the pol-Al surface the peaks in the z-distribution of the surface ions are broader here than in the charged or reconstructed versions. The net dipole moment in the un-relaxed pol-Al slab is larger than it is in the pol-AlS system (see Table 7.2). This is apparently the reason for relaxation as well as disorder being more

Figure 7.11: **Structure of the polar (111) surfaces and solutions**. See caption of Figure 7.8 for more explanations.

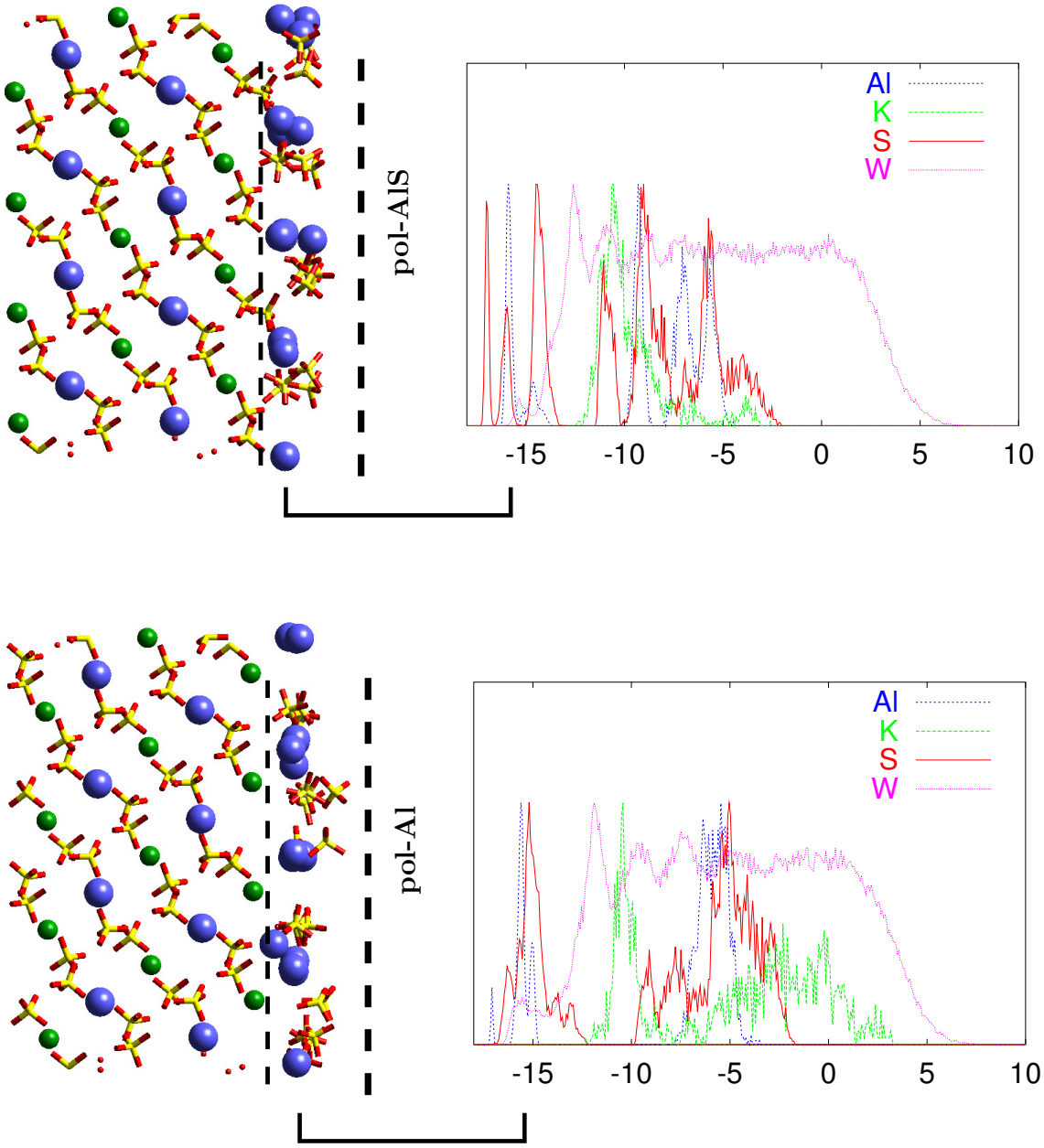

Table 7.2: **Configurational energies of PA (111) slabs**, with different surface terminations in contact with saturated PA solution.

system	<E>[a]	E_{corr}[b]	chg[c]	$\vec{p}$ [d]
	[10^3 kJ/mol]	[10^3 kJ/mol]	[e]	[eÅ]
chg-Al-t	-619.4	35.2	32.0	—
chg-AlS-t	-719.2	8.8	-16.0	—
chg-K-t	-571.7	8.8	16.0	—
chg-KS-t	-612.3	35.2	-32.0	—
pol-Al-t	-536.0	10.5	—	336.9 / 241.4
pol-AlS-t	-568.9	1.8	—	168.5 / 120.4
pol-K-t	-554.5	3.4	—	168.5 / 151.0
pol-KS-t	-536.0	8.5	—	336.9 / 251.2
rec-Al-t	-587.5	—	—	—
rec-AlS-t	-710.7	—	—	—
rec-K-t	-579.1	—	—	—
rec-KS-t	-590.1	—	—	—

[a] Average total configurational energy, incorporating E_{corr}
[b] Energy correction for charged/polar systems
[c] Net-charge of the crystal slab
[d] Dipole moment of the crystal slab before / after equilibration

pronounced in the pol-Al surface.

Configurational Energies The energies calculated for the polar slabs cannot be compared because each energy value contains the sum of two different, and unknown, surface energies, e.g for the AlS-t system: the AlS-terminated crystal-solution interface and the K-terminated crystal-vacuum interface. Because of the different stoichiometry of the simulated crystal slabs (see Table 7.1) a straight forward comparison of the energies of the

reconstructed and the charged is also not possible. To obtain strictly comparable values one would have to calculate energies with each given surface termination for increasing system sizes and for real 2-D systems (as opposed to pseudo 2-D as done here). Doing this in combination with MD simulation is computationally not feasable. However, the stoichiometries of the four systems are at least similar, and all the surfaces are of equal size. Thus we can attempt to make qualitative comparisons between the four energy values of each of those three sets.

In Table 7.2 the total average configurational energies are given. Also given are the magnitude of the net charge and the net dipole moment perpendicular to the surface and the resulting energy corrections for the systems with the polar or charged crystal slabs. The main result is: the AlS systems, chg-AlS and rec-AlS, give clearly the lowest conformational total energies as compared to the other charged or reconstructed surface terminations. This is at least in part due to the greater number of ions in the AlS systems (see parameter N_l in Table 7.1). It is not possible to correct for the different numbers of some ion types in the different systems analytically. Nevertheless there is other clearer evidence in favour of the AlS-t system: Firstly we see in Table 7.2 that the magnitude of the net charge of the chg-AlS-t system is lower than the values for both the chg-KS-t and the chg-Al-t systems. The resulting lower charge density in the surfaces of the AlS-terminated charged system can be expected to lead to a smaller repulsion of likely charged ions in this surface and thereby to a greater stability. Secondly the dipole moment of the relaxed pol-AlS surface has the smallest value compared to the other terminations Just like the lower charge density of the chg-AlS-t system this can be expected to result in an increased relative stability. Thus the energies, net dipoles or net charges confirm the structural results in suggesting that the Al-S-t surface is the most stable.

7.7 Discussion

The following section is divided into several parts each discussing one particular question raised in this chapter.

Comparison of different models for polar surfaces

We have simulated all four un-reconstructed surface terminations in a polar and a charged version. The results of the two simulations cannot be compared directly because the dipole correction term, only used in the simulations of the polar systems (see sections 3.6.2 and 3.5.4), affects not only the energy but also the forces on the atoms and thereby the structure of the flexible part of the crystal and the solution. However, the same surface terminations turned out to be stable with both methods. And also of the reconstructed, i.e., neither charged nor polar, surfaces the Al-t and AlS-t terminations turned out to be the most stable. This gives us some confidence into our results because apparently the applied methodologies for modelling the polar surfaces do not influence the results unduely.

The RMSDs and the relaxation of the surface atoms are generally larger with the polar than with the charged versions. This is obviously caused by the forces due to the dipole correction term because the forces on the flexible surface atoms resulting from the charged and from the polar rigid crystal slabs, respectively, must be similar in magnitude. Thus the deviation of the atomic positions in the surface from their bulk positions would be comparable without the correction term. It is not surprising that the forces due to the dipole correction have a considerable effect because they are proportional to the magnitude of the total dipole moment of the simulation box. Since most of the ions in the crystal are frozen the large dipole moment originating from the polar crystal slab cannot be reduced by relaxation. Hence I consider the charged version as a more realistic representation of the system because a setup like this could theoretically occur in nature while the polar version, as modelled here, is extremely unlikely to be observed; the homogeneous charge background (in contrast to the non-homogeneous charge distribution to be found above real polar surfaces) introduces errors. In the future these could be evaluated by comparing the resulting liquid structure to a system with a surplus of explicit counter ions in the solution. Thus, in contrast to the the dipole correction term, the homogeneous background charge can be seen as a systematically improve-able first order approximation. The high

charge density in the charged system, caused by the small system size, i.e., the small number of (111) layers, has a pronounced effect in the Al-t system where the ordering of the solution is much more distinctive in the charged as opposed to the polar system. However, in the AlS-t systems, where the charge density of the charged version is lower, the solution structure of the polar and the charged systems still show some differences but the overall extent of ordering of the solution slabs is comparable. Although the simulation cell used here, with a crystal slab with a net-charge compensated by a homogeneous background charge, is only a crude approximation to a realistic charged crystal, it apparently gives consistent results. I conclude that, when theoretically investigating the structure of any polar surface, the consideration of charged crystal slabs, in addition to reconstructed ones is advisable. A more systematic investigation of the applicability of this method is subject to future work.

The structure of the PA (111) surface

In our simulations the PA solution above the surfaces is at the saturation concentration. For a real system this corresponds to a steady state with the crystal dissolving and growing at the same velocity. PA grows layer-wise via a screw dislocation mechanism. Growth and dissolution happens at step and kink sites on the crystal surface at low super-saturations. Under these conditions we must expect to find one stable surface cut that represents the termination found on growing PA (111) layers (see Figure 7.2) with other possible terminations dissolving. Via this criterion I can exclude all the KS-t and K-t surfaces which are dissolving. Both the reconstructed, the charged and the polar AlS-t and Al-t terminations are relatively stable. A strong point against the reconstructed Al-t surface, as already discussed in Section 7.6.1, is the fact that potassium ions block the empty aluminium sites produced by the reconstruction thereby thwarting further crystal growth. Evidence in favour of the AlS-t termination in both the charged and the reconstructed systems is that the amplitudes of the vibrations perpendicular to the surface are larger with the Al-t system as compared to AlS-t. The charge density on the chg-AlS-t surface

is half as high as on the chg-Al-t surface and we have seen that this high charge density in the chg-Al-t surface causes a strong field and in turn a far-reaching ordering of ion layers in the solution above the surface. This of course reduces the entropy of the system and by that increases the free energy making the occurrence of this type of surface termination generally less likely.

With all the evidence gathered so far I expect the real PA (111) surface to be terminated by an aluminium-sulfate layer. It is not possible at this point to determine clearly whether a reconstructed termination with only a fraction of the sites in the outer most sulfate layer occupied (rec-AlS-t) or a charged termination with a full sulfate layer on top of the surface (chg-AlS-t) is more likely to occur on a real crystal in aqueous solution. However, since the stability of both terminations seems to be quite similar I would expect both terminations — and everything in between — to be found on real surfaces with the actual sulfate coverage depending on the sulfate concentration in the solution.

The dominating mechanism for the stabilisation of polar (111) faces

Thus this theoretical investigation cannot determine undisputedly whether reconstruction or the enrichment of counter ions above a charged and un-reconstructed surface plays the major role in stabilising the PA (111) surface. However, we did find that in a simulation of the systems at atomic scale resolution with a reasonable model potential, a charged surface can be as stable as the corresponding reconstructed one. As long as there is no experimental evidence to prove the opposite we must assume the chg-AlS-t model representing a valid structure of the PA (111) surface. This is a non-trivial finding, with implications beyond the PA case, because the existence of such an un-reconstructed termination of a polar ionic crystal surface is usually excluded a priori.

Implications of the results for crystal agglomeration

At the first glance the results discussed above seem to contradict experimental findings according to which the force needed to detach two agglomerated (111) surfaces

increases with increasing super-saturation and hence increasing sulfate partial pressure [Pratola et al.(2002)Pratola, Simons, and Jones]. According to our theoretical predictions increased super-saturation would increase the polar character of the (111) faces, giving rise to electrostatic double layer effects which in turn increase the repulsion between two such surfaces. However, I expect that the increased agglomeration strength with higher super-saturation, as observed experimentally, is not a direct consequence of the surface structure. It is probably caused to a large extent by the simple fact that increased super-saturation results in faster crystal growth. Consequently any crystalline bridge between two attached surfaces has grown more and therefore the measured forces to break it are stronger. In addition it is well known [Hansen and Lowen(2000)] that equally charged crystal surfaces can attract each other in the presence of multi-valent counter-ions as is the case here.

Another experimental finding is that, independent of the super-saturation, a pair of two (100) or two (110) faces agglomerates stronger than a pair of (111) faces. This must be a consequence of the involved surface structures and the structures proposed here can easily explain this phenomenon: If two (100) or two (110) faces attach a crystalline bridge can be formed without any further rearrangement of ions or molecules because only by lateral movement two attached (110) or (100) surfaces can build a perfect crystal structure (see Figure 7.5). For two (111) faces this is different because in whatever way we bring them together they cannot directly attach to form a perfect crystalline bridge. Firstly the polar surfaces are more relaxed than the non-polar surfaces and this relaxation must be reversed. Secondly additional ions from the solution are needed in order to build a stoichiometrically perfect crystal bridge. With the termination proposed here, a mixture between rec-AlS-t and chg-AlS-t, additional sulfate and potassium ions have to be brought in position before a continuous PA crystal can be formed. This requires time and energy and therefore the strength of a crystalline bridge between two (111) faces will be weaker than that between two (100) or (110) faces for similar growth times.

7.8 Summary

We have established a theoretical model for PA surfaces that predicts a surface structure terminated by a full aluminium layer and an outermost sulfate layer with coverage varying between 0.75 and 1 depending on the sulfate concentration in solution. The fact that a single termination out of the four possible ones is by far the most stable is compatible with the experimental finding of PA (111) surfaces grow via screw-dislocations building large flat terraces. With the proposed surface structure we can also explain the experimental finding of different agglomeration forces between different combinations of PA faces and the relative order of these forces. By establishing the stability of a charged, rather than the reconstructed ionic crystal surface usually assumed, we question the common practice of excluding the existence of such surface terminations a priori.

The positions of the ions in the surface were found to be very close to the corresponding positions in the perfect bulk crystal structure of PA. In further simulations involving these surfaces it is therefore well justified to use crystal slabs that are completely rigid up to the top most aluminium layer followed by a flexible sulfate layer that can adjust to the conditions in the adjacent solution.

Chapter 8

Forces Between Nano-Crystallites in Aqueous Solution

In this chapter we will finally turn to the key question inspiring this project: Can we quantitatively predict crystal agglomeration from the knowledge of the material properties and process parameters ? The results presented here cannot give a clear answer to this question but it can be seen as non trivial step towards this final goal.

In Section 8.1 a way for the calculation of the potential of mean force between two meso-scale particles in solution is discussed. Although this quantity is not going to be used and, in fact, not calculated in any of the work reported further on, this section is included here since the potential of mean force is the principal quantity that is required to estimate agglomeration efficiencies as discussed in Section 2.2. The remainder of this chapter is organised as follows: The system geometries and computational algorithms I use to estimate the forces between two nano-crystallites in solution are presented in Section 8.2. The choice of the material used for the preliminary calculations and the classical force field used to model this material are discussed in Section 8.3. After a short account on the computational details of the MD simulations in Section 8.4 results obtained with the model used here are presented and discussed. This results section is divided into three parts: In the first part in Section 8.5 we look at results of some calculations performed

to establish the validity of the model we use to simulate the crystallites. The calculated agglomeration forces and other results obtained for a system of two KCl nano-crystallites in solution are given in Section 8.6. In the third part, Section 8.7, I present results for the same KCl-solution system as obtained with a slightly different model that takes into account the lateral flexibility of the crystallites. Finally in Section 8.8 the results are discussed and summarised.

8.1 Calculating the Potential of Mean Force

The potential of mean force (PMF) is the one dimensional section of the free energy surface $\Delta G(\zeta)$ between two molecular configurations connected by a well defined *reaction path* where ζ is a generalised coordinate, for example, the dihedral angle of a flexible molecule or the distance between ligand and receptor in solution. It is useful especially for quantifying the influence of a solvent on the stability of a given configuration of solute molecules. In this case we require the PMF where ζ corresponds to δ the distance of approach of two crystallites in solution. There exist efficient methods for the calculation of free energy differences via Molecular Dynamics or Monte Carlo simulations [Beveridge and Dicapua(1989), Straatsma et al.(1992)Straatsma, Zacharias, and Mccammon,
Kumar et al.(1992)Kumar, Bouzida, Swendsen, Kollman, and Rosenberg, Roux(1995)] Their application to the given problem, however, does not seem to be straight forward.

In a comparatively simple way for calculating a PMF via Molecular Dynamics simulation two molecules (or nano-particles, colloids, surfaces, etc.), A and B, are immersed into a solution. While their respective distance δ is constrained to one single value δ_i the remaining system, essentially the solvent, is simulated un-restrained at a given temperature. The average force on the particles due to interactions with the solvent and with each other, in the direction of the line between, e.g., the two centers of mass $\mathbf{r}_{AB}$ (the

reaction coordinate) is calculated as

$$\langle F \rangle = \left\langle (\mathbf{F}_A - \mathbf{F}_B) \frac{\mathbf{r}_{AB}}{r_{AB}} \right\rangle \tag{8.1}$$

This is repeated for a range of different separations δ_i, giving the average force as a function of the distance. The resulting function $\langle F(\delta) \rangle$ is then integrated numerically from $\delta = \infty$ to $\delta = \delta_0$ to give the free energy difference between the two particles at infinite separation and at some finite distance δ_0 — frequently taken to be the contact distance,

$$\mathrm{PMF}(\delta_0) = \Delta G(\delta_0) = \int_{\infty}^{\delta_0} \langle F(\delta) \rangle \, d\delta \approx \sum_{\infty}^{\delta_0} \langle F(\delta) \rangle \, \Delta\delta \tag{8.2}$$

In practice the upper integration boundary is not taken to be infinity but rather a finite distance where the interaction between the two particles in solution is negligible or can be approximated by some mean field theoretical approach.

Proceeding thus we introduce an error in the calculated PMF [Sprik and Ciccotti(1998)] because the geometry of the system we want to simulate requires the application of a special set of holonomic constraints, as will be seen in the next section. The question how to correct free energy results obtained in simulations with constraints has triggered a considerable debate in the last decade.[Straatsma et al.(1992)Straatsma, Zacharias, and Mccammon, Pearlman(1993), Mulders et al.(1996)Mulders, Kruger, Swegat, and Schlitter, Den otter and Briels(1998), Sprik and Ciccotti(1998), Gullingsrud et al.(1999)Gullingsrud, Braun, and Schulten, Darve and Pohorille(2001)] It is unclear whether any of the proposed methods can be applied to the present problem. The constraints applied to the system studied here (see Section 8.2) are more complex and affect more degrees of freedom than a simple constraint of the distance between the centers of mass of two molecules. Therefore a free energy calculated with the model outlined below is theoretically not well defined. For now I simply define a quantity by Equation 8.2 and call it potential of mean force. I expect that meaningful results can be obtained with this expression if one uses the obtained uncorrected value of ΔG only to compare similar systems with the same

constraints, dimensions and geometrical characteristics. This seems to be common practice and the method has been applied to calculate the PMF between two molecules in solution [Perera and Berkowitz(1993)] or between one molecule in solution and a surface.[Shinto et al.(1998)Shinto, Sakakibara, and Higashitani]

In the context of free energy difference calculations the forces (or energies) are sometimes not calculated for a discrete set of values of ζ, but ζ is varied continuously between the two end-points within a single simulation run, thereby minimising the error introduced by the numerical integration [Straatsma et al.(1986)Straatsma, Berendsen, and Postma]. This so called, *slow growth thermodynamic integration*, however, is still a matter of debate[Mitchell and Mccammon(1991), Straatsma and Mccammon(1991)] since the simulated system is supposed to be in thermodynamic equilibrium over the whole range of ζ to obtain a valid free energy difference. Thus, unless ζ is varied extremely slowly, a large hysteresis is obtained between forward (growing ζ) and backward (decreasing ζ) simulation runs. The slow equilibration of the system will in fact turn out to be the major obstacle we encounter in this work, as will be discussed below.

8.2 Calculation of Inter Particle Forces, the System Geometry

The system we want to model consists of two microscopic particles immersed into an infinite solution, and we are interested in the variation of the forces between the two particles while they approach each other. The separations we are interested in lie in a range between zero and about two nanometers (see Fig. 2.1B). At this distance the DLVO theory[Israelachvili(1991)] breaks down due to structural forces caused by the finite volume and distinctive structure of the solvent molecules[Israelachvili and Mcguiggan(1988)] and we need to model the solvent as discrete molecules rather than a continuum. The determination of forces between particles in solution is generally assumed to be easier when the distance r between them is large (In the DLVO theory these forces are essentially

VdW forces, for macroscopic particles typically proportional to r^{-2}, the proportionality constant (the so called Hamacker constant) being determined either in experiment or via some theoretical calculation of the dispersion interactions between the materials in question). Interestingly enough this assumption turns out to be wrong at closer inspection: Ackler et al.[Ackler et al.(1996)Ackler, French, and Chiang] determined the Hamacker constant with different experimental and theoretical methods for a range of materials and found differences in the obtained values for a given material of up to a factor of seven. Although some progress seems to have been made — in a recent publication [Andersson et al.(1998)Andersson, Hult, Apell, Langreth, and Lundqvist] VdW forces between parallel and distant surfaces were calculated with a density functional theoretical approach, quasi ab initio — this is somewhat worrying. However, investigating this question in more depth would exceed the scope of this thesis by far and we therefore leave this question open for now.

Once two particles are closer than a few nano-meters the approaching surfaces can be modelled as two infinite, parallel and flat surfaces enclosing a pore filled with solvent. Especially for crystals that grow layer-wise this is a reasonable approximation that would allow us to reduce the system size dependence of the calculated properties by using periodic boundary conditions. This model or variations thereof have been used in a large number of studies of the effective forces between colloidal particles, crystal or metallic surfaces separated by an electrolyte solution. In most of these publications a primitive model electrolyte (PME) or some mean field approximation (e.g. Poisson Boltzmann Equation) was used to represent the solution phase.[Marcelja(2000), Henderson et al.(2000)Henderson, Bryk, Sokolowski, and Wasan, Forsman et al.(1998)Forsman, Jonsson, and Akesson, Rivera and Sorensen(1994), Bratko and Henderson(1994), Sorensen and Sloth(1992), Bratko et al.(1991)Bratko, Henderson, and Blum Feller and Mcquarrie(1993)] It has been suspected for some time and only recently it has been shown unambiguously [Yang et al.(2002)Yang, Yiacoumi, and Tsouris] that these simplified models can not even qualitatively account for some important structural details of an ionic solution in a narrow slit-pore between two surfaces. In the accessible literature

I have found only one example [Yang et al.(2002)Yang, Yiacoumi, and Tsouris] of such a calculation with explicit representation of all molecules in the solution (ions and water) in a pore for varying pore widths. In this study an aqueous ionic solution consisting of water and NaCl was modelled as a mixture of Lennard Jones spheres with, in the case of the water, variable atomic charges. The surfaces were modelled as charged, flat and hard walls. These simulations in the canonical ensemble, however, were only done after the ionic concentration in the pore as a function of the pore diameter was established via a numerical solution of the Poisson Boltzmann Equation. Hence we are facing results that have been obtained by a combination of simple mean field approximation followed by explicit, detailed simulation of the system. The fact that the structural results obtained with a mean field approximation alone differ from those found when using explicit solution molecules remains valid. However, it is all but clear whether this method can be applied to accurately model a realistic system because the concentration of the ions in the pore and the resulting structure are obtained in a non-consistent way. Thus we will try here to calculate both the concentration and the structural features of the solution using a model where all the involved ions and molecules are simulated explicitly. Why this is complicated and, to the best of our knowledge, has not been done so far for a comparable system is discussed in the following.

Although the diffusion coefficient of solvent molecules in a pore can be markedly smaller than it is in the bulk [Mansour et al.(2002)Mansour, Dimeo, and Peemoeller, Sansom et al.(1996)Sansom, Kerr, Breed, and Sankararamakrishnan,
Gallo et al.(1999)Gallo, Rovere, Ricci, Hartnig, and Spohr], the velocity of a nano-crystallite in a liquid will still be slower than the velocity of individual solvent molecules by several orders of magnitude. Therefore it is generally assumed that there is a thermodynamic equilibrium between the liquid phase in the pore between two particles and in the surrounding bulk solution down to very small separations close to the contact distance. The concentration(s) of liquids and liquid mixtures in confined geometries, such as microscopic pores, in contact and in equilibrium with a bulk solution of the same material at a given temperature are generally

not equal to the bulk concentrations and will vary with varying pore diameter d_p.[Han et al.(1993)Han, Cushman, and Diestler, Yethiraj and Hall(1991)] This density as a function of d_p is not known a priori and must therefore be allowed to change. The conserved quantity in such a case is the chemical potential μ_i. That is, we simulate the liquid at the same constant chemical potential at each given separation between the two particles (surfaces). Algorithms for generating such a μVT ensemble with Monte Carlo or Molecular Dynamics simulations do exist and have been applied to a wide range of systems [Adams(1975), Mezei(1987), Shelley and Patey(1994), Yau et al.(1994)Yau, Liem, and Chan, Macedonia and Maginn(1999)], but so far none of these algorithms is powerful enough to cope with an aqueous ionic solution at ambient conditions. Some of these algorithms and a possible alternative will be discussed in the two following sections.

8.2.1 Slit-pore at Constant Chemical Potential

If we want to establish the properties of a fluid in a confined geometry the *in vivo* version of this fluid is, in many interesting cases, in contact with some bulk phase at constant temperature and pressure. Since the explicit simulation of this bulk phase *in silico* is usually very expensive in terms of the required computational resources one tries to establish the constant chemical potential by other means. Most published results of molecular simulations of fluids in confined geometries were obtained with algorithms producing a grand canonical (GCE) or μVT ensemble [Brovchenko and Geiger(2002), Brovchenko et al.(2001)Brovchenko, Geiger, and Paschek, Schoen et al.(1998)Schoen, Gruhn, and Diestler Schoen and Diestler(1997), Cracknell et al.(1995)Cracknell, Nicholson, and Quirke, Somers and Davis(1992), Lupkowski and Vanswol(1991), Schoen et al.(1989)Schoen, Rhykerd, Cushman, a Luzar et al.(1987)Luzar, Bratko, and Blum, Vanmegen and Snook(1981)] as discussed in Section 3.6.3.

A number of improved algorithms have been proposed over the last two decades [Mezei(1987), Shing and Azadipour(1992),

Vega et al.(1994)Vega, Shing, and Rull, Shelley and Patey(1994), Yau et al.(1994)Yau, Liem, and Chan, Macedonia and Maginn(1999)], There is one interesting method devised by Shing et al.[Shing and Azadipour(1992), Vega et al.(1994)Vega, Shing, and Rull] which provides for constant chemical potential in MD or MC simulations, without the need for particle insertion/deletions, by separate canonical ensemble simulations with a range of different particle numbers in parallel. The method seems to be very efficient for pure substances but less so for mixtures. An estimate for the chemical potential of each component needs to be calculated continuously, and for each combination of particle numbers a separate initial configuration must be equilibrated. An estimate of the required CPU time implies that this algorithm is not applicable to our problem.

Another algorithm that efficiently circumvents the problem with vanishing insertion probabilities was proposed by Cagin and Pettitt.[Cagin and Pettitt(1991)] Here particles are not inserted or deleted in one step but gradually, reminiscent of a thermodynamic integration. Although one can show that this algorithm produces a Grand Canonical ensemble,[Lynch and Pettitt(1997)] its applicability for the problem at hand is questionable. There are always one or more fractional particles present in the sample, something that does of course not correspond to anything happening in reality. Having such fractional particles present in a narrow slit-pore might introduce undesired effects that are hard to quantify.

An alternative family of algorithms [Wang and Fichthorn(2000), Schoen et al.(1994)Schoen, Diestler, and Cushman, Svensson and Woodward(1994)] renders the chemical potential in an MC or MD simulation constant by appropriate control of certain components of the stress tensor in the simulation box. Here particle insertions or deletions into/from the system are not necessary as well, and hence the simulation of very dense fluids is possible. However, these methods only work for pure substances and cannot be applied to mixtures, such as an ionic solution, in which the chemical potentials of more then one substance need to be controlled simultaneously. For ionic solutions one usually falls back upon primitive

model electrolytes [Otto and Patey(2000), Wu et al.(1998)Wu, Bratko, and Prausnitz, Forsman et al.(1998)Forsman, Jonsson, and Akesson, Bratko and Henderson(1994), Bratko et al.(1991)Bratko, Henderson, and Blum], a model which must be considered as a too great simplification, as explained in the previous section. Recently Shelley and Patey reported a simulation of an aqueous ionic solution at constant chemical potential with explicit water molecules [Shelley and Patey(1999), Shelley and Patey(1994)]. They used a variant of a configuration biased GCMC algorithm to achieve this goal but the atomic charges of the ions used there are markedly smaller than one elementary charge and the temperature is 500 K or higher. Currently these conditions seem to represent the upper boundary of what can be done with grand canonical simulation algorithms. However, here we are interested in the simulation of an aqueous ionic solution with explicit representation of the water molecules at ambient conditions. Such a system seems to be out of range with currently available methods.

Another complication arises because we are essentially interested in agglomeration in the regime of super saturated solutions. In other words, we have a non-equilibrium system rendering the concept of chemical potential useless since μ is an equilibrium property and consequently not well defined in a super-saturated solution.

To conclude, we cannot use one of the established grand canonical MD or MC algorithms for our system and in the next section we investigate a possible alternative.

8.2.2 Direct Simulation of a Particle Reservoir: The Immersed Sandwich

At the current state of the art the above mentioned problems can only be solved by going the *brute force* way, using a system geometry as sketched in Figure 8.1. Thus we include a minimum amount of bulk liquid into the simulation in order to obtain a system with constant chemical potential. With increasing computer power this ansatz has become affordable and has been applied to a few simple systems so far [Yethiraj and Hall(1991), Shinto et al.(1999)Shinto, Miyahara, and Higashitani, Wallqvist and Berne(1995),

Figure 8.1: **System geometry for the simulation of a slit pore in contact with bulk solution.**

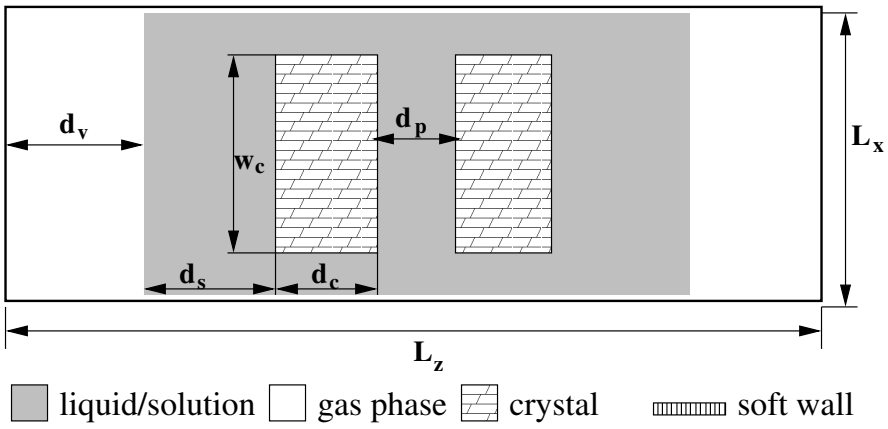

Zhang et al.(2001)Zhang, Balasundaram, Gehrke, and Jiang]

The simulation box shown in Figure 8.1 is periodically repeated in all three dimensions. Two crystallites, represented by a rigid lattice of ions, are completely immersed into a liquid solution. In the y-dimension the crystal as well as the solution attach continuously to their periodic replica resulting in two rows of infinitely long crystal slabs immersed into a slab of solution (the "immersed sandwich"). The slit pore between the two crystal slabs is in contact with two layers of solution at the other side of each crystallite. These solution layers are just big enough to have a region of constant density in the direction perpendicular to the slit-pore and thereby bulk properties. This bulk phase in turn is in contact with a gas phase. The resulting phase boundary reduces the thermodynamic degrees of freedom and ensures that on average the partial pressure of each components in the solution and in the gas phase is equal and constant as long as the values for the total volume and the temperature let the system reside in the two phase region in the phase diagram. This phase boundary allows us to use a comparatively small bulk volume, just big enough to serve as an efficient buffer for ions. In other studies a relatively large and computationally inefficient bulk volume, filling the whole simulations box, was used [Shinto et al.(1999)Shinto, Miyahara, and Higashitani,

Wallqvist and Berne(1995)] in combination with MD at constant temperature and pressure. At room temperature the dilute gas-phase region in our model will be essentially empty most of the time, i.e., a vacuum separating the periodic images in the z-dimension. This empty region is required to obtain an effectively 2-D-periodic system. [Yeh and Berkowitz(1999)] In Section 3.5.4 is was confirmed that with such an, appropriately dimensioned, empty space we can use a 3-D Ewald Summation to account for the long range interactions. This is computationally more efficient than most of the dedicated algorithms accounting for the long range interactions in systems with two-dimensional periodicity.[Crozier et al.(2000)Crozier, Rowley, Spohr, and Henderson, Grzybowski et al.(2000)Grzybowski, Gwozdz, and Brodka] Here we are going to use only simple crystals with Type I faces (see Section 7.2) leaving the entire system with a vanishing average net dipole moment. Therefore an empty space of at least 25Å should suffice to guarantee negligible forces acting between periodic images in the direction normal to the surfaces (here the z-dimension).

The setup sketched above has the advantage that the total forces on the crystallites, including the forces due to the surrounding bulk solution, can be calculated consistently within one simulation run. It can also be used for the simulation of moderately supersaturated solutions because it consists only of bulk solution and flat surfaces. For many, if not most, materials it has been established that in the regime of small up to moderate super-saturation crystal growth only takes place at s.pdf and kinks in the surface while the largest parts of the crystal surface and thereby very likely those parts that approach each other during agglomeration are flat, i.e., not growing.[J.(1993)]

Before we can apply the method proposed here to realistic systems we need to address the following features: The obvious disadvantage of the chosen system setup is the relatively large system size required which exceeds the size of a corresponding simulation including only the slit pore by at least one order of magnitude. Another aspect is the equilibration which might proceed prohibitively slow due to the comparatively long and *winded* path a solvent molecule or an ion has to travel from the bulk to the pore. The value of the surface surface forces per area calculated for such a system will depend on

the system size, primarily on the parameter w_c, the width of the crystal slabs in the x-dimension. However, we are primarily interested in the effect of an ionic solute and its concentration on the relative forces between two crystals in an aqueous solution. We expect that this effect can already be seen for comparatively small values of w_c. While the absolute value of the calculated forces per surface area will probably vary with w_c when w_c is smaller than a certain threshold, the relative values as calculated with different compositions of the solution will be much less affected by the system size. In any case it will be necessary to establish a minimum size of w_c required to obtain reproducible results. It has been shown [Gao et al.(1997)Gao, Luedtke, and Landman] that the relative arrangement of two structured surfaces in the plane parallel to those surfaces can have a distinct influence on the liquid structure and the resulting forces acting between them. On the other hand side it may increase the system size dependence of the measured forces if we let the crystallites move in the x-y-plane because then the portion of the pore covered by crystal surfaces on both sides will be smaller.

In the following we report results of a number of calculations done to test the feasibility of the method and the validity of various assumptions. We perform simulations with pure water and with a saturated KCl solution. We test the dependence on system size and for different pore widths δ_p we monitor the convergence of the measured forces and the liquid density in the pore. To test the influence of the lateral mobility of the crystallites we try out and compare two approaches: i) We fix the positions of the crystallites in the x-y-plane completely so that they are in register, i.e., at the relative position corresponding to the energy minimum of the bare crystallites. ii) We let the two crystallites move according to the frictional forces from the solution in the x and y-dimensions parallel to the interfaces. Some details about the implementation of these two approaches are given in Section 8.4.

8.3 The Material and Model Potentials

For our test calculations we use a material that is comparatively simple and easy to model computationally. This is primarily done in order to minimise artifacts due to shortcomings

of the force field and other approximations made in classical molecular simulation. The second criterion being the availability of experimental as well as theoretical results for the material, we finally decided to use potassium chloride (KCl). It has been shown that at moderate super-saturations KCl grows in flat layers [Polak and Sangwal(1999)] and consequently large flat and well defined surfaces are exposed to the solution. For this reason the possibility of crystal growth events modifying the measured forces in an unpredictable manner can be taken as highly unlikely.

8.3.1 The Solution

All the Model Potentials used here are purely classical empirical force fields. For modelling the water we use the extended simple point charge model (SPC/E) which describes the water-water interactions by a combination of a Lennard Jones potential between the oxygen sites and Coulomb interactions between partial charges on the oxygens and hydrogens. For the interactions between water and the crystal components K^+ and Cl^- we also use a combination of Lennard-Jones and Coulomb potentials with a set of parameters published in a paper of Linden-Bell et al.[Rasaiah and Lynden-bell(2001)] In this paper the authors give as original source for the parameters a personal communication with Dang. One could expect polarisability to play a non negligible role in the simulation of surfaces. This question has recently been addressed [Yeh and Berkowitz(2000)] in a publication presenting results of simulations of water between two silver surfaces and under the influence of an additional external inhomogeneous electric field. Using a polarisable and a non polarisable water model resulted in structural and dielectric properties obtained with both models that agreed within the respective error bars. Given this result and the fact that polarisable model potentials are generally quite expensive in terms of the required CPU-time we will only use the non polarisable SPC/E model in all the simulations. Both the KCl parameters of Dang and the SPC/E parameters are listed in Table 8.1.

8.3.2 The Crystal

We are primarily interested in the dynamics of the solution between the crystal faces and the resulting structural forces. For KCl, a crystal with the cubic rock salt structure, non-polar low index faces, as used here, can be expected to show only a minimum degree of relaxation. For these reasons we decided to use completely rigid crystal lattices in the simulations. In order to investigate the validity of taking the crystal to be rigid we perform a few test calculations with rigid and flexible crystals.

Applying the commonly used Lorentz-Berthelot mixing rules to generate van der Waals parameters for the K-K, Cl-Cl and K-Cl interactions from the parameters used for the K-O, Cl-O and O-O atom pairs in the solution and combining these with the formal ionic charges results in parameters that hopelessly underestimate the KCl lattice parameter upon lattice energy minimisation. The only other model potential for the K-Cl VdW interactions we found employs a Buckingham potential [Binks(1994)] the parameters of which were fitted to reproduce a number of properties of the crystal. Electrostatic interactions between formal charges are complemented by a shell model to account for polarisability of the chloride ion. The shell model, frequently used for lattice energy minimisations of inorganic materials, is rarely used in MD simulations because it requires a quite time consuming iteration-procedure for finding the positions of the massless shells at each MD-timestep. Although improvements have been proposed, most notably the adiabatic shell model by Fincham et al.[Mitchell and Fincham(1993)], the computational efficiency of rigid ion models is still higher by a factor of at least five. Therefore we generated a new KCl force field. In this rigid ion model, henceforth labelled FF1, the charges used to calculate the Coulomb interactions are taken to be the formal ionic charges. For the parameter σ of a Lennard Jones potential we use scaled Pauling ionic radii [Huheey(1983)] while the parameter ϵ was fitted to reproduce the crystal structure upon lattice energy minimisation using GULP [Gale(1997)]. Thereby care was taken to obtain parameters that resulted in the energy minimum of the Cl-Cl VdW interactions being approximately ten times as low as the according K-K minimum with the K-Cl minimum being in be-

Table 8.1: **Force field parameters used here;** The KCl-parameters of Dang the water-KCl interactions and the SPC/E potential for water-water interactions were both used in all simulations. For the KCl interactions within the crystals we compare a rigid ion potential (FF1) and a shell model potential (FF2); in the latter only the Cl-ion has a shell (sh) and a core (co) while K is here a rigid ion as well; units: energies (ϵ, A, C): kJ/mol; length ($d, \sigma, 1/\rho$): Å; charge (q): e.

FF1		**FF2** [Binks(1994)]			
σ (K)	3.46	A (K-K)	$2.1122\ 10^5$	A (Cl_{sh}-Cl_{sh})	$3.1807\ 10^5$
ϵ (K)	0.36	ρ (K-K)	0.1916	ρ (Cl_{sh}-Cl_{sh})	0.3289
σ (Cl)	4.71	C (K-K)	0.0	C (Cl_{sh}-Cl_{sh})	$1.0391\ 10^4$
ϵ (Cl)	2.11	A (K-Cl_{sh})	$7.7400\ 10^5$	q (K)	1.0
q (K)	1.0	ρ (K-Cl_{sh})	0.2840	q (Cl_{sh})	-1.984
q (Cl)	-1.0	C (K-Cl_{sh})	0.0	q (Cl_{co})	0.984

KCl-water (Dang et al.[Rasaiah and Lynden-bell(2001)])

σ (K)	3.25	σ (Cl)	3.785	q (K)	1.0
ϵ (K)	0.5216	ϵ (Cl)	0.5216	q (Cl)	-1.0

SPC/E water [Berendsen et al.(1987)Berendsen, Grigera, and Straatsma]

σ (O)	3.169	q (O)	-0.8476	d_{OH}	1.63299
ϵ (O)	0.6502	q (H)	0.4238	α_{HOH}	104.47°

tween. Thus we account qualitatively for the larger polarisability and thereby dispersion interactions of the Cl^- ions. In Table 8.1 the parameters of both force fields are given.

8.4 Simulation Conditions & Computational Details

Unless stated otherwise the following simulation methods and parameters are used in all the simulations reported in this chapter: The long range interactions are accounted for by the use of Smooth Particle Mesh Ewald [Essmann et al.(1995)Essmann, Perera, Berkowitz, Darden, Lee, and Pedersen] with an approximate relative accuracy of 5×10^{-6}. The real space part of the Ewald Summation and all short range interactions are truncated at 9 Å. A dipole correction term as discussed in Section 3.6.1 is applied to ensure independence of the results from interactions between periodic replicas in the z-direction perpendicular to the interfaces. The timestep is 0.002 ps and the temperature is kept constant at 300 K by use of a Nose-Hoover type thermostat [Hoover(1985)] with a relaxation time constant of 0.1 ps. As starting configurations we use crystal slabs with the ions in the experimental bulk lattice positions, built with the *Cerius*^{2} surface builder module,[Mol(1999)] with the exposed KCl (110) or (100) surfaces parallel to the x,y-plane. Upon these crystallites we superimpose a regular lattice of the appropriate amount of solute/solvent molecules and all those molecules with a distance to the crystal below a certain threshold value are removed. All configurations obtained in this way are equilibrated for at least 50 ps before a production run is started. All calculations are done using the program DL_POLY.[Smith et al.(2002)Smith, Yong, and Rodger]

The two KCl nano-crystallites, as shown in Figure 8.1, are simulated as rigid bodies in all cases apart from one test simulation discussed in Section 8.5. The translational and rotational motion of the crystallites are simulated in two different manners: i) both crystals are "frozen" in their initial positions in perfect register, i.e., with each chloride ion on one surface being opposite a potassium ion on the other surface, and vice versa; only the solution molecules are allowed to move during the simulation. ii) the positions of crystals are constrained in the z-dimension, i.e., the distance between the two opposing surfaces is held constant at a given value of d_p. The rotational degrees of freedom are also constrained to their initial values so that the two crystal surfaces and their surface

lattice vectors are always parallel. The crystals are, however, allowed to move laterally with respect to each other, in the x and the y-dimension parallel to the interfaces. This is achieved by summing up the forces in the x and y direction on all atoms in each crystal. Then the average forces are calculated, and the forces in the x and y directions on each atom are assigned these average values. Forces in the z direction are set to zero. An additional external potential is applied to ensure that the two crystallites do not move too far away from each other in the x-direction so that always a slit pore with a given minimum length remains. This external potential, U_{ext}, and the resulting force, F_{ext}, depend only on the x-position of each atom.

$$\begin{aligned} U_{ext}(x) &= C \cdot (x - x_0 - \delta x)^{-9} + F_0(x - x_0 - \delta x), x > x_0 \\ U_{ext}(x) &= C \cdot (x + x_0 + \delta x)^{-9} - F_0(x - x_0 - \delta x), x < -x_0 \qquad (8.3) \\ F_{ext}(x) &= -9\ C \cdot (x - x_0 - \delta x)^{-10} - F_0, x > x_0 \\ F_{ext}(x) &= -9\ C \cdot (x + x_0 + \delta x)^{-10} + F_0, x < -x_0 \qquad (8.4) \\ F_0 &= 9\ C \cdot \delta x^{-10} \end{aligned}$$

The parameters used in all the simulations reported are C = 700 kJ/mol and $x_0 = 11.66$ Å. The outermost atoms in the x-dimension in each crystallite in the initial configuration, when they are in perfect register, are at $x = \pm\ 9.99$ Å and the distance between in the x-dimension between the two crystals in perfect register and in perfect mismatch respectively is $\delta_x = 2.22$ Å. Thus the crystallites can respond to the frictional forces from the solution and move unimpeded through a relative distance of $1.5 \cdot \delta_x$. If the distance between their centers of mass in the x-direction exceeds $1.5\ \times \delta_x$ a steep repulsive potential sets in. Thereby the two surfaces can explore every possible mutual arrangement in the x-y-plane without them drifting apart completely in the x-direction. Via the second terms on the right hand sides of Eqn. 8.3 and 8.4 the potential and the resulting force are shifted, or tapered, so that no discontinuity in the force on a particle occurs as the external potential sets in.

Table 8.2: **Lattice parameters (in Å) and elastic constants (in GPa) of KCl**, after lattice energy minimisation with two different model potentials

	a	c_{11}	c_{12}	c_{44}
FF1	4.4398	7.52	1.33	1.33
FF2	4.4504	4.83	0.84	0.84
exp[a]	4.4398	4.5±0.4	0.628±0.006	0.690±0.03

[a]Experimental values are taken from [Landolt(1993)]

8.5 Results I, Model Potentials and Rigid Crystals

Both the SPC/E water model and the parameters for the KCl-water interactions from Dang et al. have been used before in published studies. Therefore we use these parameters without any further scrutiny and concentrate on the KCl-KCl interaction parameters and the ramifications of the crystal being simulated as rigid body without internal degrees of freedom. We calculate structural results obtained for a water layer upon a crystal slab with flexible ions where the ion ion interactions are described either by the rigid ion force field devised here (FF1) or with the shell model potential mentioned in Section 8.3.2 (FF2). These results are compared to results obtained for a water layer upon a completely rigid crystal.

In Table 8.2 the lattice parameters and elastic constants calculated with both force fields considered here are compared to experimental values. The elastic constants as calculated with FF2 are considerably closer to the corresponding experimental values than those calculated with FF1 while the lattice constant is reproduced sufficiently accurately with both forcefields.

In the following structural properties obtained via MD are compared. We perform MD

simulations of a system consisting of 356 water molecules above the (110)-face of A KCl crystal. The crystal consists of each 160 Cl^- and K^+ ions arranged in four layers perpendicular to the 110 direction. Starting from the initial configuration, the perfect crystal lattice and randomly situated water molecules positioned in a box of 25.1×22.2×67.5 $Å^3$, each simulation includes an equilibration period of 50 ps and a production period of 200 ps. More simulations of equal length are performed for the (100) KCl surface with 2×175 ions and 315 water molecules in a 22.2×22.2×67.5 $Å^3$ box. In all cases the box dimensions used lead to a system with a vacuum layer of at least 20 Å between the water-vacuum and the crystal-vacuum interfaces. In the first simulation set up (A) the whole crystal is kept rigid by setting the force on the ions to zero at each time-step. In the second (B) the ions interact via the FF1 potential. In both simulations, A and B, the total volume of the simulation box was held constant. In the third simulation run (C) conditions were identical to B apart from the integration algorithm which here included a Nose Hoover barostat [Melchionna et al.(1993)Melchionna, Ciccotti, and Holian] keeping the pressure constant at 0 Pa and allowing for isotropic volume fluctuations. In Figure 8.2 snapshots are shown of the final configurations of systems A-C.

Obviously the crystal lattices in simulations B and C start to dissolve. Usually both crystal growth and dissolution are processes that proceed via lattice defects, s.pdf and kinks.[J.(1993)] Since here the initial configuration was a perfect crystal surface the dissolution of the crystal is probably an artifact due to the inaccurate force field. It is worth mentioning, however, that some degree of realism is retained because after a closer look at the final configurations one realises that in both cases B and C the crystals rearranged so that eventually a {100} face is exposed towards both the vacuum and the water interface. The {100} faces, on the other hand side, are, according to experiment and attachment energy predictions, the morphologically most important and thereby most stable faces [Polak and Sangwal(1999)]. Therefore the observed reconstruction of the (110) face can be seen as a realistic and desirable feature of the simulations. This phenomenon, called micro-faceting, is well known and has been observed in experiment on a number of crystal surfaces.[J.(1993)] Not surprisingly the reconstruction in the NPT ensemble (C),

Figure 8.2: **Snapshots of KCl + water systems after 240 ps MD**. For each system the exposed surface, the force field used for the ion-ion interactions in the crystal (unless the crystal is rigid), and the ensemble (constant volume (V) or pressure (P)) are indicated.

A: (110), rigid, V

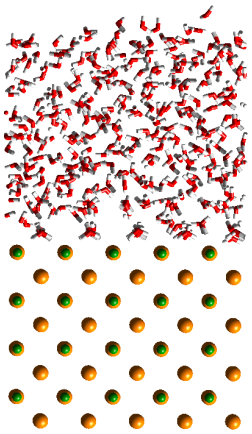

B: (110), FF1, V

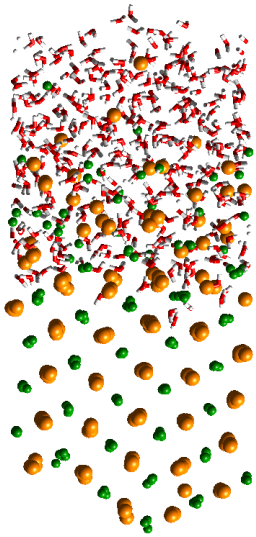

C: (110), FF1, P

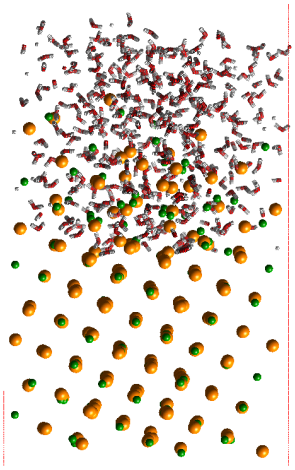

D: (100), rigid, V

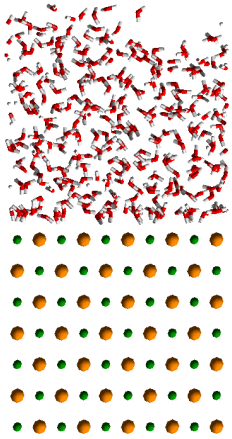

E: (100), FF1, V

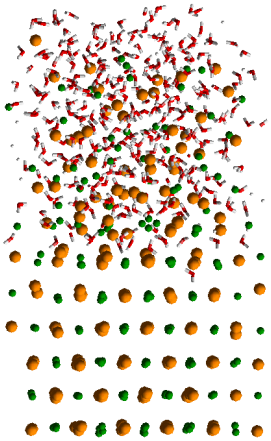

F: (100), FF2, V

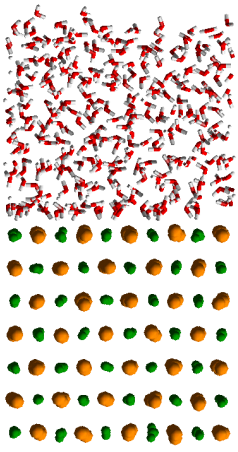

Figure 8.3: **Average mass and charge densities**, as function of the coordinate z of the water atoms for the rigid crystal with FF1 (D) and the flexible crystal with FF2 (F)

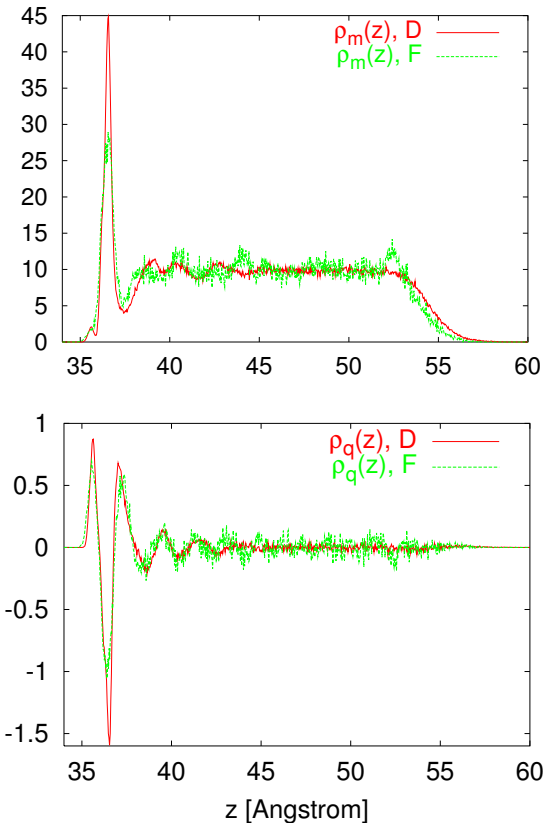

Figure 8.4: **Snapshots of the KCl-water interface after 240 ps MD**

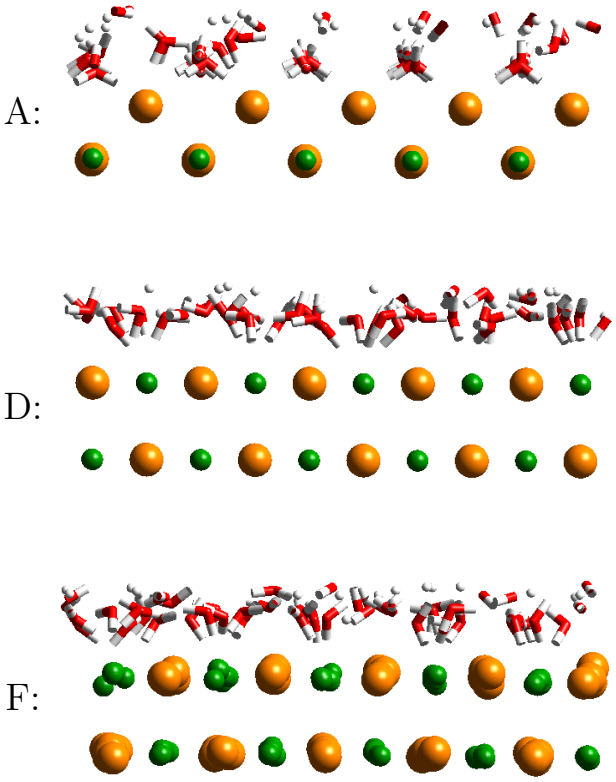

where the lattice parameters can vary to allow for a *smoother* transition between the two states looks somewhat more regular than it does in the NVT simulation (B). It would be interesting performing longer simulation runs in order to find out whether the dissolution of the crystal will stop at a certain degree of saturation of the solution.

To establish whether the dissolution of the crystals in runs B and C was really due to the poor force field or rather due the unstable (110) surface we did three more simulations with (100) faces as starting configuration. In the first one (D) the crystal is again held rigid, in the second (E) we use FF1 and in the third (F) we use FF2. All three simulations

are performed at constant volume. Comparing snapshots E and F in Figure 8.4 it becomes evident that the dissolution is definitely a consequence of the model potential FF1. There clearly are some lattice vibrations with FF2 but the surface remains intact while when using FF1 the crystal layer closest to the crystal water interface has already dissolved after 240 ps.

Of paramount interest here are the details of the structure of the water close to the surface. Since for the results obtained with the FF1 force field this surface is not well defined we compare only the rigid and the FF2 surface structures as shown in Figure 8.4. For A, the rigid (110) surface, most of the water molecules in the first layer are sitting either halfway between two surface chloride anions with the hydrogens pointing towards the Cl^- or directly above a potassium cation with the hydrogens pointing towards the solution. The water above the (100) surface is less ordered for both the rigid (D) and the flexible (F) crystals. Here most of the water molecules are oriented with their H-H axes approximately perpendicular to the surface with one of the hydrogens pointing towards a chloride anion. The higher order above the (110) face results necessarily in a lower contribution to the entropy for this system which in turn raises the free energy, contributing to the lower stability of the {110} family of faces as compared to {100}. When comparing D and F in Figure 8.4 a straightforward conclusion is not possible. As can be seen from the slightly more pronounced peaks in the Chloride-Hydrogen radial distribution functions (not shown here) there is a higher degree of order in model D. These differences, however, are relatively small and the positions of the first three peaks are very similar for the D and the F model. Similar information can be extracted from the charge and mass density along the z-axes as shown in Figure 8.3. We conclude that the rigidity of the crystal has some influence on the structure of the water close to the surface. The differences, however, are small and if one is primarily interested in the forces between surfaces as a function of their separation, i.e., essentially energy differences rather than absolute energies the rigid surface is expected to be a valid approximation. Thus in all the simulations reported below we use "frozen" crystallites and apply the potential by Dang et al. to model the interactions between the ions within the crystal and in solution.

The interaction between two ions residing in different crystal slabs is also described by this potential since here only the r^{-6} dispersion term is important and there is no reason to assume that the according parameter in one empirical force field is any better than the one in another empirical force field. Moreover the direct crystal crystal interactions and forces are comparatively small as will be seen below, and they can easily be corrected a posteriori if this turns out to be necessary.

8.6 Results II, Structure and Forces in the Frozen Sandwich

After having established the validity of the force field and the rigid crystal approximation we now turn to the main results of this chapter: The forces and liquid structure as calculated with the system geometry proposed in section 8.2.2 (Figure 8.1). In most of the test calculations for the force field we used the (110) rather than the morphologically more important (100) face. Since here we are primarily interested in establishing the feasibility and the efficiency of the simulation method rather than making realistic estimates for the agglomeration of KCl crystals we continue using the (110) faces Simulations are performed for a range of pore widths, i.e., we adjust the position of the crystallites along the z-dimension to obtain a range of pores with a diameter d_p varying between 15.6 and 6 Å. For each value of d_p an MD simulation is performed with all crystal ions "frozen" in their initial position (perfect fcc-lattice with experimental values for the lattice parameter, two opposed (110) faces) throughout the simulation and in perfect register, i.e., each Cl^- ion in the uppermost layer of one surface directly opposed by a K^+ ion on the other surface and vice versa. Parameters of all the simulations performed with this system are summarised in Table 8.3.

Table 8.3: **Setups for Simulations with the System Geometry Sketched in Figure 8.1**

label	d_p/Å[a]	N_{H_2O}[b]	N_{KCl}[c]	L_x/Å[d]	L_z/Å[e]	time/ps[f]
w-6.0	6.0	1526	0	32.2	129.95	(300+) 400
w-6.2	6.2	1526	0	32.2	129.95	400
w-6.4	6.4	1526	0	32.2	129.95	(310+) 670
w-6.6	6.6	1526	0	32.2	129.95	400
w-6.8	6.8	1526	0	32.2	129.95	(440+) 700
w-6.8-x	6.8	2042	0	36.7	129.95	380
s-6.0	6.0	1292	117	32.2	129.95	(486+) 200
s-6.4	6.4	1292	117	32.2	129.95	(344+) 400
s-6.8	6.8	1292	117	32.2	129.95	(180+) 400
s-6.8-z	6.8	1292	117	32.2	144.00	140
s-6.8-w	6.8	1547	140	32.2	144.00	140
s-dz	10.0-4.0	1292	117	32.2	129.95	320

[a]Pore-width, taken as the distance between opposing atoms on the two surfaces in the pore

[b]Number of water molecules

[c]Number of KCl formula units in solution

[d]Simulation box length parallel to the crystal face

[e]Simulation box length perpendicular to the crystal face

[f]Total simulation time. Numbers in brackets give additional equilibration time during which no forces were calculated.

8.6.1 Neat Water

In the following results are presented of simulations with neat water as liquid phase. In particular we discuss the simulations labelled w-6.0 - w-6.8 in Table 8.3. Although this kind of system could be studied with an efficient grand canonical MC or MD algorithm we use the extended system here to get results that are directly comparable to the simulations with the ionic solution.

Equilibration

The volume and consequently the density of the slit pore cannot be defined unambiguously because the liquid-solid interfaces parallel to the crystal surfaces are structured. Here we estimate the extension of the pore in the z direction to be d_p-d_{100}(KCl), i e., the distance between opposing atoms in register on the two crystal surfaces minus the spacing between two neighbouring KCl (100) layers in the crystal. In Figure 8.5 the resulting number densities of water in the pore obtained for different pore widths are displayed as a function of simulation time. Of special interest here is the question whether these densities converge within a reasonable amount of time. For the slit pores with d_p = 6.0, 6.2 and 6.4 Å the density appears to reach a steady equilibrium value after only 200 ps, both starting with an initial concentration higher (for d_p = 6.0 Å) or lower (for d_p = 6.0 Å) than the final equilibrium value. Somewhat worrying is the fact that for d_p = 6.6 and 6.8 Å the density changes rather distinctively after a simulation time of about 350 and 600 ps respectively. Due to the intricate geometry of the systems they possibly can spend a long time in a meta-stable state before reaching the equilibrium density. Whether this is really the case or whether we merely see some rather large density fluctuations here can only be established by doing longer simulation runs.

The number density calculated as the average density of the two liquid layers parallel to and outside the pore in the region where the density distribution along the z-axes is constant amounts to 0.0325±0.0017 $Å^{-3}$ which, as to be expected, is close to the number density of water at ambient conditions (0.03343 $Å^{-3}$). The uncertainty introduced by the approximative determination of the pore densities is possibly larger than the difference between the bulk and pore densities found here. Thus a straight forward comparison is not advisable. With more confidence we can compare the five pore densities with one another. Here we find the lowest densities for d_p = 6.2 and 6.4 Å; the other three pore widths show clearly higher densities.

Figure 8.5: **Time development of the water densities in the pore**, for the systems labelled w-6.0 - w-6.8 in Table 8.3, units: $Å^{-3}$ and ps; crosses: instantaneous values, full line: time average; note the different time intervals!

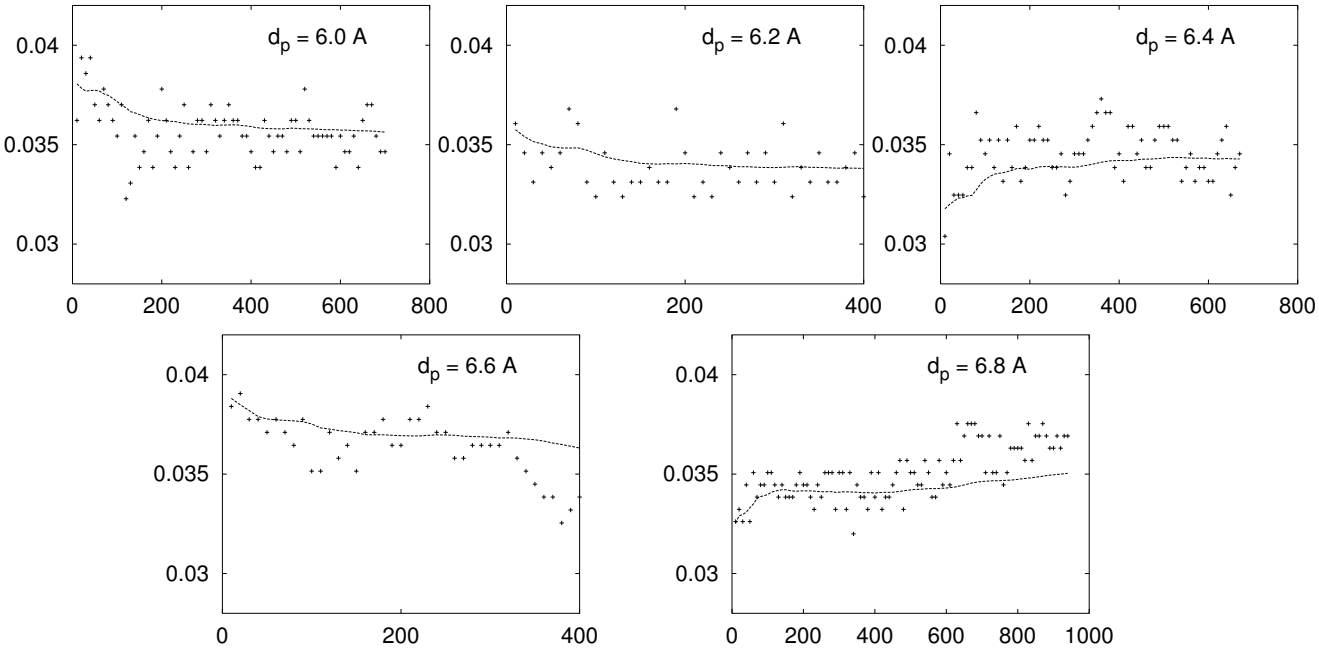

Structure

The reason for these differences becomes clear if we look the average distribution of the water molecules across the pores as shown in Figure 8.6. There the oxygen, hydrogen and charge densities along the z-axis, i.e., across the pore and along the x-axes, i.e., parallel to the surfaces are shown for all considered values of d_p. In all cases we clearly see a stratification or layering of the water which is most pronounced for $d_p = 6.0$ Å since here one layer of water nearly exactly fits into the pore with the oxygens at the center and the hydrogen atoms pointing towards the surfaces. For this system the density in the innermost region of the pore is nearly constant, i.e., there is barely any translational movement of the water molecules and they are virtually frozen in this region. In Figure 8.7 we show the projection on the x-y-plane of trajectories of a few randomly chosen water oxygens in the pore over a period of 300 ps. Once trapped in a convenient position in

Figure 8.6: **Structure of the water in the pore with geometry A**. Relative oxygen, hydrogen and charge densities across the pore (left) and as function of the x-dimension within the pore (right)

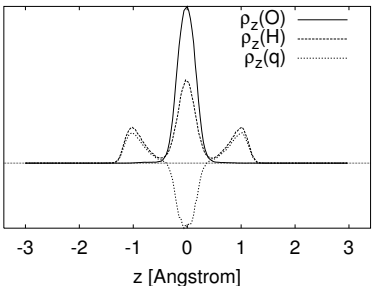

$\mathbf{d}_p = \mathbf{6.0}$ **Å**

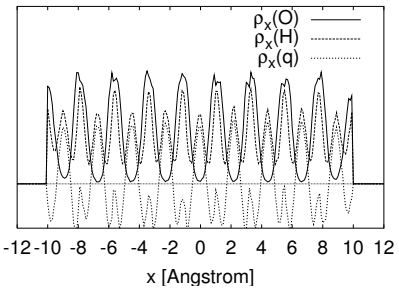

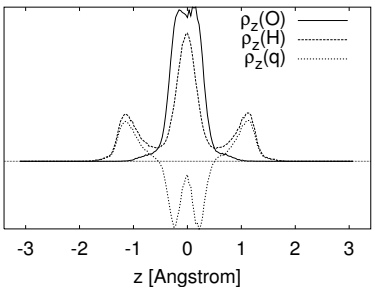

$\mathbf{d}_p = \mathbf{6.2}$ **Å**

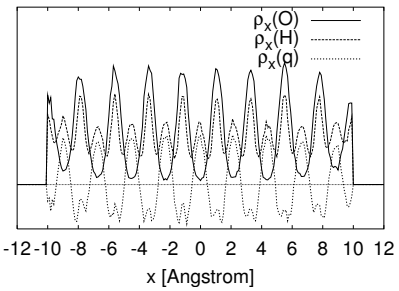

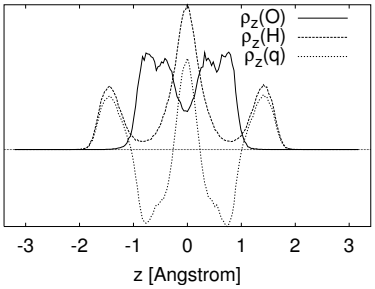

$\mathbf{d}_p = \mathbf{6.4}$ **Å**

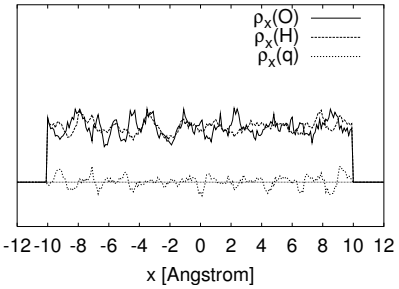

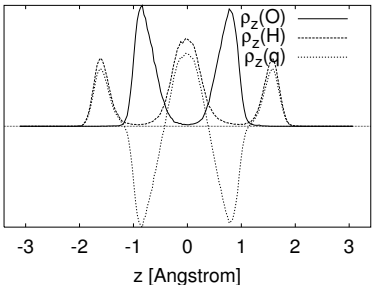

$\mathbf{d}_p = \mathbf{6.6}$ **Å**

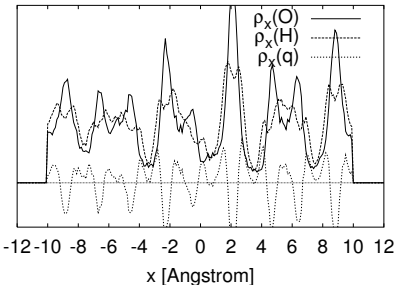

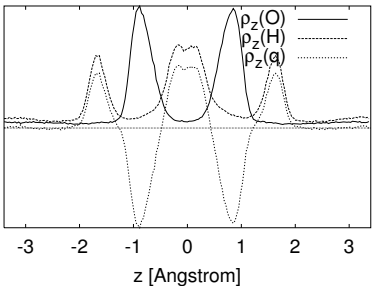

$\mathbf{d}_p = \mathbf{6.8}$ **Å**

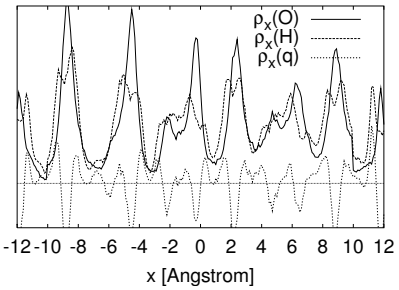

the 2-D lattice the water molecules cannot escape from there anymore at the temperature of 300 K used here. The water in the pore has lost its liquid character. There is no more translational diffusion, and the water is effectively frozen. This effect is, in part, due to the presence of the frozen crystal ions, resulting in crystallites with a temperature of zero K. In a real crystal at a finite temperature, however, the atoms on the surface vibrate around their equilibrium position with a rather narrow amplitude (RMSD $\sim$ 0.3 Å [Dove(1993)]) which was also found in the simulations of the flexible crystal with the FF2 forcefield in Section 8.5. Given the resulting small deviations of the crystal atoms from their average position the cave represented by two parallel crystal surfaces will still be an effective prison for the confined water molecules at finite temperatures. As will be shown below there is also a very high energy barrier preventing the crystallites from detaching once they have come so close that only a single water layer fits into the pore. It follows that at a temperature of 300 K two crystallites with only a single water layer left in between two of their surfaces must already be considered as agglomerated. The implications for the interpretation of the results obtained here will be discussed in the concluding section of this chapter.

At a separation of 6.2 Å we have still approximately one layer of water, however, the central peak is already split into two sub-peaks most clearly to be seen from the charge density across the pore. For the w-d68 system we can see two clearly separated water layers in Figure 8.6. The corresponding charge density reveals that the hydrogen atoms reside mainly in the space between the two oxygen layers and between the layers and the crystal surfaces. At a surface surface separation of 6.4 Å we get an entirely different picture. There is still some stratification left but the number of water layers fitting into the pore at this separation is apparently a non integer number resulting in considerable loss of order which is clearly shown by the mass and charge densities profiles parallel to the surfaces. For the larger separations, 6.6 and 6.8 Å the order is partially restored.

Figure 8.7: **Trajectories of some water oxygens in the 6.0 Å pore**, over a time interval of 300 ps.

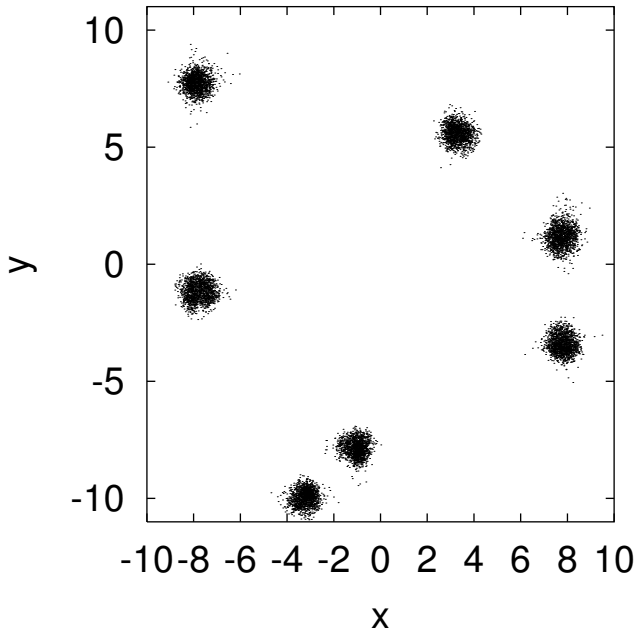

Figure 8.8: **Summation of the Forces**. To estimate the variation of the forces with the lateral distance to the center of the pore they are summed up separately for stacks of crystal ions labelled 1-5.

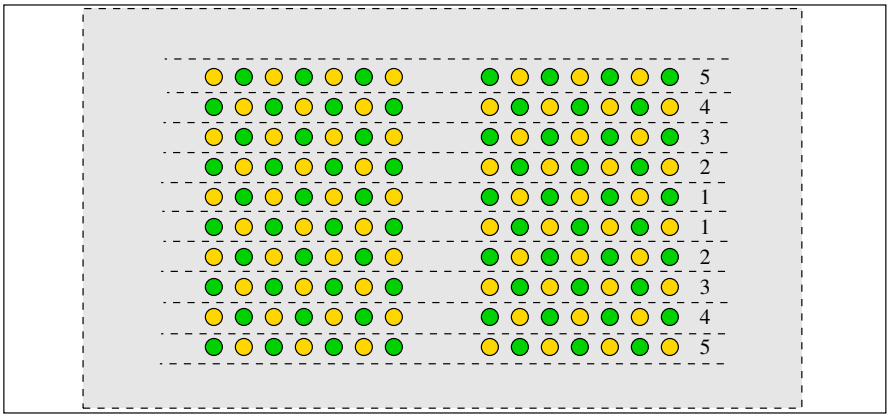

Forces

The less order there is the less well the water fits into the pore and the larger its "frustration", which is reflected by repulsive structural forces. The resulting oscillating character of the forces between surfaces separated by a slit pore is a well known phenomenon and has been observed in experiment [Israelachvili and Mcguiggan(1988)] as well as in theoretical calculations.[Parsonage and Nicholson(1987), Somers and Davis(1992), Svensson and Woodward(1994)] It remains to be established whether reasonable and reproduceable forces can be obtained in spite of the edge effects caused by the system geometry used here. In Figure 8.9 the forces on the crystal ions are displayed for different lateral distances from the center of the pore (explained in Figure 8.8) as a function of time. For the small surface surface separation (d_p=6.0Å, see Fig. 8.9a) the force varies barely with the lateral distance from the center. At a distance of d_p=6.8Å (see Fig. 8.9b), however, the differences become large. For the other surface surface separations (not shown here) these variations lie in between the two extreme cases shown in Fig. 8.9. In Fig. 8.10 the average forces and error bars are shown as a function of the lateral distance. We want to stress that the error bars given here and for all the following results have been calculated as the root mean square deviation (RMSD) of the *instantaneous* values of the

Figure 8.9: **Forces between the crystallites for different lateral distances from the pore center** (as defined in Fig. 8.8) and for surface surface distances of a) 6.0 Å and b) 6.8 Å.

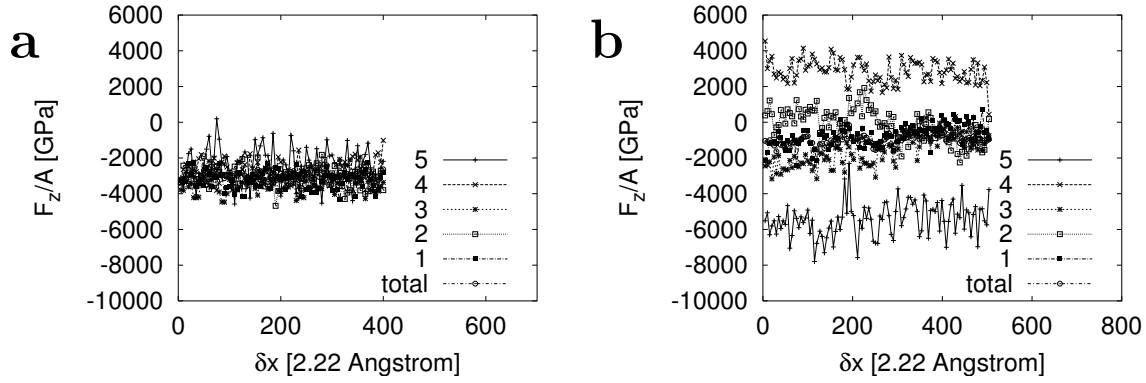

force. This is very conservative, resulting in larger error bars as would be obtained by considering sub-averages rather than instantaneous values to calculate the RMSD, as is frequently done in the context of molecular simulation. We can see that with decreasing distance to the pore center the forces converge towards a value that presumably lies within the error bars of the total average. In Section 8.6.3 more results will be given to clarify the influence of the edge effects seen here. In Fig. 8.10 we see the time development of the running average of the inter surface forces for surface separations ranging from 6.0 to 6.8 Å. We can see that the forces have converged to steady mean values within a simulation time of less than 100 ps for $d_p = 6.0$ and 6.8 Å respectively. For the remaining distances we apparently need to simulate the system for more the 500 ps to reach the mean value as can be seen from the curve for $d_p = 6.4$ Å. This is also in accordance with the observed slow convergence of the densities at these densities. As we saw in Figure 8.6 the liquids in the pores with d_p=6.4 and 6.6 Å show less ordered structures. This is presumably the reason for the comparatively long time needed for these systems to equilibrate. The average total forces as obtained for different surface separations are compared in Fig. 8.11a. Both the total and the structural forces are shown. The structural forces are the total forces on the crystallites minus the contribution due to the direct interactions between the two crystallites — the latter we call vacuum forces here. The range of d_p values considered

Figure 8.10: **a) Averages and RMSD values of the forces for different lateral distances dx**. The total mean values are given at dx = 0. b) Time development of the average total forces for different surface separations.

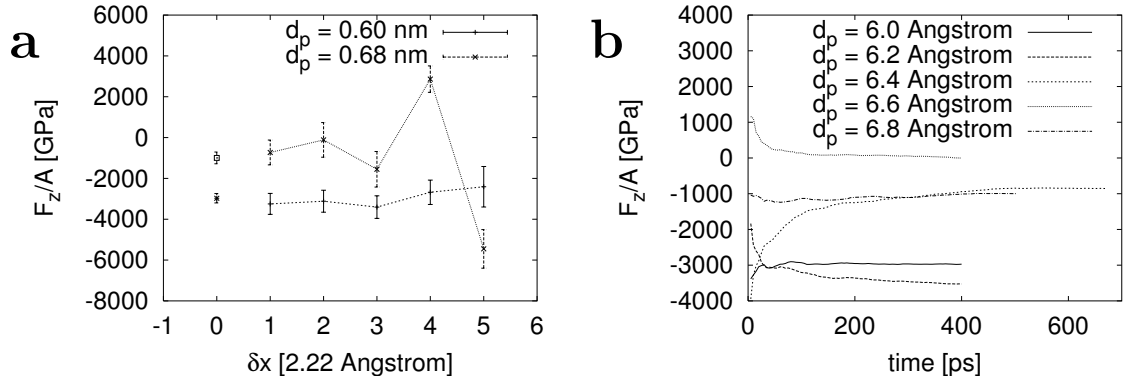

Figure 8.11: **The average total and structural forces (and the RMSDs) for different surface separations**. In both diagrams the same data is shown on a different scale.

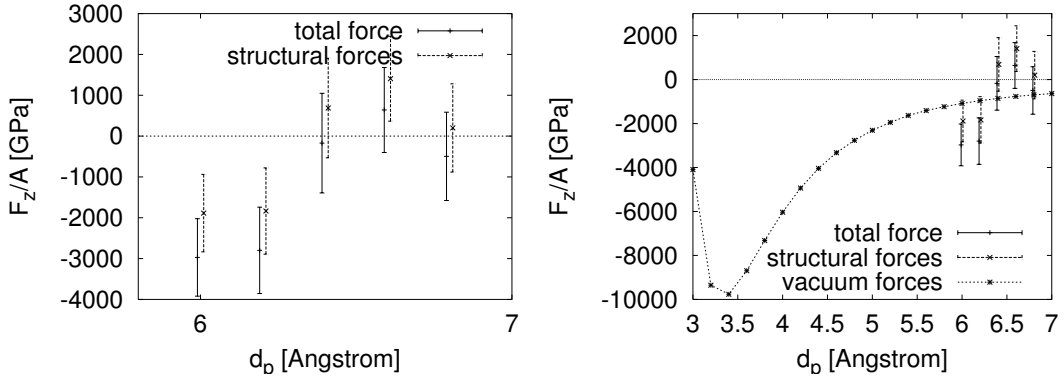

here is too small to give a comprehensive picture. Nevertheless we can already see that for varying surface distance the total forces change in an oscillating rather than a monotonous fashion. It can be expected that for some distance slightly larger than 6.8 Å two layers of water will fit exactly into the pore and the structural forces become attractive again. For clarity we also show the same forces on a different scale in Fig. 8.11b. Here the force between the two crystallites in vacuum is given for comparison.

Figure 8.12: **Number of K^+ (left) and Cl^- (right) ions in the pore**, for different values of d_p

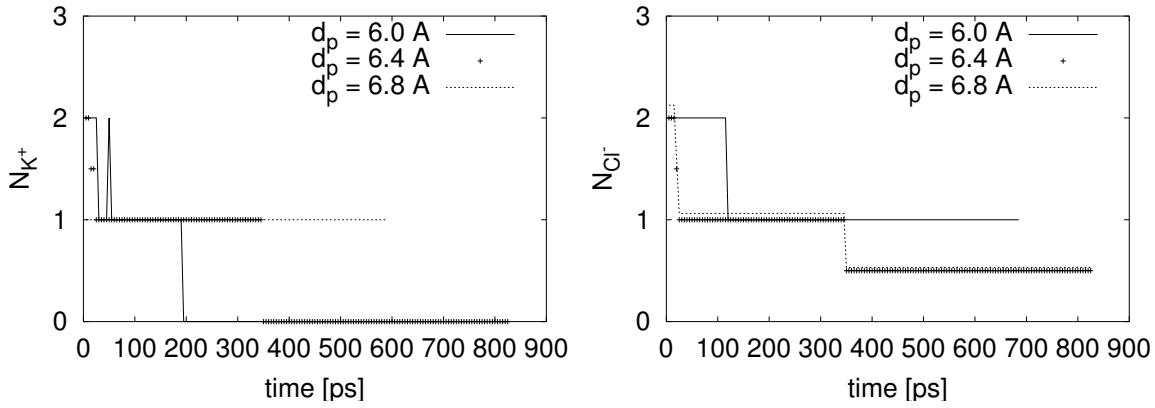

8.6.2 KCl Solution

For the results we present in this section the neat water was replaced by a saturated KCl solution (labelled s-6.0, s-6.4 and s-6.8 in Table 8.3). The saturation concentration of KCl at room temperature is 37 g/100 ml solvent, corresponding to about 11.04 water molecules per KCl formula unit as used here.

Equilibration

Figure 8.12 shows the number of K^+ and Cl^- ions in the pore as a function of simulation time for different d_p values. Development of the number of water molecules over the same time-span is shown in Figure 8.13. We see that for d_p = 6.0 and 6.8 Å the number of water molecules converges very fast and fluctuates around its mean value while for d_p = 6.4 Å we have a discontinuity after approximately 300 ps. This can be explained by looking at Figure 8.12 where we see that one Cl^- and two K^+ ions leave the pore of the s-d64 system at the same time as the water density increases. Generally the density of ions in the pore turned out to be surprisingly low for the pore widths studied here. The ratio between the numbers of water molecules and ions in the pore is at least twice as high as it is in the bulk. One might argue that this is an artifact due to a low initial concentration in the pore and the slow diffusion of the ions in this confined environment.

Figure 8.13: **Number of water molecules in the pore** for different values of d_p

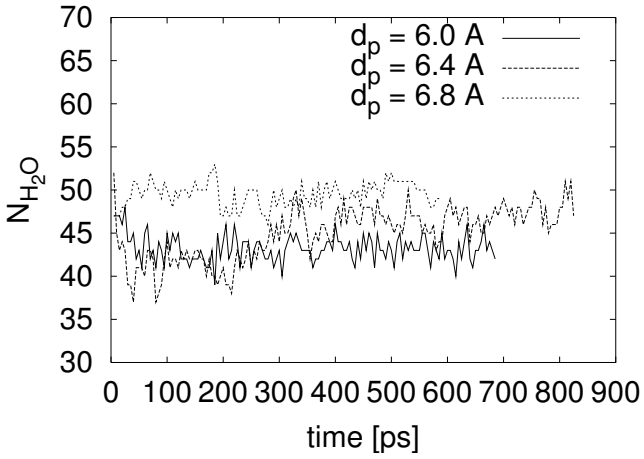

This, however, is unlikely since in the s-d64 system the initial configuration held 7 K^+ and 8 Cl^- ions equally distributed throughout the pore. Both these numbers drop to two within only 20 ps simulation time (this event can not be seen in Figure 8.12 where the equilibration times are not included). In other words, equilibration proceeds extremely fast, at least when the ionic concentration in the pore is too high. Generally the density fluctuations of the ionic solution in the pore are larger than they are for pure water. This is clearly a consequence of the increased disorder in the pore due to the presence of the ions.

Forces

The forces as a function of the lateral distance to the center of the pore show a similar trend as they did in the simulations with pure water. The fluctuations, however, are more erratic as they are for pure water (see Fig.8.14), since now the structure of the liquid is disturbed by the ions in the pore. For example in Figure 8.14a we see that the forces on the crystal ions in region 3 are shifted to a more positive, i.e., repulsive value as compared to the pure water case where the structural forces are virtually independent of the lateral distance to the pore center. Precisely in this region, however, there is a single Cl-ion trapped (see the arrow in Figure 8.15) which distorts the hydrogen bonding structure

Figure 8.14: **Forces as function of lateral ion positions** with a) d_p = 6.0 Å, b) d_p = 6.4 Å, c) d_p = 6.8 Å. d) Time development of the running averages of the total force for the three separations.

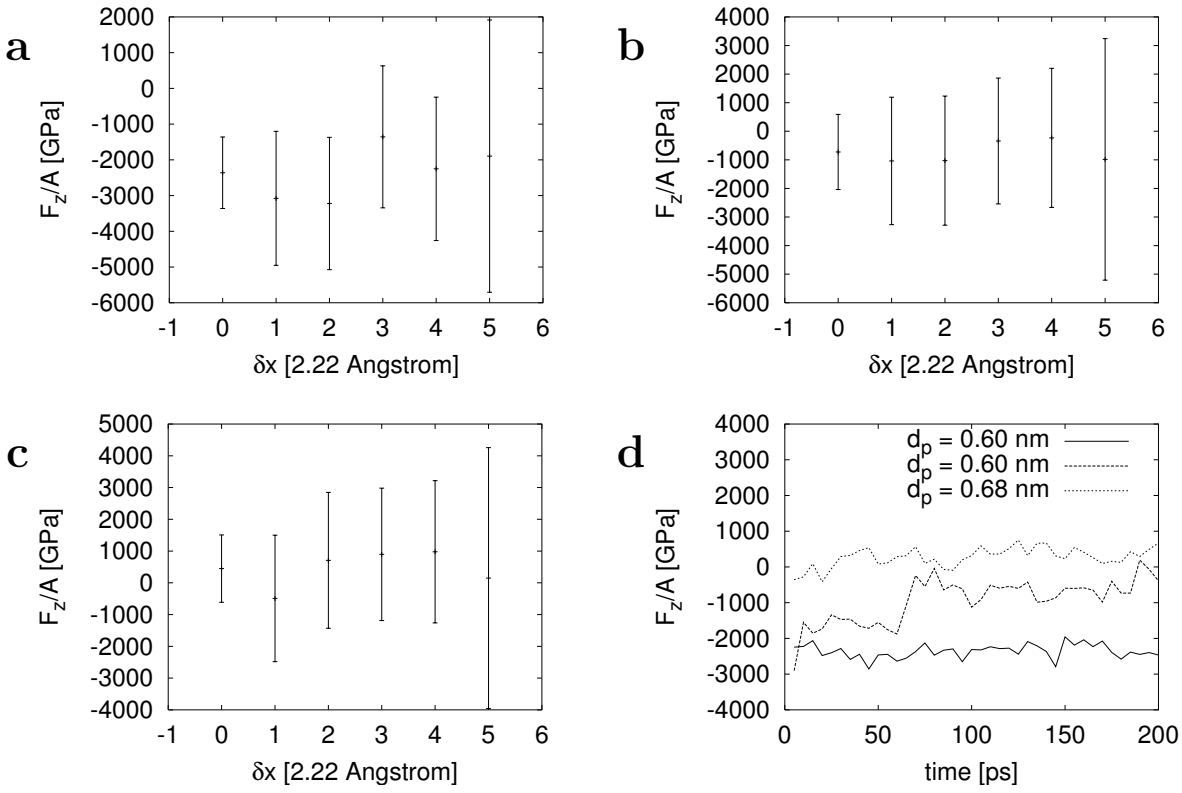

of the surrounding water decisively and reduces thereby the attractive structural forces. Because in all simulations the number of ions in the pore remains constant after a short equilibration period the total forces between the crystallites converge relatively fast (see Fig.8.14d). In Figure 8.16 the average total and structural forces for the three different surface separations considered here and the forces calculated in vacuum are given. Since the calculations so far are confined to only three different separations we cannot give a comprehensive interpretation but the results are illustrative nevertheless. The most important finding here is that the inter surface forces between the KCl crystallites in neat water and in saturated KCl solution, respectively, differ, if only slightly, as to be seen in Fig. 8.17. Since the statistics of our runs are rather poor so far the differences are within the error bars but the qualitative diagrams for the effect on the structure (Figure 8.15)

Figure 8.15: **Snapshots of the pore with d_p = 6.0 Å**, with neat water and KCl solution. The single Cl-ion left in the pore causes repulsion between the crystallites.

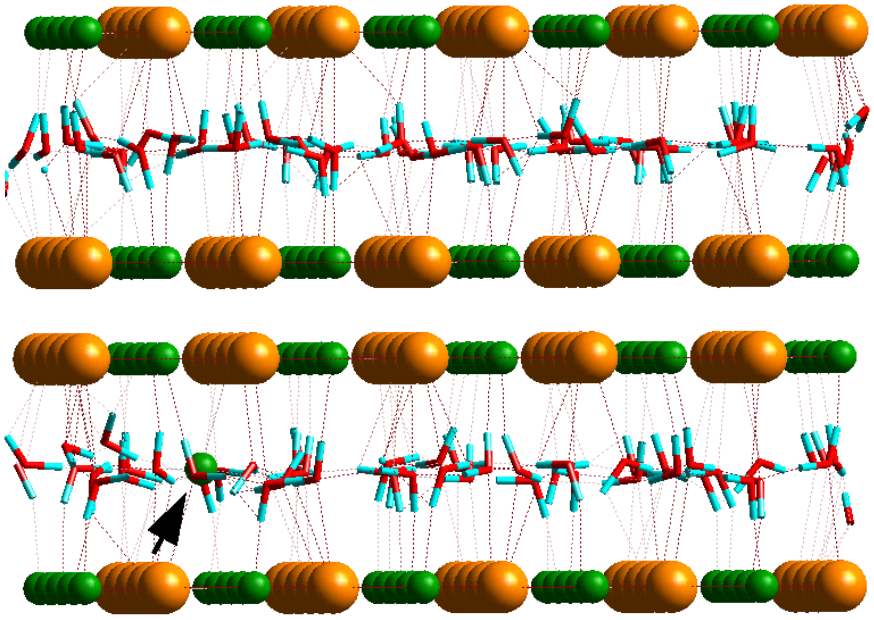

Figure 8.16: **The average total and structural forces for different surface separations**. In both diagrams the same data is shown on a different scale.

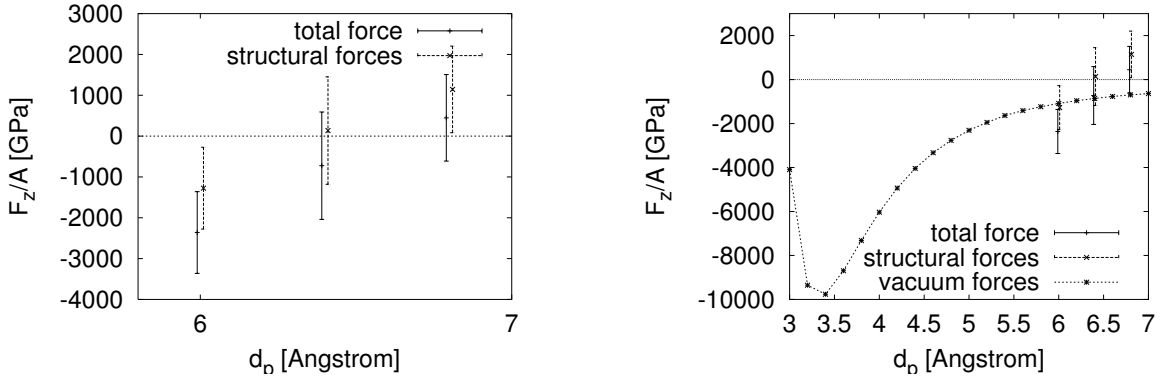

Figure 8.17: **Comparison of the inter surface forces in neat water and in saturated KCl solution.**

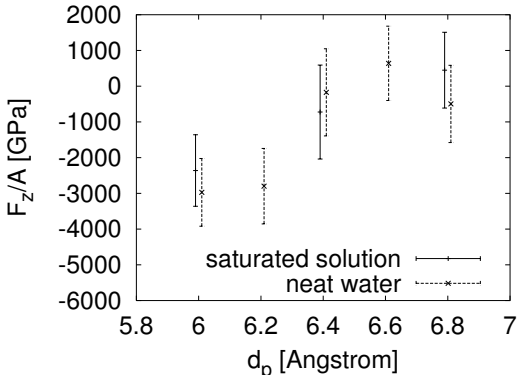

suggest a real effect.

8.6.3 System Size

Although it looks as though the forces calculated in the simulations presented so far are rather well converged in most cases we still have to establish the system size dependence of their magnitudes. Unfortunately the systems used so far are already quite close to the upper boundary of the computational resources we have at our disposal. On the other hand side it is unclear whether the simulation of two infinite surfaces, as frequently used for simpler materials, comes much closer to the truth than our system here since in a real system we find irregularities like surface s.pdf, kinks, grain boundaries, interstitial atoms, lattice defects, etc. Crystal agglomeration can not be seen as the direct attachment of two plain surfaces. There is some experimental evidence that no or only relatively small parts of the surfaces attach directly while the solid bridge between the two crystallites or at least its major part is formed by subsequent crystal growth.[Pratola et al.(2002)Pratola, Simons, and Jones] It is unlikely that these small parts that do attach look very much like the system we model here, but it might still be a better approximation than two infinite surfaces. To get a more comprehensive picture we nevertheless investigated the consequence of increasing the system size on the forces.

Bulk Volume and Simulation Box-length L_z

As a first and computationally less challenging test we increased L_z, the size of the system in the direction perpendicular to the surfaces and the total number of solvent molecules. we do not vary the thickness of the crystallites in the z-direction since in Section 6 we have already shown that the thickness used here can be considered is large enough. A result which is also in accord with the findings presented by other authors for similar systems [Oyen and Hentschke(2002)] We compare results obtained with the setups labelled s-6.8, s-6.8-z and s-6.8-w in Table 8.3. Thus we have two KCl crystallites separated by a distance of 6.8 Å in saturated KCl solution combined with a permutation of two different values for L_z (129.95 and 144.0 Å) and two different numbers of water molecules (1292 and 1547 H_2O) In Fig. 8.18 the total force F_z between the crystallites as a function of time is shown for the three systems. Due to the large fluctuations of the forces a comparison is not easy, however, the mean values obtained for the three systems are within their respective error-bars, with F_z/A(s-6.8) = 448±1060, F_z/A(s-6.8-z) = 695±1020 and F_z/A(s-6.8-w) = 596±1000 GPa. We can conclude that i) the forces are converged with respect to the number of solution molecules ii) the extension of the simulation box in the z-direction is large enough to exclude artifacts introduced by interactions with periodic images across the cell boundary in the z-direction. This is essentially a confirmation of the results obtained in Chapter 6 for the structural properties.

We stress that it is not completely clear whether these results are rather due to the large error bars we are ready to accept here than due to a true convergence of the results with system size. Longer simulations with a greater variation of the system size would have to be done in order to establish the system size dependence of the results unambiguously.

Variation of the Surface Width

The main concern when considering the system size is the width of the crystallites in the x direction, since the larger this width is the less pronounced are the edge effects going to

Figure 8.18: **Running averages of forces** calculated for varying number of solvent molecules and varying length of the simulation cell (See text for explanation of the labels).

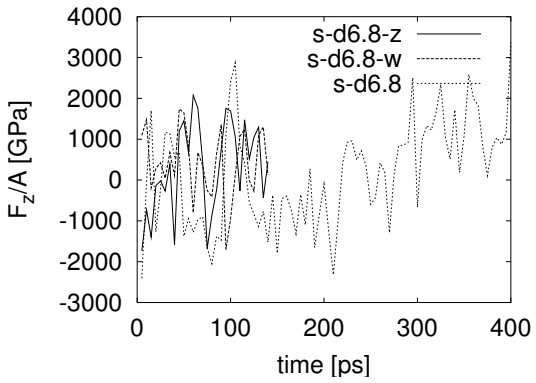

be. These edge effects, as shown above, lead to large fluctuations in the forces measured at different lateral distances from the pore center.

In a first attempt to assess the influence of the bulk-pore interface on the forces we compare the results calculated for systems with different lengths of the pore in the x-dimension, w_c. One geometry, labelled X (w-6.8 in Table 8.3), includes a crystal with ten layers of ions perpendicular to the surface in the x-dimension, just as all the systems used for the previously presented simulations, and is compared to a second, labelled XII (w-6.8-x in Table 8.3), with twelve corresponding layers. In both systems the surface surface separation is $d_p = 6.8$ Å and neat water is used as the liquid phase. The results, shown in Figure 8.19 look actually very good. The magnitude and sign of the fluctuations of the forces close to the bulk-pore interface agree well for both systems just as do the two total mean values of the forces. We conclude that that the average forces per area as obtained with the (X) system geometry are converged with respect to the surface area.

In a more rigorous attempt to assess the influence of the edge effects we performed another test comparing results obtained with two sets of three different systems with surface surface separations of 6.0, 6.4 and 6.8 Å and with pure water as solvent. The first set of results, labelled (X) is obtained with the system geometry A we used for all our previous calculations. where the number of layers of ions perpendicular to the surface in the x-dimension is 10. For the second set labelled (inf) we use a geometry that includes

Figure 8.19: **Comparison of the calculated structural forces between nanocrystallites with 10 layers (X) and 12 layers (XII) of atoms in the x-direction**. Here δx is the x-component of the distance of an ion from the edge, i.e., from the bulk-pore interface. At δx=7 the force is given averaged over the whole surface area. For clarity one of the two curves (XII) is shifted by 0.2 towards positive δx.

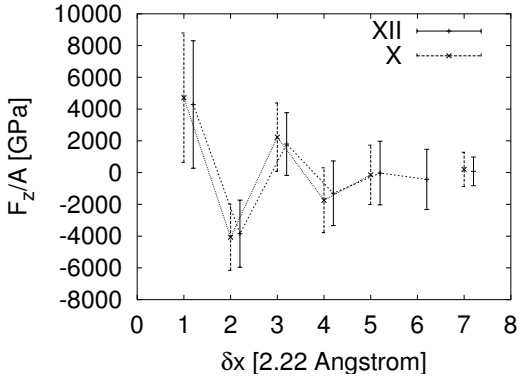

only the liquid in the pore and the confining crystal slabs spanning the whole simulation box in the x-dimension, parallel to the slit pore. Here no bulk phase is included in the simulation box and the crystallites comprise parallel slabs with infinite extension in the x,y-plane. This is the geometry commonly used in combination with grand canonical simulation algorithms. Normally we do not know the density of the liquid in such a pore for a given chemical potential in advance. Here, however, we can use the densities as obtained in the corresponding (X)-runs. Due to the finite length of the pore used there and the resulting edge effects ρ(x), the density distribution along the x-axis, not only fluctuates but may also have a gradient going from the edge towards the pore center. A reasonable estimate of the corresponding density in the (inf) geometry was obtained by calculating the density in the (X)-systems for different lateral distances to the pore center δx, followed by an extrapolation of the density $\rho(\text{inf}) \approx \rho(\delta\text{x}\rightarrow 0)$. The conclusions drawn from the results in Fig. 8.19 are undoubtedly confirmed. Figure 8.20 shows that the forces in the systems where the crystals have a finite length in the x-dimension fluctuate much stronger than they do when the crystal slabs are infinite, but the total averages of the structural forces are clearly within their respective error bars. We conclude that the forces per area are virtually independent of the with of the crystallites (the parameter w_c) for

Figure 8.20: **Structural Forces per area and their RMSDs as a function of the lateral distance to the pore center δx**, calculated in geometries with a length of the pore of 10 crystal layers (X) versus infinite pores (inf). At δx=0 the means of the force across the whole pore length is given

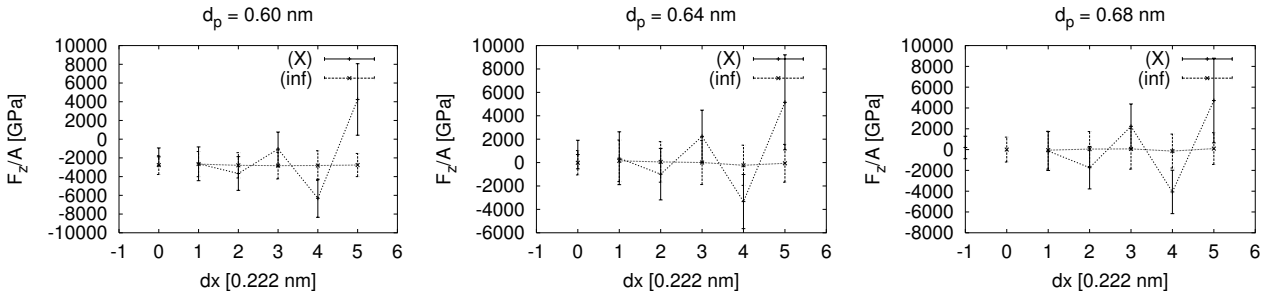

$w_c \geq 20.0$ Åor 10 crystal layers.

8.6.4 Explicit Non-Equilibrium

We have seen that the equilibration in the pore between the two nano crystallites proceeds rather slowly. The system geometry used here can be expected to be decidedly more "porous" than the real system of two approaching crystalline surfaces. because about every 20 Å the surfaces are perforated, leaving a channel that connects the pore region to the bulk solution. Therefore the equilibration times found here are to be seen as a lower boundary to those to be observed in nature. Hence the question arises whether in a real system the liquid in the pore is in equilibrium at all. If this is not the case simulations as those reported above are probably of limited usefulness for assisting the interpretation of experimental results. In order to gain some insight into what happens if the liquid in the pore is not in equilibrium during the agglomeration process we set up another model in which a saturated KCl solution around the two crystallites is equilibrated at a surface distance of 10 Å. After the equilibration period the crystallites are moved at a constant velocity towards each other during a single simulation run until they reach a final distance of 4 Å. Due to our limited computational resources we can only model a very high velocity which here was taken to be 2 m/s. Although this is the typical speed

of the tip of a propeller used to stir the solution in an industrial crystalliser it is probably an unrealistic high value for the approach of two crystallites because their relative speed will be damped considerably by the viscous forces due to the solution. Nevertheless we hope to gain some qualitative insights.

In Figure 8.21 we can see the total force between the two crystallites as they cover the distance of 6 Å. For comparison the forces calculated for three distances at equilibrium are also given. Apparently the velocity of approach is so high that the solution molecules are squeezed and partially get stuck between the two surfaces so that we end up with large repulsive forces. Although the relative velocity of the crystallites is much too high the reality presumably lies somewhere in between the extreme case shown here and a system at exhaustive equilibrium with the bulk. The confinement of the liquid in a structured pore might promote the persistence of meta-stable states or local minima in the solution between the surfaces resulting in equilibration times that exceed the time available as two particles in a heavily stirred solution approach each other. For want of sufficient computational resources we have to leave this question subject to further research and for now make the following ad-hoc assumption: If the density in the pore differs from the equilibrium density in the course of a real agglomeration event it is plausible to expect this density to be higher than the equilibrium density since here we look at agglomeration, as opposed to the detachment, of particles. It follows that if we start a simulation at a given value of d_p with a density in the pore that is clearly higher than the equilibrium density and after some time reach a steady state and converged forces at a lower density then this might be a either the global minimum or equilibrium for this pore width or alternatively it is a meta-stable state or a local minimum. That is, given that the used force field and other approximations made are accurate enough, the measured forces, once they have converged to a steady mean value and stayed there sufficiently long, do correspond to the forces found in a real system no matter which of the two, the equilibrium or a meta-sable state, is represented by the liquid in the pore.

Quite likely this is merely an academic question since, as we have shown above, we do reach a steady state in most cases within less than 500 ps and there is no reason to

Figure 8.21: **Forces between two nano-crystallites approaching each other at a speed of 2 m/s in saturated KCl solution**; comparison to forces calculated at constant surface separation.

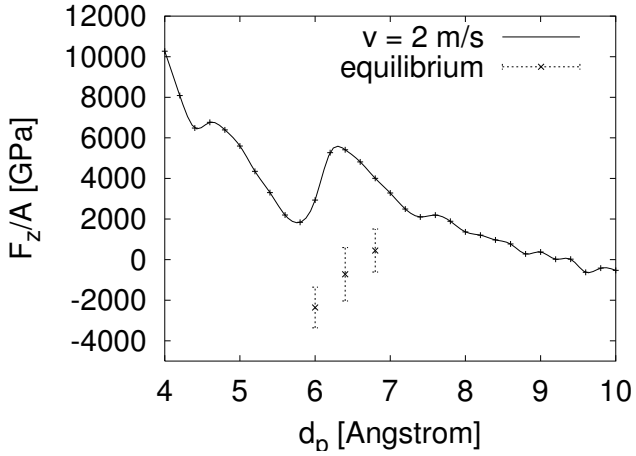

assume that this steady state does not correspond to the equilibrium state. Those systems for which the forces and densities converge rather slowly have a surface separation that results in frustrated and disordered liquid; this, rather than a meta-stable state being probably the cause for the observed large fluctuations and the ensuing slow convergence.

8.7 Results III, Structure and Forces obtained with a Mobile Sandwich

In all the simulations presented so far the two opposing micro-crystallites are held in perfect register. With structured surfaces, such as the ones we use here, it can make a qualitative difference for the forces if one allows the surfaces to move laterally and relative to each other because their optimal position for a given solvent can vary with varying surface surface distance. Somers at al. [Somers and Davis(1992)] performed grand canonical Monte Carlo simulations in which they studied the structure and diffusivity of a Lennard-Jones fluid and the resulting normal pressure in a narrow pore with walls made of an (100) surface of a face-centered-cubic lattice of Lennard Jones atoms. For pore widths $d_p \leq 2.75\sigma$, with σ being the Lennard Jones parameter (diameter) of the atoms representing the liquid, they found noticeable differences between structures and forces obtained with the walls in different registries.

With the system geometry used here the force components parallel to the crystal solution interface, i.e., here the x-y-plane, originating from interactions with the solution molecules in the bulk region and in the vertical conjunction connecting the slit-pore and the bulk solution are of course zero on average due to the symmetry of the system shown in Figure 8.1. However, with the molecules in the slit-pore having a distinct shape and size, the most stable arrangement of the two surfaces, corresponding to the lowest free energy, has not necessarily the two surfaces in perfect register, resulting in non-zero average forces on the crystallites in the x and/or y direction.

As a preliminary test the non-equilibrium simulation discussed in the last part of Section 8.6 is repeated with two crystallites that can move laterally in the x-dimension through a distance 1.5 times as long as the difference between the two extreme configurations perfect register and perfect mismatch as detailed in Section 8.4. In the y-direction no constraints are applied and the crystallites can move un-impeded responding to any frictional forces from the solution molecules. In Figure 8.22 the consequence of keeping

Figure 8.22: **Forces between two nano-crystallites approaching each other at a speed of 2 m/s in saturated KCl solution**; comparison to forces calculated with crystallites that can adjust their relative position in the x-y-plane.

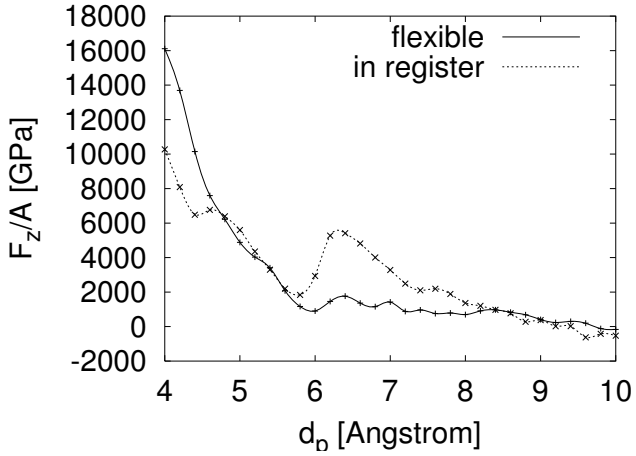

the crystallites fixed in their initial positions on the x,y-plane is clearly to be seen. The strong repulsion observed in the rigid system at a separation of about 6.5 Å is decisively reduced. At very small distances the repulsion in the mobile system becomes larger than it is in the rigid one. This is likely to be mainly caused by the different liquid densities in the pore. At all separations $d_p \leq 8.0$ Å there are about 10 % more molecules in the pore in the mobile system. This is apparently so because with crystallites that can adjust their relative positions in the x,y-plane more solvent molecules fit into the last one or two layers of water. These molecules however cannot be squeezed out of the pore anymore once they are there and the surfaces continue their approach because they get effectively stuck. As mentioned above this scenario represents an extreme case because the relative velocity of the crystallites is very high. Nevertheless it is confirmed that the lateral mobility of the surfaces does make a noticeable difference. In a real system we cannot expect the relative position of two surfaces being constrained exactly at one point. The distance between the surfaces in and out of register is in the range of a few Ångstoms, i.e., extremely small. Thus, in experiments with the surface force apparatus where the position of the crystals in the plane parallel to the interface is nominally fixed there will certainly be enough leeway left for the crystals to explore the whole range of possible mutual arrangements.

Table 8.4: **Details for the equilibrium simulations with flexible crystallites**. The box dimensions are $L_x = 32.2$ Å, $L_y = 22.2$ Å and $L_z = 129.95$ Å and the number of water molecules is 1526 throughout. The total number of solvated KCl formula units is 117 in all the systems labelled fs.

water			solution				
label	d_p[a]/Å	time[b]/ps	label	d_p/Å	N_{KCl}^{pore}[c]	m_{cryst}[d]/10^4 amu	time/ps
fw60	6.0	800	fs60	6.0	6	2.61	800
fw64	6.4	800	fs64	6.4	8	2.61	800
			fs64-mpi	6.4	12	2.61	600
			fs64-lpi	6.4	2	2.61	600
fw68	6.8	800	fs68	6.8	9	2.61	800
fw72	7.2	800	fs72	7.2	10	2.61	800
			fs72-mpi	7.2	16	2.61	600
fw100	10.0	800	fs100	10.0	16	2.61	200
fw156	15.6	800	fs156	15.6	30	2.61	200
			fs72-m	7.2	10	2610	600

[a]Pore-width, taken as the distance between opposing atoms on the two surfaces.
[b]Total simulation time, including equilibration phase
[c]Number of ions in the pore at t=0.
[d]Total mass of the KCl crystallites.

Thus we run the danger of introducing artifacts into our results unless we let the crystallites move in the x-y-plane so that they can explore each possible relative arrangement. In the following we look at more results obtained with the same system geometry and size as used in the preceding section, the difference being that now the nano-crystallites can adjust their relative positions in the x-y-plane and thereby respond to the frictional forces exerted by the solution in the slit-pore. With this setup we simulate again two KCl nano-crystallites with opposing (110) faces in both neat water and saturated KCl

solution. Both simulations with constant and with varying pore widths are included. The surface separations used in the equilibrium simulations are d_p = 6.0, 6.4, 6.8, 7.2, 10.0 and 15.6 Å. For the initial configuration of these simulations we choose the concentration of ions and water in the pore so that both are about 5% above the bulk concentration. More details of the simulations are given in Table 8.4

8.7.1 Motion of the Nano-Crystallites

Figure 8.23 shows the relative motion of the two crystallites in solution and in pure water. We clearly see that the configuration corresponding to the two crystallites being in register is not adopted in all systems. For most of the separations the configuration corresponds in fact to the surfaces being out of register. Only for two cases with pure water as the liquid phase in combination with pore-widths, d_p = 6.0 and 6.4 Å we find the surfaces in or close to register. With saturated KCl solution as the liquid medium the surfaces are in mismatch even at the smallest separations. This is apparently due to ions from the solution residing in positions in between two equally charged surface ions thereby building an energetically favourable +/–/+ or –/+/– string of ions that resembles the structure of the ions in the solid crystal. This can also be seen in snapshots of the configuration in the pore (not shown here). It also explains why the motions of the crystal surfaces are strongly correlated up to a separation of 10 Å while there seems to be barely any correlation left at this distance with pure water in the pore. For all separations up to 7.2 Å the range of the relative motion is very narrow and hence the motions of the two crystallites are clearly correlated for both system types. Since in most cases the surfaces are not in register this correlation must be mediated by the liquid in the pore and not by direct interactions between the two bare crystallites. With d_p = 15.6 Å neither water nor KCl solution can maintain an effective lateral correlation between the two surfaces.

Figure 8.24 shows the trajectories in the x-y-plane of ions in the pore. Both the absolute and the relative motion are shown. The latter is the absolute motion of a particle minus the motion that the center of mass of the two nano-crystallites undergoes

Figure 8.23: **200 ps trajectory of the relative positions of the crystallites** for pores filled with pure water (W) or saturated KCl solution (S) and for various pore widths d_p. The boxes span a range of $-1 < x < 1$ and $-1 < y < 1$ with one unit of length corresponding to 2.22 Å. The center of each box (0,0) corresponds to the crystallites being in perfect register; (0.5,0.5), (-0.5,0.5), etc.: surfaces are out of register; Due to the symmetry of the crystal all possible positions (x,y) with $(|x|, |y|) = (0.5,0.5)$ are equivalent, the same is true for all possible positions with $(|x|, |y|) = (0,0.5)$ and $(|x|, |y|) = (0.5,0)$. Note that for d_p up to 7.2 Å the arrangement of the two crystallites is virtually constant but depends clearly on the presence of ions.

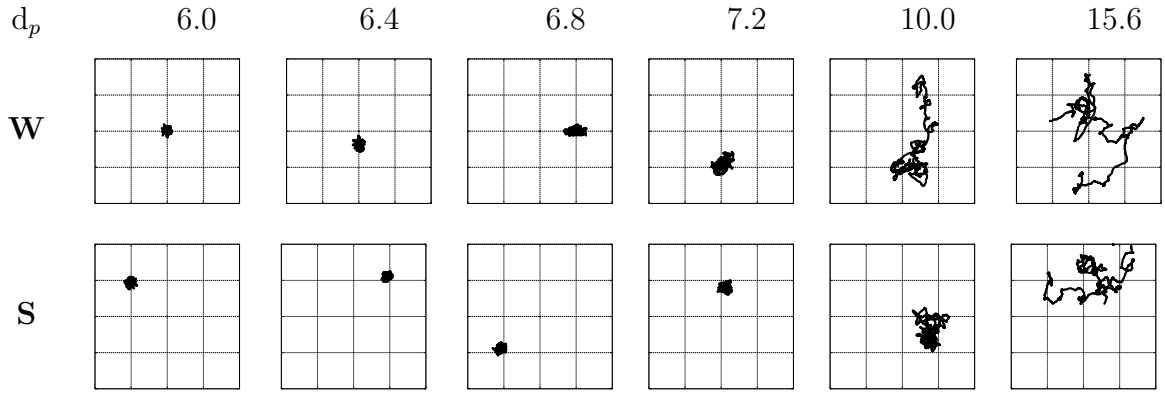

at the same time. The fact that the distribution of the particles is clearly narrower in the latter case is evidence for a tight correlation between the particles and the surfaces. More evidence is given by the fact that the relative positions of ions in the pore clearly reflect the pattern of the surface, with the average distance between each combination of ion-types in the pore being very close to corresponding value in the crystal surface. A picture like the ones in Figure 8.24 is less instructive for larger pore separations because in this case there are too many ions in the pore and the image gets blurred. Single ions and water molecules, however, are still correlated to the surfaces also at larger separations.

From a one-dimensional density distribution of the water in the pore as function of the z-coordinate (see Fig. 8.27) one can clearly see that three distinctive water layers are accommodated in the pore with $d_p = 15.6$ Å. Water molecules and ions in the middle layer can move relatively freely while those in the two layers next to the surfaces are more or less tightly attached to the surface. Figure 8.25 shows typical trajectories for two water

Figure 8.24: **200 ps Trajectories of K^+ and Cl^- ions in the pore**; K^+: dark gray, Cl^-: light gray; x *times* y = 7.7 × 22.2 Å^2 sections of the pore are shown; The horizontal boundaries of each diagram at y = ± 11.1 Åare periodic boundaries; various surface separations are compared; in the top row (ABS) the projection of the absolute particle motion on the x-y-plane is drawn. The bottom row (REL) shows the same trajectories corrected for the motion of the crystals (see text for explanation).

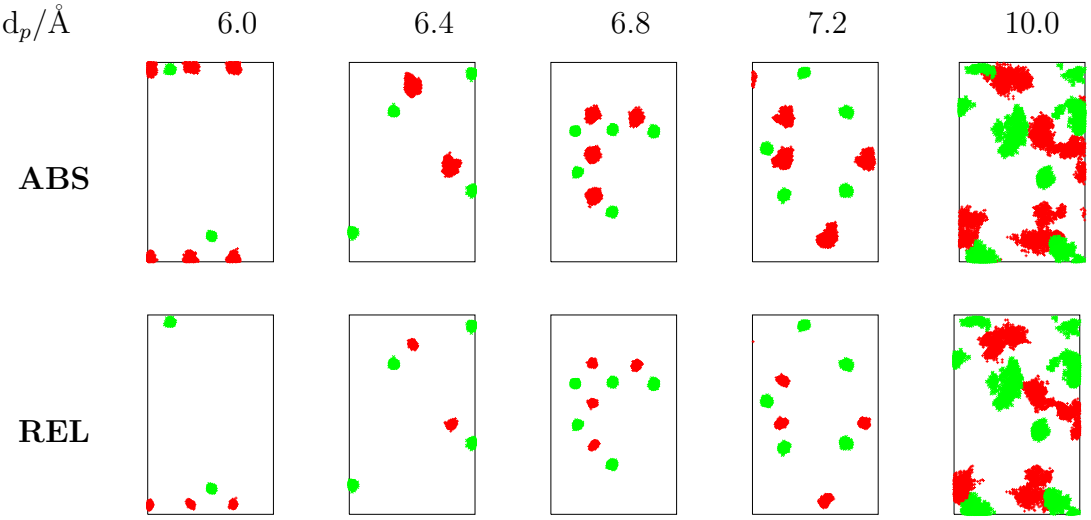

molecules one in the middle layer and another one attached to a surface.

8.7.2 Structure

In Figure 8.26 and 8.27 the density distributions across (z) and alongside (x) the pore are shown. The structure of the liquid in the pore is similar to the structure obtained with frozen crystallites, but the order in the x-dimension parallel to the surfaces is less pronounced. The decrease of order, however, is exaggerated due to the moving crystallites. We have seen that the molecules in the pore interact specifically with the surface structure. Here the absolute, rather than the relative distribution functions are shown. Therefore the resulting image is somewhat blurred. A genuine difference to the simulations with frozen crystallites is the fact that the latter result in a less ordered structure at a surface separation of d$_p$ = 6.4 Å as compared to both d$_p$ = 6.0 and 6.8 Å while with mobile crystallites the order decreases monotonically with increasing pore width. This can be

Figure 8.25: **The trajectories of two water molecules in a pore with d_p = 15.6 Å projected on the x-z-plane**. The two horizontal lines indicate the position of the surfaces (actually the plane going through the centers of mass of the outermost surface atoms). One of the water molecules resides in the central water layer while the other is attached to the bottom surface resulting in restricted mobility.

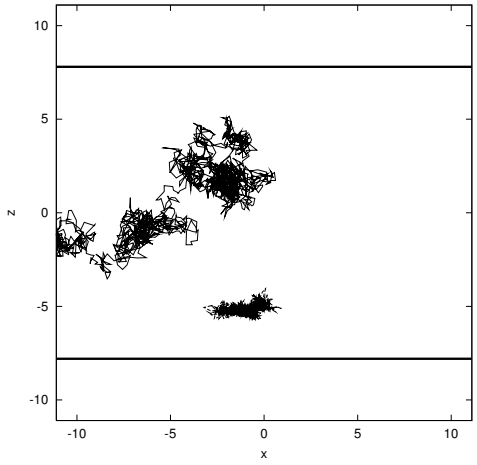

readily understood as a consequence of the lateral mobility of the surfaces. In Figure 8.23 we see that at d_p = 6.4 Å the two surfaces are somewhat out of register on average which apparently allows for an energetically more favourable and at the same time more ordered structure of the liquid in the pore. With frozen crystallites it is impossible for the system to transform into this state. The water molecules do not fit properly into the pore and a disordered structure results. Particularly interesting are the distribution functions obtained with the saturated KCl solution. Figure 8.26 clearly reveals that the positions of ions in the pore are well defined with the ions being virtually immobile for surface separations up to 7.2 Å. At a separation of d_p = 10.0 Å there is still some correlation between the ions in solution and in the surface structure left while at d_p = 15.6 Å the ions can apparently move unimpeded through the whole length of the pore, though this is probably only true for ions that are not situated in a liquid layer next to one of the surfaces. The z-distribution functions in Figure 8.27 show that there are such distinctive ionic layers, one for $d_p \leq 6.8$ Å, two for d_p = 7.2 Å, three for d_p = 10.0 Å and at least four with d_p = 15.6 Å. In all the density distributions we see that the water oxygens can

Figure 8.26: **Density profiles parallel to the interfaces** water (full thin line), K^+ (thick line) and Cl^- (dashed line) in the pore. Densities are given in $Å^{-3}$ as a function of the x-coordinate in the pore for various pore widths d_p (both in units of Å); left: saturated KCl solution, right: neat water;

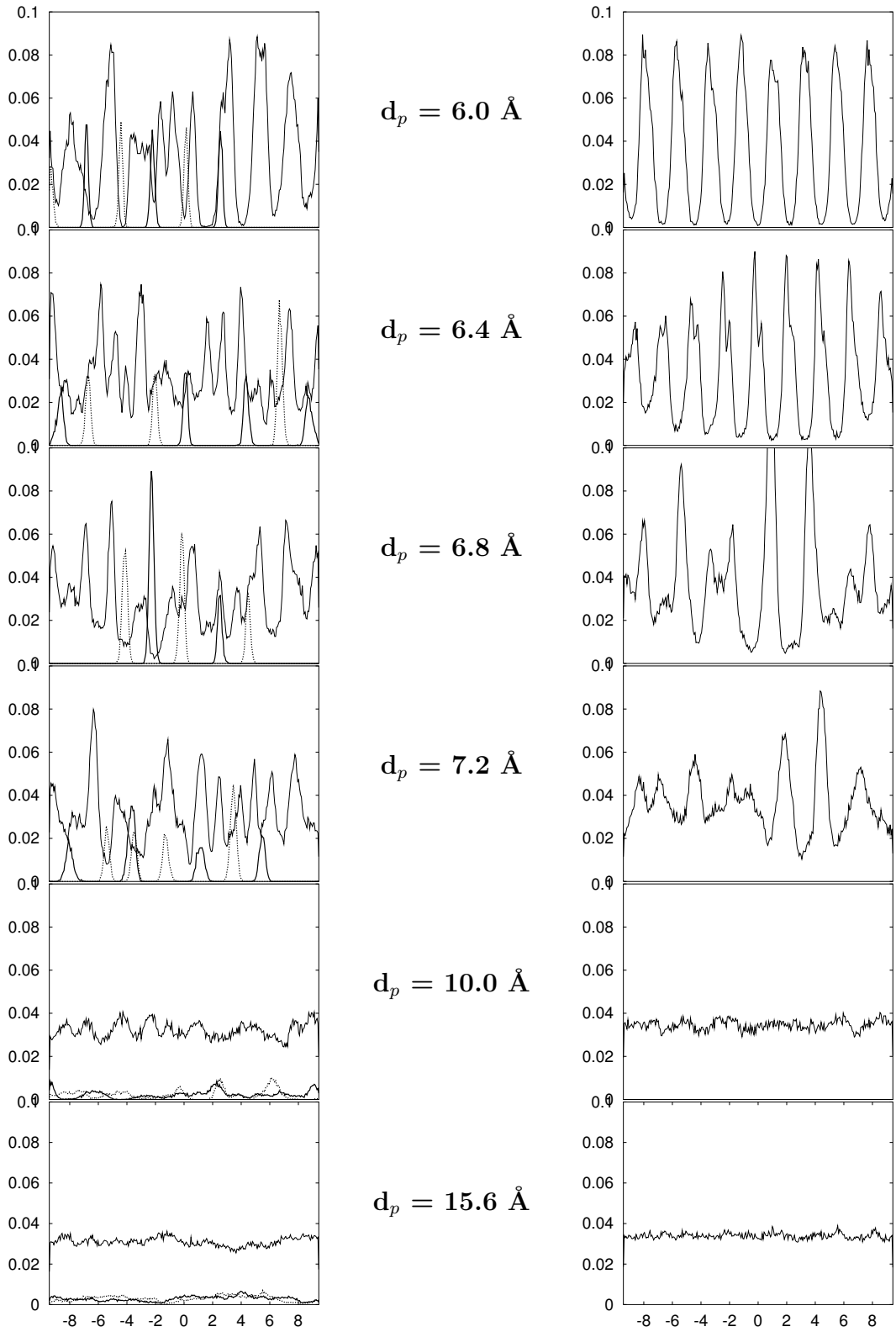

Figure 8.27: **Density profiles normal to the surfaces** water (full thin line), K^+ (full line) and Cl^- (dashed line) in the pore; Densities are given in $Å^{-3}$ as a function of the z-coordinate in the pore and the pore width d_p (both in units of Å); left: saturated KCl solution, right: neat water;

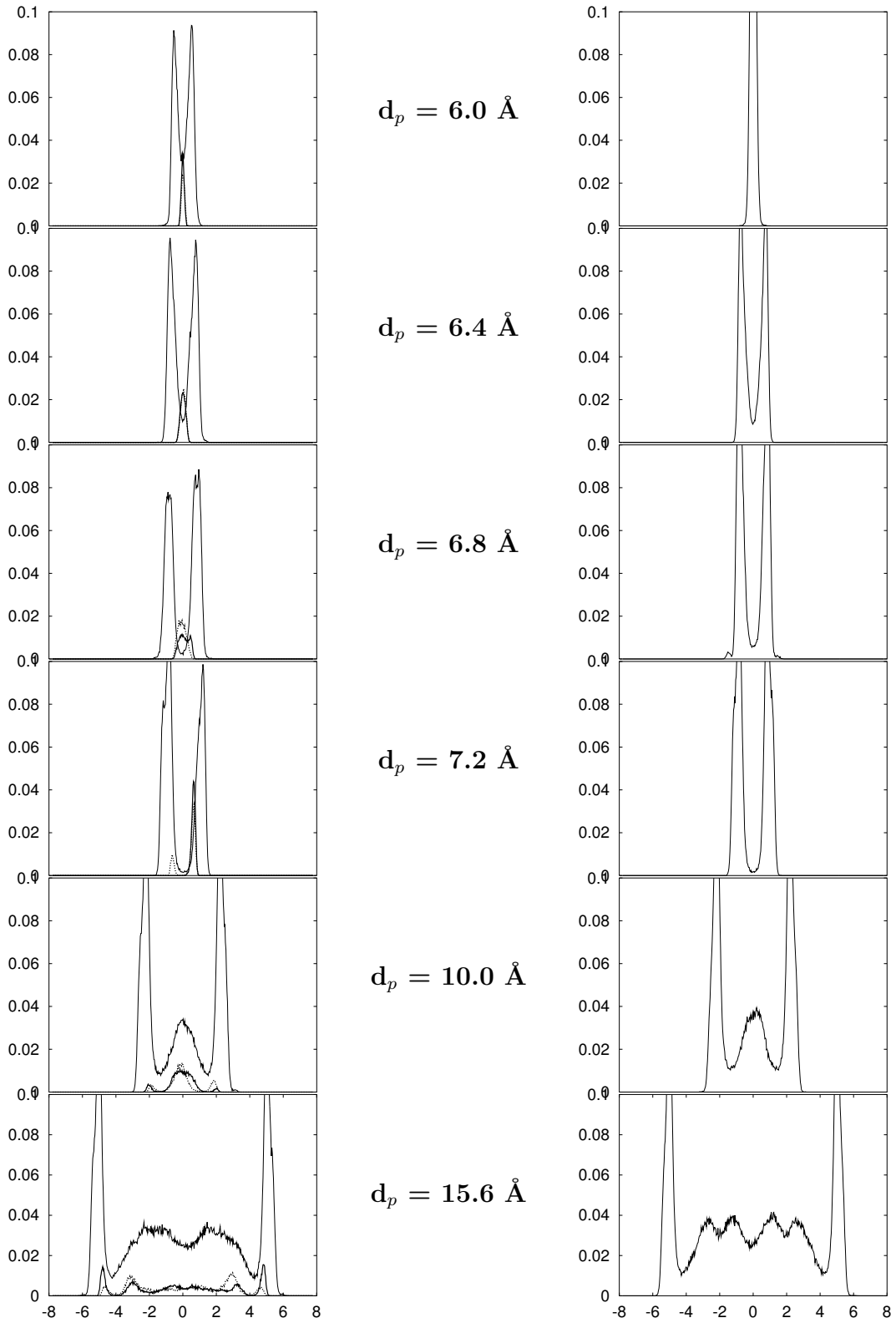

come closer to the surface than any of the ions. Even those ions that reside in one of the layers next to a surface are in all cases at least partially hydrated. Snapshots of the liquid structure (not shown here), however, reveal that, at all separations d_p, some of the ions attach directly to a surface with no water molecules left in between solution and surface ion.

Figure 8.28: **Pair distribution functions of ions in the pore**; data is displayed for various pore widths and for the homogeneous bulk solution. The functions are not normalised, In the case of d_p=6.4 Åthere were too few Cl ions in the pore to obtain a Cl-Cl pair correlation function; see text for more explanation.

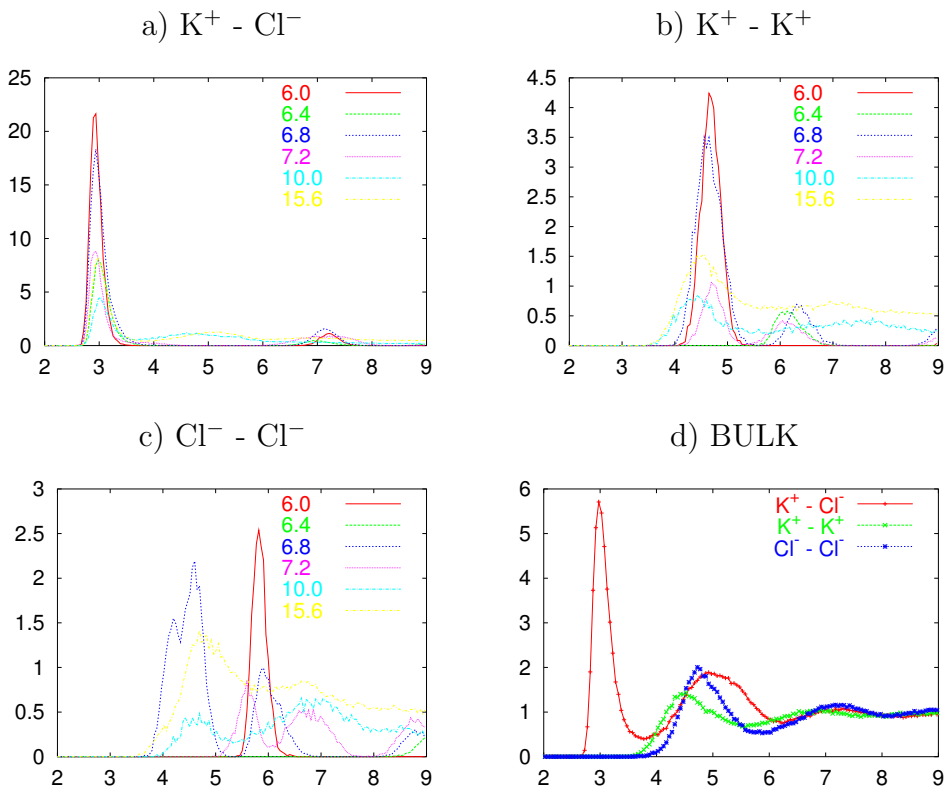

Of some interest are also the radial pair distribution functions shown in Figure 8.28. As discussed in Section 2.3.2 a recently proposed method for the simulation of aqueous ionic solutions uses a primitive model electrolyte in combination with effective ion-ion pair potentials derived from potentials of mean force in order to account for the solvent effects. Since there is a direct relationship between the pair distribution function and the potential of mean force calculated for any pair of molecules in a solution [Hansen and McDonald(1996)] we can check the viability of this model by comparing radial correlation functions for the ions in the pore at different surface separations. The differences between the correlation functions at different surface separations as shown

in Figures 8.28a-c must not be over-rated since all the functions have been scaled as if they were calculated for an isotropic solution. Since the number of other molecules surrounding each ion in a slit pore is of course smaller than it is in the bulk and this number depends on the pore width it is hard to obtain functions that can be compared quantitatively. However, we can assume that notwithstanding which kind of scaling is applied to the functions the positions of the first, second, etc. peak must be the same for the functions obtained in the pore and in the bulk if the latter are to be used to model a solution in a confined environment. The absence of a first peak in the Cl^--Cl^-order correlation function for some values of $d_p$is actually an artifact due to the small systems sizes considered here. However, for all the other pairs and surface separations we can identify the first peak and compare its location to the corresponding value in the bulk shown in Figures 8.28d. In short, we see that this value seems to depend quite sensitively on the pore width. The least variation we see for the K^+-Cl^- correlation function. For the two anion and cation pairs, however, the positions of the peaks clearly varies with the value of the pore width d_p and differences of up to 0.3 Å between values obtained at different d_p and in the bulk, respectively, can be observed. It has been shown before that small variations in the effective pair potentials used can have a profound influence on the results of simulations of ionic solutions with the above mentioned extended primitive model.[Otto and Patey(2000)] The results obtained here show that the pair distribution functions, and therefore the potential of mean force, show significant variations depending on the width of the pore. Therefore it seems dangerous to use ion-ion potentials of mean force as calculated in a bulk solution to model the effective interactions of ions in confined geometries as has been proposed by Marcelja.[Marcelja(1997)]

8.7.3 Equilibration

An important question to answer is whether the slit-pore is in equilibrium with the bulk. All the systems considered here were set up with an initial configuration of the nano-crystallites in perfect register and with a water and ion density in the pore which is

slightly higher than the corresponding bulk densities (making the assumption that the pore volume can be approximated by taking the extension of the pore in the z-dimension to be d_p-d_{hkl}^{110}(KCl), where d_{hkl}^{110}(KCl) is the layer distance of the (110) KCl crystal face). We do so because we expect equilibration to proceed faster under these conditions. Surplus molecules that are squeezed in between two surfaces must be expected to leave the pore faster than molecules entering a pore with a concentration slightly lower than its equilibrium value.

In Figure 8.29 the time-development of the number of water molecules in the pore is shown for all the considered systems. The water densities seem to converge fast and then fluctuate around equilibrium values for most of the systems. Only the water in the KCl solution at $d_p = 6.8$ Å appears to not having equilibrated within 800 pico seconds. Due to the rather small system size used here the relative large fluctuations at small separations must be considered as normal. One feature in Figure 8.29 that attracts our attention is the fact that the water density in the $d_p = 6.0$ Å pore is nearly constant with only water in the pore while we see much larger fluctuates when the pore is filled with aqueous KCl solution. The presence of the ions renders the structure of the liquid in the pore less ordered and thereby increases the fluctuations. In Table 8.5 the average number of water molecules and ions in the pore is given for the various values of d_p. For the concentration of the ions in the pore, as given in Table 8.5, it is much less clear whether it has converged in the simulation time used here. We have already seen in the preceding section that the mobility of the molecules in the pore is severely restricted. Especially at small d_p values there is virtually no exchange of ions between the pore and the rest of the system. The standard deviations of the number of ions in the pore as given in Table 8.5 are somewhat misleading here. By looking at the actual trajectories of the ions in the pore it becomes clear that for pore widths $d_p < 10.0$ Å the variations suggested by these standard deviations are a consequence of finite and small pore volume considered here. Some of the ions are close to the pore/bulk interface and although they barely move in the x-direction their position very close the border of the volume considered here for counting the ions feigns a variation of the number of ions in the pore.

Figure 8.29: **Number of water molecules in the pore as a function of the simulation time in pico seconds**, for the solution (right) and the pure water system (left). From top to bottom (both left and right): d_p = 15.6, 10.0, 7.2, 6.8, 6.4 and 6.0 Å.

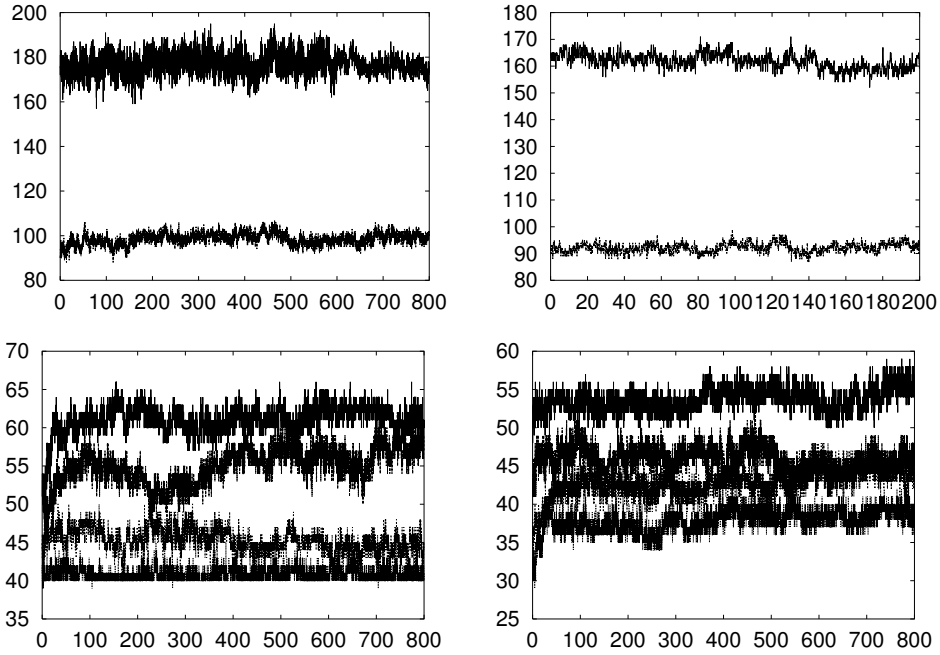

Although the number of ions in the pore is virtually constant we cannot know whether the system is in chemical equilibrium with the bulk (and the correct ionic concentration was obtained by chance from the start) or in some local minimum stabilised by the energy barrier for ions entering or leaving the pore. In order to shed some light onto this question three more 600 ps simulations, labelled fs64-mpi, fs64-lpi and fs72-mpi, were performed. The setup of these simulations is identical to the ones labelled fs64 and fs72, with the only difference being that in the additional simulations a different number of ions was situated in the pore at the start of the simulation (see Table 8.4). The overall number of ions is the same in all setups. The outcome of this experiment is: The number of ions in the pore at the beginning and at the end of each simulation is the same and also does not change in between. The quite discouraging conclusion is that for pore widths up to 7.2 Å the ionic density in the pore depends very sensitively on the initial configuration and does not

Table 8.5: **Number of molecules in the pore and the standard deviations.** The considered volume is terminated in the z-direction by the crystal surfaces, in the y-direction by periodic boundaries at ± 11.1 Å. Extension in the x direction is 9.43 Å, centered around the center of the crystallites, ensuring that only molecules are counted that are entirely in the pore even at the maximum possible relative displacement of the surfaces.

d_p	H_2O^a	σ	H_2O^b	σ	K^+	σ	Cl^-	σ
6.0	40.9	1.31	38.5	1.39	2.99	0.06	2.53	0.50
6.4	44.3	1.57	44.5	1.19	3.97	0.14	4.00	0.00
6.8	56.3	1.79	45.0	1.79	3.99	0.09	4.99	0.11
7.2	61.6	1.30	54.1	1.79	5.00	0.00	5.00	0.00
10.0	98.9	3.10	92.1	1.78	6.42	0.95	6.28	0.45
15.6	176.4	5.26	161.8	2.86	15.02	0.92	15.38	0.70

[a] pure water

[b] aqueous solution

change noticeably within the simulation times used here. In other words, we do not know what the equilibrium concentration of ions in the pore is a priori and we have also no chance of finding this value by a simulation of the type presented here. Further evidence herefore is given in Table 8.6 where we give the mean square displacement of the ions and the water in the pore in the x-direction for different values of the pore width. The mean square displacement per time unit is directly proportional to the diffusion coefficient of a molecular species in a given solution. The numbers in Table 8.6 clearly reflect the fact that at small pore widths the mobility of the ions is severely restricted. Even at a pore width of 15.6 Å the diffusivities of the molecules in the pore, water as well as ions, have less than half the value found for these molecules in a separate simulation we performed of a KCl bulk solution at ambient pressure and temperature. In fact the values given in Table 8.6 provide a too optimistic picture: the mobility of ions in the pore and between

Table 8.6: **The 1-D mean square displacement for water and ions in the pore**, calculated from 100 ps trajectories and there from 2000 sub-averages of each 10 ps simulation time. For comparison the values calculated for a saturated KCl bulk solution are also given.

	1-D MSD / $10^{-9}m^2s^{-1}$						
d_p/Å	6.0	6.04	6.8	7.2	10.0	15.6	bulk
H_2O^a	0.37	0.11	0.37	0.59	1.56	3.26	
H_2O^b	0.16	0.25	0.25	0.12	0.82	1.35	3.31
K^+	0.16	0.16	0.17	0.08	0.61	0.87	2.01
Cl^-	0.16	0.17	0.18	0.07	0.31	0.97	1.74

[a] water in pure water.

[b] water in saturated KCl solution.

bulk and pore is not only much lower than in the bulk but practically zero under the given conditions. The small but non-zero values for the mean square displacement at small pore widths in Table 8.6 are probably an artefact due to relatively short time-windows (10 ps) used in the calculation of the mean square displacement.

Two questions that follow immediately are: 1) How long would it actually take for such a system to equilibrate ? Can we expect the chemical potential of each molecular species' being equal in the pore and in the bulk, or is the activation energy barrier for the transport of molecules in between pore and bulk so high that equilibration will not happen in a finite amount of time ? 2) Does the ionic concentration in the pore have a significant effect on the forces between the crystallites ? This is vital to establish whether the relative speed of approach and hence degree of equilibration will have a major impact on agglomeration forces.

In the next section we look at the forces and in the last section of this chapter more will be said about the equilibration issue.

8.7.4 Forces

The forces calculated for various systems with constant pore widths and their error estimates are given in Table 8.7. The error estimates are the standard deviations of the averages of subsets of each 10 pico seconds. In the light of the findings presented in the preceding section the results must be interpreted with some care. Since we can by no means take it as granted that the ionic concentration in the pores corresponds to the equilibrium concentration it is pointless comparing the forces obtained with a particular KCl concentration (here we only considered two: zero and experimental saturation concentration) for different surface separations because the number of ions in the pore at each separation might correspond to an equilibrium with different bulk concentrations or to a different speed of approach of the surfaces for that matter. Another complication arises from the relatively large error bars we encounter here. In fact this does not come as a surprise since it is well known that the pressure and related quantities show very large fluctuations in Molecular Dynamics simulations because of the small system sizes normally used. For separations greater than 7.2 Å the results obtained here for the forces are of the same order of magnitude as their error bars. The error bars for most quantities calculated via Molecular Dynamics simulations are normally proportional to the inverse square root of the simulation time. Thus, if we wanted the error bars to reduce by a factor of ten the simulation time would have to increase by a factor 100. Although this would be feasible, but just, with state of the art computer hardware it is questionable whether this would be worthwhile since this still would leave the equilibration problem to be solved.

Nevertheless, there are a number of insights that can be gained by comparing the calculated forces. Firstly we can confirm the result obtained in the non-equilibrium simulation with the moving crystallites as discussed earlier in this section: allowing the crystallites to move laterally as opposed to keeping them frozen with the surfaces in register can result in noticeably different forces. For the results obtained with saturated KCl solution, the differences are in part due to a different number of ions in the pore. For example, the huge difference (-4.4 vs -159.5 10^{-6} N) found between the forces obtained with mobile and

Table 8.7: **Average total force between the nano-crystallites**, in KCl solution (S) and pure water (W) for different constant pore widths d_p and for mobile and rigid nano-crystallites. The error estimate, σ, is the standard deviation calculated from sub-averages of each 10 ps.

	Force / 10^{-6} N							
	mobile x-tals				frozen x-tals			
d_p	S	σ	W	σ	S	σ	W	σ
6.0	**-4.4**	7.0	**-146.8**	5.2	**-159.5**	5.5	**-115.9**	4.4
6.4	**-5.2**	7.4	**2.1**	7.9	**-8.8**	14.0	**-28.0**	11.0
6.4	**6.4**[a]	8.8						
6.4	**26.5**[b]	12.1						
6.8	**-9.3**	8.7	**3.5**	14.9	**-28.3**	8.5	**30.1**	9.9
6.8	**1.8**[c]	11.6						
7.2	**41.8**	10.8	**4.0**	9.0				
7.2	**34.9**[d]	17.6						
10.0	**-0.6**	6.9	**-9.6**	5.0				
15.6	**8.1**	4.1	**2.7**	4.3				

[a] less ions in pore (fs64-lpi)
[b] more ions in pore (fs64-mpi)
[c] heavier crystallites (1000×, fs68-m)
[d] more ions in pore (fs72-mpi)

frozen crystallites at a surface separation of 6.0 Å (fs60 vs s60) must be a consequence of the different number of ions (3 KCl vs 1 Cl) found in the pore. By comparing results obtained with pure water, however, we see that the influence of freezing the crystallites on the forces is a genuine effect: at d_p = 6.4 Å the force equals 2.1 ± 7.9 10^{-6} N with mobile and -28.0 ± 11.0 10^{-6} N with frozen crystallites.

By comparing the three force values obtained with the mobile crystallites at a surface

separation of d_p = 6.4 Å and the two at d_p = 7.2 Å we can assess the influence of the ionic concentration in the pore on the forces. While the two force values obtained at d_p = 7.2 Å are within their respective error bars there is a clear effect to be seen at d_p = 6.4 Å. Interestingly enough the magnitude of the force is not a monotonous function of the concentration. The force is at a minimum at an intermediate number of ions in the pore (8 vs 12 and 2). The cause for the force minimum found here is probably the fact that via correlations between solvated ions in the pore and oppositely charged ions in the surface an effective attraction results. For higher ionic concentrations this attraction is probably over-compensated by repulsion due to the increased osmotic pressure in the pore.

In Table 8.7 there is also the result of one additional simulation (s068-m) that has not been discussed so far. Here we assigned higher masses to the atoms in the crystallites so that the total mass of each crystallite is thousand times its original value. This experiment is performed in order to establish whether the fast relative motion, or vibration of the two crystallites influences the forces. If this was the case we would have an additional problem because then the efficiency of agglomeration in solution would depend on the size and the mass of the involved particles. Strictly speaking and in a thermodynamic sense the force and the potential energy in such a system cannot be a function of the mass. However, the particles considered here are very small, each consisting of not more than 175 KCl formula units. This is decisively smaller than the average size of the particles in whose agglomeration behaviour we are interested here. We have seen in Section 8.6.2 that with crystallites that are completely frozen equilibration of the ionic concentration in the pore does happen much faster resulting in a different liquid composition and thereby structure in the pore. The reason why this does not happen with mobile crystallites is probably that there, due to the very small inertia of the crystallites used here, the two surfaces can adopt nearly instantaneously the energetically most favourable lateral arrangement, corresponding to the specific number of water and ions in the pore at the beginning of the simulation. Once the crystallites having transformed to such a favourable configuration, a local energy minimum, a further variation of the pore densities is probably very "costly".

If the mass and inertia of the crystallites is much higher the densities in the pore would have more time to adjust themselves before the relative position of the crystallites reaches a local minimum. If we use artificially heavy atoms with a thousandfold mass as compared to the real atomic masses of K and Cl the vibrational speed of the particles slows down by a factor of $1/\sqrt{1000}$. With the same initial configuration as used for the light system the heavy system results in the same number of ions in the pore. The forces in units of 10^{-6} N between the crystals are 1.8 ± 11.6 for the heavy and -9.3 ± 8.7 for the corresponding lighter system. The two forces are only just within their respective error-bars. This is only one single result and further work with a variation of the initial concentration of ions in the pore would be necessary to confirm its validity. We can draw, however, the tentative conclusion that the mass and thereby the velocity of the thermal motion of the crystallites has a comparatively small influence on the equilibration in the pore and the resulting structural forces per unit area between two particles in solution.

8.7.5 Non-Equilibrium

As discussed in Section 8.7.3, the simulation setup used here cannot guarantee to provide ionic densities in narrow pores that correspond to densities in chemical equilibrium with the bulk phase. Consequently the condition of constant chemical potential throughout the system, bulk and slit pore, which is normally taken to be required for such simulations is not fulfilled. The question is whether this is an artifact of the current simulation method, or whether this is a genuine effect also to be found in real systems. If we consider such real systems the question is: Will equilibration happen fast enough as to guarantee chemical equilibrium at every point during the approach of two particles ? In order to shed some light onto this question we perform more non-equilibrium simulations of crystallites approaching each other at a constant speed. Agglomeration, including the growth of a solid bridge between two particles is a very slow process. If we only look at aggregation of two particles in solution, as the prerequisite for agglomeration, i.e., we consider the time span between the moment when two particles in solution just start

"seeing" each other and their final aggregation, this probably still takes longer than any of the simulation runs performed here at constant surface separation (800 ps). In the following results are shown for two KCl nano-crystallites with mobility in the x-y-plane (as discussed in Section 8.4) for the equilibrium simulations. The liquid phase is, again, a saturated KCl solution. We discuss forces and structural features obtained in simulations of two particles bridging the distance from a separation of 15.6 Å down to 6.0 Å in 0.48, 1.92 and 4.8 nano seconds respectively. The corresponding speed of approach is 2.0, 0.5 and 0.2 m/s, respectively. We do not use heavy ions here as done in one of the previously discussed simulations. However, if, for the sake of the argument, we consider a particle with a mass of 2610 atomic mass units, as the ones used in the simulation labelled s068-m discussed above, the diameter of such a particle, if it consisted of real KCl instead of the heavy atoms used in s068-m, is approximately 20 nm which is a small but still realistic size for particles undergoing agglomeration. The average thermal velocity per degree of freedom at 300 K is according to elementary statistical mechanics about 1 m/s for such a particle. This, however, is only the instantaneous velocity and the average distance over which it travels with this speed, the mean free path, is extremely small. Such a particle when embedded in a solvent normally undergoes a Brownian motion which can be described by a Langevin Dynamics. In its simplest form the equation of motion is [Elimelech et al.(1985)Elimelech, Gregory, Jia, and Williams]

$$\dot{p}(t) = -\zeta p(t) + F(t) + p^G(t) \tag{8.5}$$

where $\mathbf{p}$ is the momentum vector, $\mathbf{F}$ the inter-particle force vector, ζ the friction coefficient and $\mathbf{p}^G$ a random term including the average effect of collisions between the particle and numerous solvent molecules. The friction coefficient is frequently taken to be constant. For particles that undergo aggregation this is not a good approximation because the viscosity of the intervening liquid and thereby the restoring frictional forces distinctly increase at a very close distance.[Elimelech et al.(1985)Elimelech, Gregory, Jia, and Williams] This reduces the relative speed considerably. We do not know how high the resulting speed of approach really is, and there seems to be no clear answer to this question given in the

Figure 8.30: **Non-equilibrium: force acting between moving crystallites**, left: comparison of three different speeds of approach; the forces measured at constant pore width (v = 0 m/s) are also given including the error-bars. right: the forces measured at v = 0.5 m/s while decreasing the surface-surface distance from 15.6 to 6.0 Å (fwd) or while increasing it from 6.0 to 11 Å (bwd). Units are 10^{-6} N (y) and Å(x).

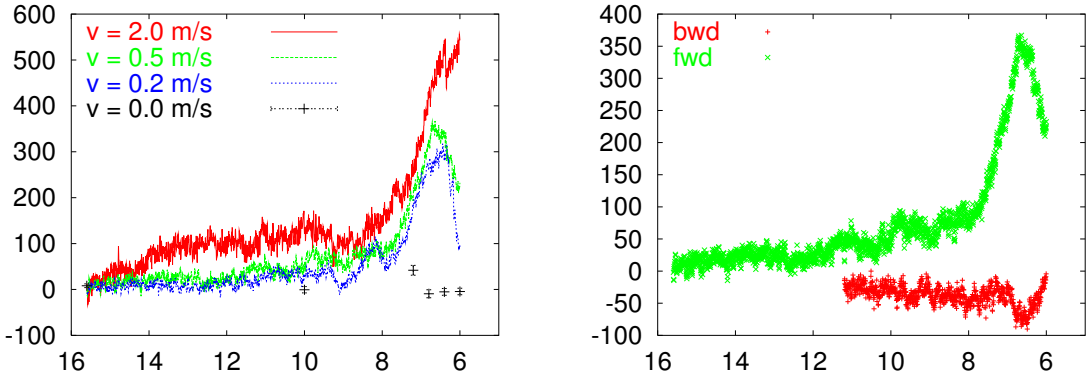

literature, but the speeds used here are probably higher than the relative speeds of the majority of particles in a real solution. Nevertheless we will gain qualitative insights from such an *in-silico* experiment.

The inter-surface forces, obtained in the non-equilibrium simulations as a function of the distance or pore width is shown on the left hand side of Figure 8.30 for the three different speeds of approach considered here. Also shown are the forces calculated in "equilibrium" as given in Table 8.7. The term equilibrium refers here to the results discussed in the preceding sections where the systems were simulated for 800 ps at constant surface separation and not to the true thermodynamic equilibrium state. The "equilibrium forces" are hence to be seen merely as indicative since the actual ionic densities which, as we have seen in the preceding section, influence the forces are "ad hoc values" here.

A large repulsive force builds up as the two surfaces approach each other. Not surprisingly this force decreases with decreasing speed of approach v. and is at a minimum for v = 0 m/s, i.e., at constant pore width. The repulsive pressure will be the sum of a kinetic contribution due to the velocity of the approaching surfaces, and an energetic contribution because solution molecules in the pore cannot relax fast enough to a structure with

Figure 8.31: **Non-equilibrium: number of water molecules in the pore**, as a function of the surface separation, for three different speeds of approach.

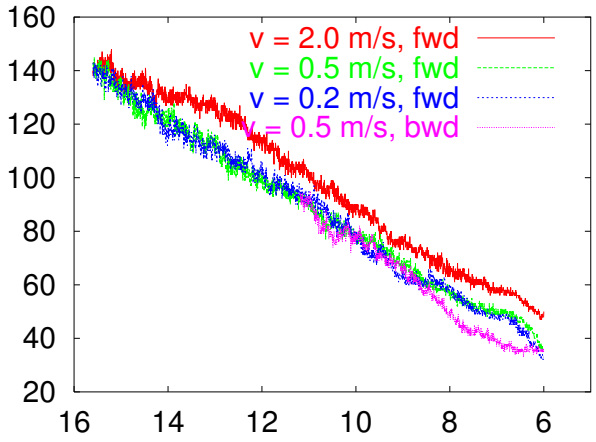

a low energy. At a speed of 2 m/s and to a smaller extent also at the two lower speeds we have probably also an osmotic contribution, i.e., the density of the water and ions in the pore is too high. Since we do not know the true equilibrium concentrations of water and ions as a function of the pore width the importance of this latter contribution is not completely clear. If we look at the number of water molecules in the pore as a function of the pore width for the different speeds of approach as shown in Figure 8.31 we see that at v = 2 m/s the density is decidedly higher than it is at the two lower velocities. At v = 0.5 m/s the density is still somewhat higher than it is at v = 0.2 m/s. This difference, however, is small and does not extend over the whole range of separations. This leads to the conjecture that a speed not much lower than 0.2 m/s might be low enough to ensure a density close to to the equilibrium density in the pore. It does look now as if there was something wrong with the reasoning here. Have we not found that equilibrium cannot be reached even with a velocity as low as 0 m/s, i.e., at constant pore width ? Are there two different kinds of equilibria ? Possibly we should turn away from the concept of equilibrium altogether, and rather talk about the *low speed limit* of the densities in a slit pore between two approaching particles. For pore widths of $d_p \leq 7.2$ Å we saw that no exchange of ions between bulk and pore took place over a time span of 800 ps

and we put forward the conjecture that there might be an energy barrier so high as to prevent equilibration indefinitely.* That is, what ever ionic density prevails in the pore after the particles have approached each other at a finite speed arriving at a particular separation will remain there until the particles are moved further apart or together. Thus, the concept of constant chemical potential seems to be not appropriate for the problem at hand. If we talk about aggregation of particles the low speed limit as proposed above might be more useful.

When we start the simulation from a configuration that has been equilibrated at d_p = 6.0 Å followed by retracting the surfaces at constant speed of 0.5 m/s we observe an effect opposite to the case of approaching surfaces: The right hand side of Figure 8.30 shows that the force is highly attractive and much lower than it is at constant separation. In a first phase the solution molecules apparently cannot enter the pore fast enough, resulting in a "negative osmotic pressure" and thereby attraction between the surfaces. It is interesting, however, that the densities in the pore resulting with surfaces retracting and the densities obtained with approaching surfaces already converge at a distance of only about 9 Å. Not only the water density but also the ionic densities converge for the two simulations at a distance of around 9.0 Å as shown in Figure 8.32 At this separation between two and three relaxed solution layers will fit into the pore. This agrees well with the finding in Section 8.7.3 according to which the mobility of the molecules in the pore at constant surface separation, d_p, switches from a vibrational to a translational regime somewhere between d_p = 7.2 and 10.0 Å. In contrast to the densities the forces of the forward and backward simulations still clearly differ at 11 Å, the largest separation included in the simulation with retracting crystallites. A very similar behaviour was found by Biesheuvel [Biesheuvel(2002)] who calculated the interaction forces between surfaces with ionisable surface groups via a semi-empirical relation including time dependent surface charge regulation. He argues that both the large repulsion at small separations and a strong attraction at retraction as measured experimentally with the surface force appara-

*This energy barrier could actually be determined relatively easily by calculating the potential of mean force for an ion "dragged" out of the pore.

tus can be explained via this model while other models that assume equilibrium between bulk and pore throughout the experiment fail to do so.

Due to limited time and hardware resources we unfortunately cannot tackle another interesting question here: At what velocities will the densities and forces obtained with approaching and retracting surfaces converge ? This convergence can of course only be reached when the number of ions and water molecules in the pore at the smallest surface separation, here 6.0 Å, is the same. This condition is not fulfilled for the forward and backward simulations at v = 0.5 m/s discussed here. With the surfaces retracting there are 3 K^+ and 2 Cl^- in the pore at d_p = 6.0 Å while with the approaching surfaces 8 K^+ and 6 Cl^- are in the pore at this surface separation. However, the ion densities are already the same at about 9 Å.

One aspect not discussed so far is the ratio between K^+ and Cl^- ions in the pore. Since here we are dealing with an overall neutral system and non-polar surfaces one would expect the content of the pore to be neutral as well, no matter what the speed of approach or which pore width we look at. The ion/water ratios given for both K^+ and Cl^- in Figure 8.32, however, reveal that the pore is not necessarily neutral. Interpreting these results is obviously limited by the small system size we use, but nevertheless, they raise an interesting question. The difference between the relative K^+ and Cl^- concentrations in the pore at d_p = 6.0 Å after the approach at 2.0 m/s looks quite prominent in Figure 8.32 but in fact this difference only corresponds to 3 atoms (5 K^+, 5 Cl^- vs 5 K^+, 8 Cl^-). However, since the difference persists over most of the pore widths and can be found for both v = 2.0 and v = 0.5 m/s it is probably a genuine property of the material under the given conditions rather than a statistical fluctuation. One might suspect that this effect is caused by the chloride ions attaching closer to the surfaces. However, although snapshots of the configurations (not shown here) do show this effect the difference is minute and probably within the error bars. This is also confirmed by plots of the average ion densities as a function of the distance from the surfaces. Therefore the reason for the local net-charge in the pore is probably simply the different size of the hydrated potassium and chloride ions.[Kiriukhin and Collins(2002)] Potassium and its first solvation shell is somewhat big-

Figure 8.32: **Non-equilibrium: relative K^+ (red) and Cl^- (green) densities**, as a function of the surface separation. Here the densities are given as the number of K^+ or Cl^- ions divided by the number of water molecules in the pore. Top: forward vs. backward (see caption of Figure 8.30), bottom: two different speeds of approach (0.2 vs 2.0 m/s). Note that the ratio in the bulk phase for both K^+ and Cl^- is about 0.08.

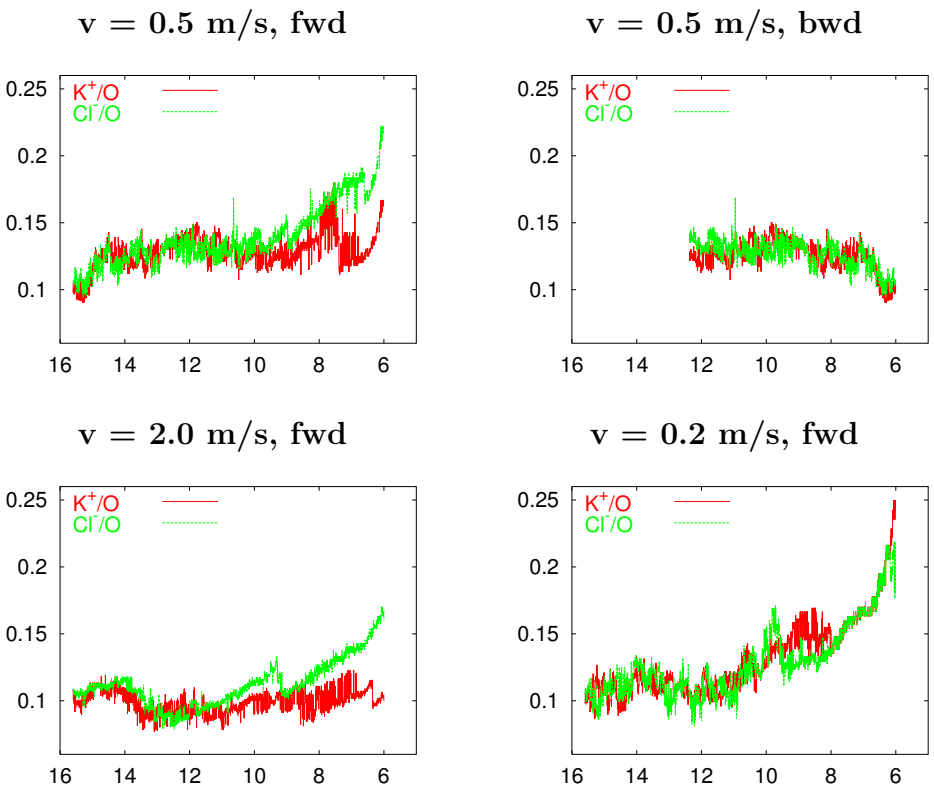

ger than the corresponding chloride complex. Since here we study a confined system, i.e., an environment where space is generally a scarce commodity, it is straightforward to assume that the smaller chloride complex fits easier into the narrow pore. The fact that this effect apparently grows stronger with increasing speed of approach also agrees with this assumption. A clear confirmation of this hypothesis would require a detailed analysis of the hydrogen-bonding structure in the pore and the hydration shells of the ions. This is beyond the scope of this work, and a clear result would probably be hard to obtain due to the small system size considered here.

Finally we turn to another result of the non-equilibrium simulations: the charge density

in the pore. Calculating the absolute charge density as a function of the absolute z-coordinate would be pointless since the surfaces are moving continuously. Therefore we show here the charge density as a function of the absolute distance from the crystal solution interface. In all the plots discussed in the following the partial charges of the water oxygen and hydrogen are included into the calculated charge distributions. Since water must actually be seen as being a dipole rather than two separate charges and since the concept of partial charges is generally ill-defined it is unclear how valid this is. However in nearly all of the other studies published in this field (see Section 2.3.2) a primitive model electrolyte is used. Thus, the charge densities above a surface normally only include the ions while the water is completely neglected because in a primitive model electrolyte the water is taken to be a homogeneous background dielectric without any structure. We assume that using the concept of partial charges is still a better approximation than this gross simplification. In Figure 8.33 the density distribution above the KCl surface is compared for two different speeds of approach, v = 0.2 vs 2.0 m/s. Also included is the charge distribution obtained in the equilibrium simulation of the widest pore considered here with $d_p = 15.6$ Å, which is here taken as an approximation to the charge distribution at infinite surface separation. For the calculation of the charge densities in the two non-equilibrium cases only configurations for pore widths between 15.6 and 13.2 Å were considered so that any differences are mainly due to the different speed and not due to interactions with the other surface and different solution structure in the middle of the pore. The result is rather striking in that the density distribution above the surface seems to be nearly independent of the speed of approach. There are some differences between the results obtained with the two finite velocities but they are rather small and by no means qualitative. Comparison of speed of approach of 0.0 (constant d_p) with 0.2 m/s reveals that there is barely any difference. Thus the structure of the solution immediately above the surface, i.e., essentially in what is called the Stern layer, remains practically unchanged when accelerating the surface from 0.0 to 0.2 m/s. Both the maximum and minimum closest to the surface, i.e., at the smallest values of the abscissa, originate mainly from water hydrogens and oxygens. The ions only contribute to the second peak. The first

Figure 8.33: **Non-equilibrium: charge density above surface**. The charge density is calculated for a slab of 4 Å thickness above the surface for two different speeds of approach and compared to the same result from the equilibrium simulation are at d_p = 15.6 Å. In the two non-equilibrium cases the summation includes all the configurations obtained for a pore width, 15.6 > d_p > 13.2 Å; Units are Å (x) and e/Å^3 (y). Note that the partial charges of the water atoms are included here.

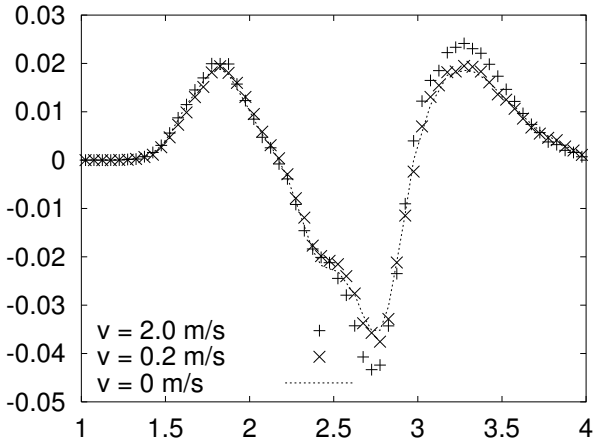

peak, throughout all surface separations and velocities of approach, is due to the water hydrogens that point at the chloride ions in the crystal surface and the first minimum is accordingly due to the oxygens bound to the hydrogens in the first peak.

If the two surfaces come ever closer the shape of the charge distribution changes somewhat. In Figure 8.34 the charge distribution above the surface is again compared for v = 0.2 and 2.0 m/s. This time, however, the comparison is made for four different ranges of pore widths. The total distance bridged by the particles (15.6 - 6 Å) is divided into four equally spaced ranges (15.6↔13.2↔10.8↔8.4↔6.0) and the corresponding sub-sets of configurations are summed up separately. At v = 0.2 m/s the charge density barely changes its shape down to a pore width of 8.4 Å. Only during the final 2.4 Å the entire distribution appears to be shifted along the z-coordinate, the shape of the function still remaining very similar to the equilibrium shape. As the pore width decreases beyond a certain minimum distance the whole first layer apparently gets somewhat pushed towards the surface with the internal structure of the layer barely changing. For a speed of

Figure 8.34: **Non-equilibrium: The average charge density as a function of the distance to the surface (in units of Å) for various pore width ranges.** Speed of approach: left: v = 2.0 m/s, right: v = 0.5 m/s, bottom: v = 0.2 m/s

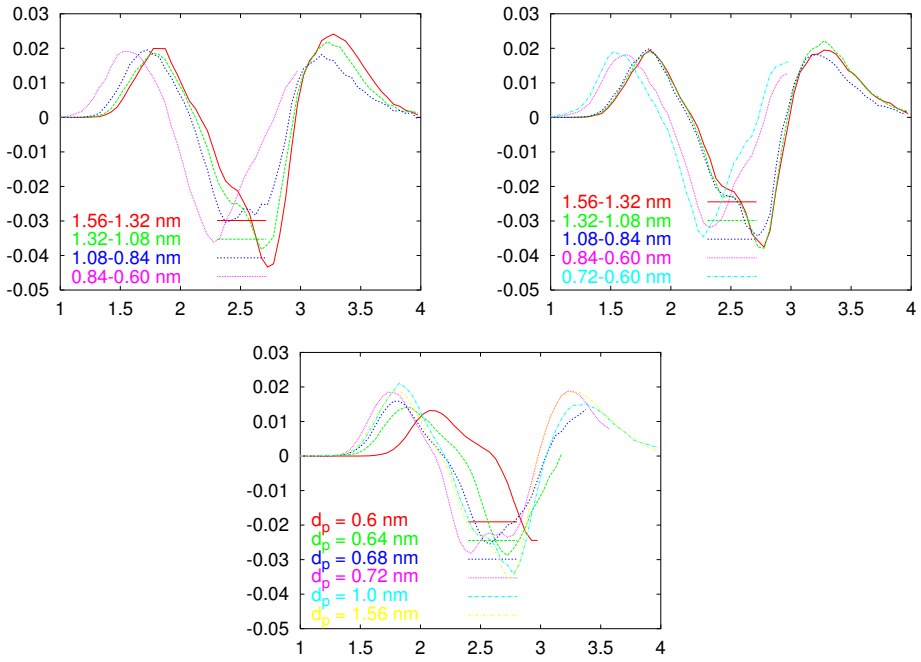

approach of 2.0 m/s the picture is similar, only the distortion of the distribution sets in already at a separation of about 10 Å but a clear shift of the distribution towards the surface only sets in at around 8.4 Å, just as found for the slower approach. Interesting is a comparison with a zero velocity case, i.e., the simulations at constant pore-width. Down to a separation of 10.0 Å the shape of the distribution function remains very similar to the one obtained at $d_p = 15.6$ Å. At a pore width of 7.2 Å the distribution becomes distorted and obtains a shape very similar to the one found at a speed of 2.0 m/s for the range 10.8 - 8.4 Å. The most striking difference to the non-equilibrium results is found at small separations of 6.4 and 6.0 Å. In contrast to distribution functions calculated at a finite speed the squeezing of the layer reverses here, and the function expands away from the surface. Unfortunately we cannot determine unambiguously whether this sudden change of shape and position of the charge distribution is a genuine difference between the static and dynamic simulations or simply due a comparatively low initial density of solution in

the pore at d_p = 6.4 and 6.0 Å.

8.8 Discussion

The results given in this chapter clearly raise more questions than they give answers. Hence the final section is deliberately called discussion rather than conclusions. There are, however, some points that could be clearly established. The results in Section 8.5 suggest that the usage of rigid crystals without internal degrees of freedom is a reasonable approximation for a system as simple as the KCl-solution interface. A thorough investigation of issues concerning the force field as, for example, ramifications of not considering polarisability of the solution molecules is not subject of this work. If a number of other problems, most notably the equilibration question, are solved addressing this question should be straightforward task.

One clear result found here is the fact that keeping the surfaces in register, or at any other constant relative arrangement, for that matter, results in a distinct alteration of the obtained structure and forces. The mobile representation of the system is undoubtedly the more realistic one. The forces as a function of the pore-width, measured with mobile crystallites and pure water as the liquid phase, are considerably damped as compared to those obtained with frozen crystallites (Table 8.7). This is a consequence of the fact that with variable registry the water molecules can adopt energetically more favourable positions in the pore, reducing the forces in the repulsive regime. In the attractive regime the magnitude of the forces is also reduced because with mobile crystallites more solution molecules fit into the pore increasing the repulsion between the surfaces due to structural forces. If the crystallites are mobile the degree of order in the liquid in the slit-pore seems to decrease monotonously with increasing surface separation. This is not observed with frozen crystallites. If the liquid phase is a KCl solution the situation is more complicated. The number of different pore widths and KCl concentrations used here is too few to give a clear picture. However, we clearly saw that the presence of ions can effect the preferred registry and thereby partially override the effect of the water on the registry, especially for small pore widths (see Figure 8.23). These are effects that clearly cannot be assessed with simpler models where the water is treated as continuum. They are

substantial at pore widths smaller than about ten Ångstrom and, most importantly, alter the forces as shown in Table 8.7. Hence the usage of explicit water and ion models is to be strongly recommended in such calculations. The effect will probably be smaller with highly charged surfaces since here the strong electrostatic interactions could override the dependence of the forces on the registry. However, we have seen in snapshots and density distribution functions that the water shows a distinctive directional order in narrow pores and therefore its treatment as a background continuum cannot be justified.

Generally the forces between two KCl nano-crystallites with parallel opposing (110) faces depend very sensitively on the number of ions in the slit-pore between the surfaces. Depending on the pore-width the ions can promote both attraction, via the alignment of a cat-ion between two surface an-ions or vice versa, and repulsion, via breaking of attractive hydrogen bond chains, between the surfaces. This dependence of the inter particle forces on the ionic concentration was to be expected. Somewhat surprising, however, is the fact that the forces also depend very sensitively on the initial conditions, i.e., the number of ions in the pore in the starting configuration. In other words, the exchange rate of ions between the pore and the bulk is practically zero for pore widths $d_p \leq 10$ Å. We have seen that that for such surface separations, not exceeding the width of two solution layers, the correlation between the molecules in the pore and the surface structure is so strong that the ions are effectively immobilised. This effect would also prevail in systems with a geometry that facilitated equilibration for larger pore widths, for example, if an extended bulk region was put immediately next to the pore instead of the narrow vertical slit-pore that connects pore and bulk in the simulations reported here. It not only renders the interpretation of the obtained forces difficult but also raises a the principal question whether it is reasonable to perform a simulation of slit pores with structured surfaces containing aqueous ionic solutions at constant chemical potential.

Results of the non-equilibrium simulations of two crystallites approaching each other with constant velocity revealed that the forces as well as the liquid densities in the pore as a function of the pore separation are very similar for speeds of 0.2 and 0.5 m/s. That is, the forces and densities might converge to constant values at a speed not much lower

than 0.2 m/s. I presume that the forces and densities obtained thus are more appropriate for assessing the influence of inter-particle forces on crystal aggregation.

Irrespective of the equilibration question there is another point that has not been discussed so far. The following is highly speculative. If we look at the magnitude of the forces we find that the values in the repulsive regime are very high indeed. For example with mobile crystallites, saturated KCl solution and a pore width of 7.2 Å we obtain an average force of $4.2 \cdot 10^{-5}$ N. Taking into account the surface areas involved here, about 500 Å^2, we obtain a pressure of $8.4 \cdot 10^{12}$ Pa or $8.4 \cdot 10^6$ MPa. The interface between two crystallites that have agglomerated in an experiment has been shown to contain many water inclusions in a region parallel to the attached surfaces.[**?**] The plausible explanation is that in reality agglomeration is not the attachment of two large, perfectly flat and aligned surfaces. Probably only a small fraction of the surfaces of two approaching crystallites does actually come into contact while those areas that do not attach seamlessly remain separated by a solvent inclusion or subsequently attach via further crystal growth, the latter process happening on a longer time scale than the actual aggregation event. If we take this into account and make the ad hoc assumption that only 1 % of two surfaces do come into close contact the value of the force discussed above reduces by a factor of hundred to $8.4 \cdot 10^4$ MPa. This is still considerably larger than pressure fluctuations in small water samples.[**?**] Thus we have to make one out of two assumptions: 1) two aggregating crystallites never come closer than about one nano-meter. Once they have approached that far they get possibly caught in a secondary minimum where they stay long enough for crystal growth to take over and finish the agglomeration process. 2) Other processes that are out of the range of the present simulation method could play a role allowing the crystallites to come so close that only one solution layer is left in between parts of the two surfaces. For the system considered here this approximately corresponds to the simulations at $d_p = 6.0$ Å. I expect this last solution layer to remain in the crystal in any case since the solution molecules cannot escape from the pore anymore; they are highly ordered if not crystalline, practically immobile and large attractive forces prevail. The processes promoting the approach past the high repulsive maxima separating

pores with 2, 3 and possibly more water layers might involve a shifting of the crystallites parallel to the surfaces or lattice defects on the surfaces that accidentally suppress liquid structures between the surfaces that would otherwise lead to strong repulsion.

Establishing which of these mechanisms dominates or whether we find different mechanisms for different materials would require a more extended study of the subject and is beyond the scope of this work. In fact the results presented in this chapter look rather discouraging. However, there are some positive aspects as well. It could be shown that the charge density above the crystal surfaces remain nearly identical to the density above a free surface. This is a confirmation for the applicability of simpler models for larger surface separations since these models often assume a constant surface charge or potential.[Elimelech et al.(1985)Elimelech, Gregory, Jia, and Williams] We have also seen that the water density in the pore equilibrates relatively fast in the simulations with pure water. Although we cannot be sure to have reached equilibrium at the smallest separations ($d_p \leq 6.4$ Å) it seems to be a reasonable approximation to simulate pure water in the slit-pore at constant chemical potential with one of the algorithms discussed in Section 3.6.3. If we performed such a simulation of water at constant chemical potential and put one additional molecule of a different type into the pore we could study the effect of this molecular species in a low concentration limit on aggregation forces and compare the effect of different additives.

Chapter 9

Summary, Conclusions, Outlook

The purpose of this work was to investigate systematically in how far models for crystal agglomeration can be improved and given a sounder physical basis by the means of atomic scale simulation. In Chapter 2 I reviewed traditional models for crystallisation and agglomeration; the role molecular simulation currently plays in this field was discussed and the limitations highlighted. A thorough literature review revealed that specific interactions and correlations between structured surfaces and solution molecules and in between solution molecules must be accounted for in an accurate calculation of inter particle forces. Hence the commonly applied mean field approximations have only limited predictive power in many cases.

After an overview over the general methodology of molecular simulation in Chapter 3 I did a first study to scrutinise the applicability of molecular simulation in the context of modelling intermolecular interactions in crystalline material. I compared the performance of different model potentials or force fields in the prediction of crystal morphologies via the attachment energy model. It turned out that predicted morphologies are rather insensitive to the model potential in most cases. Thus any incorrect predictions are probably caused by assumptions inherent to the attachment energy model, most notably the neglect of any account for solvent, rather than by limitations of the classical model potentials.

A more ambitious undertaking was establishing the structure of potash alum sur-

faces in contact with aqueous solution in Chapter 7. For tackling this problem I first devised a classical model potential for potash alum as described in Chapter 5. The resulting rigid ion potential could be shown to reproduce the crystal structure and elastic constants reasonably well upon lattice energy minimisation of the experimental structure. The correct crystal structure was maintained in a Molecular Dynamics simulation at a temperature of 300 K, this being a test that is rarely applied when modelling inorganic materials. The experimentally confirmed dynamical crystal disorder in potash alum could also be reproduced at least qualitatively; a result that gave us some confidence into the quality of this very simple model potential. Another pre-requisite for a successful modelling of interfaces, in particular those including ionic materials, is the correct treatment of electrostatic long range interactions. In Chapter 6 results are reported for a number of test simulations showing that a generalised reaction field algorithm [Hummer et al.(1994)Hummer, Soumpasis, and Neumann] is efficient in terms of computational speed but can not properly account for long range interactions in systems with 2-D periodicity. A Smooth particle Mesh Ewald algorithm in combination with a dipole correction term [Yeh and Berkowitz(1999)] turned out to be a good compromise providing accurate results at reasonable computational speed. After having established both the applicability of the force-field and the most efficient way to deal with electrostatic long range interactions I performed a number of Molecular Dynamics simulations of various potash alum surfaces in contact with saturated aqueous potash alum solution. I could establish that the morphologically most important face of potash alum, the (111) face, is terminated by sulfate anions and likely to have a comparatively high surface charge density. This is in accord with the experimental finding [Pratola et al.(2002)Pratola, Simons, and Jones] that the force required to pull apart a pair of surfaces attached in aqueous solution is larger for pairs of neutral (220) or (200) faces than it is for a pair of (111) faces. It could not be established clearly whether the sulfate terminated surface slab is fully occupied or partially reconstructed since this is likely to depend on the partial pressure of sulfate anions in the solution. Finding any quantitative relation to describe this dependence would be very demanding, if not impossible,

with currently available theoretical methods and computational tools.

Finally, in Chapter 8 I report the results of Molecular Dynamics simulations of two potassium chloride nano-crystallites in aqueous solution. A number of authors noted that the commonly used primitive model which neglects specific solvent-surface and solvent-ion interactions (see Ref. [Hansen and Lowen(2000)] and references therein) might be an inadequate simplification when simulating this kind of system. Only recently this conjecture was scrutinised by Yang et al. [Yang et al.(2002)Yang, Yiacoumi, and Tsouris] who found distinctive differences in the ion density distribution as obtained with a primitive model and with explicit water. These findings are confirmed here for a system that is qualitatively different from the one studied by Yang et al. [Yang et al.(2002)Yang, Yiacoumi, and Tsouris] and considerably more realistic. Both neat water and an ionic solution in a mobile slit pore with a structured surface cause, due to specific surface-ion correlations and the polar nature of water, a variety of effects that could certainly not be predicted by a mean field approach such as a primitive model or a numerical solution of the Poisson Boltzmann Equation. Most notably both water and ions do have a distinct influence on the preferred registry of two crystal surfaces once they are closer than about ten Ångstrom. A method was introduced only recently [Marcelja(1997)] where the specific influence of solvent molecules is accounted for by using the potential of mean force, as effective ion-ion potentials in a primitive model electrolyte. The results I present here shed some doubt on the applicability of this method since I find that ion-ion pair correlation functions, and thereby the potential of mean force, in solution in a slit pore depend very sensitively on the pore-width while the potentials of mean force commonly applied in this method are previously determined in a separate simulation of a bulk sample.

I did encounter fundamental problems resulting from the extremely slow equilibration of the ionic concentrations in the narrow slit pore in between the two crystal surfaces. Although these problems could not be resolved here I consider the obtained results of some importance since they highlight a problem that might be a general issue in the simulation of confined systems in contact with a bulk phase. In the best part of the work

published in this field so far, constant chemical potential of the species in and outside the pore is taken for granted and the time dependence of the equilibration is not considered at all.

Considering the huge pressure needed to expel the last few layers of water between the surfaces, as discussed in Section 8, two principal questions stand at the end of this thesis: Do two crystals that agglomerate in solution touch each other at all or is the agglomeration rather promoted by, possibly accelerated, crystal growth between two close surfaces ? And: If the crystallites do approach up to a very close distance, is the solution in the resulting slit-pore in equilibrium with the bulk solution or not ? The work presented here is evidence for the answer to the second question being a clear no, at least for pore-widths smaller than about one nano-meter. I could not give a clear answer to the first question, hence this problem remains an interesting subject for future research.

With hindsight to the results obtained here I must state that we are still far from the goal I originally set out to achieve and that more work needs to be done before we can give reasonably accurate and reliable theoretical estimates of aggregation efficiencies of particular crystalline materials from first principles. As shown here the classical empirical model potentials used seem to be a minor problem while the main problem remains the efficient incorporation of events on very different length and time scales. We need to include both an accurate and explicit description of the atomic scale interactions as well as equilibration events on a time-scale of at least micro-seconds into our models. With current computational hardware and algorithms this cannot be done. In spite of this rather sobering result it would be worthwhile to investigate whether we can assess the influence of various additives on agglomeration efficiencies. As a first approximation one could do simulations of a slit-pore with water in the Grand Canonical ensemble with one of the algorithms discussed in Section 8.2.1. One, or a few, additional molecule(s) of a different species would represent some additive and would not be subject to insertions or deletions. If we find additives that can specifically bind to a given surface topology, the concentration and consequently the equilibration question are probably of secondary importance and meaningful results can be obtained. Because the explicit simulation of

the bulk phase is not necessary here, an additional advantage of such an approach would be that larger pores can be simulated for longer times, and hence the error bars would decrease considerably. While being less rigorous, such an approach could still give us a way to estimate, at least semi-quantitatively, agglomeration efficiencies from first principles.

Bibliography

[Mersmann and Braun(2001)] Mersmann, A.; Braun, B. In *Crystallization Technology Handbook*; Marcel Dekker: New York, 2001; Chapter Agglomeration.

[Overbeek(1999)] Overbeek, T. *Adv. Colloid Interface Sci.* **1999**, *83*, IX–XI.

[Israelachvili(1991)] Israelachvili, J. N. *Intermolecular and surface forces*; Academic Press: London, 1991.

[Israelachvili and Mcguiggan(1988)] Israelachvili, J. N.; Mcguiggan, P. M. *Science* **1988**, *241*, 795–800.

[Hansen and Lowen(2000)] Hansen, J. P.; Lowen, H. *Annu. Rev. Phys. Chem.* **2000**, *51*, 209–242.

[Hounslow et al.(1988)Hounslow, Ryall, and Marshall] Hounslow, M. J.; Ryall, R. L.; Marshall, V. R. *AICHE J.* **1988**, *34*, 1821–1832.

[Mersmann et al.(2002)Mersmann, Braun, and Loffelmann] Mersmann, A.; Braun, B.; Loffelmann, M. *Chem. Eng. Sci.* **2002**, *57*, 4267–4275.

[von Smoluchowski(1917)] von Smoluchowski, M. *Zeitschr. Phys. Chem.* **1917**, *92*, 129.

[Gardner et al.(1998)Gardner, Theis, and Young] Gardner, K. H.; Theis, T. L.; Young, T. C. *Colloid Surf. A-Physicochem. Eng. Asp.* **1998**, *141*, 237–252.

[Elimelech et al.(1985)Elimelech, Gregory, Jia, and Williams] Elimelech, M.; Gregory, J.; Jia, X.; Williams, R. *Particle Deposition and Aggregation*; Butterworth-Heinemann Ltd.: Oxford, 1985.

[Fuchs(1934)] Fuchs, N. *Zeitschr. Phys.* **1934**, *89*, 736.

[Han and Lee(2002)] Han, M.; Lee, H. *Colloid Surf. A-Physicochem. Eng. Asp.* **2002**, *202*, 23–31.

[Docoslis et al.(2001)Docoslis, Wu, Giese, and Van oss] Docoslis, A.; Wu, W.; Giese, R. F.; Van oss, C. J. *Colloid Surf. B-Biointerfaces* **2001**, *22*, 205–217.

[Nikolakis et al.(2000)Nikolakis, Kokkoli, Tirrell, Tsapatsis, and Vlachos] Nikolakis, V.; Kokkoli, E.; Tirrell, M.; Tsapatsis, M.; Vlachos, D. G. *Chem. Mat.* **2000**, *12*, 845–853.

[Kallay and Zalac(2002)] Kallay, N.; Zalac, S. *J. Colloid Interface Sci.* **2002**, *253*, 70–76.

[McQuarrie and Simon(1997)] McQuarrie, D. A.; Simon, J. D. *Physical Chemistry, A Molecular Approach*; University Science Books: Sausalito, Calif., 1997.

[Oyen and Hentschke(2002)] Oyen, E.; Hentschke, R. *Langmuir* **2002**, *18*, 547–556.

[Derjaguin and Landau(1941)] Derjaguin, B. V.; Landau, L. *Acta Physicochimica (USSR)* **1941**, *14*, 633.

[Verwey and Overbeek(1948)] Verwey, E. J.; Overbeek, J. *Theory of the Stability of Lyophobic Colloids*; Elsevier: Amsterdam, 1948.

[Hamaker(1937)] Hamaker, H. *Physics* **1937**, *4*, 1058.

[London(1930)] London, F. *Z. Physik* **1930**, *63*, 245–279.

[Lifshitz(1956)] Lifshitz, E. *Sov. Phys. JETP* **1956**, *2*, 73.

[Ackler et al.(1996)Ackler, French, and Chiang] Ackler, H. D.; French, R. H.; Chiang, Y. M. *J. Colloid Interface Sci.* **1996**, *179*, 460–469.

[Thennadil and Garcia-rubio(2001)] Thennadil, S. N.; Garcia-rubio, L. H. *J. Colloid Interface Sci.* **2001**, *243*, 136–142.

[Biesheuvel(2001)] Biesheuvel, P. M. *J. Colloid Interface Sci.* **2001**, *238*, 362–370.

[Yotsumoto and Yoon(1993)] Yotsumoto, H.; Yoon, R. H. *J. Colloid Interface Sci.* **1993**, *157*, 426–433.

[Van oss et al.(1999)Van oss, Docoslis, Wu, and Giese] Van oss, C. J.; Docoslis, A.; Wu, W.; Giese, R. F. *Colloid Surf. B-Biointerfaces* **1999**, *14*, 99–104.

[Ninham(1999)] Ninham, B. W. *Adv. Colloid Interface Sci.* **1999**, *83*, 1–17.

[Wu et al.(1999)Wu, Bratko, Blanch, and Prausnitz] Wu, J. Z.; Bratko, D.; Blanch, H. W.; Prausnitz, J. M. *J. Chem. Phys.* **1999**, *111*, 7084–7094.

[Wu et al.(2000)Wu, Bratko, Blanch, and Prausnitz] Wu, J. Z.; Bratko, D.; Blanch, H. W.; Prausnitz, J. M. *Phys. Rev. E* **2000**, *62*, 5273–5280.

[Rouzina and Bloomfield(1996)] Rouzina, I.; Bloomfield, V. A. *J. Phys. Chem.* **1996**, *100*, 9977–9989.

[Wu and Prausnitz(2002)] Wu, J. Z.; Prausnitz, J. M. *J. Colloid Interface Sci.* **2002**, *252*, 326–330.

[Greberg and Kjellander(1998)] Greberg, H.; Kjellander, R. *J. Chem. Phys.* **1998**, *108*, 2940–2953.

[Lado et al.(1983)Lado, Foiles, and Ashcroft] Lado, F.; Foiles, S. M.; Ashcroft, N. W. *Physical Review* **1983**, *A28*, 2374–2379.

[Burak and Andelman(2001)] Burak, Y.; Andelman, D. *J. Chem. Phys.* **2001**, *114*, 3271–3283.

[Marcelja(1997)] Marcelja, S. *Colloid Surf. A-Physicochem. Eng. Asp.* **1997**, *130*, 321–326.

[Otto and Patey(2000)] Otto, F.; Patey, G. N. *J. Chem. Phys.* **2000**, *113*, 2851–2855.

[Lee et al.(2002)Lee, Chan, and Tang] Lee, M.; Chan, K. Y.; Tang, Y. W. *Mol. Phys.* **2002**, *100*, 2201–2211.

[Kinoshita et al.(1996)Kinoshita, Iba, and Harada] Kinoshita, M.; Iba, S. Y.; Harada, M. *J. Chem. Phys.* **1996**, *105*, 2487–2499.

[Rick(2001)] Rick, S. W. *J. Chem. Phys.* **2001**, *114*, 2276–2283.

[Yang et al.(2002)Yang, Yiacoumi, and Tsouris] Yang, K. L.; Yiacoumi, S.; Tsouris, C. *J. Chem. Phys.* **2002**, *117*, 8499–8507.

[Metropolis et al.(1953)Metropolis, Rosenbluth, Rosenbluth, Teller, and Teller] Metropolis, N.; Rosenbluth, A. W.; Rosenbluth, M. N.; Teller, A. H.; Teller, E. *J. Chem. Phys.* **1953**, *21*, 1087–1091.

[Alder and Wainwright(1959)] Alder, B. J.; Wainwright, T. E. *J. Chem. Phys.* **1959**, *31*, 459–466.

[Rahman(1964)] Rahman, A. *Physical Review* **1964**, *136*, A405–A411.

[Rahman and Stillinger(1971)] Rahman, A.; Stillinger, F. H. *J. Chem. Phys.* **1971**, *55*, 3336–3359.

[Wesseling(2000)] Wesseling, P. *Principles of Computational Fluid Dynamics*; Springer: Berlin Heidelberg New York, 2000.

[Hoover and Hoover(2001)] Hoover, W. G.; Hoover, C. G. *Computing in Science & Engineering* **2001**, *3*, 78–85.

[Hoogerbrugge and Koelman(1992)] Hoogerbrugge, P. J.; Koelman, J. *Europhysics Letters* **1992**, 155–160.

[Jensen(1999)] Jensen, F. *Computational chemistry*; John Wiley & Sons Ltd.: Chichester, 1999.

[Hansen and McDonald(1996)] Hansen, J.-P.; McDonald, I. R. *Theory of Simple Liquids*; Academic Press Ltd.: London, 1996.

[Frisch et al.(1998)Frisch, Trucks, Schlegel, Scuseria, Robb, Cheeseman, Zakrzewski, Montgomery, Jr., Str
Frisch, M. J. et al. *Gaussian 98, Revision A.9*, program, 1998, Gaussian, Inc., Pittsburgh PA.

[Allen and Tildesley(1987)] Allen, M.; Tildesley, D. *Computer Simulation of Liquids*; Clarendon Press: Oxford, 1987.

[Frenkel and Smit(2001)] Frenkel, D.; Smit, B. *Understanding Molecular Simulation: From Algorithms to Applications, second edition*; Academic Press: London, 2001.

[Levine(1991)] Levine, I. N. *Quantum Chemistry*; Prentice Hall Inc.: Englewood Cliffs, New Jersey, 1991.

[van Duijneveldt et al.(1994)van Duijneveldt, van Duijneveldt-van Derijdt, and van Lenthe] van Duijneveldt, F. B.; van Duijneveldt-van Derijdt, J. G.; van Lenthe, J. H. *Chem. Rev.* **1994**, *94*, 1873–1885, not copied.

[Tzeli et al.(2000)Tzeli, Mavridis, and Xantheas] Tzeli, D.; Mavridis, A.; Xantheas, S. S. *J. Chem. Phys.* **2000**, *112*, 6178–6189.

[van Mourik and Gdanitz(2002)] van Mourik, T.; Gdanitz, R. J. *J. Chem. Phys.* **2002**, *116*, 9620–9623.

[Williams(2001)] Williams, D. E. *J. Comput. Chem.* **2001**, *22*, 1154–1166.

[Stone(1985)] Stone, A. J. *Molecular Physics* **1985**, *56*, 1047–1064.

[Buckingham(1967)] Buckingham, A. D. *Adv. Chem. Phys.* **1967**, *12*, 107–142.

[Jeziorski et al.(1994)Jeziorski, Moszynski, and Szalewicz] Jeziorski, B.; Moszynski, R.; Szalewicz, K. *Chem. Rev.* **1994**, *94*, 1887–1930.

[Stone(1996)] Stone, A. J. *The Theory of Intermolecular Forces*; Oxford University Press: Oxford, 1996.

[Beyer et al.(2001)Beyer, Lewis, and Price] Beyer, T.; Lewis, T.; Price, S. L. *Crystengcomm* **2001**, art. no.–44.

[Celebi et al.(2000)Celebi, Angyan, Dehez, Millot, and Chipot] Celebi, N.; Angyan, J. G.; Dehez, F.; Millot, C.; Chipot, C. *J. Chem. Phys.* **2000**, *112*, 2709–2717.

[Dick and Overhauser(1958)] Dick, B.; Overhauser, A. *Phys. Rev.* **1958**, *B112*, 90.

[Hermida-ramon et al.(1998)Hermida-ramon, Engkvist, and Karlstrom] Hermida-ramon, J. M.; Engkvist, O.; Karlstrom, G. *J. Comput. Chem.* **1998**, *19*, 1816–1825.

[Nobeli et al.(1998)Nobeli, Price, and Wheatley] Nobeli, I.; Price, S. L.; Wheatley, R. J. *Mol. Phys.* **1998**, *95*, 525–537.

[Hayes and Stone(1984)] Hayes, I. C.; Stone, A. J. *Mol. Phys.* **1984**, *53*, 83–105.

[Stone(1993)] Stone, A. J. *Chem. Phys. Lett.* **1993**, *211*, 101–109.

[Axilrod and Teller(1943)] Axilrod, M.; Teller, E. *J. Chem. Phys.* **1943**, *11*, 299.

[Groenenboom et al.(2000)Groenenboom, Mas, Bukowski, Szalewicz, Wormer, and Van der avoird] Groenenboom, G. C.; Mas, E. M.; Bukowski, R.; Szalewicz, K.; Wormer, P. E. S.; Van der avoird, A. *Phys. Rev. Lett.* **2000**, *84*, 4072–4075.

[Atkins(1988)] Atkins, P. W. *Physical chemistry*; Oxford University Press: Oxford, 1988.

[Gay and Berne(1981)] Gay, J. G.; Berne, B. J. *J. Chem. Phys.* **1981**, *74*, 3316–3319.

[Williams(1966)] Williams, D. E. *J. Phys. Chem.* **1966**, *45*, 3370.

[Verlet(1967)] Verlet, L. *Physical Review* **1967**, *159*, 98–103.

[Brooks et al.(1983)Brooks, Bruccoleri, Olafson, States, Swaminathan, and Karplus] Brooks, B. R.; Bruccoleri, R. E.; Olafson, B. D.; States, D. J.; Swaminathan, S.; Karplus, M. *J. Comput. Chem.* **1983**, *4*, 187–217, The respective latest version of the all-atom force-field by Alex D. MacKerell Jr. *et al.* is included with the current version of the program.

[Scott et al.(1999)Scott, Hunenberger, Tironi, Mark, Billeter, Fennen, Torda, Huber, Kruger, and Van gu Scott, W. R. P.; Hunenberger, P. H.; Tironi, I. G.; Mark, A. E.; Billeter, S. R.; Fennen, J.; Torda, A. E.; Huber, T.; Kruger, P.; Van gunsteren, W. F. *J. Phys. Chem. A* **1999**, *103*, 3596–3607.

[Halgren(1999)] Halgren, T. A. *J. Comput. Chem.* **1999**, *20*, 730–748.

[Price(2000)] Price, S. L. In *Reviews in Computational Chemistry*; Wiley-VCH, Inc: New York, 2000; Vol. 14, Chapter Toward more Accurate Model Intermolecular Potentials for Organic Molecules.

[Gasteiger and Marsili(1980)] Gasteiger, J.; Marsili, M. *Tetrahedron* **1980**, *36*, 3219–3228.

[No et al.(1990)No, Grant, and Scheraga] No, K. T.; Grant, J. A.; Scheraga, H. A. *J. Phys. Chem.* **1990**, *94*, 4732–4739, habet.

[Maple et al.(1994)Maple, Hwang, Stockfisch, Dinur, Waldman, Ewig, and Hagler] Maple, J. R.; Hwang, M. J.; Stockfisch, T. P.; Dinur, U.; Waldman, M.; Ewig, C. S.; Hagler, A. T. *J. Comput. Chem.* **1994**, *15*, 162–182.

[Mulliken(1955)] Mulliken, R. S. *J. Chem. Phys.* **1955**, *23*, 1833–1846.

[owdin(1970)] owdin, P.-O. L. *Adv. Quantum. Chem.* **1970**, *5*, 185.

[Bader(1990)] Bader, R. *Atoms in Molecules: A Quantum Theory*; Oxford University Press: Oxford, 1990.

[Stone and Alderton(1985)] Stone, A. J.; Alderton, M. *Mol. Phys.* **1985**, *56*, 1047–1064.

[Bayly et al.(1993)Bayly, Cieplak, Cornell, and Kollman] Bayly, C. I.; Cieplak, P.; Cornell, W. D.; Kollman, P. A. *J. Phys. Chem.* **1993**, *97*, 10269–10280.

[Cornell et al.(1993)Cornell, Cieplak, Bayly, and Kollman] Cornell, W. D.; Cieplak, P.; Bayly, C. I.; Kollman, P. A. *J. Am. Chem. Soc.* **1993**, *115*, 9620–9631.

[Allinger et al.(1989)Allinger, Yuh, and Lii] Allinger, N. L.; Yuh, Y. H.; Lii, J.-H. *J. Am. Chem. Soc* **1989**, *111*, 8551.

[Berendsen et al.(1987)Berendsen, Grigera, and Straatsma] Berendsen, H. J. C.; Grigera, J. R.; Straatsma, T. P. *J. Phys. Chem.* **1987**, *91*, 6269–6271.

[Kaminski et al.(2002)Kaminski, Stern, Berne, Friesner, Cao, Murphy, Zhou, and Halgren] Kaminski, G. A.; Stern, H. A.; Berne, B. J.; Friesner, R. A.; Cao, Y. X. X.; Murphy, R. B.; Zhou, R. H.; Halgren, T. A. *J. Comput. Chem.* **2002**, *23*, 1515–1531.

[Halgren and Damm(2001)] Halgren, T. A.; Damm, W. *Curr. Opin. Struct. Biol.* **2001**, *11*, 236–242.

[Catlow and Cormack(1987)] Catlow, C. R. A.; Cormack, A. N. *Int. Rev. Phys. Chem.* **1987**, *6*, 227–250.

[Kim et al.(1994)Kim, Moller, Tildesley, and Quirke] Kim, K. S.; Moller, M. A.; Tildesley, D. J.; Quirke, N. *Mol. Simul.* **1994**, *13*, 77–99.

[Catlow and Thomas(1992)] Catlow, C. R. A.; Thomas, J. M. *Philos. Trans. R. Soc. Lond. Ser. A-Math. Phys. Eng. Sci.* **1992**, *341*, 255–268.

[Catlow et al.(1993)Catlow, Thomas, Freeman, Wright, and Bell] Catlow, C. R. A.; Thomas, J. M.; Freeman, C. M.; Wright, P. A.; Bell, R. G. *Proc. R. Soc. London Ser. A-Math. Phys. Eng. Sci.* **1993**, *442*, 85.

[Bingham et al.(1989)Bingham, Cormack, and Catlow] Bingham, D.; Cormack, A. N.; Catlow, C. R. A. *J. Phys.-Condes. Matter* **1989**, *1*, 1205–1212.

[Hartzell et al.(1998)Hartzell, Cygan, and Nagy] Hartzell, C. J.; Cygan, R. T.; Nagy, K. L. *J. Phys. Chem. A* **1998**, *102*, 6722–6729.

[Wawak et al.(1998)Wawak, Pillardy, Liwo, Gibson, and Scheraga] Wawak, R. J.; Pillardy, J.; Liwo, A.; Gibson, K. D.; Scheraga, H. A. *J. Phys. Chem. A* **1998**, *102*, 2904–2918.

[Motherwell et al.(2002)Motherwell, Ammon, Dunitz, Dzyabchenko, Erk, Gavezzotti, Hofmann, Leusen, L Motherwell, W. D. S. et al. *Acta Crystallogr. Sect. B-Struct. Sci.* **2002**, *58*, 647–661.

[Klepeis et al.(2003)Klepeis, Pieja, and Floudas] Klepeis, J. L.; Pieja, M.; Floudas, C. A. *Comput. Phys. Commun.* **2003**, *151*, 121–140.

[Press et al.(1994)Press, Teukolsky, Vetterling, and Flannery] Press, W. H.; Teukolsky, S. A.; Vetterling, W. T.; Flannery, B. P. *Numerical Recipies in C*, 2nd ed.; Cambridge University Press: Cambridge, UK, 1994.

[Kirkpatrick et al.(1983)Kirkpatrick, Gelatt, and Vecchi] Kirkpatrick, S.; Gelatt, C. D.; Vecchi, M. P. *Science* **1983**, *220*, 671–680.

[Wales and Scheraga(1999)] Wales, D. J.; Scheraga, H. A. *Science* **1999**, *285*, 1368–1372.

[Taylor et al.(1997)Taylor, Barrera, Allan, and Barron] Taylor, M. B.; Barrera, G. D.; Allan, N. L.; Barron, T. H. K. *Phys. Rev. B* **1997**, *56*, 14380–14390.

[Allan et al.(2001)Allan, Barrera, Barron, and Taylor] Allan, N. L.; Barrera, G. D.; Barron, T. H. K.; Taylor, M. B. *Int. J. Thermophys.* **2001**, *22*, 535–546.

[Miller and Wales(1999)] Miller, M. A.; Wales, D. J. *J. Chem. Phys.* **1999**, *111*, 6610–6616.

[Dinner and Karplus(1998)] Dinner, A. R.; Karplus, M. *Nat. Struct. Biol.* **1998**, *5*, 236–241.

[Doye and Wales(1996)] Doye, J. P. K.; Wales, D. J. *J. Chem. Phys.* **1996**, *105*, 8428–8445.

[Dill(1993)] Dill, K. A. *Curr. Opin. Struct. Biol.* **1993**, *3*, 99–103.

[Dill et al.(1993)Dill, Fiebig, and Chan] Dill, K. A.; Fiebig, K. M.; Chan, H. S. *Proc. Natl. Acad. Sci. U. S. A.* **1993**, *90*, 1942–1946.

[Beyer and Price(2000)] Beyer, T.; Price, S. L. *J. Phys. Chem. B* **2000**, *104*, 2647–2655.

[Vesely(2001)] Vesely, F. J. *Computational Physics - An Introduction*; Kluwer Academic: New York-London, 2001.

[Posch et al.(1990)Posch, Hoover, and Holian] Posch, H. A.; Hoover, W. G.; Holian, B. L. *Ber. Bunsen-Ges. Phys. Chem. Chem. Phys.* **1990**, *94*, 250–256.

[Holian et al.(1990)Holian, Degroot, Hoover, and Hoover] Holian, B. L.; Degroot, A. J.; Hoover, W. G.; Hoover, C. G. *Phys. Rev. A* **1990**, *41*, 4552–4553.

[R. P. Feynman and Sands(1963)] R. P. Feynman, R. B. L.; Sands, M. *The Feynman Lectures on Physics, Vol 1, Chapter 9 ("Newton's Laws of Dynamics")*; Addison-Wesley: ?, 1963.

[Smith and T.R. Forester(2001)] Smith, W.; T.R. Forester, T. R. *THE DL_POLY_2 USER MANUAL*, http://www.dl.ac.uk/TCS/Software/DL_POLY/USRMAN/USRMAN.html, 2001.

[McQuarrie(2000)] McQuarrie, D. A. *Statistical Mechanics*, 2nd ed.; University Science Books: Sausalito, Calif., 2000.

[Hoover(1985)] Hoover, W. G. *Phys. Rev. A* **1985**, *31*, 1695–1697.

[Ewald(1921)] Ewald, P. *Ann. Phys.* **1921**, *64*, 253–287.

[Schreiber and Steinhauser(1992)] Schreiber, H.; Steinhauser, O. *Chem. Phys.* **1992**, *168*, 75–89.

[Boresch and Steinhauser(1997)] Boresch, S.; Steinhauser, O. *Ber. Bunsen-Ges. Phys. Chem. Chem. Phys.* **1997**, *101*, 1019–1029.

[Toukmaji and Board Jr.(1996)] Toukmaji, A. Y.; Board Jr., J. A. *Comp. Phys. Comm.* **1996**, *95*, 73–92.

[Sagui and Darden(1999)] Sagui, C.; Darden, T. A. *Annu. Rev. Biophys. Biomolec. Struct.* **1999**, *28*, 155–179.

[Fincham(1994)] Fincham, D. *Molec. Sim.* **1994**, *13*, 1–9.

[Adams and Durey(1986)] Adams, D. J.; Durey, G. S. *J. Comp. Phys.* **1986**, *72*, 156–176.

[Barker and Watts(1973)] Barker, J. A.; Watts, R. O. *Mol. Phys.* **1973**, *26*, 789–792.

[Neumann(1985)] Neumann, M. *J. Chem. Phys.* **1985**, *82*, 5663.

[Hummer et al.(1994)Hummer, Soumpasis, and Neumann] Hummer, G.; Soumpasis, D. M.; Neumann, M. *J. Phys.-Condes. Matter* **1994**, *6*, A141–A144.

[Perera and Berkowitz(1993)] Perera, L.; Berkowitz, M. L. *J. Phys. Chem.* **1993**, *97*, 13803–13806.

[Bocker et al.(1995)Bocker, Nazmutdinov, Spohr, and Heinzinger] Bocker, J.; Nazmutdinov, R. R.; Spohr, E.; Heinzinger, K. *Surf. Sci.* **1995**, *335*, 372–377.

[Marmier et al.(1999)Marmier, Hoang, Girardet, and Lynden-bell] Marmier, A.; Hoang, P. N. M.; Girardet, C.; Lynden-bell, R. M. *J. Chem. Phys.* **1999**, *111*, 4862–4864.

[Wensink et al.(2000)Wensink, Hoffmann, Apol, and Berendsen] Wensink, E. J. W.; Hoffmann, A. C.; Apol, M. E. F.; Berendsen, H. J. C. *Langmuir* **2000**, *16*, 7392–7400.

[Shelley and Patey(1996)] Shelley, J. C.; Patey, G. N. *Mol. Phys.* **1996**, *88*, 385–398.

[Feller et al.(1996)Feller, Pastor, Rojnuckarin, Bogusz, and Brooks] Feller, S. E.; Pastor, R. W.; Rojnuckarin, A.; Bogusz, S.; Brooks, B. R. *J. Phys. Chem.* **1996**, *100*, 17011–17020.

[Spohr(1997)] Spohr, E. *J. Chem. Phys.* **1997**, *107*, 6342–6348.

[Hummer and Soumpasis(1994)] Hummer, G.; Soumpasis, D. M. *Phys. Rev. E* **1994**, *49*, 591–596.

[Heyes et al.(1977)Heyes, Barber, and Clarke] Heyes, D. M.; Barber, M.; Clarke, J. H. R. *Faraday Transactions* **1977**, *73*, 1485.

[Yeh and Berkowitz(1999)] Yeh, I. C.; Berkowitz, M. L. *J. Chem. Phys.* **1999**, *111*, 3155–3162.

[Leeuw et al.(1980)Leeuw, Perram, and Smith] Leeuw, S. W. D.; Perram, J. W.; Smith, E. *Proceedings of the Royal Society of London Series A* **1980**, *373*, 27–56.

[Hummer(2002)] Hummer, G. Personal Communication, 2002.

[Van eijck and Kroon(2000)] Van eijck, B. P.; Kroon, J. *J. Phys. Chem. B* **2000**, *104*, 8089–8089.

[Wedemeyer et al.(2000)Wedemeyer, Arnautova, Pillardy, Wawak, Czaplewski, and Scheraga] Wedemeyer, W. J.; Arnautova, Y. A.; Pillardy, J.; Wawak, R. J.; Czaplewski, C.; Scheraga, H. A. *J. Phys. Chem. B* **2000**, *104*, 8090–8092.

[Pillardy et al.(2000)Pillardy, Wawak, Arnautova, Czaplewski, and Scheraga] Pillardy, J.; Wawak, R. J.; Arnautova, Y. A.; Czaplewski, C.; Scheraga, H. A. *J. Am. Chem. Soc.* **2000**, *122*, 907–921.

[Kantorovich(1999)] Kantorovich, L. N. *Phys. Rev. B* **1999**, *60*, 15476–15479.

[Kantorovich and Tupitsyn(1999)] Kantorovich, L. N.; Tupitsyn, I. I. *J. Phys.-Condes. Matter* **1999**, *11*, 6159–6168.

[Widmann and Adolf(1997)] Widmann, A. H.; Adolf, D. B. *Comput. Phys. Commun.* **1997**, *107*, 167–186.

[Jorge and Seaton(2002)] Jorge, M.; Seaton, N. A. *Mol. Phys.* **2002**, *100*, 2017–2023.

[Kuhn and Rehage(1997)] Kuhn, H.; Rehage, H. *Ber. Bunsen-Ges. Phys. Chem. Chem. Phys.* **1997**, *101*, 1493–1500.

[De souza and Maier(2003)] De souza, R. A.; Maier, J. *Phys. Chem. Chem. Phys.* **2003**, *5*, 740–748.

[Miteva et al.(1997)Miteva, Demirev, and Karshikoff] Miteva, M.; Demirev, P. A.; Karshikoff, A. D. *J. Phys. Chem. B* **1997**, *101*, 9645–9650.

[Vila et al.(1998)Vila, Ripoll, Vorobjev, and Scheraga] Vila, J. A.; Ripoll, D. R.; Vorobjev, Y. N.; Scheraga, H. A. *J. Phys. Chem. B* **1998**, *102*, 3065–3067.

[Wagner and Simonson(1999)] Wagner, F.; Simonson, T. *J. Comput. Chem.* **1999**, *20*, 322–335.

[Lyubartsev and Laaksonen(1998)] Lyubartsev, A. P.; Laaksonen, A. *J. Biomol. Struct. Dyn.* **1998**, *16*, 579–+.

[Refson()] Refson, K. *Moldy-Manual*; Rutherford Appleton Laboratory, Chilton, UK, http://server.ccl.net/cca/software/SOURCES/C/moldy/moldy-manual.pdf.

[Hummer et al.(1996)Hummer, Pratt, and Garcia] Hummer, G.; Pratt, L. R.; Garcia, A. E. *J. Phys. Chem.* **1996**, *100*, 1206–1215.

[Bogusz et al.(1998)Bogusz, Cheatham, and Brooks] Bogusz, S.; Cheatham, T. E.; Brooks, B. R. *J. Chem. Phys.* **1998**, *108*, 7070–7084.

[Channon et al.(1998)Channon, Catlow, Gorman, and Jackson] Channon, Y. M.; Catlow, C. R. A.; Gorman, A. M.; Jackson, R. A. *J. Phys. Chem. B* **1998**, *102*, 4045–4048.

[Grey et al.(2002)Grey, Nicholson, Gale, and Peterson] Grey, T. J.; Nicholson, D.; Gale, J. D.; Peterson, B. K. *Appl. Surf. Sci.* **2002**, *196*, 105–114.

[Kamberaj and Helms(2001)] Kamberaj, H.; Helms, V. *Comput. Phys. Commun.* **2001**, *141*, 375–402.

[and Nicholson and Parsonage(1982)] and Nicholson, D.; Parsonage, N. G. *Computer Simulation and the Statistical Mechanics of Adsorption*; Academic Press: London , New York, 1982.

[Adams(1975)] Adams, D. J. *Molecular Physics* **1975**, *29*, 307–311.

[Lupkowski and Vanswol(1991)] Lupkowski, M.; Vanswol, F. *J. Chem. Phys.* **1991**, *95*, 1995–1998.

[Mezei(1987)] Mezei, M. *Mol. Phys.* **1987**, *61*, 565–582.

[Shing and Azadipour(1992)] Shing, K. S.; Azadipour, S. R. *Chem. Phys. Lett.* **1992**, *190*, 386–390.

[Vega et al.(1994)Vega, Shing, and Rull] Vega, L. F.; Shing, K. S.; Rull, L. F. *Mol. Phys.* **1994**, *82*, 439–453.

[Shelley and Patey(1994)] Shelley, J. C.; Patey, G. N. *J. Chem. Phys.* **1994**, *100*, 8265–8270.

[Yau et al.(1994)Yau, Liem, and Chan] Yau, D. H. L.; Liem, S. Y.; Chan, K. Y. *J. Chem. Phys.* **1994**, *101*, 7918–7924.

[Macedonia and Maginn(1999)] Macedonia, M. D.; Maginn, E. J. *Mol. Phys.* **1999**, *96*, 1375–1390.

[Grimbergen et al.(1998)Grimbergen, Reedijk, Meekes, and Bennema] Grimbergen, R. F. P.; Reedijk, M. F.; Meekes, H.; Bennema, P. *J. Phys. Chem. B* **1998**, *102*, 2646–2653.

[Liu et al.(1995)Liu, Boek, Briels, and Bennema] Liu, X.-Y.; Boek, E. S.; Briels, W. J.; Bennema, P. *J. Chem. Phys.* **1995**, *103*, 3747–3754.

[Boek et al.(1994)Boek, Briels, and Feil] Boek, E. S.; Briels, W. J.; Feil, D. *J. Phys. Chem.* **1994**, *98*, 1674–1681.

[Bravais(1886)] Bravais, A. *Etudes Crystallographiques*; Gauthiers-Villars: Paris, 1886.

[Friedel(1907)] Friedel, M. G. *Bull. Soc. Fr. Mineral.* **1907**, *30*, 326–455.

[Donnay and Harker(1937)] Donnay, J. D. H.; Harker, D. *Am Mineral* **1937**, *22*, 446.

[Hartman and Perdok(1954)] Hartman, P.; Perdok, W. G. *Acta Crystallogr.* **1954**, *8*, 49–52.

[Hartman and Bennema(1980)] Hartman, P.; Bennema, P. *J. Crystal Growth* **1980**, *49*, 145–156.

[Vandervoort(1991)] Vandervoort, E. *J. Cryst. Growth* **1991**, *110*, 662–668.

[Winn and Doherty(1998)] Winn, D.; Doherty, M. F. *AIChE J* **1998**, *44*, 2501–2514.

[Meenan(1997)] Meenan, P. Crystal Morphology Predictive Techniques To Characterize Crystal Habit: Application to Aspirin. *Separation and purification by crystallization*, Washington, DC, 1997.

[Qingwu et al.(1997)Qingwu, Sheen, Shepherd, Sherwood, Simpson, and Hammond] Qingwu, W.; Sheen, D. B.; Shepherd, E. E.; Sherwood, J. N.; Simpson, G. S.; Hammond, R. B. *J. Crystal Growth* **1997**, *181*, 418–426.

[Clydesdale et al.(1998)Clydesdale, Roberts, Telfer, Saunders, Pugh, Jackson, and Meenan] Clydesdale, G.; Roberts, K. J.; Telfer, G. B.; Saunders, V. R.; Pugh, D.; Jackson, R. A.; Meenan, P. *J. Phys. Chem. B* **1998**, *102*, 7044–7049.

[Clydesdale et al.(1991)Clydesdale, Docherty, and Roberts] Clydesdale, G.; Docherty, R.; Roberts, K. J. *Comput. Phys. Commun.* **1991**, *64*, 311–328.

[Clydesdale et al.(1997)Clydesdale, Roberts, Telfer, and Grant] Clydesdale, G.; Roberts, K. J.; Telfer, G. B.; Grant, D. J.-W. *J. Pharm. Sci.* **1997**, *86*, 135–140.

[Berkovitch-Yellin(1985)] Berkovitch-Yellin, Z. *J. Am. Chem. Soc.* **1985**, *107*, 8239–8253.

[Hobza et al.(1997)Hobza, Kabelac, Sponer, Mejzlik, and Vondrasek] Hobza, P.; Kabelac, M.; Sponer, J.; Mejzlik, P.; Vondrasek, J. *J. Comput. Chem.* **1997**, *18*, 1136–1150.

[Gundertofte et al.(1996)Gundertofte, Liljefors, and Norrby] Gundertofte, K.; Liljefors, T.; Norrby, P. O. *J. Comput. Chem.* **1996**, *17*, 429–449.

[Halgren(1999)] Halgren, T. A. *J. Comput. Chem.* **1999**, *20*, 730–748.

[Docherty and Roberts(1988)] Docherty, R.; Roberts, K. J. *J. Cryst. Growth* **1988**, *88*, 159–168.

[Allen et al.(1987)Allen, Kennard, Watson, Brammer, Orpen, and Taylor] Allen, F. H.; Kennard, O.; Watson, D. G.; Brammer, L.; Orpen, A. G.; Taylor, R. *J. Chem. Soc.-Perkin Trans.* **1987**, *12*, S1–S19.

[Winkler and Dunitz(1975)] Winkler, F.; Dunitz, J. *Acta Crystallogr.* **1975**, *B31*, 286–292.

[Kabo et al.(1992)Kabo, Kozyro, Krouk, Sevruk, Yursha, Simirsky, and Gogolinsky] Kabo, G. J.; Kozyro, A. A.; Krouk, V. S.; Sevruk, V. M.; Yursha, I. A.; Simirsky, V. V.; Gogolinsky, V. I. *J. Chem. Thermodyn.* **1992**, *24*, 1–13.

[Kampermann et al.(1995)Kampermann, Sabine, Craven, and Mcmullan] Kampermann, S. P.; Sabine, T. M.; Craven, B. M.; Mcmullan, R. K. *Acta Crystallogr.* **1995**, *A51*, 489–497.

[Mansson et al.(1970)Mansson, Rapport, and Westrum] Mansson, M.; Rapport, N.; Westrum, J., E.F. *J. Am. Chem. Soc.* **1970**, *92*, 7296–7299.

[Semmingsen(1988)] Semmingsen, D. *Acta. Chim. Scan. Ser. A* **1988**, *42*, 279–283.

[Barone et al.(1990)Barone, Dellagatta, Ferro, and Piacente] Barone, G.; Dellagatta, G.; Ferro, D.; Piacente, V. *J. Chem. Soc.-Faraday Trans.* **1990**, *86*, 75–79.

[Leviel et al.(1981)Leviel, Auvert, and Savariault] Leviel, J. L.; Auvert, G.; Savariault, J. M. *Acta Crystallogr.* **1981**, *B37*, 2185–2189.

[Dewit et al.(1983)Dewit, Vanmiltenburg, and Dekruif] Dewit, H. G. M.; Vanmiltenburg, J. C.; Dekruif, C. G. *J. Chem. Thermodyn.* **1983**, *15*, 651–663.

[Swaminathan et al.(1984)Swaminathan, Craven, Spackman, and Stewart] Swaminathan, S.; Craven, B. M.; Spackman, M. A.; Stewart, R. F. *Acta Crystallogr.* **1984**, *B40*, 398–404.

[Filippini and Gavezzotti(1993)] Filippini, G.; Gavezzotti, A. *Acta Crystallogr.* **1993**, *B49*, 868–880.

[Gavezzotti and Filippini(1994)] Gavezzotti, A.; Filippini, G. *J. Phys. Chem.* **1994**, *98*, 4831–4837.

[Hagler et al.(1979)Hagler, Dauber, and Lifson] Hagler, A. T.; Dauber, P.; Lifson, S. *J. Am. Chem. Soc.* **1979**, *101*, 5111–5121.

[Williams and Cox(1984)] Williams, D. E.; Cox, S. R. *Acta Ctrystallogr.* **1984**, *B40*, 404–417.

[Coombes et al.(1996)Coombes, Price, Willock, and Leslie] Coombes, D. S.; Price, S. L.; Willock, D. J.; Leslie, M. *J. Phys. Chem.* **1996**, *100*, 7352–7360.

[Mol(1999)] *Cerius*^{2} *Modelling Environment*; Molecular Simulations Inc: San Diego, CA, 1999.

[Hagler et al.(1974)Hagler, Euler, and Lifson] Hagler, A. T.; Euler, E.; Lifson, S. *J. Am. Chem. Soc.* **1974**, *96*, 5319–5327.

[Chirlian and Francl(1987)] Chirlian, L. E.; Francl, M. M. *J. Comput. Chem.* **1987**, *8*, 894–905.

[Breneman and Wiberg(1990)] Breneman, C. M.; Wiberg, K. B. *J. Comput. Chem.* **1990**, *11*, 361–373.

[M. J. Frisch et al.(1998)] M. J. Frisch et al., *Gaussian 98 (Revision A.6)*; Gaussian, Inc.: Pittsburgh PA, 1998.

[Stone(1998)] Stone, A. J. *GDMA: distributed multipoles from Gaussian98 wavefunctions*; University of Cambridge, 1998, http://fandango.ch.cam.ac.uk.

[Stone et al.(2000)Stone, Dullweber, Engkvist, Fraschini, Hodges, Meredith, Popelier, and Wales] Stone, A. J.; Dullweber, A.; Engkvist, O.; Fraschini, E.; Hodges, M. P.; Meredith, A. W.; Popelier, P. L. A.; Wales, D. J. *Orient: a program for studying interactions between molecules, version 4.2*; University of Cambridge, 2000, http://fandango.ch.cam.ac.uk.

[Engkvist et al.(2000)Engkvist, Price, and Stone] Engkvist, O.; Price, S. L.; Stone, A. J. *PCCP Phys. Chem. Chem. Phys.* **2000**, *2*, 3017–3027.

[Rohl and Gay(1996)] Rohl, A. L.; Gay, D. H. *J. Cryst. Growth* **1996**, *166*, 84–90.

[Willock et al.(1995)Willock, Price, Leslie, and Catlow] Willock, D. J.; Price, S. L.; Leslie, M.; Catlow, C. R. A. *J. Comput. Chem.* **1995**, *16*, 628–647.

[Beyer and Price(2000)] Beyer, T.; Price, S. L. *Cryst. Eng. Comm.* **2000**, *34*, year.

[Gavezzotti and Filippini(1997)] Gavezzotti, A.; Filippini, G. Energetic Aspects of Crystal Packing: Experiment and Computer Simulations. In *Theoretical Aspects and computer Modeling of the Molecular Solid State*; Gavezzotti, A., Ed.; John Wiley and sons: Chichester, 1997; Chapter 3, p 97.

[Day et al.(2001)Day, Price, and Leslie] Day, G. M.; Price, S. L.; Leslie, M. *Crystal Growth & Design* **2001**, *1*, 13–27.

[Davey and Rütti(1976)] Davey, R. J.; Rütti, A. *J. Crystal Growth* **1976**, *32*, 221–226.

[Walker et al.(1998)Walker, Roberts, and Maginn] Walker, E. M.; Roberts, K. J.; Maginn, S. J. *Langmuir* **1998**, *14*, 5620–5630.

[Mayo et al.(1990)Mayo, Olafson, and Goddard] Mayo, S. L.; Olafson, B. D.; Goddard, W. A. *J. Phys. Chem.* **1990**, *94*, 8897–8909.

[Rappe and Goddard(1991)] Rappe, A. K.; Goddard, W. A. *J. Phys. Chem.* **1991**, *95*, 3358–3363.

[Geertman and Vanderheijden(1992)] Geertman, R. M.; Vanderheijden, A. E. D. M. *J. Cryst. Growth* **1992**, *125*, 363–372.

[Docherty et al.(1993)Docherty, Roberts, Saunders, Black, and Davey] Docherty, R.; Roberts, K. J.; Saunders, V.; Black, S.; Davey, R. J. *Faraday Disc.* **1993**, *95*, 11–25.

[Feigelson et al.(1985)Feigelson, Route, and Kao] Feigelson, R. S.; Route, R. K.; Kao, T. M. *J. Cryst. Growth* **1985**, *72*, 585–594.

[Davey et al.(1986)Davey, Fila, and J.] Davey, R.; Fila, W.; J., G. *J. Cryst. Growth* **1986**, *79*, 607–613.

[George et al.(1995)George, Harris, Rohl, and Gay] George, A. R.; Harris, K. D. M.; Rohl, A. L.; Gay, D. H. *J. Mater. Chem.* **1995**, *5*, 133–139.

[Su et al.(1992)Su, Li, Pan, Wu, and Yang] Su, G. B.; Li, Z. D.; Pan, R. F.; Wu, D. X.; Yang, T. Q. *J. Cryst. Growth* **1992**, *119*, 368–370.

[Beyer et al.(2001)Beyer, Day, and Price] Beyer, T.; Day, G. M.; Price, S. L. *J. Am. Chem. Soc.* **2001**, *123*, 5086–5094.

[Gonze et al.(2002)Gonze, Beuken, Caracas, Detraux, Fuchs, Rignanese, Sindic, Verstraete, Zerah, Jollet, Gonze, X. et al. *Comput. Mater. Sci.* **2002**, *25*, 478–492.

[Dovesi et al.(2000)Dovesi, Orlando, Roetti, Pisani, and Saunders] Dovesi, R.; Orlando, R.; Roetti, C.; Pisani, C.; Saunders, V. R. *Phys. Status Solidi B-Basic Res.* **2000**, *217*, 63–88.

[Yeh and Berkowitz(2000)] Yeh, I. C.; Berkowitz, M. L. *J. Chem. Phys.* **2000**, *112*, 10491–10495.

[Larson and Cromer(1967)] Larson, A. C.; Cromer, D. T. *Acta Crystallographica* **1967**, *A22*, 793–800.

[Sakuntala et al.(2000)Sakuntala, Akhilesh, Chandra Shekar, and Sahu] Sakuntala, T.; Akhilesh, K. A.; Chandra Shekar, N. V.; Sahu, P. C. *J. Phys.: Condens. Matter* **2000**, *12*, 4417–4432.

[Allan et al.(1993)Allan, Rohl, Gay, Catlow, Davey, and Mackrodt] Allan, N. L.; Rohl, A. L.; Gay, D. H.; Catlow, C. R. A.; Davey, R. J.; Mackrodt, W. C. *Faraday Discuss.* **1993**, *95*, 273–280.

[Borodin et al.(2001)Borodin, Bell, Li, Bedrov, and Smith] Borodin, O.; Bell, R. L.; Li, Y.; Bedrov, D.; Smith, G. D. *Chem. Phys. Lett.* **2001**, *336*, 292–302.

[Martin and K.(1981)] Martin, R. M.; K., K. *Phys. Rev.* **1981**, *B24*, 2081–2088.

[Ghosez et al.(1998)Ghosez, Michenaud, and Gonze] Ghosez, P.; Michenaud, J. P.; Gonze, X. *Phys. Rev. B* **1998**, *58*, 6224–6240.

[Gale(2000)] Gale, G. D. *Phys. Rev.* **2000**, *B62*, 6224–6240.

[Cannon et al.(1994)Cannon, Pettitt, and Mccammon] Cannon, W. R.; Pettitt, B. M.; Mccammon, J. A. *J. Phys. Chem.* **1994**, *98*, 6225–6230.

[Gale(1997)] Gale, J. D. *J. Chem. Soc.-Faraday Trans.* **1997**, *93*, 629–637.

[Rudolph et al.(2000)Rudolph, Mason, and Pye] Rudolph, W. W.; Mason, R.; Pye, C. C. *Phys. Chem. Chem. Phys.* **2000**, *2*, 5030–5040.

[Pye and Rudolph(2001)] Pye, C. C.; Rudolph, W. W. *J. Phys. Chem. A* **2001**, *105*, 905–912.

[Caminiti et al.(1979)Caminiti, G., and G.] Caminiti, R.; G., P.; G., P. *Chemical Physics Letters* **1979**, *64*, 391–395.

[Smith and Forester(1996)] Smith, W.; Forester, T. R. *J. Mol. Graph.* **1996**, *14*, 136–141.

[Marcus(1988)] Marcus, Y. *Chem. Rev.* **1988**, *88*, 1475.

[Bol and Welzen(1977)] Bol, W.; Welzen, T. *Chem. Phys. Lett.* **1977**, *49*, 189.

[Ohtaki and Radnai(1993)] Ohtaki, H.; Radnai, T. *Chem. Rev.* **1993**, *93*, 1157.

[McCall and Douglas(1965)] McCall, D. W.; Douglas, D. C. *J. Phys. Chem.* **1965**, *69*, 2001.

[Rasaiah and Lynden-bell(2001)] Rasaiah, J. C.; Lynden-bell, R. M. *Philos. Trans. R. Soc. Lond. Ser. A-Math. Phys. Eng. Sci.* **2001**, *359*, 1545–1574.

[Crozier et al.(2000)Crozier, Rowley, Spohr, and Henderson] Crozier, P. S.; Rowley, R. L.; Spohr, E.; Henderson, D. *J. Chem. Phys.* **2000**, *112*, 9253–9257.

[Sinfelt(2002)] Sinfelt, J. H. *Surf. Sci.* **2002**, *500*, 923–946.

[Vlieg(2002)] Vlieg, E. *Surf. Sci.* **2002**, *500*, 458–474.

[Haberlein and Tschiersch(1994)] Haberlein, H.; Tschiersch, K. P. *Pharmazie* **1994**, *49*, 769–775.

[Talapin et al.(2002)Talapin, Poznyak, Gaponik, Rogach, and Eychmuller] Talapin, D. V.; Poznyak, S. K.; Gaponik, N. P.; Rogach, A. L.; Eychmuller, A. *Physica E* **2002**, *14*, 237–241.

[Vanenckevort et al.(1981)Vanenckevort, Bennema, and Vanderlinden] Vanenckevort, W. J. P.; Bennema, P.; Vanderlinden, W. H. **1981**, *124*, 171–191.

[Reyhani et al.(1999)Reyhani, Freij, and Parkinson] Reyhani, M. M.; Freij, S.; Parkinson, G. M. *J. Crystal Growth* **1999**, *198-199*, 258–263.

[Amara et al.(2001)Amara, Ratsimba, Wilhelm, and Delmas] Amara, N.; Ratsimba, B.; Wilhelm, A. M.; Delmas, H. *Ultrason. Sonochem.* **2001**, *8*, 265–270.

[Pratola et al.(2002)Pratola, Simons, and Jones] Pratola, F.; Simons, S. J. R.; Jones, A. G. *Chem. Eng. Res. Des.* **2002**, *80*, 441–448.

[Tasker(1979)] Tasker, P. W. *J. Phys. C: Solid State Phys.* **1979**, *12*, 4977–4984.

[Maki et al.(1999)Maki, Ichinose, Sekiguchi, Ohashi, Nishihara, Haneda, and Tanaka] Maki, H.; Ichinose, N.; Sekiguchi, S.; Ohashi, N.; Nishihara, T.; Haneda, H.; Tanaka, J. *Jpn. J. Appl. Phys. Part 1 - Regul. Pap. Short Notes Rev. Pap.* **1999**, *38*, 2741–2744.

[Harding(1999)] Harding, J. H. *Surf. Sci.* **1999**, *422*, 87–94.

[Mocuta et al.(2000)Mocuta, Barbier, and Renaud] Mocuta, C.; Barbier, A.; Renaud, G. *Appl. Surf. Sci.* **2000**, *162*, 56–61.

[Barbier et al.(1998)Barbier, Renaud, and Stierle] Barbier, A.; Renaud, G.; Stierle, A. *Surf. Sci.* **1998**, *404*, 757–760.

[Barbier et al.(2000)Barbier, Mocuta, Kuhlenbeck, Peters, Richter, and Renaud] Barbier, A.; Mocuta, C.; Kuhlenbeck, H.; Peters, K. F.; Richter, B.; Renaud, G. *Phys. Rev. Lett.* **2000**, *84*, 2897–2900.

[Jones et al.(1996)Jones, Rawlings, Foord, Egdell, Pethica, Wanklyn, Parker, and Oliver] Jones, F. H.; Rawlings, K.; Foord, J. S.; Egdell, R. G.; Pethica, J. B.; Wanklyn, B. M. R.; Parker, S. C.; Oliver, P. M. *Surf. Sci.* **1996**, *359*, 107–121.

[Becker and Gasharova(2001)] Becker, U.; Gasharova, B. *Phys. Chem. Miner.* **2001**, *28*, 545–556.

[Carlsson(2001)] Carlsson, J. M. *Comput. Mater. Sci.* **2001**, *22*, 24–31.

[Wander and Harrison(2001)] Wander, A.; Harrison, N. M. *J. Chem. Phys.* **2001**, *115*, 2312–2316.

[Norenberg and Harding(2001)] Norenberg, H.; Harding, J. H. *Surf. Sci.* **2001**, *477*, 17–24.

[Safran(1994)] Safran, S. A. *Statistical Thermodynamics of Surfaces, Interfaces, and Membranes*; Addison-Wesley Pub.: Reading, Mass., 1994.

[Hodel et al.(1993)Hodel, Simonson, Fox, and Brunger] Hodel, A.; Simonson, T.; Fox, R. O.; Brunger, A. T. *J. Phys. Chem.* **1993**, *97*, 3409–3417.

[Smith and Lynden-bell(1999)] Smith, P.; Lynden-bell, R. M. *Mol. Phys.* **1999**, *96*, 1027–1032.

[Grochola et al.(2002)Grochola, Russo, Snook, and Yarovsky] Grochola, G.; Russo, S. P.; Snook, I. K.; Yarovsky, I. *J. Chem. Phys.* **2002**, *116*, 8547–8555.

[Broughton and Gilmer(1986)] Broughton, J. Q.; Gilmer, G. H. *J. Chem. Phys.* **1986**, *84*, 5759–5768.

[Lill and Broughton(2000)] Lill, J. V.; Broughton, J. Q. *Model. Simul. Mater. Sci. Eng.* **2000**, *8*, 345–355.

[Heifets et al.(2000)Heifets, Kotomin, and Maier] Heifets, E.; Kotomin, E. A.; Maier, J. *Surf. Sci.* **2000**, *462*, 19–35.

[Watson et al.(1997)Watson, Oliver, and Parker] Watson, G. W.; Oliver, P. M.; Parker, S. C. *Phys. Chem. Miner.* **1997**, *25*, 70–78.

[Aquilano et al.(1997)Aquilano, Rubbo, Catti, and Pavese] Aquilano, D.; Rubbo, M.; Catti, M.; Pavese, A. *J. Cryst. Growth* **1997**, *182*, 168–184.

[Conesa(1995)] Conesa, J. C. *Surf. Sci.* **1995**, *339*, 337–352.

[Gillan et al.(1996)Gillan, Kantorovich, and Lindan] Gillan, M. J.; Kantorovich, L. N.; Lindan, P. J. D. *Curr. Opin. Solid State Mat. Sci.* **1996**, *1*, 820–826.

[Nygren et al.(1996)Nygren, Pettersson, Freitag, Staemmler, Gay, and Rohl] Nygren, M. A.; Pettersson, L. G. M.; Freitag, A.; Staemmler, V.; Gay, D. H.; Rohl, A. L. *J. Phys. Chem.* **1996**, *100*, 294–298.

[Fiorentini and Methfessel(1996)] Fiorentini, V.; Methfessel, M. *J. Phys.-Condes. Matter* **1996**, *8*, 6525–6529.

[Boettger et al.(1998)Boettger, Smith, Birkenheuer, Rosch, Trickey, Sabin, and Apell] Boettger, J. C.; Smith, J. R.; Birkenheuer, U.; Rosch, N.; Trickey, S. B.; Sabin, J. R.; Apell, S. P. *J. Phys.-Condes. Matter* **1998**, *10*, 893–894.

[Wright et al.(2001)Wright, Cygan, and Slater] Wright, K.; Cygan, R. T.; Slater, B. *Phys. Chem. Chem. Phys.* **2001**, *3*, 839–844.

[Baudin et al.(2000)Baudin, Wojcik, and Hermansson] Baudin, M.; Wojcik, M.; Hermansson, K. *Surf. Sci.* **2000**, *468*, 51–61.

[Pojani et al.(1997)Pojani, Finocchi, Goniakowski, and Noguera] Pojani, A.; Finocchi, F.; Goniakowski, J.; Noguera, C. *Surf. Sci.* **1997**, *387*, 354–370.

[Oviedo and Gillan(2000)] Oviedo, J.; Gillan, M. J. *Surf. Sci.* **2000**, *463*, 93–101.

[Swamy et al.(2002)Swamy, Muscat, Gale, and Harrison] Swamy, V.; Muscat, J.; Gale, J. D.; Harrison, N. M. *Surf. Sci.* **2002**, *504*, 115–124.

[Adamson and Gast(1997)] Adamson, A. W.; Gast, A. P. *Physical Chemistry of Surfaces*; John Wiley & Sons, Inc.: New York, 1997.

[Smith and Fincham(1993)] Smith, W.; Fincham, D. *Mol. Simul.* **1993**, *10*, 67–71.

[Dove(1993)] Dove, M. T. *Introduction to Lattice Dynamics*; Cambridge University Press: Cambridge, 1993.

[Beveridge and Dicapua(1989)] Beveridge, D. L.; Dicapua, F. M. **1989**, *18*, 431–492.

[Straatsma et al.(1992)Straatsma, Zacharias, and Mccammon] Straatsma, T. P.; Zacharias, M.; Mccammon, J. A. *Chem. Phys. Lett.* **1992**, *196*, 297–302.

[Kumar et al.(1992)Kumar, Bouzida, Swendsen, Kollman, and Rosenberg] Kumar, S.; Bouzida, D.; Swendsen, R. H.; Kollman, P. A.; Rosenberg, J. M. *J. Comput. Chem.* **1992**, *13*, 1011–1021.

[Roux(1995)] Roux, B. *Comput. Phys. Commun.* **1995**, *91*, 275–282.

[Sprik and Ciccotti(1998)] Sprik, M.; Ciccotti, G. *J. Chem. Phys.* **1998**, *109*, 7737–7744.

[Pearlman(1993)] Pearlman, D. A. *J. Chem. Phys.* **1993**, *98*, 8946–8957.

[Mulders et al.(1996)Mulders, Kruger, Swegat, and Schlitter] Mulders, T.; Kruger, P.; Swegat, W.; Schlitter, J. *J. Chem. Phys.* **1996**, *104*, 4869–4870.

[Den otter and Briels(1998)] Den otter, W. K.; Briels, W. J. *J. Chem. Phys.* **1998**, *109*, 4139–4146.

[Gullingsrud et al.(1999)Gullingsrud, Braun, and Schulten] Gullingsrud, J. R.; Braun, R.; Schulten, K. *J. Comput. Phys.* **1999**, *151*, 190–211.

[Darve and Pohorille(2001)] Darve, E.; Pohorille, A. *J. Chem. Phys.* **2001**, *115*, 9169–9183.

[Shinto et al.(1998)Shinto, Sakakibara, and Higashitani] Shinto, H.; Sakakibara, T.; Higashitani, K. *J. Chem. Eng. Jpn.* **1998**, *31*, 771–779.

[Straatsma et al.(1986)Straatsma, Berendsen, and Postma] Straatsma, T. P.; Berendsen, H. J. C.; Postma, J. P. M. *J. Chem. Phys.* **1986**, *85*, 6720–6727.

[Mitchell and Mccammon(1991)] Mitchell, M. J.; Mccammon, J. A. *J. Comput. Chem.* **1991**, *12*, 271–275.

[Straatsma and Mccammon(1991)] Straatsma, T. P.; Mccammon, J. A. *J. Chem. Phys.* **1991**, *95*, 1175–1188.

[Andersson et al.(1998)Andersson, Hult, Apell, Langreth, and Lundqvist] Andersson, Y.; Hult, E.; Apell, P.; Langreth, D. C.; Lundqvist, B. I. *Solid State Commun.* **1998**, *106*, 235–238.

[Marcelja(2000)] Marcelja, S. *Langmuir* **2000**, *16*, 6081–6083.

[Henderson et al.(2000)Henderson, Bryk, Sokolowski, and Wasan] Henderson, D.; Bryk, P.; Sokolowski, S.; Wasan, D. T. *Phys. Rev. E* **2000**, *61*, 3896–3903.

[Forsman et al.(1998)Forsman, Jonsson, and Akesson] Forsman, J.; Jonsson, B.; Akesson, T. *J. Phys. Chem. B* **1998**, *102*, 5082–5087.

[Rivera and Sorensen(1994)] Rivera, S. R.; Sorensen, T. S. *Mol. Simul.* **1994**, *13*, 115–160.

[Bratko and Henderson(1994)] Bratko, D.; Henderson, D. *Phys. Rev. E* **1994**, *49*, 4140–4144.

[Sorensen and Sloth(1992)] Sorensen, T. S.; Sloth, P. *J. Chem. Soc.-Faraday Trans.* **1992**, *88*, 571–589.

[Bratko et al.(1991)Bratko, Henderson, and Blum] Bratko, D.; Henderson, D. J.; Blum, L. *Phys. Rev. A* **1991**, *44*, 8235–8241.

[Feller and Mcquarrie(1993)] Feller, S. E.; Mcquarrie, D. A. *Mol. Phys.* **1993**, *80*, 721–728.

[Mansour et al.(2002)Mansour, Dimeo, and Peemoeller] Mansour, F.; Dimeo, R. M.; Peemoeller, H. *Phys. Rev. E* **2002**, *66*, art. no.–041307.

[Sansom et al.(1996)Sansom, Kerr, Breed, and Sankararamakrishnan] Sansom, M. S. P.; Kerr, I. D.; Breed, J.; Sankararamakrishnan, R. *Biophys. J.* **1996**, *70*, 693–702.

[Gallo et al.(1999)Gallo, Rovere, Ricci, Hartnig, and Spohr] Gallo, P.; Rovere, M.; Ricci, M. A.; Hartnig, C.; Spohr, E. *Philos. Mag. B-Phys. Condens. Matter Stat. Mech. Electron. Opt. Magn. Prop.* **1999**, *79*, 1923–1930.

[Han et al.(1993)Han, Cushman, and Diestler] Han, K. K.; Cushman, J. H.; Diestler, D. J. *Mol. Phys.* **1993**, *79*, 537–545.

[Yethiraj and Hall(1991)] Yethiraj, A.; Hall, C. K. *Mol. Phys.* **1991**, *73*, 503–515.

[Brovchenko and Geiger(2002)] Brovchenko, I.; Geiger, A. *J. Mol. Liq.* **2002**, *96-7*, 195–206.

[Brovchenko et al.(2001)Brovchenko, Geiger, and Paschek] Brovchenko, I. V.; Geiger, A.; Paschek, D. *Fluid Phase Equilib.* **2001**, *183*, 331–339.

[Schoen et al.(1998)Schoen, Gruhn, and Diestler] Schoen, M.; Gruhn, T.; Diestler, D. J. *J. Chem. Phys.* **1998**, *109*, 301–311.

[Schoen and Diestler(1997)] Schoen, M.; Diestler, D. J. *Phys. Rev. E* **1997**, *56*, 4427–4440.

[Cracknell et al.(1995)Cracknell, Nicholson, and Quirke] Cracknell, R. F.; Nicholson, D.; Quirke, N. *Phys. Rev. Lett.* **1995**, *74*, 2463–2466.

[Somers and Davis(1992)] Somers, S. A.; Davis, H. T. *J. Chem. Phys.* **1992**, *96*, 5389–5407.

[Schoen et al.(1989)Schoen, Rhykerd, Cushman, and Diestler] Schoen, M.; Rhykerd, C. L.; Cushman, J. H.; Diestler, D. J. *Mol. Phys.* **1989**, *66*, 1171–1182.

[Luzar et al.(1987)Luzar, Bratko, and Blum] Luzar, A.; Bratko, D.; Blum, L. *J. Chem. Phys.* **1987**, *86*, 2955–2959.

[Vanmegen and Snook(1981)] Vanmegen, W. J.; Snook, I. K. *J. Chem. Phys.* **1981**, *74*, 1409–1411.

[Cagin and Pettitt(1991)] Cagin, T.; Pettitt, B. M. *Mol. Phys.* **1991**, *72*, 169–175.

[Lynch and Pettitt(1997)] Lynch, G. C.; Pettitt, B. M. *J. Chem. Phys.* **1997**, *107*, 8594–8610.

[Wang and Fichthorn(2000)] Wang, J. C.; Fichthorn, K. A. *J. Chem. Phys.* **2000**, *112*, 8252–8259.

[Schoen et al.(1994)Schoen, Diestler, and Cushman] Schoen, M.; Diestler, D. J.; Cushman, J. H. *J. Chem. Phys.* **1994**, *100*, 7707–7717.

[Svensson and Woodward(1994)] Svensson, B.; Woodward, C. E. *J. Chem. Phys.* **1994**, *100*, 4575–4581.

[Wu et al.(1998)Wu, Bratko, and Prausnitz] Wu, J. Z.; Bratko, D.; Prausnitz, J. M. *Proc. Natl. Acad. Sci. U. S. A.* **1998**, *95*, 15169–15172.

[Shelley and Patey(1999)] Shelley, J. C.; Patey, G. N. *J. Chem. Phys.* **1999**, *110*, 1633–1637.

[Shinto et al.(1999)Shinto, Miyahara, and Higashitani] Shinto, H.; Miyahara, M.; Higashitani, K. *J. Colloid Interface Sci.* **1999**, *209*, 79–85.

[Wallqvist and Berne(1995)] Wallqvist, A.; Berne, B. J. *J. Phys. Chem.* **1995**, *99*, 2893–2899.

[Zhang et al.(2001)Zhang, Balasundaram, Gehrke, and Jiang] Zhang, L. Z.; Balasundaram, R.; Gehrke, S. H.; Jiang, S. Y. *J. Chem. Phys.* **2001**, *114*, 6869–6877.

[Grzybowski et al.(2000)Grzybowski, Gwozdz, and Brodka] Grzybowski, A.; Gwozdz, E.; Brodka, A. *Phys. Rev. B* **2000**, *61*, 6706–6712.

[J.(1993)] *Handbook of Crystal Growth*; J., H. D. T., Ed.; 1993; Vol. 2B.

[Gao et al.(1997)Gao, Luedtke, and Landman] Gao, J. P.; Luedtke, W. D.; Landman, U. *Phys. Rev. Lett.* **1997**, *79*, 705–708.

[Polak and Sangwal(1999)] Polak, W.; Sangwal, K. *Cryst. Res. Technol.* **1999**, *34*, 655–660.

[Binks(1994)] Binks, D. J. Ph.D. thesis, University of Surrey, Chemistry, 1994.

[Mitchell and Fincham(1993)] Mitchell, P. J.; Fincham, D. *J. Phys.-Condes. Matter* **1993**, *5*, 1031–1038.

[Huheey(1983)] Huheey, J. E. *Inorganic Chemistry: Principles of structure and reactivity*; Harper International: New York, 1983.

[Essmann et al.(1995)Essmann, Perera, Berkowitz, Darden, Lee, and Pedersen] Essmann, U.; Perera, L.; Berkowitz, M. L.; Darden, T.; Lee, H.; Pedersen, L. G. *J. Chem. Phys.* **1995**, *103*, 8577–8593.

[Smith et al.(2002)Smith, Yong, and Rodger] Smith, W.; Yong, C. W.; Rodger, P. M. *Mol. Simul.* **2002**, *28*, 385–471.

[Landolt(1993)] Landolt, H. H. *Numerical data and functional relationships in science and technology : new series, Landolt-Bö rnstein*; Springer: Berlin, 1993; Vol. III, 29a.

[Melchionna et al.(1993)Melchionna, Ciccotti, and Holian] Melchionna, S.; Ciccotti, G.; Holian, B. L. *Mol. Phys.* **1993**, *78*, 533–544.

[Parsonage and Nicholson(1987)] Parsonage, N. G.; Nicholson, D. **1987**, *83*, 663–673.

[Biesheuvel(2002)] Biesheuvel, P. M. *Langmuir* **2002**, *18*, 5566–5571.

[Kiriukhin and Collins(2002)] Kiriukhin, M. Y.; Collins, K. D. *Biophys. Chem.* **2002**, *99*, 155–168.